A CD8$^+$ killing assay to measure T cell responses to infection with SARS-nCoV-2

Uvedhna Padia

218010260

Supervisor: Prof Zaza M. Ndhlovu

Co-supervisor: Dr Andrea O. Papadopoulos

A dissertation submitted to the Discipline of Virology in the School of Laboratory Medicine and Medical Sciences, College of Health Sciences at the University of KwaZulu-Natal in part fulfilment of the degree, Master of Science.

2024

PREFACE

The experimental procedures presented in this thesis were performed at the Africa Health Research Institute, Nelson R. Mandela School of Medicine, University of KwaZulu Natal, Durban, South Africa. This study was performed under the supervision of Prof. Zaza Ndhlovu and Dr Andrea Papadopoulos. This dissertation represents the original work of the author and has not been submitted for any degree or examination at any other university. Where the work of others has been used, the authors have been duly acknowledged.

[redacted]

Uvedhna Padia (Student)

[redacted]

Prof. Zaza Ndhlovu (Supervisor)

[redacted]

Dr Andrea Papadopoulos (Co-supervisor)

PLAGIARISM DECLARATION

I, Uvedhna Padia declare that:

(i) The research reported in this thesis, except where otherwise indicated, is my original research.

(ii) This thesis has not been submitted for any degree or examination at any other university.

(iii) This thesis does not contain other persons' data, pictures, graphs or other information, unless specifically acknowledged as being sourced from other persons.

(iv) This thesis does not contain other persons' writing, unless specifically acknowledged as being sourced from other researchers. Where other written sources have been quoted, then:

a) Their words have been re-written, but the general information attributed to them has been referenced.

b) Where their exact words have been used, then their writing has been placed in italics and inside quotation marks and referenced.

(v) Where I have reproduced a publication of which I am an author, co-author, or editor, I have indicated in detail which part of the publication was actually written by myself alone and fully referenced such publications.

(vi) This thesis does not contain text, graphics or tables copied and pasted from the Internet, unless specifically acknowledged, and the source being detailed in the thesis and in the References sections.

_____

Uvedhna Padia (Student)

17 July 2024

_____

Date

ETHICS APPROVAL

The ethics approval for this study was obtained from the Biomedical Research Committee of the Nelson R. Mandela School of Medicine, University of KwaZulu Natal, Durban, South Africa. The ethics approval reference number is as follows: **BREC/00006446/2023**

PRESENTATIONS

1. Uvedhna Padia, Zaza Ndhlovu, Andrea Papadopoulos. Measuring $CD8^+$ T cell responses: A pseudovirus approach. AHRI Indaba seminar series, 30th September 2022, Africa Health Research Institute, Durban, South Africa (Oral presentation).

2. Uvedhna Padia, Zaza Ndhlovu, Andrea Papadopoulos. A $CD8^+$ pseudovirus killing assay to measure T cell responses to infection with SARS-CoV-2. Immuno-Zambia Conference, 8th December 2022, M'kango Golfview Hotel, Lusaka, Zambia (Poster presentation).

3. Uvedhna Padia, Zaza Ndhlovu, Andrea Papadopoulos. A $CD8^+$ killing assay to measure T cell responses to infection with SARS-CoV-2. AHRI Research Day, 19th October 2023, K-RITH Tower Building, Nelson R Mandela School of Medicine, Durban, South Africa (Oral presentation)

4. Uvedhna Padia, Zaza Ndhlovu, Andrea Papadopoulos. Developing a $CD8^+$ Killing Assay for Quantitative Measurement of Immune-Mediated Elimination of SARS-CoV-2 Infected Cells. International Union of Immunological Sciences (IUIS) Conference, 30 November 2023, Cape Town International Convention Centre, Cape Town, South Africa (Poster presentation).

ACKNOWLEDGEMENTS

I would like to extend my gratitude to Professor Zaza Ndhlovu and Dr Andrea Papadopoulos for their careful prioritisation and critique on all aspects of this research project. Your patience and support throughout my Master's degree has been invaluable.

My sincere thanks to the following stakeholders, whose contributions made this study possible: AHRI Biorepository Core, AHRI Clinical Core (Farina Karim), COMMIT-KZN (Willem Hanekom, Bernadett Gosnell and Yunus Moosa), Sigal Lab (Alex Sigal, Kajal Reedoy, Zesuliwe Jule, Yashica Ganga and Khadija Khan) and the AHRI Mechanisms study team.

I am profoundly grateful to the participants of the HPP Acute and Elite controller cohorts, the Botswana-Harvard AIDS Institute Partnership (BHP) cohort and the Females Rising through Education, Support and Health (FRESH) cohort. Your involvement was essential to the success of this research. A special thank you to the Moore Group and Dr Thandeka Moyo-Gwete at the National Institute of Communicable Diseases (NICD) for their collaboration.

I extend my appreciation to the following funders: National Research Foundation (NRF), Sub-Saharan African Network for TV/HIV Research Excellence (SANTHE), Wellcome Trust and the Bill and Melinda Gates Foundation.

Lastly, I would like to thank the members of the Ndhlovu Lab for their unwavering encouragement and guidance over the last two years. It has been a privilege working alongside such talented and supportive colleagues. I can only hope to one day become as exceptional a scientist as each of you.

DEDICATION

For Umesh, Yashica, Tahil and Yastaav Padia. I'm going to put this on the fridge.

And for Bella the cat who did absolutely nothing, which was all she needed to do.

TABLE OF CONTENTS

ABSTRACT

The coordinated efforts of the innate and adaptive immune systems are essential for the effective control and clearance of novel SARS-CoV-2 (SARS-nCoV-2) infection. While the innate immune response provides an immediate but non-specific defense, the adaptive immune response offers specificity and long-lasting protection. Although anti-SARS-nCoV-2 immune responses are well-characterized, T cell responses are equally important. But, the role of cytolytic $CD8^+$ T cell responses in vaccine-induced protection against SARS-nCoV-2 is poorly understood, partly because of a lack of robust assays which accurately measure virus-specific $CD8^+$ T cell (CTL) cytotoxicity. The aim of this study was to develop an assay capable of measuring SARS-nCoV-2 specific CTL responses to both COVID-19 vaccines and natural infection. This study evaluated two fluorescence-based killing assays. The pseudovirus-based killing assay aimed to optimize a spike pseudotyped reporter virus to infect target cells for a SARS-nCoV-2-specific $CD8^+$ T cell killing assay. The second assay measured cytotoxic $CD8^+$ T cell responses by labelling antigen-presenting target cells with different concentrations of carboxyfluorescein succinimidyl ester (CFSE), whereby fluorescence loss represented killing by autologous effector cells. For the pseudovirus approach, multiple transfection methods and target cell infection conditions were tested towards achieving a robust fluorescence readout in target cells. However, the assay did not produce a sufficient fluorescence readout to measure $CD8^+$-mediated elimination of target cells. For the CFSE-based assay, different concentrations of CFSE were tested and optimized for antigen-specific and non-specific target cells respectively, followed by optimizing co-culture with autologous $CD8^+$ T cells, both for *ex vivo* killing measurements or following cultured expansion of T cells. The assay was validated using peripheral blood mononuclear cells (PBMCs) from people living with HIV (PLWH). The assay was then used to compare SAR-nCoV-2 specific CTL killing responses in PLWH and without HIV (PLWoH) vaccinated with Oxford/AstraZeneca, Coronavac or Ad26COV2.S. SARS-nCoV-2-specific $CD8^+$ killing activity was generally low in COVID-19 vaccine recipients. Marginally higher responses were observed in PLWH receiving vector-based vaccines Oxford/AstraZeneca and Ad26COV2.S, than PLWoH. Overall, a CFSE-based $CD8^+$ killing assay that can measure COVID-19 vaccine responses was successfully developed. Additionally, this assay can be adapted to measure CTL responses to other viruses and natural viral infections.

LIST OF TABLES

LIST OF FIGURES

LIST OF ABBREVIATIONS

Abbreviation	Full name
ACE2	Angiotensin-Converting Enzyme 2
AIDS	Acquired Immunodeficiency Syndrome
AIM	Activation-Induced Marker
APC	Antigen Presenting Cell
ART	Antiretroviral Therapy
BSA	Bovine Serum Albumin
$CD4^+$ T cells	Cluster of Differentiation 4 Positive T cells
$CD8^+$ T cells	Cluster of Differentiation 8 Positive T cells
CFSE	Carboxyfluorescein Succinimidyl Ester
CMV	Cytomegalovirus
COVID-19	Coronavirus Disease 2019
CTL	Cytotoxic T Lymphocyte
DMEM	Dulbecco's Modified Eagle Medium
DMSO	Dimethyl Sulfoxide
DNA	Deoxyribonucleic Acid
ELISA	Enzyme-Linked Immunosorbent Assay
ELISpot	Enzyme-Linked Immunospot Assay
FACS	Fluorescence Activated Cell Sorting
FBS	Fetal Bovine Serum
FSC	Forward Scatter
GFP	Green Fluorescent Protein
hACE2	Human Angiotensin Converting Enzyme
HEK	Human Embryonic Kidney
HIV	Human Immunodeficiency Virus
ICS	Intracellular Cytokine Staining
IFN	Interferon
IFN-γ	Interferon Gamma
IGRA	Interferon Gamma Release Assay
IL	Interleukin
LB	Luria Bertani
mAbs	Monoclonal Antibodies
MACS	Magnetic Activated Cell Sorting
MFI	Median Fluorescence Intensity

MHC	Major Histocompatibility Complex
MLV	Murine Leukaemia Virus
mRNA	Messenger Ribonucleic Acid
nAbs	Neutralizing Antibodies
NK	Natural Killer
PAMP	Pathogen-Associated Molecular Pattern
PBMC	Peripheral Blood Mononuclear Cells
PBS	Phosphate-Buffered Saline
PEI	Polyethylenimine
PI	Propidium Iodide
PLWH	People Living with HIV
PLWoH	People Living without HIV
PRR	Pattern Recognition Receptors
PVNA	Pseudovirus Neutralization Assay
RBD	Receptor Binding Domain
RNA	Ribonucleic Acid
RPMI 1640	Roswell Park Memorial Institute 1640
RT-PCR	Reverse Transcription Polymerase Chain Reaction
SARS-CoV	Severe Acute Respiratory Syndrome
SARS-nCoV-2	Novel Severe Acute Respiratory Syndrome Coronavirus 2
SSC	Side Scatter
ssRNA	Single Stranded Ribonucleic Acid
TCR	T Cell Receptor
TLR	Toll-Like Receptor
TMPRSS2	Transmembrane Serine Protease 2
TNF-α	Tumor Necrosis Factor Alpha
VIA	Viral Inhibition Assay
VOC	Variant of Concern
VOI	Variant of Interest
VSV	Vesicular Stomatitis Virus
VUM	Variant Under Monitoring
WHO	World Health Organization
YFP	Yellow Fluorescent Protein

CHAPTER 1: LITERATURE REVIEW

1.1. The COVID-19 pandemic

In December of 2019, an unidentified pneumonia outbreak was reported in Wuhan, Hubei province, central China (Zhou et al., 2020b). It was further reported that these pneumonia cases grew exponentially and led to approximately 80 deaths by the end of January 2020 (Zhou et al., 2020b). Following isolation and genomic analysis of this pathogen, it was found that the pathogen was a novel coronavirus closely related to severe acute respiratory syndrome coronavirus (SARS-CoV), hence the name SARS-nCoV-2 (novel severe acute respiratory syndrome coronavirus 2) was adopted (Ciotti et al., 2020). SARS-nCoV-2 is a betacoronavirus which falls under the subgenus *Sarbecovirus* and is considered highly similar to bat SARS-like coronaviruses (Cui et al., 2019, Ciotti et al., 2020, Wu et al., 2020). The rapid spread of SARS-nCoV-2 around the world and the thousands of deaths caused by the coronavirus disease (COVID-19) led to the declaration of a global pandemic by the World Health Organization in March of 2020 (Ciotti et al., 2020). Since the start of the pandemic, South Africa has recorded more than four million cases of COVID-19 and over 100 000 COVID-19-related deaths (Jassat et al., 2024).

COVID-19 is characterised by mild flu-like symptoms such as fever, dry cough and headaches or may present asymptomatic in some diagnosed individuals (Karim et al., 2021b), although cases tend to be more severe in individuals with underlying comorbidities such as obesity, diabetes, chronic kidney disease and human immunodeficiency virus (HIV) (Mellor et al., 2021). In severe cases of COVID-19, infected patients may experience breathing difficulties, pneumonia, stroke and even death (Zhou et al., 2020b). South Africa has continued to experience challenges in its healthcare service delivery due to a lack of funding, inadequate recruitment in rural areas and unequal distribution of resources which were further exacerbated by the COVID-19 pandemic (Mbunge, 2020). In addition, South Africa has the highest number of people living with HIV (PLWH) in the world, which has added to the severe burden on both the healthcare and economic sectors (Bulled and Singer, 2020). People living with HIV may experience severe immune dysfunction which further exacerbates the harmful effects of SARS-nCoV-2 associated with underlying immunosuppression (Williamson et al., 2020, Karim et al., 2021b). During HIV infection, many aspects of the adaptive immune response become dysregulated which may result in prolonged infection due to the ineffective control and clearance of SARS-nCoV-2 (Karim et al., 2021a, Karim et al., 2021b).

1.1.1 SARS-nCoV-2 entry mechanism

The cell surface receptor, angiotensin-converting enzyme 2 (ACE2,) is a well-characterised and critical host entry receptor for other coronaviruses including SARS-CoV and HCoV-NL-63 and mediates entry of SARS-nCoV-2 into human cells (Kumar et al., 2021). The ACE2 receptor is highly expressed in multiple cell types which may contribute to higher COVID-19 vulnerability within these cell types. In addition to its high expression levels in pulmonary tissue which contributes to its ability to cause severe lung damage, Zheng (2021) has noted that the organs of the digestive system, namely the intestine, gallbladder, duodenum and ileum, as well as the kidneys have high expression levels of ACE2 (Daniloski et al., 2021). This is consistent with findings related to the clinical manifestations of COVID-19 such as kidney failure and gastrointestinal symptoms such as diarrhoea (Guan et al., 2020). Structural differences in the receptor binding domain (RBD) of SARS-nCoV-2 enable the virus to have a significantly higher ACE2 binding affinity than the SARS-CoV RBD (Mittal et al., 2020, Shang et al., 2020). To gain entry into the host cell, as depicted in **Figure 1.1.**, ACE2 must bind to the RBD of SARS-nCoV-2 spike (S) protein which is facilitated by the process of membrane fusion (Jackson et al., 2022). To initiate membrane fusion, and subsequently allow the virus to enter a host and release its genetic material, viral entry proteins are required to undergo a conformational change (Kumar et al., 2021). Before fusion occurs, the S protein adopts a "metastable state" which is an intermediate state that is prone to transformation into a lower-energy, more stable state (Jackson et al., 2022). This is necessary to provide sufficient energy to overcome the natural repulsive forces that the virus encounters with cellular membranes.

The transition of the S protein is facilitated by two proteolytic cleavage steps after ACE2 has been engaged. The first of these is localized at the S1-S2 boundary and is carried out by host cell proteases such as furin and transmembrane protease, serine 2 (TMPRSS2). The importance of this cleavage step is in the fact that it primes the S protein for further conformational changes, thereby facilitating the transition to a more stable energy state. TMPRSS2, which is located on the surface of the host cell, cleaves the S protein during viral entry, thus contributing to the activation of the S2 subunit (Shang et al., 2020). Furin, a cellular protease, cleaves the S protein at the S1-S2 boundary during the virus's maturation in the host cell's secretory pathway (Shang et al., 2020, Jackson et al., 2022). After the initial cleavage, a second proteolytic cleavage occurs at the S2' site, which is critical for the complete activation of the S protein. This cleavage is carried out by endosomal proteases such as cathepsins, which are non-specific proteases that participate in degradation of proteins in the endosomes and lysosomes, and promotes the fusion of the viral and cellular membranes in the endosome (Kumar et al., 2021, Jackson et al., 2022). This co-ordinated two-step proteolytic activation process ensures the fusion peptide, a hydrophobic region within the S2 subunit, is optimally exposed thereby facilitating its insertion into the host cell membrane. As the fusion peptide inserts into the host cell membrane, the S2 subunit undergoes further conformational changes and transitions into a more extended structure. This

leads to the formation of a stable post-fusion conformation, which allows the viral and cellular membranes to merge, consequently releasing the viral genome into the cytoplasm of the host cell (Whittaker et al., 2021, Jackson et al., 2022). The entry of SARS-nCoV-2 into host cells is a delicate process and plays a role in the virus's efficiency in utilising the host cell's machinery for its replication and propagation (Whittaker et al., 2021). Understanding these entry mechanisms provides insights for the development of spike-directed vaccines (Seyedpour et al., 2021).

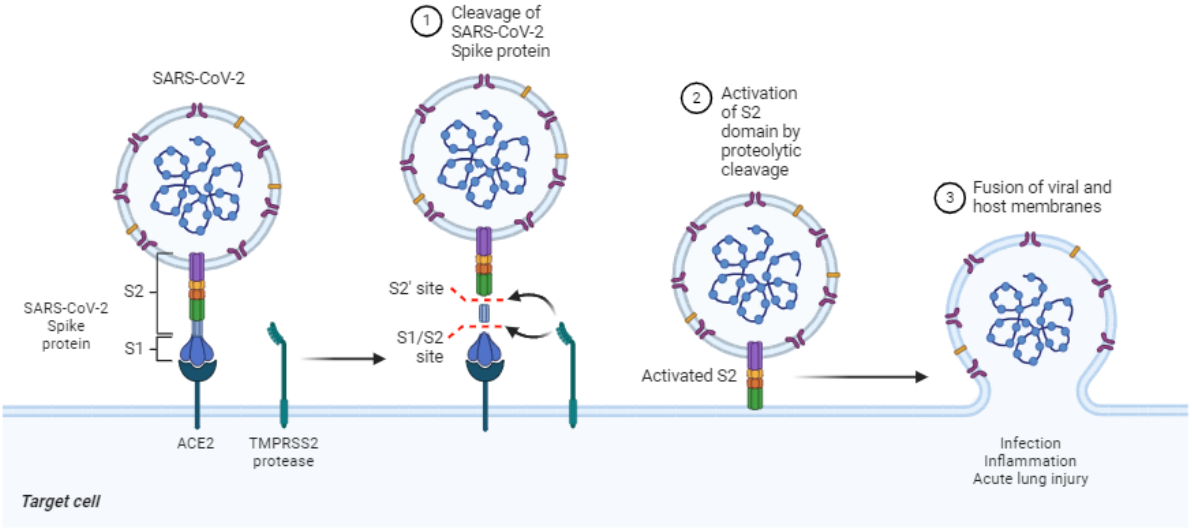

Figure 1.1.: Schematic representation of SARS-nCoV-2 infection of target cells expressing angiotensin converting enzyme 2 (ACE2) (created in BioRender, adapted from Hartenian et al. (2020) and Kumar et al. (2021)).

1.1.2. Emergence of SARS-nCoV-2 variants

Coronaviruses accumulate mutations through the process of recombination when variants with different mutations infect the same host (Gribble et al., 2021, Jackson et al., 2021, Tegally et al., 2021). During viral replication, random mutations may be introduced into the viral genome due to the error-prone nature of viral RNA-dependent RNA polymerase (RdRp) and despite the presence of a proofreading exonuclease (Lou et al., 2021, Tegally et al., 2021). Furthermore, the mutation rate or the rate at which a virus evolves is a key contributor to the emergence of SARS-nCoV-2 variants (Markov et al., 2023). The mutation rate may also be defined as the rate at which genetic changes emerge per every replication cycle and it is estimated that the mutation rate of SARS-nCoV-2 is approximately $1 \times 10^{-6} – 2 \times 10^{-6}$ mutations per nucleotide per replication cycle (Amicone et al., 2022, Markov et al., 2023). This rate is below the ranges of other RNA viruses like hepatitis C and human immunodeficiency virus (HIV) which lack an exonuclease proofreading mechanism in their replication machinery (Markov et al., 2023). As

the virus spread and replicated further over the course of the pandemic, chronic infection increased the likelihood of adaptive mutation by the virus (Lou et al., 2021).

The WHO has developed a SARS-nCoV-2 Variant Classification scheme comprised of two main categories: variants of concern (VOC) and variants of interest (VOI). A VOC refers to those SARS-nCoV-2 variants that are capable of drastically altering COVID-19 epidemiology by hindering the effectiveness of vaccines and neutralizing antibodies (nAbs) and increasing transmissibility. A VOI, on the other hand, refers to SARS-nCoV-2 variants possessing predictable mutations which are known to affect the characteristics of viruses such as their infectivity, immune evasion or disease severity (Mistry et al., 2021). An additional category was also included referring to variants under monitoring (VUM) which are those variants with specific mutations known to affect viral characteristics and which may potentially pose a threat to public health in the future, although there is no current evidence of epidemiological or phenotypic impact (Choi and Smith, 2021). The five major SARS-nCoV-2 variants of concern recognized by the WHO are: Alpha B.1.1.7 which was first identified in the United Kingdom, Beta B.1.351 which was first reported in South Africa, Gamma P.1 which was first reported in Brazil, Delta B.1.617.2 which was first identified in India and Omicron B.1.1.529 (Khan et al., 2022, Keeton et al., 2022) which was first discovered in South Africa (Mistry et al., 2021).

The first notable mutation which allowed the virus to adapt to its new human host was a point mutation in the spike protein translating to the substitution of a glycine residue in place of aspartate at amino acid 614 (D614G) of SARS-nCoV-2 (Mittal et al., 2022, Tian et al., 2022). The D614G mutation is present in all VOC with several clinical infection and animal studies demonstrating that the virus bearing the D614G mutation is more infectious than the Wuhan-Hu-1 isolate (Mittal et al., 2022, Tian et al., 2022). It has been observed that the infection efficiency of D614G pseudovirus was eight to ten fold higher than the wildtype strain (Zhou et al., 2020a) and clinical samples infected with D614G mutant strain had a higher titre of SARS-nCoV-2 RNA suggesting a higher infectivity than the wildtype strain (Daniloski et al., 2021). Daniloski et al. (2021) also demonstrated that the D614G mutation increased entry efficiency for the virus across a wide range of human cell types ranging from lung and liver to colon using both a replication-competent SARS-nCoV-2 virus and a pseudotyped lentiviral system. It is hypothesized that D614G can shift the RBD to an “up” conformation, hence promoting binding with the ACE2 receptor and therefore more efficient virion infectivity (Zhou et al., 2020a).

Another mutation contributing to the enhanced infectivity of VOC is N501Y, which is a key substitution in the RBD, present in the Alpha, Beta, Gamma and Omicron VOCs (Tao et al., 2021, Dejnirattisai et al., 2022). This mutation increases ACE2 binding affinity as well as viral replication in the cells of the upper airway in humans and in the upper respiratory tract of hamsters (Liu et al., 2021b). D614G and N501Y are also associated with resistance to the current COVID-19 vaccines and an enhanced reinfection rate (Araf et al., 2022). Another substitution, E484K, may also increase binding affinity to

human ACE2 with some studies suggesting that E484K and N501Y may further enhance binding affinity when combined (Nelson et al., 2021, Zahradník et al., 2021). L452R is another RBD mutation present in the Delta VOC which can enhance the binding affinity of RBD to ACE2, thereby increasing the likelihood of the virus infecting host cells (Tian et al., 2022). Pseudotyped viruses containing L452R demonstrated higher levels of cellular entry in lung organoids compared with pseudotyped viruses containing only D614G, but lower levels with pseudotyped viruses containing N501Y (Deng et al., 2021). Mutations in the vicinity of the S1/S2 furin cleavage site have occurred independently in several SARS-nCoV-2 VOCs and include N679K, Q675H/R and P681H/R (Hodcroft et al., 2021). In particular, P681H/R is associated with an increased positive charge which has been observed to affect virus tropism by increasing S1/S2 cleavage in human airway epithelial cells (Saito et al., 2021). N-terminal domain (NTD) mutations have been reported in many VOCs and commonly in individuals with prolonged SARS-nCoV-2 infections (Choi and Smith, 2021). These deletions at positions 69-70 are associated with increased viral replication (Kemp et al., 2021).

The presence of mutations among the VOC has contributed to their distinct transmissibility characteristics (Atlani-Duault et al., 2021). The emergence and spread of these VOCs is linked with the absence of robust immune protection after an initial exposure to wildtype viruses or even vaccines, a phenomenon termed “immune evasion” (Hie et al., 2021). To measure immune escape among VOCs, viral neutralization assays have been employed which measure functional nAb levels in serum and plasma (Bewley et al., 2021). Neutralization, or the reduction in viral infectivity due to the binding of antibodies to the surface of viral particles thereby blocking the viral replication cycle, is an important measure of the immune response after vaccination or recovery from COVID-19, as well as breakthrough infections (Takeshita et al., 2022, Ravlić et al., 2023). Neutralization assays are crucial for the quantification of functional nAbs in serum samples and can be used to examine the viral physiology, viral entry mechanisms and determine host tropisms (Li et al., 2017, Salata et al., 2019, Cantoni et al., 2021, Bewley et al., 2021). Pseudovirus neutralization assays (PVNAs) have been widely used to evaluate nAb responses against wildtype SARS-nCoV-2 and different VOCs in plasma from vaccinated individuals (Cantoni et al., 2021, Donofrio et al., 2021, Zhang et al., 2022). Donofrio et al (2021) has described a simplified pseudovirus neutralization assay in which all steps can be performed in the same plate within a standard biosafety level 2 laboratory. Furthermore, the assay was used to determine the neutralizing potency of nAbs derived from serum samples as serum neutralizing activity has been closely correlated with protection in several COVID-19 infections (Donofrio et al., 2021). PVNAs were used to verify the first human monoclonal antibody that neutralizes both SARS-CoV and SARS-nCoV-2, 47D11 (Wang et al., 2020). In addition, plaque reduction neutralization tests have been used which measure nAbs by *in vitro* virus neutralization (Bewley et al., 2021).

The Alpha variant is estimated to be 43% to 100% more transmissible than the wildtype but is neutralized by convalescent sera and is not associated with an increased reinfection risk (Dejnirattisai

et al., 2022). On the other hand, the Beta variant is up to 50% more transmissible than the wildtype if immune escape is minimal (Choi and Smith, 2021, Bushman et al., 2021). Multiple studies have reported that 40% to 50% of convalescent serum samples exhibit no neutralizing activity against the Beta variant or pseudovirus, although T cell responses are mostly intact even when antibody responses wane (Sherina et al., 2021). The Delta variant has evolved a heightened transmission ability over other SARS-nCoV-2 variants (Cele et al., 2022). While it does not show a significant level of evasion from plasma immunity elicited by ancestral strains, it does demonstrate escape from Beta antibody immunity (Liu et al., 2021a). Most recently, the emergence of the Omicron variant led to a surge of infections worldwide as a result of its 32 mutations in the S protein which has made the variant more resistant to nAbs induced by natural infection or vaccination (Liu et al., 2021a, Khan et al., 2022). Five subvariants of Omicron have subsequently been detected, namely BA.1, BA.2, BA.3, BA.4 and BA.5. The continuously evolving nature of the SARS-nCoV-2 variants has greatly contributed to its enhanced transmissibility and immune evasion capabilities. For these reasons, identifying conservative correlates of immune protection are necessary for lasting control of COVID-19.

1.2. Antiviral immune responses

Given that the COVID-19 landscape has evolved rapidly since the start of the pandemic, understanding how immunity translates into protection is imperative. Most viral infections are efficiently resolved by the two arms of the immune system: the innate immune response and the adaptive immune response (Seth et al., 2006). The first line of defence is the innate immune system which recognizes foreign viral material and activates a signalling cascade which controls the spread of the virus to neighbouring cells (Castro Dopico et al., 2022). In the case of respiratory viruses like SARS-nCoV-2, the initial encounter occurs in the upper respiratory tract through the nasal epithelium, tonsils and adenoids where mucosal immunity development is activated (Primorac et al., 2022). Innate immunity is first induced by pattern recognition receptors (PRRs) present on the cells of the innate immune system (such as phagocytic and dendritic cells) that detect molecular structures shared by pathogens of various origins (pathogen-associated molecular patterns, PAMPs) (Seth et al., 2006, Primorac et al., 2022). Toll-like receptors (TLRs) 3, 7, 8 and 9 are the major PRRs that recognize virally-derived nucleic acids and activate signalling cascades that result in the induction of type I interferons (IFNs) (Seth et al., 2006). An impaired IFN type I response, which is characterized by the absence of IFN-β and low IFN-α activity, has been observed in severe patients and is associated with an exacerbated inflammatory response (Hadjadj et al., 2020, Arunachalam et al., 2020). Subsequent adaptive immune responses are orchestrated by the innate immune response and involve antibodies produced by plasma cells from bone marrow-derived B lymphocytes (B cells) and effector thymus-produced lymphocytes (T cells) (Ramasamy, 2020).

1.2.1. The anti-viral adaptive immune response

The adaptive immune response is comprised of three major cell types: B cells, $CD4^+$ helper T cells and $CD8^+$ cytotoxic T cells, as depicted in **Figure 1.2.** (Ramasamy, 2020, Sette and Crotty, 2021). Dimeric immunoglobulin (Ig) A antibodies, when transported through the mucosal epithelium to the upper respiratory tract (URT) airway, can attach to proteins on the virion membrane, agglutinate virions, and prevent them from binding to epithelial cells (Ramasamy, 2020). Similarly, IgG and IgM antibodies in the nasal mucosa can neutralize virions and activate the classical complement pathway to destroy virions and infected cells. Additionally, viral particles encounter major histocompatibility complexes (MHC) I and II as well as natural killer (NK) cells (Primorac et al., 2022). MHC-I molecules, which are expressed on all cells with a nucleus serves mainly as an antigen recognition mechanism for $CD8^+$ T cells (Primorac et al., 2022). MHC-II molecules, which are embedded in the membranes of antigen-presenting cells (macrophages, monocytes, dendritic cells and B cells) activate B cell proliferation and differentiation as well as $CD4^+$ T cells (Lima et al., 2022). Furthermore, $CD4^+$ T cells in URT lymphoid tissues can stimulate B cells and lead to immunoglobulin class switching, where B cells change the

class of antibodies they produce, and antibody affinity maturation, where antibodies are primed for more effective pathogen-specific binding (Ramasamy, 2020). The humoral-mediated response, mainly comprised of B cells, has been studied extensively as B cells produce antibodies that are able to bind to viral particles present in the blood and mucosal surfaces, thus preventing the spread of infection (Alrubayyi et al., 2021). The evaluation of humoral immunity represents only one aspect of immunological memory. For this reason, the study of cellular immune responses (T cells) is also important in formulating a holistic understanding of the immune response to SARS-nCoV-2.

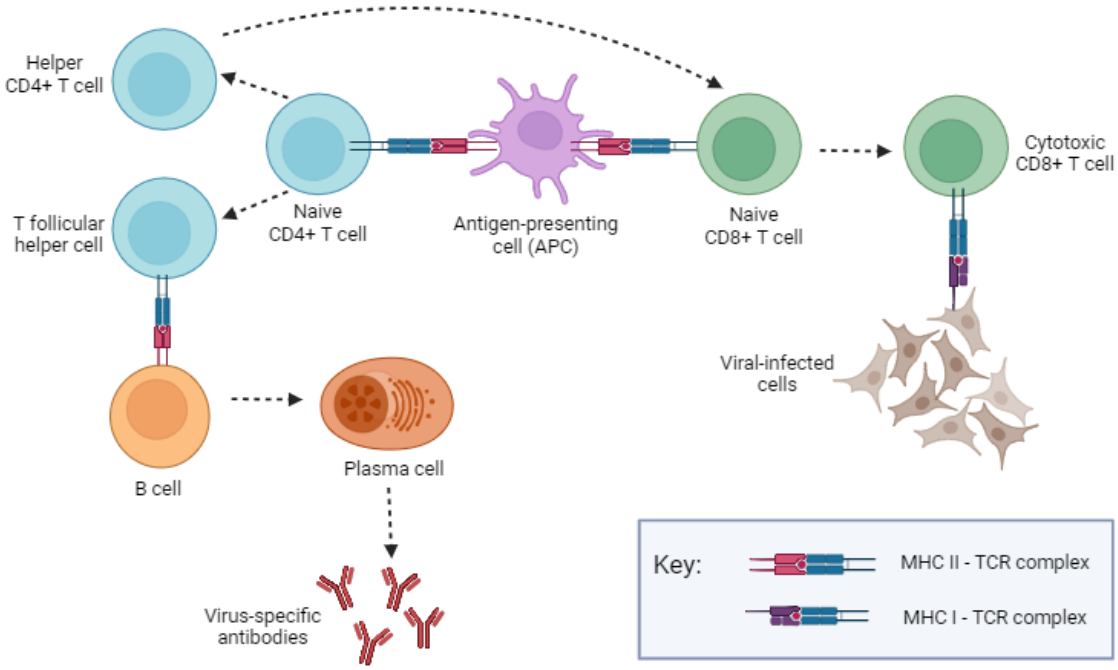

Figure 1.2.: Schematic representation of antiviral adaptive immunity showing the interaction between helper $CD4^+$ T cells, naïve $CD4^+$ T cells, antigen-presenting cells (APC), naïve $CD8^+$ T cells, cytotoxic $CD8^+$ T cells, and B cells leading to the production of virus-specific antibodies. The diagram details the role of MHC I - TCR and MHC II - TCR complexes as indicated in the key (created in BioRender, adapted from Mistry et al, (2021)).

1.2.2. Antibody responses to SARS-nCov-2

The antibody response plays a critical role in the control and clearance of SARS-nCoV-2 infection and can be divided into two phases. During the extrafollicular (EF) phase, B cells are activated to differentiate rapidly into relatively short-lived plasma cells outside the follicle a few days after infection (Qi et al., 2022). The EF cells are often of the IgM isotype but can switch to IgG or IgA in response to viral infections. The germinal centre (GC) phase takes several days to a week to start but can last for many months (Elsner and Shlomchik, 2020, Qi et al., 2022). Antigen-specific B cells experience somatic hypermutation where their genetic material is altered to enhance their effectiveness and

undergo affinity-maturation, which leads to the development of isotype-switched and high-affinity plasma cells (Qi et al., 2022). These plasma cells establish a durable reservoir primarily situated in the bone marrow. Both the extrafollicular (EF) and germinal centre (GC) phases generate antigen-specific memory B cells, which can persist beyond the resolution of the initial infection (Palm and Henry, 2019). In blood vessels, memory B cells join the circulatory system in surveillance and plasma cells migrate towards inflammatory sites to fight off infections (Qi et al., 2022).

It has been reported that most individuals infected with SARS-nCoV-2 seroconvert within 2 weeks post symptom onset and produce antibodies predominantly recognizing the viral spike and nucleocapsid proteins (Long et al., 2020, Suthar et al., 2020, Premkumar et al., 2020). Elevated serum levels of total or nAbs in the blood are often associated with more severe cases of COVID-19, but do not guarantee improved disease outcomes from the initial infection (Robbiani et al., 2020, Chen et al., 2020b, Dan et al., 2021). Early studies have suggested that the mortality rate among hospitalized COVID-19 patients could be lowered by administering convalescent plasma, although this finding was not reported by a larger controlled trial (Hueso et al., 2020, Klassen et al., 2021, Abani et al., 2021). The presence of nAbs that prevent the virus from entering cells via the ACE2 receptor is a good indicator of the effectiveness of preventive vaccines. After infection or vaccination, the concentration of these nAbs against SARS-nCoV-2 peaks within the first few weeks, but then it gradually decreases, which leads to waning immunity and a higher risk of reinfection by the original viral strain or new SARS-nCoV-2 variants of concern (VOC) or variants of interest (VOI) (Wajnberg et al., 2020, Isho et al., 2020, Seow et al., 2020). These studies highlight the importance of timing in the initiation and maintenance of antibody responses.

1.2.3. First generation COVID-19 vaccines elicit short-lived antibody responses

Modern vaccination can be largely attributed to the efforts of Edward Jenner, an 18th century English physician. Jenner noticed how milkmaids infected with cowpox virus were immune to smallpox and decided to inject pus from a pustule of a cowpox patient into a young child who was challenged with smallpox. The child survived the challenge and this became one of the most influential findings of modern medicine (Kayser and Ramzan, 2021). It is noteworthy that prior to this discovery, cultures in the Middle East, Africa and Asia Minor were already using inoculation to immunize children which firmly established the concept that a person who recovered from a disease generally did not experience the disease again (Kayser and Ramzan, 2021). An alternative to this inoculation process at the time was fairly common in China and India which involved nasal insufflation of cotton buds containing a small amount of a smallpox-derived powder, likely from smallpox scabs (Vargha and Wilkins, 2023). Since Jenner's breakthrough discovery, many types of vaccines have been developed against diseases such as

diphtheria, polio and hepatitis which are provided as paediatric vaccines, although novel methods and vaccine strategies are continuously evolving (Dai and Gao, 2021, Kayser and Ramzan, 2021).

Vaccination is largely considered the most effective method of preventing and controlling the spread of SARS-nCoV-2 (Mohseni Afshar et al., 2023, Wang et al., 2023a). The current vaccine landscape is wide-ranging and several vaccine strategies have been developed for SARS-nCoV-2 vaccines since December 2020 to minimize the effects of COVID-19 and achieve herd immunity (**Table 1.1.**). Immunotherapy is an effective clinical treatment strategy for infectious diseases and involves the passive immunization of antibodies, either laboratory-produced or from the blood of infected patients, which identify epitopes on the viral particle (Sheikhshahrokh et al., 2020). Given that SARS-nCoV and SARS-nCoV-2 use the same cell entry receptor, ACE2, neutralizing monoclonal antibodies targeting the RBD in the spike protein of SARS-CoV can be used for SARS-nCoV-2 and effectively inhibit the virus by binding to ACE2 and prevent cellular entry (Sheikhshahrokh et al., 2020). While this strategy does not necessarily prevent infection, it may increase humoral protection against SARS-nCoV-2 infection by targeting various S protein epitopes and functions (Sheikhshahrokh et al., 2020). Vaccination on the other hand may elicit nAbs which limit viral replication and transmission (Mostaghimi et al., 2022). Depending on the vaccination type, IgA and IgG can be transported to the mucosal surface where they hinder S protein attachment to ACE2 and initial viral clearance. If the infection of host cells is prevented, sterilising immunity is achieved and this is established if viral loads are undetectable following the vaccine challenge (Mostaghimi et al., 2022).

Inactivated virus vaccines are made non-infectious either physically or chemically and preserve the integrity of the viral particle thereby allowing multiple viral proteins to be presented for immune recognition (Dong et al., 2020, Dai and Gao, 2021). Furthermore, they can be easily produced in large quantities making them a particularly attractive vaccine strategy, although biosafety level 3 facilities are required to grow the pathogen (Dong et al., 2020). Inactivated vaccines which use whole inactivated SARS-nCoV-2 as the immunogen give rise to antibodies against the spike (S) antigen and other structural protein antigens such as envelope protein (E), matrix protein (M) and nucleocapsid protein (N) antigens (Kan and Li, 2023). The inactivated vaccine platform has been employed in the development of Coronavac by Sinovac, Covaxin by Bharat Biotech and InCov COVID-19 vaccine by Sinopharm (Kan and Li, 2023). Inactivated vaccines are particularly useful in pandemic settings when information about viral pathogens is minimal, although multiple doses of the vaccine are required to maintain immunity (Liu and Ye, 2022). Interestingly, administering a heterologous booster with Coronavac has been shown to induce a more immunogenic response compared to homologous boosting (Li et al., 2022, Jiang et al., 2023). Live-attenuated vaccines have also previously been successful in the treatment of poliomyelitis and smallpox and utilize a weakly pathogenic virus as the antigen (Minor, 2015). It should be noted, however, that there are concerns about the inclusion of epitopes which do not induce nAbs or confer protection as they may skew immune responses (Minor, 2015).

Viral vector vaccines, either replicating or non-replicating, are usually constructed from a carrier virus, such as an adeno or pox virus, and are engineered to carry a relevant viral gene – in the case of CoVs, this would be the S gene (Dong et al., 2020). The Oxford/AstraZeneca (ChAdOx1-S) vaccine, the Convidecia vaccine by CanSinoBio, the Covishield vaccine produced by the Serum Institute of India and the Ad26.COV2.S vaccine from Janssen Pharmaceuticals by Johnson & Johnson utilized this strategy whereby the vaccine encodes the S protein of SARS-nCoV-2 (García-Montero et al., 2021, Wang et al., 2023a). The immunogen is expressed in the context of heterologous infection which induces innate immune responses necessary for adaptive immunity (Afrough et al., 2019). This strategy may however recall prior immunity to the vector and is limited to presenting a small number of CoV antigens to the immune system of the host (Wang et al., 2023a). Vaccine efficacy against symptomatic SARS-nCoV-2 infection with the Delta variant has been shown to peak in the early weeks following the second dose of the ChAdOx1-S vaccine and then decreased by 20 weeks to 44.3% efficacy (Andrews et al., 2022). Waning efficacy was greater in older adults as well as those in a clinical risk group (Andrews et al., 2022). Protein subunit vaccine Nuvaxovid developed by Novavax was the first approved recombinant protein-based vaccine against SARS-nCoV-2. The vaccine consists of trimeric full-length spike glycoproteins derived from SARS-nCoV-2, which are organized into nanoparticles and combined with a saponin-based adjuvant known as Matrix-M (Firouzabadi et al., 2023). An additional protein subunit vaccine, Covovax, developed by the Serum Institute of India has been recommended for use as a booster for individuals receiving other primary vaccine regimens given its good safety profile and ability to induce a high level of binding and nAbs against SARS-nCoV-2 (Kanokudom et al., 2023).

Another popular vaccine strategy is nucleic acid vaccines such as messenger RNA (mRNA) and DNA vaccines which are delivered into human cells where they are transcribed into viral proteins. While their long-term safety profiles remain unknown, mRNA vaccines are highly potent, cost-effective and can be developed rapidly which makes them a promising alternative to conventional vaccine strategies (Dong et al., 2020). These vaccines use mRNA which provide instructions to cells to encode the SARS-nCoV-2 S protein and gives rise to a robust nAb response (Mirtaleb et al., 2023). After vaccination, immune cells then construct this S protein and display them on cell surfaces (Mirtaleb et al., 2023). The BNT162b2/COMIRNATY vaccine produced by Pfizer and mRNA-1273/Spikevax vaccine produced by Moderna are both lipid nanoparticle-formulated, nucleoside-modified RNA vaccines (Francis et al., 2022). (Mulligan et al., 2020). Patients vaccinated with BNT162b2 and mRNA-1273 vaccines have shown IgA and IgG antibodies in their saliva (Nahass et al., 2021, Woldemeskel et al., 2022). Phase I/II studies have shown that the vaccine elicited mild to moderate symptoms and caused higher neutralizing titres after the second dose compared to the COVID-19 convalescent sera panel. Notably, a decline of SARS-nCoV-2 nAbs six months after mRNA vaccination has been reported by Evans et al. (2022) with individuals vaccinated with BNT162b2 exhibiting lower nAb titres than those vaccinated with mRNA-

1273. In addition, it was reported that the Omicron variant escaped mRNA vaccine-induced immunity even three to four weeks after the second vaccine dose (Evans et al., 2022). DNA vaccines have also demonstrated great potential as therapeutics given their long shelf life, manufacturing costs and ability to enhance the induction of T cells and antibody production (Dong et al., 2020). Their disadvantage, however, is that DNA molecules must be transcribed by crossing the nuclear membrane and they generally have a low immunogenicity (Hobernik and Bros, 2018).

Although antibodies play a crucial role in the immediate defence against infection their levels naturally decrease after peaking post-vaccination, potentially reducing the efficacy of many COVID-19 vaccines in the long term. T cells, on the other hand, may provide a more durable protection as they can recognise and destroy infected cells, and memory T cells can persist for years after infection or vaccination, providing ongoing surveillance against the virus (Sette and Crotty, 2021). T cell immunity includes both $CD8^+$ cytotoxic T cells, which can directly kill virus-infected cells, and $CD4^+$ helper T cells, which support antibody production and the activation of other immune cells (Grifoni et al., 2020). Memory T cells can offer protection against severe disease, even when antibody levels have declined (Rydyznski Moderbacher et al., 2020). Therefore, understanding the T cell response to vaccination is crucial for evaluating the full scope of SARS-nCoV-2 vaccine-induced immunity.

Table 1.1.: Comparative efficacy and timelines for peak antibody responses of COVID-19 vaccines.

Type of vaccine	Vaccine name	Manufacturer	Prevention of symptomatic infection	Prevention of severe infection	Peak antibody production
mRNA	COMIRNATY/BNT162b2	Pfizer/BioNTech	~95% efficacy (Polack et al., 2020)	~97% efficacy (Polack et al., 2020)	About 7 to 14 days after second dose (Polack et al., 2020, Reynolds et al., 2023)
	Spikevax/mRNA-1273	Moderna	~94.1% efficacy	~90% efficacy	About 14 days after second dose (Baden et al., 2021, Reynolds et al., 2023)
Viral vector-based	Vaxzevria/AZD1222	AstraZeneca	~70% efficacy	~80 to 90% efficacy against severe disease	Typically 28 days after first dose (Voysey et al., 2021, Reynolds et al., 2023)
	Covishield/ChAdOx1_nCoV-19	Serum Institute of India	~67% efficacy	~13% efficacy after partial vaccination and 66.6% after full vaccination	About 15 days after second vaccination dose (Pramod et al., 2022, Joshi et al., 2023, Thomas et al., 2023)
	Ad26.COV2-S	Janssen–Cilag International	~66% efficacy	~85% efficacy against severe disease	About 14 days after a single vaccination (Sadoff et al., 2021)
	Convidecia/Ad5-nCoV	CanSinoBio	~65% efficacy after a single dose	~95% efficacy 14 days after vaccination and ~90% efficacy 28 days after vaccination (Halperin et al., 2022)	Achieved when used as a heterologous booster after primary vaccination regimen is administered (Li et al., 2022)
Inactivated virus	InCoV COVID-19 Vaccine	Sinopharm/Beijing Institute of Biological Products	~79% 14 days after the second dose (WHO, 2022)	~79% efficacy (WHO, 2022)	After second vaccine (booster) dose (Saeed et al., 2021)
	Coronavac	Sinovac Life Sciences	Efficacy varies between ~50.4% and ~57.5% among different study populations (Palacios et al., 2021, Halperin et al., 2022)	High efficacy but notable variability among different study populations	Achieved after third vaccination dose (Li et al., 2022)
	Covaxin	Bharat Biotech	~77% efficacy after phase III clinical trial (Talukder et al., 2022)	~93% efficacy after phase III clinical trial (Talukder et al., 2022)	After about 6 weeks (Asokan et al., 2024)
Protein subunit	Covovax/Nvx-CoV2373	Serum Institute of India	~50% efficacy regardless of baseline serostatus (Shinde et al., 2021)	High efficacy but notable variability among different study populations	About 15 days after booster vaccination (Lyke et al., 2023)
	Nuvaxovid	Novavax	~89% efficacy (Heath et al., 2021)	High efficacy but notable variability among different study populations	About 15 days after booster vaccination (Lyke et al., 2023)

1.2.4. Antiviral T cell responses

T cells play an important role in protection from viral infections. $CD4^+$ T cells can differentiate into a wide range of helper and effector types with the ability to recruit innate immune cells, facilitate tissue repair and instruct B cells (Sette and Crotty, 2021). In a study where healthy volunteers were challenged with influenza A virus, antibody and T cell responses before and during infection were monitored (Wilkinson et al., 2012). It was observed that pre-existing $CD4^+$ T cells responding to influenza proteins were associated with less severe illness and lower viral shedding (Wilkinson et al., 2012). During chronic viral infections when the host is unable to clear the virus, such as in chronic HIV infection, cytotoxic $CD8^+$ T cells limit disease severity and delay the progression of disease (Rosendahl Huber et al., 2014). Early studies into HIV highlighted the importance of $CD8^+$ T cells in delaying the progression of HIV where a loss of $CD8^+$ T cells coincides with disease progression (Rinaldo et al., 1995). The ability to measure these T cell immune responses is therefore a key criterion in the evaluation of viral immunity. Detecting antigen-specific immune responses at a cellular level is carried out using the enzyme-linked immunosorbent assay (ELISA), enzyme-linked immunosorbent spot (ELISpot) assay, intracellular cytokine staining (ICS) or activation-induced marker (AIM) assays, which mostly examine T cell recall response in cryopreserved peripheral blood mononuclear cells (PBMCs) (Vardhana et al., 2022). In addition, interferon-γ release assays (IGRAs) which is based on the excretion of IFN- γ as an established T cell activation marker (Tan et al., 2021).

SARS-nCoV-2-specific $CD4^+$ T cells typically undergo differentiation into Th1 cell and T follicular helper (Tfh) cells. Th1 cells exhibit antiviral effects through the production of IFN-γ and other cytokines while Tfh cells play a role in providing support to B cells which are crucial for the development of nAb responses, formation of memory B cells and long-term humoral immunity (Meckiff et al., 2020). During acute SARS-nCoV-2 infection, circulating Tfh (cTfh) cells specific to SARS-nCoV-2 are generated and have been associated with reduced disease severity (Rydyznski Moderbacher et al., 2020). There is a wide knowledge gap in the understanding of SARS-nCoV-2-specific T cell responses under various conditions such as the immediate and long-term response to natural infection as well as the immediate and long-term response to vaccination or reinfection with multiple variants (Peng et al., 2020). Vaccine efficacy has been designed based on antibody responses although these responses do not last particularly long (Jarjour et al., 2021). Memory T cells, however, can exist for years which makes their durability important for long term immune protection. This has been demonstrated in patients who previously contracted SARS-CoV in the 2003 outbreak (Le Bert et al., 2020). These patients maintained memory T cell reactivity to the nucleocapsid protein of the virus for 17 years, reiterating the long-term durability of T cell responses (Le Bert et al., 2020).

1.2.4.1 The $CD8^+$ T cell response

The $CD8^+$ T-cell response, outlined in **Figure 1.3.**, plays a crucial role in the early control and clearance of respiratory viral infections (Karlsson et al., 2020). Initially, T-cells develop and mature in the thymus, after which they enter the bloodstream and are transferred to peripheral lymphoid organs (Kudlay et al., 2022). There is continuous circulation between both the lymphoid tissue and blood which occurs until a cell encounters its specific antigen through antigen-presenting cells (APCs) and is activated (Kudlay et al., 2022). T-cells which do not encounter a specific antigen are called naïve T-cells (Karlsson et al., 2020). The T-cells which are activated start to divide and form clones which may either become $CD4^+$ T helper cells or $CD8^+$ T killer cells (Kudlay et al., 2022). Following activation, $CD8^+$ T-cells can adopt a variety of mechanisms to eradicate infected cells. Firstly, $CD8^+$ T cells can identify and mediate the killing of infected cells by the secretion of cytotoxic molecules such as perforin and granzymes, an important function in the control of viral infections and reinfections (Demers et al., 2013, Gerritsen and Pandit, 2016, Graalmann et al., 2021). This response induces apoptosis in infected cells which reduces the potential for bystander cells to become infected (Karlsson et al., 2020). The second mechanism is through the release of interleukin-2 (IL-2), tumor necrosis factor-α (TNF- α) and interferon-γ (IFN- γ) which are cytokines that promote the phagocytic properties of macrophages and possess antimicrobial effects (Kudlay et al., 2022). Additionally, the process of infection may elicit pathogen-specific memory $CD8^+$ T cells which can recognize and kill cells long after the first incidence of infection (Gerritsen and Pandit, 2016).

Memory $CD8^+$ T cells are an antigen-specific and long-lived cell population which provide an enhanced protective response when re-encountering the same antigen. These cells can persist in the absence of antigen and respond consistently to stimulation, distinguishing them from the host's random reaction to a specific antigen (Farber et al., 2016, Gerritsen and Pandit, 2016). This consistent response offers an evolutionary advantage, reducing the likelihood of the host becoming ill upon re-encountering the same antigen. This trait is inherited through the germline, contributing to the host's ability to mount an effective immune defence when encountering familiar pathogens (Farber et al., 2016). It has been observed that SARS-CoV infection induced long-lasting, strong virus-specific T cells which were detectable for up to six years in patients who had recovered from mouse-adapted SARS-CoV (MA15) infection (Yang LiTao et al., 2006). Since memory B cell responses are generally short-lived in patients infected with SARS-CoV, the development of vaccines capable of conferring long-term memory $CD8^+$ T cells is highly desirable (Yang LiTao et al., 2006). Antigen-specific $CD8^+$ T cells can be classified intro three subpopulations: antigen-specific effector memory (T_{EM}), central memory (T_{CM}) and tissue-resident memory (T_{RM}) cells. These cells are able to mediate viral clearance from the infection site rapidly by secreting effector molecules which limit viral replication (Kohlmeier et al., 2010). These findings reiterate the importance of memory $CD8^+$ T cell responses in conferring long-term immune protection.

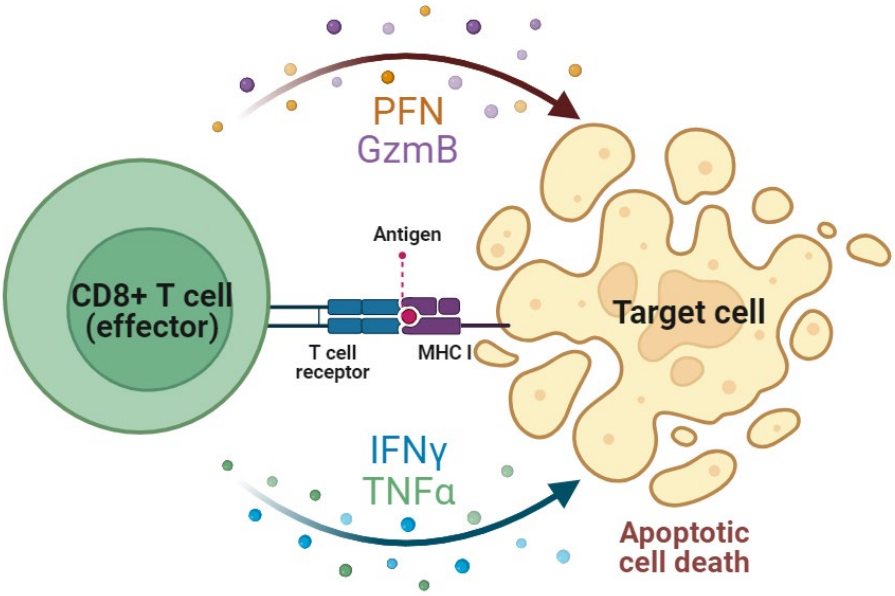

Figure 1.3.: Mechanism of $CD8^+$ T cell-mediated cytotoxicity showing interaction between MHC-I and TCR in the killing of a target cell (created in BioRender, adapted from Mistry et al. (2021))

1.2.4.2. T cell responses to SARS-nCoV-2 natural infection

Understanding immune memory after infection with SARS-nCoV-2 is an important consideration in pandemic management (Sette and Crotty, 2021). Immune memory can be generated by natural infection, vaccination or both (hybrid immunity). Dan et al. reported that the immune system's memory responses - including antibodies, $CD4^+$ T cells, $CD8^+$ T cells, and B cells - remained strong even eight months after infection (Dan et al., 2021). Around 95% of participants still had multiple measurable memory responses, including memory $CD4^+$ T cells. Interestingly, memory $CD4^+$ T cells were detectable in 93% of COVID-19 cases one month after infection, and remained at 92% even at six months post-infection (Dan et al., 2021). Memory $CD4^+$ T cells capable of identifying SARS-nCoV-2 exist in individuals who have not been exposed to the virus previously. Evidence for this comes from blood samples collected before the pandemic and it has been suggested that these cells are likely memory T cells from past infections with common cold coronaviruses (Grifoni et al., 2021, Sette and Crotty, 2021). It should be noted however that low pre-existing endemic human coronavirus (HCoV-NL63)-specific T cell frequencies are associated with impaired SARS-nCoV-2-specific T cell responses which has been observed in people living with HIV (Ng'uni et al., 2023). $CD8^+$ T cells produced in response to SARS-nCoV-2 infection mainly exhibit IFN-γ and granzyme B expression, alongside some levels of TNF and IL-24. After eight months from the infection, memory $CD8^+$ T cells with an effector memory (T_{EM}) and $CD45RA^+$ effector memory (T_{EMRA}) phenotype are more common, while there is a smaller proportion of cells with a central memory (T_{CM}) phenotype (Dan et al., 2021, Cohen et al., 2021).

1.2.4.3. T cell responses to SARS-nCoV-2 vaccination

An in-depth study of 400 South Africa healthcare workers (HCWs) was conducted with serial sampling since the first wave of SARS-nCoV-2 infections in mid-2020, which was dominated by the D614G variant (Keeton et al., 2021). Sixty HCWs who were vaccinated with the Janssen Ad26.COV2.S vaccine induced ancestral spike-specific $CD4^+$ and $CD8^+$ T cell responses in all groups (namely those who were never infected with SARS-nCoV-2 and those with PCR-confirmed infection during the first and second waves) and it was revealed that $CD8^+$ responses were present in fewer individuals prior to vaccination and did not differ significantly between all groups (Keeton et al., 2021). Further, a greater proportion of participants mounted a $CD4^+$ response compared to a $CD8^+$ response with polyfunctional profiles of vaccine responses showing $CD4^+$ T cells produced multiple cytokines at the same time while $CD8^+$ T cells produced mostly IFN-γ (Keeton et al., 2021). This study also assessed whether vaccine-induced T cells recognized Beta and Delta VOCs. The results concluded that overall robust $CD4^+$ and $CD8^+$ T cell responses are generated after vaccination, regardless of prior infection. $CD4^+$ T cells could identify Beta or Delta just as effectively as the original strain. Among 24 participants, the $CD8^+$ T cells targeting the S protein recognized Beta in 14 out of 15 responders. However, the average strength of the immune response, measured by cytokine levels, was significantly lower for Delta compared to Beta ($p=0.041$). In 15 $CD8^+$ responders, 53% experienced a two-fold or greater decrease in their response to Delta, with five individuals completely losing their ability to recognize Delta. Given that the Omicron VOC harbours considerably more mutations, the extent to which T cells can contribute to protection from SARS-nCoV-2 is of interest. Keeton et al. (2022) carried out a study assessing the ability of T cells to react to Omicron S protein in participants vaccinated with Ad26.COV2.S or BNT162b2 and unvaccinated patients. It was observed 70% of $CD4^+$ and 80% of $CD8^+$ T cell responses were maintained across the study groups. In addition, the magnitude of these cross-reactive T cells was similar for Beta and Delta VOCs (Keeton et al., 2022). This led to the conclusion that despite its observed susceptibility to nAbs, most vaccine or infection-induced T cell responses cross-recognize Omicron (Keeton et al., 2022).

1.2.4.4. T cell responses to SARS-nCoV-2 infection and vaccination in PLWH

Human Immunodeficiency Virus (HIV) primarily targets $CD4^+$ T cells (Deeks et al., 2015). During the acute phase of HIV infection, there is a substantial drop in $CD4^+$ T helper cells, while in the chronic phase a continuous decrease in the $CD4^+$ count leads to the onset of acquired immunodeficiency syndrome (AIDS) (Peng et al., 2020). Although antiretroviral therapy (ART) suppresses HIV infection, systemic immune activation may persist years after being on an ART regimen and result in low $CD4^+/CD8^+$ ratios (Peng et al., 2020). Significantly lower nAb responses have been observed in PLWH at one to three months after mRNA vaccination (Schmidt et al., 2022, Spinelli et al., 2022). Because vaccine-induced nAbs have been primed to the ancestral S protein in first-generation vaccines, it is

important to consider how well they are able to neutralize VOCs. No significant differences have been observed between PLWH and controls when evaluating BNT162b2 mRNA vaccine-elicited antibody neutralization against the Alpha, Beta and Gamma VOCs (Woldemeskel et al., 2022) as well as adenovirus-vectored vaccine responses (Pourcher et al., 2022).

Following natural infection by SARS-nCoV-2, people living with HIV (PLWH) experience blunted immunity to the virus which in turn creates a favourable environment for the hypermutation of SARS-nCoV-2 (Young, 2022). Nkosi et al. (2022) has described a cohort in South Africa infected with SARS-nCoV-2 during the first infection waves. This study observed that individuals with HIV viraemia showed significantly reduced $CD4^+$ T cell and $CD8^+$ T cell responses, as well as altered cytokine production profiles, when compared with people living without HIV (PLWoH) or PLWH with healthy $CD4^+$ T cell counts (Nkosi et al., 2022). Among PLWoH, those who were infected in the first wave produced T cells recognizing Beta spike peptides, while second-wave participants responded to wildtype spike peptides. The observed cross-reactivity was absent in HIV-viraemic individuals and was reduced in HIV-suppressed individuals (Nkosi et al., 2022). This diminished cross-reactivity may be linked to deficiencies in memory B cell responses, reduced B and T cell repertoires and HIV-induced modulation of B cell maturation pathways in the same cohort following SARS-nCoV-2 infection (Turner et al., 2021, Krause et al., 2022). In addition, there is evidence that nAbs play a role in clearing SARS-nCoV-2 and are necessary for such clearance during recovery from HIV-induced immunosuppression. Although SARS-nCoV-2 can develop significant resistance to neutralization during prolonged infection in advanced HIV cases, existing population immunity poses a challenge to viruses that have evolved in this way (Karim et al., 2024).

SARS-nCoV-2-specific T cell responses after vaccination vary depending on the individual's immunological status, the vaccine type and time interval following completion of a vaccination series (Höft et al., 2024). In studies using three types of vaccines (mRNA, viral-vectored, and inactivated), no notable disparities in spike-specific IFN-γ production were observed between 2 weeks and 6 months after completing the primary vaccination (Oyaert et al., 2022, Woldemeskel et al., 2022, Frater et al., 2021, Feng et al., 2022). These studies utilized various assays such as flow cytometry, ELISpot, and IGRAs to assess T-cell responses. Despite finding no significant differences in the magnitude of T-cell responses, the proportion of PLWH who developed a T-cell response varied based on the immunological status of the cohort. Studies with participants having a median $CD4^+$ count between 600–900 cells/mm^3 showed a similar frequency of responders between PWH and controls (Woldemeskel et al., 2022, Frater et al., 2021, Feng et al., 2022). However, a study involving PLWH with a median $CD4^+$ count of 254 cells/mm^3 reported that 32% had no T-cell response, while only 12% of the control group failed to mount a response at all. It can therefore be said that although the magnitude of T-cell responses did not significantly differ between PLWH and PLWoH in these studies, the ability to mount a T-cell response was associated with a higher $CD4^+$ count. In addition, T cells generated by

the ChAdOx1 vaccination showed robust cross-reactivity against the Beta, Gamma and Delta VOCs in PLWH (Ogbe et al., 2022).

Developing an assay to measure $CD8^+$ T cell cytotoxicity to SARS-nCoV-2 infected cells can contribute to determining the T cell repertoire against COVID-19 and whether PLWH can successfully produce a cytotoxic $CD8^+$ response. This study aims to provide an optimized $CD8^+$ T cell pseudovirus killing assay which may be used to accurately measure the responses of T cells following infection with SARS-nCoV-2. The development of a high-throughput SARS-nCoV-2 $CD8^+$ T cell pseudovirus-based killing assay is important for vaccine development and immune-based therapeutics. However, detailed optimized protocols and reagents to carry out these assays are not yet commercially available to the wider scientific community (Crawford et al., 2020). Furthermore, this study may assist in mitigating the need for biosafety-level-3 or higher facilities to carry out virus work, allowing this type of research to be more accessible to research scientists (Yu et al., 2021). A problem related to carrying out this type of research is that SARS-nCoV-2 is a biosafety level 3 agent, therefore using live virus is not always feasible as it requires specialized training, equipment and facilities (Crawford et al., 2020). A solution to this problem would be to use a spiked pseudo lentivirus which can be modified/engineered to express a fluorescence reporter.

1.3. Measuring T cell responses

1.3.1. Methods to detect and quantify antigen-specific CD8$^+$ T cell responses

As previously highlighted, the ability to quantify these responses, particularly CD8$^+$ T cell responses, is an important requirement in evaluating the functioning of T cells and a variety of assays may be employed to track cellular immunity. The enzyme-linked immunospot (ELISpot) assay is designed to quantify antigen-specific T cells at a single cell resolution (Cox et al., 2006). In this assay, cells are stimulated and incubated on a plate coated with immobilized anti-cytokine antibodies. Cells recognizing the antigen release cytokines, which are captured locally by coating antibodies. Detection is achieved through incubation with a secondary antibody (Cox et al., 2006). A colorimetric assay then shows individually bound spots, each representing a distinct antigen-specific T cell (Cox et al., 2006). ELISpots are highly sensitive although the need for PBMC isolation which requires freezing and thawing procedures may affect cell viability after cryopreservation (Mallone et al., 2011). Enzyme-linked immunosorbent assays (ELISAs) rely on plates coated with "capture" antibodies which attach to certain cytokines and enable the quantification of their concentration in the sera of infected individuals or PBMCs stimulated with antigen-specific peptides (Schwarz et al., 2022). Both ELISAs and ELISpots are simple and cost-effective to perform, although their sensitivity in relation to other techniques is lower (Schwarz et al., 2022, Petrone et al., 2023).

Flow cytometry has been used extensively in formulating a better understanding of the behaviour of T cell subsets. In essence, flow cytometry characterizes individual cells based on proliferation and surface or intracellular markers that are stained by antibodies and is commonly performed on PBMCs (Schwarz et al., 2022). Flow cytometry can pinpoint the exact cell types secreting certain molecules and offers great resolution, unlike ELISAs which measure total cytokine concentration (Dan et al., 2016). The most common flow-based experiments which evaluate antigen-specific T cells are surface marker staining, which characterizes extracellular proteins, and intracellular cytokine staining (ICS), which characterizes intracellular proteins (Schwarz et al., 2022). When there is minimal differential cytokine expression, activation-induced marker (AIM) assays are more reliable in quantifying antigen-specific cells based on experimentally determined proteins which are upregulated in response to antigen recognition (Dan et al., 2016). It should be noted, however, that both ICS and AIM assays require costly equipment and reagents as well as a level of specialist training to ensure correct characterization of cytokines and surface antigen markers (Vardhana et al., 2022). Interferon gamma release assays (IGRAs) have been used in the detection *Mycobacterium tuberculosis* infection and have now been widely used in studies of COVID-19 patients of various clinical cohorts (Jaganathan et al., 2021, Vardhana et al., 2022). Assessing T-cell responses in whole blood by IGRAs is a simple and quick procedure, offering the additional benefit of closely resembling *in vivo* conditions compared to testing purified PBMCs (Tormo et al., 2022). However, this method may not precisely capture the complex

nature of overall immunity, which includes humoral immunity and the involvement of memory B-cells (Sette and Crotty, 2021, Tormo et al., 2022).

1.3.2. Types of killing assays

To elucidate the efficacy of the $CD8^+$ T cell response against pathogens, killing assays have been employed which measure the level of specific killing and therefore the quality of cytotoxic $CD8^+$ T cell responses. These assays assess the ability of an effector cell or molecule to kill a target during a defined period of co-culture where different ratios of effectors to targets can be compared. The chromium release killing assay, which involves labelling target cells with radioactive chromium and quantifying the amount of radioactivity released into the culture medium after the addition of effector cells, has been used for measuring virus-specific T cell-mediated cytotoxicity (Brunner et al., 1968, Scheibenbogen et al., 2000, Kiesgen et al., 2021). The standard assay is limited to a single timepoint only as it measures the release of chromium after 4 h of target and effector cell co-incubation which may exclude the assessment of killing of more resistant target cell types that may require a longer time to be killed (Kiesgen et al., 2021). Moreover, the additional costs involved in the disposal of radioactive waste as well as the requirement of a gamma counter, an expensive instrument, must be considered (Karimi et al., 2014). Lastly, the radioactive nature of this assay, and therefore its potential harm to the health of the researcher, is a safety concern (Gourdain et al., 2013, Karimi et al., 2014, Kiesgen et al., 2021). For these reasons, researchers have developed novel killing assay designs involving labelling cells with non-radioactive fluorescent dyes which provide a safer alternative to the chromium release assay.

A real-time killing assay has been described which assessed cytotoxicity of natural killer (NK) cells and is also suitable for antigen-specific cytotoxic T cells (Fassy et al., 2017). Here, target cells were loaded with cell-permeable calcein-AM dye and the labelled cells were washed and co-incubated with increasing numbers of cytotoxic NK cells. Natural killer cell-mediated cytotoxicity was measured by quantifying the number of fluorescent target cells in each well every 15 min over the course of 4 h using a Cytation 5 cell imaging multimode plate reader. This assay accurately monitors the lysis of target cells over time, as opposed to flow cytometry assays which only detects target cells undergoing apoptosis (Fassy et al., 2017). The killing kinetics of NK cells have also been measured by a similar real-time killing assay described by Kummerow et al. (2014) in comparison to two standard cytotoxicity assays, the lactate dehydrogenase (LDH) release assay and propidium iodide (PI) uptake assay (Kummerow et al., 2014). It was observed that the real-time killing assay was more sensitive compared to the LDH release assay although similar readings were noted for the PI uptake assay (Kummerow et al., 2014).

The fluorescent antigen-transfect target cell – CTL (FATT-CTL) assay measured antigen-specific cytotoxicity *ex vivo* (van Baalen et al., 2005). Target cells were generated using nucleofection with

DNA vectors encoding antigen – green fluorescent protein (GFP) proteins. Viable and dead GFP-positive cells were quantified by flow cytometry following co-culture at various effector-to-target (E:T) cell ratios with the calculation of antigen-specific target cell elimination (van Baalen et al., 2005). This assay was validated using influenza and human immunodeficiency virus (HIV)-specific CTL clones and demonstrated cytotoxicity at lower E:T cell ratios than the chromium release assay (van Baalen et al., 2005). A luciferase based viral inhibition assay (VIA) has been previously outlined by Naarding et al (2014) with the purpose of evaluating vaccine induced $CD8^+$ T-cell responses. In this assay, a replication-competent infectious molecular clone (IMC) which expresses a novel luciferase reporter (LucR), and the full-length strain-specific genome of the founder HIV-1, CH077.t, was used (Naarding et al., 2014). The application of CH077.t- LucR allowed for the comparison of VIA responses against all viral genes, thereby enabling a wider comparison of $CD8^+$ T-cell responses between different samples tested (Naarding et al., 2014). Furthermore, the development of this VIA provided a more rapid, cost-effective, and less labour-intensive luciferase readout.

A novel fluorescence target array (FTA) killing assay utilises three fluorescent dyes, carboxyfluorescein diacetate succinimidyl ester (CFSE), CellTrace Violet, and cell proliferation dye with different fluorescence emission spectra which have shown low fluorescence variability and low cell cytotoxicity (Quah et al., 2012). Flow cytometry assays are limited to typically two to seven distinguishable target cell populations, but this assay opens the possibility of potentially hundreds of different target cell populations. The FTA killing assay is a highly sensitive technique which is able to detect quantitative and qualitative differences in polyclonal CTL responses, including minor CTL subsets. This assay has great potential as a tool to evaluate the functional capacity of CTLs, following vaccination (Quah et al., 2012). A similar multiplexing approach has also been adopted by Poh et al. (2020) for a cytotoxicity assay that allows direct measurement of up to 23 different specificities of epitope-specific $C8^+$ T cells in a single reaction. This assay can further validate the epitope candidates in terms of cytotoxic potential of the cognate $CD8^+$ T cells (Poh et al., 2020).

Fluorescence-based assays are undoubtedly a valuable tool in the evaluation of the dynamics of the immune response. This study aims to optimize a fluorescence-based assay which would allow for the evaluation of cytotoxic $CD8^+$ T cell responses elicited by SARS-nCoV-2 infection or vaccination. In optimizing the fluorescence-based assay, two distinct approaches will be tested: a pseudovirus-based assay utilizing fluorescence reporter genes that are incorporated into the pseudovirus design, and a cell labelling method using fluorescent dye, carboxyfluorescein succinimidyl ester (CFSE). The pseudovirus-based assay uses reporter genes to measure the extent of target cell infection and subsequent killing by $CD8^+$ T cells. On the other hand, the CFSE-based assay allows for the distinction between cells which are antigen-specific and those which are not, and therefore the analysis of cell populations and antigen-specific killing efficiency. Using these two approaches, the study aims to establish a fluorescence-based assay for the evaluation of $CD8^+$ T cell-mediated cytotoxicity, thereby

enhancing the understanding of immune responses to SARS-nCoV-2 and informing the development of effective immunotherapies and vaccines.

Hypothesis:

Upon developing an assay to measure cytotoxic $CD8^+$ T cell responses to SARS-nCoV-2 infection or vaccination, it is hypothesized that the cytotoxic $CD8^+$ T cell responses in people living with HIV (PLWH) will be poorer compared to people living without HIV (PLWoH), given that PLWH experience dysfunctional immunity to the virus.

Aim:

To develop a fluorescence-based killing assay for evaluating SARS-nCoV-2-specific cytotoxic $CD8^+$ T cell responses elicited by SARS-nCoV-2 infection or vaccination.

Objectives:

1. To develop and optimize a pseudovirus-based assay to accurately measure target cell infection and subsequent killing by $CD8^+$ T cells isolated from individuals naturally infected with or vaccinated against SARS-nCoV-2.
2. To optimize the cell labelling method using carboxyfluorescein succinimidyl ester (CFSE) for distinguishing between peptide-presenting and non-peptide-presenting cells, enabling the analysis of antigen-specific killing efficiency by $CD8^+$ T cells from individuals naturally infected with or vaccinated against SARS-nCoV-2.

CHAPTER 2: A PSEUDOVIRUS-BASED KILLING ASSAY TO MEASURE T CELL RESPONSES TO SARS-nCoV-2

2.1. Introduction

Cytotoxic $CD8^+$ T cells play an integral role in the immune defence against viral infections. These cells effectively eliminate viral-infected cells through recognition of viral peptides presented on major histocompatibility complex (MHC) class I molecules on the surface of infected cells (Almendro-Vázquez et al., 2023). The T cell receptor (TCR) on $CD8^+$ T cells specifically binds to this complex, initiating the activation of cytotoxic T cells. Once activated, the $CD8^+$ T cells can kill the infected cells and aid in clearing the infection (Almendro-Vázquez et al., 2023). Memory $CD8^+$ T cells are a critical component of protective adaptive immunity against viral infections which is why understanding its development aids in the design of optimal vaccines (Wherry and Ahmed, 2004). Furthermore, improved understanding of the role of $CD8^+$ T cell response to SARS-nCoV-2 can inform the development of novel COVID-19 vaccines and therapeutics. In South Africa, where the prevalence of human immunodeficiency virus (HIV) is high, it is also of interest to determine how the efficacy of cytotoxic $CD8^+$ T cells is affected in people living with HIV (PLWH) or whether PLWH are able to mount a robust cytotoxic $CD8^+$ T cell response. For this reason, measuring this response by means of observing the depletion of SARS-nCoV-2-infected cells by $CD8^+$ T cells may assist in elucidating the $CD8^+$ T cell response in patients co-infected with HIV and SARS-nCoV-2. Studies of live SARS-nCoV-2 are restricted to biosafety level 3 laboratories which require specialized equipment, training and facilities (Li et al., 2018). By definition, a pseudovirus is a recombinant viral particle which derives its backbone and envelope proteins from different viruses (Li et al., 2018). Pseudoviruses are comprised of the crucial components required for viral infection, namely the envelope proteins from the virus of interest and an inner core, however native surface protein genes are absent in pseudoviruses and are therefore co-transfected with a plasmid which can express the desired surface proteins. This recombinant pseudovirus can then infect multiple host cells but it lacks the ability to self-replicate for more than a single round (Ory, 1996). For this reason, pseudoviruses are a safer and effective tool as an alternative to wildtype viruses for use in biosafety level 2 research laboratories (Sanders, 2002, Yu et al., 2021).

2.1.1. Types of pseudovirus designs

There are several designs and packaging systems that have been adopted to construct SARS-nCoV-2 pseudoviruses.

2.1.1.1.. HIV-1-based lentiviral packaging system

Lentiviral pseudoviruses are often used in the study of viral entry mechanisms and the delivery of genes (Chen and Zhang, 2021). Lentiviral vectors are able to retain the genetic sequences necessary for viral transcription, packaging and integration, however, they do not possess the genetic sequences which encode the HIV envelope proteins (Li et al., 2018, Donofrio et al., 2021). The HIV-1 packaging system is the most widely adopted pseudovirus packaging system, owing to its versatility and safety (Wang et al., 2023b). The HIV genome contains structural genes (Gag, Pol and Env), regulatory genes (Tat, Rev, Nef) and helper genes such as Vif (viral infectivity factor), Vpr (viral protein R), Vpu (viral protein U) and Vpx (viral protein X) which are cloned into either 2, 3 or 4 DNA expression vectors (Xiang et al., 2022). The structural genes, namely Gag, Pol and Env, play important roles at various stages of the viral life cycle. Gag (group-specific antigen) encodes proteins which are essential for the assembly and release of new HIV viral particles (Murphy and Saad, 2020). Pol (polymerase) encodes enzymes required for the replication of the viral genome and processing of viral proteins while Env (envelope) encodes the viral glycoproteins which are crucial for HIV to enter host cells and initiate infection (Hill et al., 2005, Murphy and Saad, 2020). Regulatory genes encoded by the HIV genome include Tat (trans-activator of transcription) which controls HIV gene expression, Rev (regulator of virion expression) which facilitates the export of unspliced or partially spliced viral RNA from the nucleus to the cytoplasm of infected cells and Nef (negative factor) which plays several roles including enhancing the infectivity of HIV by downregulating cell surface expression of major histocompatibility complex class I (MHC-I) molecules, which are involved in presenting viral antigens to cytotoxic T cells (Ali et al., 2021, Sintya et al., 2021, Xiang et al., 2022).

Crawford et al. (2020) has described a multi-vector lentiviral pseudovirus design incorporating three helper plasmids expressing HIV Gag-Pol (HDM-Hgpm2), HIV Tat (HDM-tat1b) and HIV Rev (pRC-CMV-Rev1b) all under a cytomegalovirus (CMV) promoter. The CMV promoter drives the expression of genes in a variety of cell types and the helper plasmids encoding Gag-Pol, Tat and Rev are necessary as these are HIV proteins required for effective virion assembly (Nie et al., 2017, Li et al., 2018, Chen and Zhang, 2021). Without the elements required for HIV to replicate, the pseudovirus can enter cells and deliver its genetic material without the ability to produce new viruses thereby making it safe for use in biosafety level 2 facilities. In addition, a plasmid expressing codon-optimized S protein from the SARS-nCoV-2 Wuhan-Hu-1 strain under a CMV promoter (HDM-IDTSpike-fixK), as well as a lentiviral backbone plasmid utilizing a CMV promoter to express ZsGreen, a green fluorescent protein (GFP) variant, were included in the construction of this multi-vector pseudovirus. Using codon-

optimized SARS-nCoV-2 S protein ensures its efficient expression in human cells while the inclusion of a plasmid expressing a fluorescent protein allows for the tracking and quantification of infection throughout pseudovirus-based assays (Crawford et al., 2020, Xiang et al., 2022). In the construction of an in-house multi-vector pseudovirus, a similar pseudotyping approach used by Crawford et al. (2020) was adopted with the use of identical spike-expressing and helper plasmids. However, the lentiviral backbone plasmid used did not express ZsGreen, but rather mCherry, a red fluorescent protein.

The objective of the pseudovirus strategy is to minimize recombination of the viral genes, thereby reducing the chances of reversion to the original wildtype virus. Generally, two or three plasmids are co-transfected into a cell line, usually human embryonic kidney or HEK293T cells which are a transfectable derivative of human embryonic kidney 293 cells, to produce the desired pseudoviruses (Iuchi et al., 2020). The two-vector packaging system includes a plasmid expressing the SARS-nCoV-2 S protein and an HIV-1 backbone plasmid expressing the necessary packaging proteins and signals but with the envelope gene eliminated (Chen and Zhang, 2021). Several studies have utilized this design incorporating different SARS-nCoV-2 S expression vectors of interest with HIV-1 lentiviral backbones, such as pNL4-3.Luc.R-E which contains the firefly luciferase reporter gene, as well the mCherry reporter gene (He et al., 2020, Yang et al., 2020b, Keeton et al., 2021, Izac et al., 2023). mCherry is a red fluorescent protein with an excitation peak at 587 nm and an emission peak at 610 nm (Vadakkan et al., 2009). The SARS-nCoV-2 multi-vector packaging system is comprised of a separate transfer plasmid containing a reporter gene, a packaging plasmid and SARS-nCoV-2 S protein-expressing plasmid, as opposed to a single HIV-1 backbone plasmid expressing packaging and transfer proteins together (Chen and Zhang, 2021). Crawford et al. (2020) has described a multi-vector pseudovirus design comprised of a lentiviral backbone plasmid which encodes a fluorescence reporter gene, ZsGreen which has an excitation peak at 492 nm and an emission peak at 506 nm, a plasmid expressing the SARS-nCoV-2 S protein and separate plasmids encoding non-surface packaging proteins necessary for lentivirus production (Tat, Gag-Pol and Rev). The general approach for lentiviral pseudotyping is outlined in **Figure 2.1**.

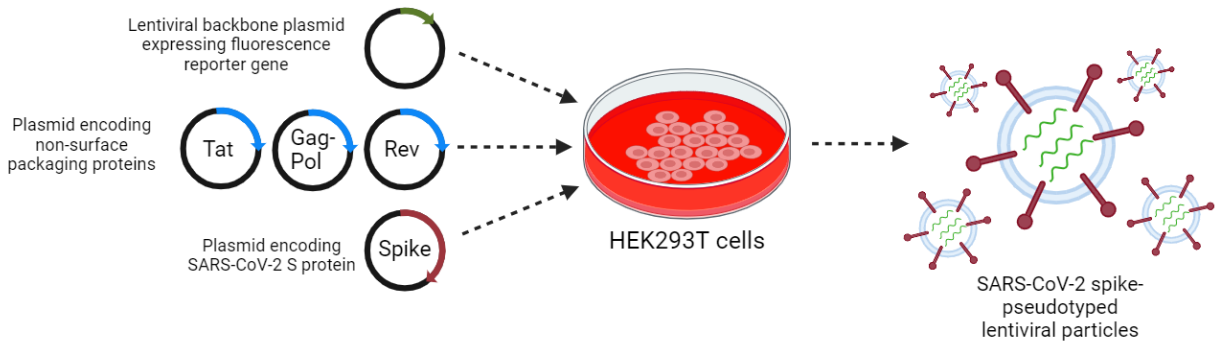

Figure 2.1.: General approach for multi-vector lentiviral pseudotyping (Made in BioRender, adapted from Crawford et al. (2020)).

2.1.1.2. VSV-based packaging system

Vesicular stomatitis virus (VSV) is a singled strand RNA (ssRNA) virus is capable of infecting a wide variety of animal cells (Xiang et al., 2022). As opposed to lentiviruses which utilize an HIV backbone, VSV possesses an envelope glycoprotein (G) which mediates its entry and it has been observed that G-deleted VSV can be complemented *in trans* with envelope glycoproteins of unrelated viruses, such as coronaviruses (Fukushi et al., 2008). The binding between glycoproteins from vesiculovirus and receptors directs the VSV-receptor complex to cellular compartments where viral fusion takes place. It has been established that the low-density lipoprotein receptor and its associated family members serve as the cellular receptors which mediate VSV's entry into cells (Munis et al., 2020). The VSV packaging system was first used to produce pseudotypes of Ebola virus (Takada et al., 1997) and has since been used in numerous viral entry studies for a variety of viruses including measles virus, leukaemia virus and hepatitis B (Tatsuo et al., 2000, Okuma et al., 2001, Saha et al., 2005). This packaging system was also used to produce SARS-CoV pseudotyped viruses due to its ability to generate high titre pseudoviruses in several different cell lines such as A549 cells, Calu cells and Vero E6 cells (Fukushi et al., 2008).

Fukushi et al. (2008) describes the protocol to develop these SARS-CoV pseudoviruses whereby 293T cells were plated onto type I collagen-coated T-75 flasks and transfected with a SARS-CoV spike protein plasmid. After incubation, the cells were inoculated with VSV pseudotypes expressing GFP. Culture supernatants containing VSV pseudotypes bearing the SARS-CoV S protein were collected, centrifuged, and filtered before storage at –80°C (Fukushi et al., 2008). Furthermore, the VSV system allows for the generation of pseudoviruses with efficient infectivity making them beneficial tools in the study of viral entry and in the development of vaccines (Xiang et al., 2022). A pseudotyped VSV bearing the full-length S protein of SARS-nCoV-2 was used in the development of a pseudovirus neutralization assay (Nie et al., 2020a). This involved infecting spike-transfected HEK293T cells with VSV*ΔG (VSV without envelope glycoprotein (G)) encoding firefly luciferase, depicted in **Figure 2.2**. After an incubation period of 1h at 37 ℃, the inoculum was removed and the cells were washed with PBS before adding medium supplemented with anti VSV-G antibody to neutralize residual input virus and prevent false-positive results (Chen and Zhang, 2021). Spike-pseudotyped particles were harvested 20 h postinoculation and were able to infect cells expressing the ACE2 receptor – infection was determined by fluorescence of the Fluc reporter gene. VSV-based pseudoviruses have therefore been invaluable in the development of neutralization assays to evaluate antibody responses to SARS-nCoV-2.

Crawford et al. (2020) has described a protocol in which VSV-G pseudotyped lentiviruses packaging the human ACE2 (hACE2) receptor were generated by co-transfection of 293T cells, a transfectable derivative of human embryonic kidney 293 cells, with pHAGE2-EF1aInt-ACE2-WT, a plasmid containing the ACE2 gene under the control of the EF1a promoter within a lentiviral vector backbone,

and lentiviral helper plasmids. The resulting lentivirus was used to infect more 293T cells and the transduced cells were sorted based on ACE2 expression using specific antibodies. Single cell clones showing a high expression of ACE2 were identified via flow cytometry and expanded, resulting in the establishment of a cell line denoted 293T-ACE2 (Crawford et al., 2020). Similarly, Khan et al. (2022) used VSV-G pseudotyped lentivirus containing hACE2 to infect H1299 cells, a lung carcinoma cell line. The transduced H1299 cells were subcloned in conditioned media over three weeks and the clones were assessed for mCherry expression upon infection with a SARS-nCoV-2 mCherry-expressing spike pseudotyped lentiviral vector using microscopy. The clone with the highest fraction of mCherry-positive cells was selected and expanded from the stock plate, denoted H1299-E3 (Khan et al., 2022).

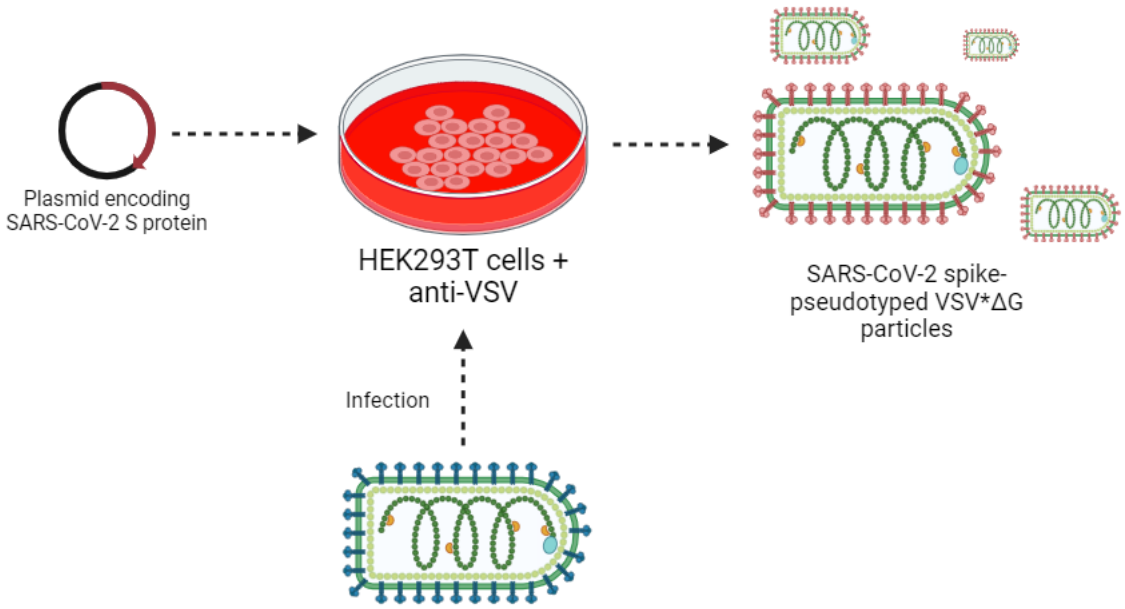

Figure 2.2.: Method for constructing SARS-nCoV-2 spike-pseudotyped VSV particles (made in BioRender, adapted from Chen and Zhang (2021)).

2.1.1.3. MLV-based packaging system

Murine leukaemia virus (MLV) is an enveloped retrovirus containing positive-strand RNA bearing three genes (Gag, Pol and Env) that encode viral capsid proteins, enzymes and envelope proteins, respectively (Chen and Zhang, 2021). Bartosch et al. (2003) has previously described a three-plasmid pseudovirus design strategy for evaluating hepatitis C viral entry comprising a transfer plasmid encoding a luciferase reporter gene, a plasmid encoding the desired envelope glycoprotein and a packaging plasmid expressing Gag and Pol but lacking the Env-coding gene (Bartosch et al., 2003). A similar design has been used to construct SARS-CoV- 2 pseudoviruses in which an MLV Gag-Pol packaging plasmid, a SARS-nCoV-2-specific S protein-encoding plasmid and a transfer plasmid encoding a luciferase reporter gene were co-transfected, as depicted in **Figure 2.3**. (Walls et al., 2020).

Zheng et al. (2021) have also used this design to generate SARS-nCoV-2 pseudoviruses for easy and rapid measurement of nAb titres in serum or plasma of COVID-19 patients (Zheng et al., 2021).

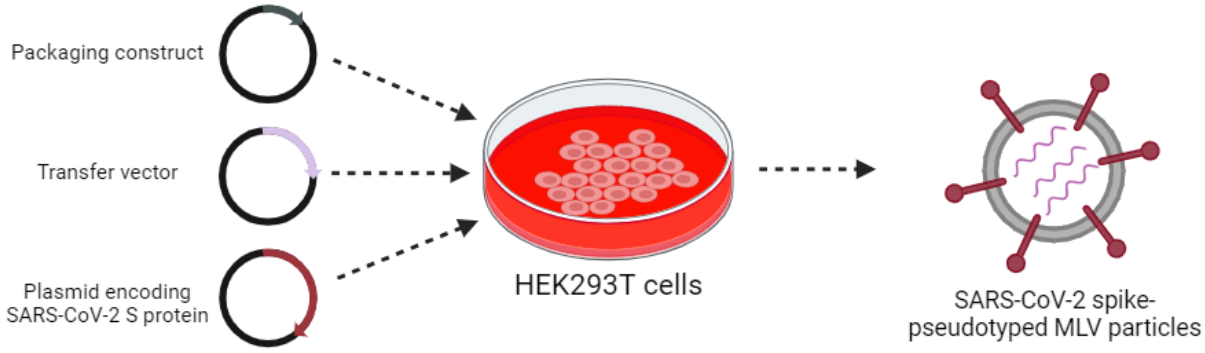

Figure 2.3.: General method for constructing SARS-nCoV-2 spike-pseudotyped MLV particles (made by BioRender, adapted from Chen and Zhang (2021)).

2.1.1.4. Pseudovirus applications

Chen et al. (2018) has described the development of an HIV-1 pseudovirus neutralization assay that utilizes the A3R5 human $CD4^+$ lymphoblastoid cell line. The study focused on optimizing various parameters such as cell counts, infection time and virus dose to enhance the efficiency of the pseudovirus production system (Chen et al., 2018). The A3R5 pseudovirus assay demonstrated significantly higher sensitivity in detecting the inhibitory effects of both monoclonal nAbs and plasma samples against tier 1 and tier 2 virus strains when compared to a standard fluorescence assay (Chen et al., 2018). In another study by Mavhandu et al. (2020), HIV-1 subtype C pseudoviruses with a luciferase reporter were used to test the inhibitory effects of selected plant substances and reverse transcriptase (RT) inhibitors Zidovudine (AZT) and nevirapine (NVP) in 293T cell transfections. While AZT and NVP effectively inhibited wildtype pseudoviruses in a dose-dependent manner, pseudoviruses with RT resistance mutations showed limited suppression (Mavhandu et al., 2020). Notably, catechin from *Peltophorum africanum* and a methanol extract from *Elaeodendron transvaalense* demonstrated potent inhibition of HIV-1-C and HIV-1-B pseudoviruses, suggesting the assay's potential for identifying novel RT inhibitors. Heyndrickx et al. (2008) has described an assay in which five replication-competent HIV-1 isolates and corresponding Env pseudoviruses were generated by co-transfecting HEK293T cells with specific plasmids. Primary PBMCs from a single donor and GFP-transduced human osteosarcoma cells (Ghost) cells expressing $CD4^+$ and either chemokine receptor 5 (CCR5) or chemokine receptor 4 (CXCR4) were used as target cells. Pseudoviruses were pre-incubated with different antiviral compounds and added to the Ghost cells or PBMCs, with infection levels measured via luciferase activity. Replication-competent viruses were similarly tested in PBMCs, with HIV p24 antigen levels measured after seven days (Heyndrickx et al., 2008). It was observed that the pseudovirus

stocks showed higher infectivity in Ghost cells compared to the PBMCs, although both pseudovirus assays (in Ghost and PBMCs) were more sensitive compared to the replication-competent virus PBMC assay, indicated by dose responses curves (Heyndrickx et al., 2008). This assay confirmed that pseudovirus-based assays are useful to evaluate antiviral infectivity.

2.1.2. Applications of SARS-nCoV-2 pseudoviruses

In conducting *in vitro* studies on the interactions between viruses and host cells, pseudoviruses have previously been employed (Steffen and Simmons, 2016). More recently, SARS-nCoV-2 pseudoviruses were used to demonstrate that SARS-nCoV-2 infection is dependent on angiotensin-converting enzyme 2 (ACE2) and transmembrane protease, serine 2 (TMPRSS2) (Hoffmann et al., 2020). Here, both SARS-nCoV-2 and SARS-CoV spike proteins were incorporated into VSV particles (Hoffmann et al., 2020). Using a panel of well-characterized cell lines of both human and animal origin (including A549, Calu-3 and H1299), it was tested which cells were susceptible to SARS-nCoV-2 spike-driven entry. All cell lines tested were susceptible to entry by the recombinant SARS-CoV or SARS-nCoV-2 -VSV pseudovirus particle, suggesting similar entry receptors between SARS-CoV and SARS-nCoV-2 (Hoffmann et al., 2020). In addition, a lentiviral packaging system was used to determine cell susceptibility, virus receptor and entry pathways for SARS-nCoV-2 (Ou et al., 2020). The lentiviral packaging system was also used to construct SARS-nCoV-2 pseudoviruses to demonstrate that human monoclonal antibodies (mAbs) block SARS-nCoV-2 S protein to the ACE2 receptor, which is an important approach for understanding alternative methods for COVID-19 prevention and treatment (Chen et al., 2020a). It was observed that three monoclonal antibodies (mAbs) were neutralized by the luciferase-encoding SARS-nCoV-2 pseudotyped lentiviral as the percentage infection showed a decrease when mAb concentration was increased (Chen et al., 2020a). A spiked SARS-nCoV-2 pseudovirus has been used to establish an *in vitro* model to study the effect of SARS-nCoV-2 infection on the human brain (Yi et al., 2020). This study revealed that mature neurons in the brain express ACE2 at the soma and are susceptible to viral entry by the spike-pseudotyped SARS-nCoV-2 (Yi et al., 2020).

Antibody neutralization assays targeting the S protein on SARS-nCoV-2 pseudoviruses have been widely investigated (Nie et al., 2020b, Yang et al., 2020b, Zettl et al., 2020, Cele et al., 2021, Donofrio et al., 2021, Keeton et al., 2021, Izac et al., 2023). It has been reported that pseudovirus-based neutralization assays have showed good correlation with live virus-based assays in addition to being relatively high throughput and requiring less sample serum (Bentley et al., 2015). Pseudotyped lentiviral particles were constructed and used to measure the neutralizing activity of human sera or plasma against SARS-nCoV-2 which provided a useful complement to enzyme-linked immunosorbent assays (ELISAs) (Crawford et al., 2020). Zettl et al. (2020) conducted a study using a VSV-based SARS-nCoV-2 pseudovirus to assess nAb levels in individuals recovering from mild to moderate COVID-19.

SARS-nCoV-2 spike-pseudotyped VSV*ΔG(FLuc) was incubated with serial dilutions of serum from convalescent COVID-19 patients with the pseudotype infection rate being determined by measuring the FLuc reporter activity 18 h post-infection and it was found that the majority of patients had low levels of nAbs (Zettl et al., 2020). Nie et al. also investigated nAbs against SARS-nCoV-2 using a VSV pseudovirus packaging system. Keeton et al. (2021) performed a neutralization assay by preparing SARS-nCoV-2 pseudotyped lentiviruses via transfection with either the ancestral SARS-nCoV-2 spike variant (D614G), the Beta spike or Delta spike plasmids and a firefly luciferase-encoding lentiviral backbone plasmid (Keeton et al., 2021). Here, plasma samples from vaccine recipients were incubated with the SARS-nCoV-2 pseudotyped lentiviruses after which HEK293T cells engineered to overexpress the ACE2 receptor were added (Keeton et al., 2021). The luminescence of the luciferase reporter gene was measured and it was observed that in two groups who had prior SARS-nCoV-2 infection, there was a significant boost in neutralization after vaccination against D614G and Beta variants (Keeton et al., 2021). A notable study carried out by Garcia-Beltran et al. (2021) evaluated the potency of sera from 99 individuals who received either one or two doses of BNT162b2 or mRNA-1273 vaccines by constructing different pseudoviruses containing the S protein of 10 circulating SARS-nCoV-2 strains. The study reported that 5 out of 10 pseudoviruses harbouring mutations in the receptor binding domain (RBD) were resistant to neutralization (Garcia-Beltran et al., 2021).

Pseudoviruses have been employed to evaluate the potency of COVID-19 vaccines in both preclinical and clinical stages of development. Several vaccines, such as the S RBD subunit protein vaccine developed by Sichuan University (Yang et al., 2020a), the full-length S glycoprotein vaccine created by Novavax (Tian et al., 2021), and the mRNA vaccines from Pfizer and Moderna (Corbett et al., 2020, Mulligan et al., 2020), along with the adenovirus vector vaccine developed by Janssen and Oxford University (Mercado et al., 2020, van Doremalen et al., 2020), as well as the inactivated vaccine developed by Sinovac Biotech and Beijing Institute of Biological Products (Gao et al., 2020), utilized pseudovirus systems to assess the neutralizing ability of antibodies induced post-vaccination. Screening of small-molecule SARS-nCoV-2 inhibitors have also been carried out using SARS-nCoV-2 pseudoviruses. A lentiviral-based SARS-nCoV-2 pseudotyped particle has been used to evaluate potent membrane fusion inhibitors (Zhu et al., 2020). Pseudotyped SARS-nCoV-2 has also been used to screen for SARS-nCoV-2 entry inhibitors with 15 active drugs being identified as SARS-nCoV-2-specific entry inhibitors (Yang et al., 2021). Spiked pseudoviruses have undoubtedly contributed significantly to the understanding of SARS-nCoV-2 infection and B cell responses elicited by natural infection and vaccination. However, mechanistic studies of SARS-nCoV2 are still largely unexplored. Integrating spiked pseudoviruses in $CD8^{+}$-mediated killing assays may help to elucidate the T cell response to SARS-nCoV-2, especially in PLWH, while abrogating the complexities and risks of live virus assays. A standardised spiked-pseudovirus killing assay is lacking the literature. Thus, this project aims to develop and optimise such an assay with the end goal of assessing the killing activity of SARS-nCoV-

2-specific $CD8^+$ T cells from various clinical cohorts by co-culturing these cells with spiked pseudovirus-infected cells.

2.1.3. Development and optimization of the pseudovirus SARS-nCoV-2 killing assay

The use of pseudoviruses for the development of the SARS-nCoV-2 killing assay offers several advantages. When SARS-nCoV-2 spike pseudoviruses are used to infect ACE2-expressing target cells, they mimic the infection of SARS-nCoV-2 offering a safer alternative to using live SARS-nCoV-2. Furthermore, the incorporation of a fluorescence reporter in the design of the pseudovirus allows for the measurement of $CD8^+$-mediated killing at different ratios of effector and target cells. Additionally, the lentiviral packaging system has been widely used and is well-studied, as outlined in the literature above. To develop a pseudovirus-based killing assay, three spike pseudotyped reporter virus designs were tested: a multi-vector lentiviral pseudovirus design similar to the design used by Crawford et al. (2020), a two-vector pseudovirus design incorporating an untruncated spike plasmid, as well as a two-vector pseudovirus design incorporating truncated spike plasmid used by Keeton et al. (2021) and Moyo-Gwete et al. (2022). In optimizing the pseudovirus infection titres for these spiked pseudotyped reporter viruses, different parameters were tested including varying the incubation times post pseudovirus infection, the amount of pseudovirus used during inoculation and assessing the effect of differing dilution factors. To further optimize the spike pseudotyped reporter virus, both classical transfection and nucleofection were used to generate the pseudoviruses and their infection titres were compared to determine which transfection method generated higher titre pseudoviruses. The optimization strategy carried out for each of the pseudovirus designs is outlined in **Figure 2.4**.

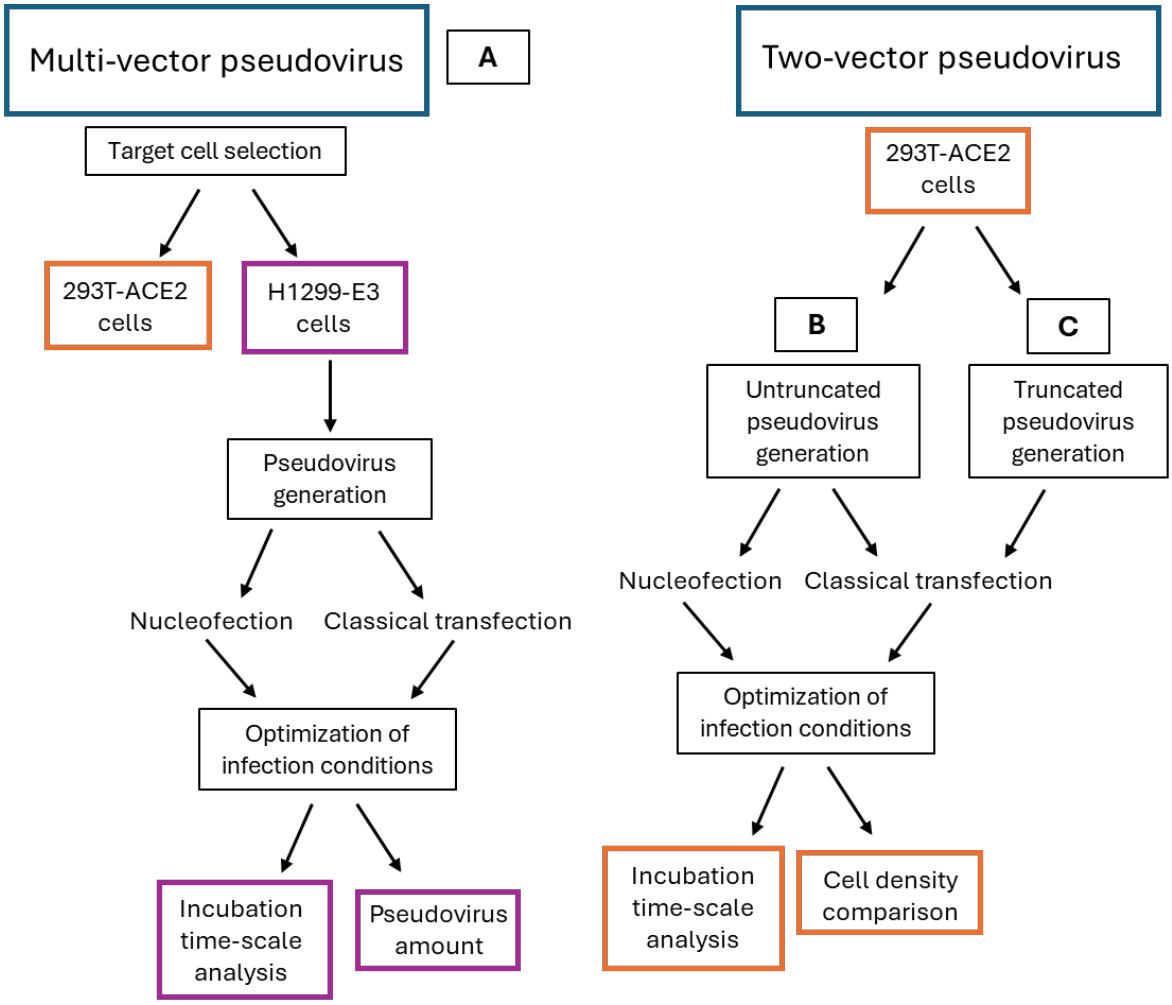

Figure 2.4.: Flow chart illustrating optimization strategy for three SARS-nCoV-2 spiked pseudovirus designs. (**A**) Multi-vector pseudovirus. (**B**) Untruncated spike two-vector pseudovirus. (**C**) Truncated spike two-vector pseudovirus.

Hypothesis:

It is hypothesized that the use of a spike pseudotyped reporter virus will serve as a robust target cell reporter to allow for the measurement of the loss of spiked pseudovirus-infected cells following co-culture with $CD8^+$ T cells isolated from individuals naturally infected with SARS-nCoV-2. This assay will provide a reliable means to assess the SARS-nCoV-2-specific cytotoxic $CD8^+$ T cell response among people living with HIV (PLWH) and people living without HIV (PLWoH), as well as the effect of vaccination on $CD8^+$ T cell responses to SARS-nCoV-2.

Aim:

To optimize a spike pseudotyped reporter virus to infect target cells for a SARS-nCoV-2-specific $CD8^+$ T cell killing assay.

Objectives:

1. To optimize the titre of wildtype spiked pseudoviruses.
2. To optimize flow-based detection of pseudovirus-infected in multiple target cells.
3. To optimize co-culture conditions for killing of pseudovirus-infected target cells by isolated $CD8^+$ T cells.
4. To perform killing assays using the optimized pseudovirus, to compare cytotoxic $CD8^+$ T cell responses to SARS-nCoV-2 natural infection, and/or vaccination in PLWH and PLWoH.

2.2. Materials and Methods

2.2.1. Summarised approach for optimisation of reporter spiked-pseudovirus generation

To optimise the generation of high titre spiked-pseudovirus, experiments were conducted using both multi-vector and two-vector pseudovirus designs. Initially, a multi-vector spiked pseudovirus, produced via classical transfection, was used to identify an optimal target cell line. This involved inoculating various cell lines with the pseudovirus at dilutions of 1:2, 1:4, and 1:8, followed by assessing infectivity using flow cytometry. Once the optimal target cell line was selected, the infection duration was optimized by exposing this cell line to the multi-vector pseudovirus at time points of 24 h, 48 h, 72 h, and 96 h, using pseudovirus dilutions of 1:1, 1:2, and 1:4. Subsequently, the multi-vector pseudovirus was produced by nucleofection to further enhance the pseudovirus titre. A similar series of experiments were performed to optimise the duration of infection. A two-vector pseudovirus incorporating an untruncated D614G plasmid was created using both classical transfection and nucleofection. The optimal infection duration for this pseudovirus was evaluated by inoculating the target cell line with pseudovirus dilutions of 1:1, 1:2, and 1:4 at 72 h and 96 h, including a VSV-GFP control for comparison. Following these experiments, a truncated version of the D614G plasmid was used to generate a two-vector spiked pseudovirus via classical transfection, identified as the superior transfection method from previous tests. This pseudovirus was applied to the target cell line at dilutions of 1:1, 1:2, and 1:4 for 96 h, and infectivity was evaluated using flow cytometry. Lastly, to optimise the pseudovirus titre further, various seeding densities were tested prior to pseudovirus inoculation. The detailed methodologies for these optimizations are outlined below.

2.2.2 Cell line culture

2.2.2.1 HEK293T cells

HEK293T cells were gifted by the HIV Pathogenesis Programme, Durban, South Africa and thawed in culture medium (DMEM supplemented with 10% heat-inactivated FBS, 1% HEPES and 1% penicillin/streptomycin (Gibco, Schwerte, Germany)). The cells were centrifuged at 1000 rpm for 10 min and the supernatant was discarded. The cells were resuspended in 5 ml culture medium before being transferred to a vented T_{25} culture flask. The HEK293T cells were incubated at 37°C in 5% CO_2 with daily monitoring of cell growth.

2.2.2.2 HEK293T cells expressing angiotensin converting enzyme 2 receptor (293T-ACE2)

HEK293T cells engineered to overexpress the ACE2 receptor (293T-ACE2 cells) were a gift from the Moore group, HIV & SARS-CoV-2 Virology Section, National Institute of Communicable Diseases, Johannesburg, South Africa. Cells were thawed and cultured in Dulbecco's Modified Eagle Media

(DMEM) (Gibco, Schwerte, Germany) supplemented with 10% heat inactivated FBS, 1% L-glutamine, 3 mg/ml puromycin and 10 mg/ml gentamycin, and incubated at 37°C and 5% CO_2.

2.2.2.3 H2199-E3 cells

H1299-E3 cells were gifted by the Sigal group, Africa Health Research Institute, Durban, South Africa (Cele et al., 2021, Khan et al., 2022). The cells were cultured in RPMI 1640 medium supplemented with 10% heat inactivated fetal bovine serum (FBS) (Gibco, Schwerte, Germany), 1% HEPES buffer solution, 1% non-essential amino acids, 1% sodium pyruvate and 1% L-glutamine (Gibco, Schwerte, Germany), and incubated at 37°C and 5% CO_2.

2.2.2.4 Trypsinization

At 80 – 90% cell confluency, the culture medium was decanted from the T_{25} flask and the cells were washed once with 10 ml PBS before the addition of 500 µl 0.05% trypsin-EDTA (1X) (Gibco, Schwerte, Germany). The cells were incubated for 5 min at 37°C in 5% CO_2 and the trypsinization reaction was neutralized thereafter with 10 ml culture medium once the cells had been detached. The cells were passaged twice before proceeding to nucleofection or classical transfection.

2.2.3 Plasmids used, propagation and isolation

2.2.3.1 List of plasmids used for reporter spiked pseudovirus generation

Plasmids used in this study are described in **Table 2.1.**

Table 2.1.: Plasmids required for generation of a reporter spiked-pseudovirus

Plasmid	Source	Relevant citations
5-vector spiked pseudovirus		
mCherry	A gift from the Sigal group at AHRI, Durban, South Africa.	(Crawford et al., 2020, Cele et al., 2021)
HDM-IDTSpike-fixK		
HDM-Hgpm2		
HDM-tat1b		
pRC-CMV-Rev1b		
2-vector spiked pseudovirus		
pBR43-ΔEnv-NefSF2GFP	A gift from the Brockman Lab	(Gao et al., 1996, Ohagen et al., 2003)

D614G	A gift from the Moore group, HIV & SARS-CoV-2 Virology Section, NICD, Johannesburg, South Africa.	(Keeton et al., 2021, Moyo-Gwete et al., 2023)
Truncated D614G	A gift from Thandeka Moyo-Gwete, NICD, Johannesburg, South Africa.	
pCMV-VSV-g	A gift from Bob Weinberg (Addgene plasmid # 8454)	(Stewart et al., 2003)

2.2.3.2 Plasmid propagation in Escherichia coli

Luria-Bertani (LB) broth (ThermoFisher Scientific, Eugene, Oregon, United States) was prepared by adding two tablets to 100 ml dH_2O and autoclaved in a Schott bottle. The broth was allowed to cool before 50 ml broth was transferred to sterile conical flasks, after which 500 µl *Escherichia coli* transformed with respective plasmid DNA was added to each of the flasks. The flasks were gently swirled before the addition of 50 µl ampicillin to each flask. The flasks were left to shake at 150 rpm in a 30°C automatic shaker for 72 h.

2.2.3.3 Bulk plasmid isolation

Following the shaking incubation, plasmid isolation was carried out using the ZymoPURE™ Plasmid Midiprep Kit (Zymo Research Corporation, Irvine, California, United States). In brief, 50 ml of the bacterial culture was centrifuged at 4000 rpm for 10 min in a 50 ml Falcon tube. The supernatant was decanted and the bacterial cells were resuspended in 8 ml ZymoPURE™ P1. The solution became viscous after the addition of 8 ml ZymoPURE™ P2 which indicated lysis completion and at this point, 8 ml ZymoPURE™ P3 was added to the solution to neutralize the reaction. The neutralized lysate was loaded into the ZymoPURE™ Syringe Filter-X and clarified into a 50 ml Falcon tube. ZymoPURE™ Binding Biffer was added to the cleared lysate and mixed thoroughly before being inserted into to the Zymo-Spin™ V-PS Column Assembly. The mixture was centrifuged at 500 × *g* for 2 min until all the cleared lysate had passed through the column. The column was washed with 5 ml ZymoPURE™ Wash 1 and 2, discarding the flow-through each time. A final wash was performed with ZymoPURE™ Wash 2 followed by centrifugation to remove the residual wash buffer. The purified DNA was then eluted by transferring the column into a clean Eppendorf tube, incubating at room temperature for 5 min and centrifuging at 10 000 × *g* for 1 min. The eluted plasmid DNA was stored at ≤ -20°C.

2.2.4 Transfection methods for pseudovirus generation

2.2.4.1 Classical transfection

On the day before transfection, ~5 × 10^5 HEK293T cells were seeded on a 6-well plate in 2 ml culture medium without antibiotics so the cells were 80% confluent at the time of transfection. For each transfection sample, complexes were prepared by diluting 4 µg of total DNA in 250 µl DMEM without additives in Eppendorf tubes. Total DNA encompassed multiple vectors described in **Table 2.2**. In separate Eppendorf tubes, 8 µl polyethyleneimine (PEI) was diluted with 250 µl DMEM without additives for each transfection sample and incubated for 5 min. The diluted PEI was combined with the diluted DNA and incubated for a further 30 min at room temperature. To each well of HEK293T cells, 500 µl of the transfection was added in a drop-wise fashion, forming a spiral from the outside inwards. The plate was incubated at 37°C and 5% CO_2 for 4 to 6 hours before the DMEM was removed and replace with complete DMEM with antibiotics. The supernatants were harvested and filtered through a 0.45 µm syringe filter 72 h post-transfection before being frozen in 500 µl aliquots at -80°C in cryovials.

2.2.4.2 Nucleofection

The nucleofection was carried out as per the Amaxa™ 4D-Nucleofector™ kit manufacturer's protocol. In brief, the appropriate Nucleofector™ program was selected on the 4D-Nucleofector™ System. An aliquot of DMEM was pre-warmed to 37°C while HEK293T cells at 80-90% confluency were harvested by trypsinization described above. The cells were resuspended in 10 ml culture medium and an aliquot of cells were counted to determine cell density. Following counting, ~5 × 10^5 cells per condition were centrifuged at 1000 rpm for 10 min. The supernatant was discarded and the pellet was resuspended in 100 µl room temperature 4D- Nucleofector™ Solution per condition. Pseudoviral plasmid DNA was prepared and added to each of the mastermixes according to **Table 2.2** after which they were transferred to Nucleocuvette™ Vessels. The Nucleocuvette™ Vessels were carefully placed in the 4D-Nucleofector™ X Unit and the nucleofection was run to completion. After nucleofection, the cells were removed from the Nucleocuvette™ Vessels for each condition and resuspended in 2 ml pre-warmed culture medium in a 6-well plate. The cells were incubated at 37°C in 5% CO_2 incubator for 72 h. After the 72 h incubation, the pseudovirus was harvested from each well by filtering culture supernatant through a 0.45 µm syringe filter before being frozen in 500 µl aliquots at -80°C in cryovials.

Table 2.2.: Amounts of plasmid DNA required to construct a reporter spiked-pseudovirus using classical transfection and nucleofection.

Plasmid	Amount per classical transfection (µg)	Amount per nucleofection (µg)
5-vector spiked pseudovirus		
mCherry	1	1
HDM-IDTSpike-fixK	0.34	0.34
HDM-Hgpm2	0.22	0.22
HDM-tat1b	0.22	0.22
pRC-CMV-Rev1b	0.22	0.22
2-vector spiked pseudovirus		
pBR43-ΔEnv-NefSF2GFP	3.2	3.2
D614G/truncated or D614G or pCMV-VSV-g	0.8	0.8

2.2.5 Infection of 293T-ACE2 or H1299-E3 cells with spiked-pseudovirus

2.2.5.1. Standard infection protocol

One day before infection, ~1.25 × 10^4 target cells in a final volume of 100 µl were seeded in a flat-bottom 96-well plate. For the inoculation process 100 µl of the respective pseudovirus was added to the target cells (as per above culture conditions) which were then subjected to serial dilutions of pseudovirus to media. Specifically, the pseudovirus was diluted at ratios of 1:1, 1:2, and 1:4. The cells were incubated at 37°C in 5% CO_2 for each specified incubation time. Following respective incubation times, 25 µl trypsin-EDTA (1X) was added to each well to detach the cells. The cells were incubated for 15 min at 37°C in 5% CO_2 after which they were transferred to a U-bottom 96-well plate and pelleted at 1800 rpm for 6 min. Two washing steps were performed using 200 µl 3% bovine serum albumin (BSA) (Sigma, Munich, Germany) in phosphate buffered saline (PBS) (Gibco, Schwerte, Germany) to remove unbound pseudovirus and debris. The cells were resuspended after the final wash in 1% BSA in PBS before performing fluorescence activated cell sorting (FACS) preparation and evaluation of the infection efficiency at each time point and under the various dilution conditions.

2.2.5.2 Optimisation of infection protocol

Target cells were infected as described above in duplicate plates, each pertaining to a specific infection duration: 24 h, 48 h, 72 h and 96 h. The cells were incubated at 37°C in 5% CO_2 for each specified incubation time before removing for FACS preparation and analysis.

2.2.5.3 Optimisation of cell-to-virus infection ratio

As described above, target cells were seeded in a 96-well plate one day before infection. Initially, 50 µl of pseudovirus was added to the target cells in a 1:2 dilution. The cells were then subjected to serial dilutions of 1:4 and 1:8. After experimentation, 100 µl of pseudovirus was tested instead of the initial 50 µl for all subsequent experiments

2.2.5.4 Optimisation of target cell density

To assess the effect of cell seeding density on the pseudovirus titre, varying densities of 293T-ACE2 cells were tested. Cells were seeded in a 96-well plate at densities of ~1.25×10^4, ~2.5×10^4 and ~5×10^4 cells per well. The seeding was performed one day prior to infection, and the cells were infected according to the protocol described above.

2.2.6. FACS for 5-vector mCherry spike pseudovirus after 293T-ACE2 or H1299-E3 cell infection

Flow cytometry was performed on the LSR Fortessa™ using the BD FACSDiva™ software and analysis was performed on FlowJo v10.8.1. 293T-ACE2 and H1299-E3 cells were initially gated based on forward scatter (FSC-A) and side scatter (SSC-A). Gating was refined to single cells for both cell types, and the subsequent fluorescence channels utilized to detect infection in H1299-E3 cells were PE-CF594 for mCherry and AF488 for YFP. These channels were used to detect the expression of mCherry and YFP, indicative of multi-vector pseudovirus infection. For 293T-ACE2 cells, the fluorescence channels utilized to detect multi-vector pseudovirus infection were PE-CF594 for mCherry and FSC-A. Statistical analyses were performed using GraphPad Prism 10.0.3 (GraphPad Software, Inc, San Diego, CA).

2.2.7. FACS for 2-vector GFP spike pseudovirus after 293T-ACE2 infection

Flow cytometry was performed on the LSR Fortessa™ using the BD FACSDiva™ software and analysis was performed on FlowJo v10.8.1. 293T-ACE2 cells were initially gated based on forward scatter (FSC-A) and side scatter (SSC-A). Gating was refined to single cells, and the subsequent fluorescence channels utilized to detect two-vector pseudovirus infection in 293T-ACE2 cells were AF488 for YFP expression and FSC-A. Statistical analyses were performed using GraphPad Prism 10.0.3 (GraphPad Software, Inc, San Diego, CA).

2.3. Results

2.3.1 Selection of optimal target cell line for SARS-nCoV-2 pseudovirus infectivity

When conducting viral infectivity assays involving human cell lines, it is important to understand which cell lines are susceptible to the virus and to what degree (Pires De Souza et al., 2022). The ACE2 receptor is the main entry receptor used by SARS-nCoV-2 to gain entry into host cells (Jackson et al., 2022) and given that several cell lines do not naturally express the ACE2 receptor at high levels, it is necessary to generate transient and stable cell lines which highly express ACE2 to facilitate infection by SARS-nCoV-2 pseudoviruses (Crawford et al., 2020, Cele et al., 2021, Khan et al., 2022). The infection protocol, whereby target cells were adhered to a microplate and inoculated with pseudovirus was described previously (Crawford et al., 2020). However, the lentiviral backbone plasmid used in this study did not express ZsGreen, but rather mCherry, a red fluorescent protein, which is compatible with H1299-E3 cells. These H1299-E3 cells were engineered with fluorescent nuclei where the mCherry gene was included in the lentiviral vector to serve as a marker for successful transduction and to facilitate the tracking of infected cells. The strong expression of mCherry in these cells allowed for quantification of infection rates using flow cytometry (Khan et al., 2022).

To assess the infectivity of a multi-vector wildtype spiked pseudovirus generated by classical transfection (Crawford et al., 2020), two target cell lines, H1299-E3 cells and 293T-ACE2 cells, were infected using 50 µl of the in-house multi-vector pseudovirus, depicted in **Figure 2.5** (**A**) and (**B**). Flow cytometry analysis revealed that H1299-E3 cells produced more mCherry signal than 293T-ACE2 cells, suggesting greater levels of spiked pseudovirus infection in H1299-E3 cells, as illustrated in **Figure 2.5** (**C**) and (**D**). This was evident in the infectivity percentages at different pseudovirus dilution factors where 50 µl of the pseudovirus was added to 100 µl of cells (1:2 dilution) and then serially diluted at 1:4 and 1:8 dilutions. Furthermore, **Figure 2.5** (**E**) showed that the percentage of mCherry fluorescence peaked at the 1:2 dilution for both the 293T-ACE2 and H1299-E3 cells. This was additionally confirmed by the bar graph in **Figure 2.5** (**F**) showing the median fluorescence intensity (MFI) where the MFI peaked at the 1:2 dilution for the H1299-E3 cells. Consequently, it was determined that for optimal infectivity, the H1299-E3 cell line is the most suitable for conducting pseudovirus infections.

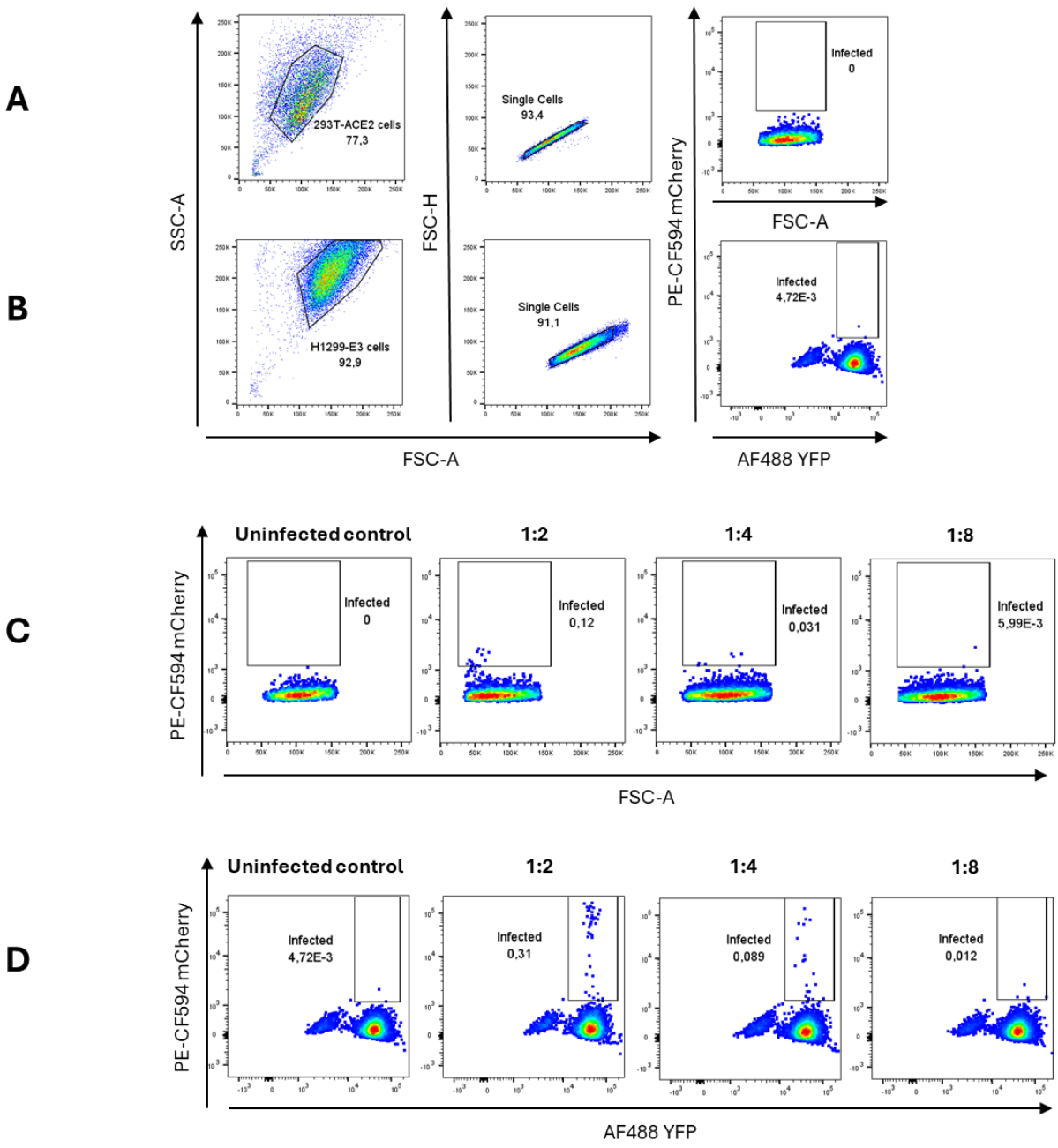
A
B
SSC-A
FSC-A
293T-ACE2 cells
77,3
H1299-E3 cells
92,9
FSC-H
Single Cells
93,4
Single Cells
91,1
PE-CF594 mCherry
AF488 YFP
Infected
0
Infected
4,72E-3
C
Uninfected control
1:2
1:4
1:8
Infected
0
Infected
0,12
Infected
0,031
Infected
5,99E-3
D
Infected
4,72E-3
Infected
0,31
Infected
0,089
Infected
0,012

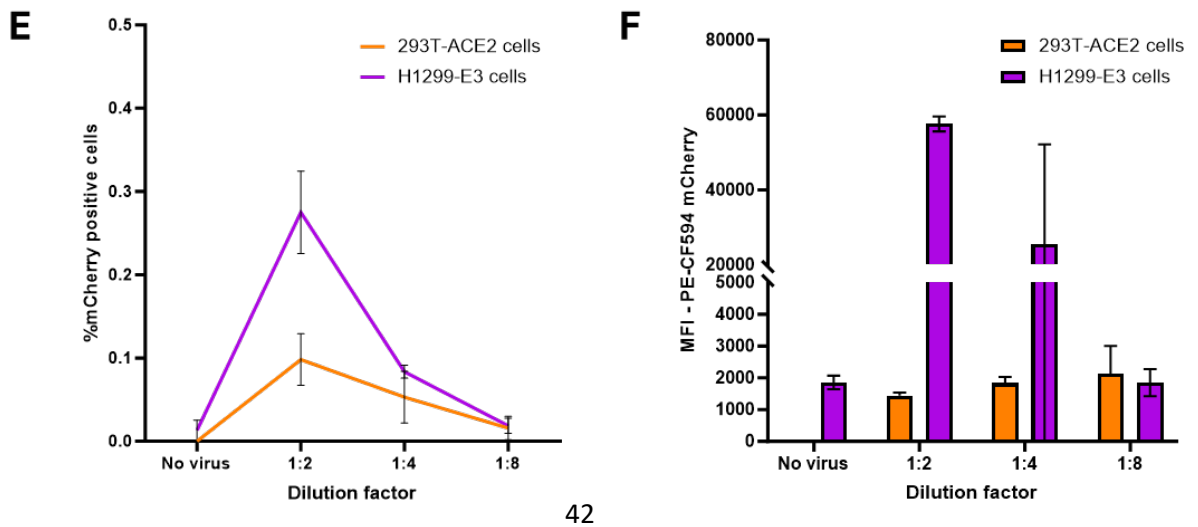
E
%mCherry positive cells
293T-ACE2 cells
H1299-E3 cells
No virus
1:2
1:4
1:8
Dilution factor
F
MFI - PE-CF594 mCherry
293T-ACE2 cells
H1299-E3 cells
No virus
1:2
1:4
1:8
Dilution factor

Figure 2.5.: Comparative analysis of in-house multi-vector pseudovirus infection in 293T-ACE2 cells and H1299-E3 cells. (**A**) Gating strategy for uninfected control 293T-ACE2 cells, showing the main cell population and single cells, with no indication of infection in the PE-CF594 mCherry versus AF488 YFP plot. (**B**) Gating strategy for uninfected control H1299-E3 cells, also displaying the primary cell population and single cells, with minimal cell infection in the PE-CF594 mCherry versus AF488 YFP plot. (**C**) Representative flow cytometry plots displaying infection percentages in 293T-ACE2 cells following infection with in-house multi-vector SARS-nCoV-2 spiked pseudovirus at different dilutions (1:2, 1:4, 1:8). (**D**) Representative flow cytometry plots displaying infection percentages in H1299-E3 cells following infection with in-house multi-vector SARS-nCoV-2 spiked pseudovirus at different dilutions (1:2, 1:4, 1:8). (**E**) Graph comparing the relative infection rates between 293T-ACE2 cells and H1299-E3 cells across various dilutions (1:2, 1:4 and 1:8). (**F**) Bar graph illustrating the median fluorescence intensity (MFI) of infected 293T-ACE2 and H1299-E3 cells.

2.3.2. Infection optimization of multi-vector pseudovirus generated by classical transfection

In order to obtain a high pseudovirus infection titre, and therefore an efficient flow cytometry readout which would allow the quantification of the reduction in pseudovirus fluorescence as a function of killing by $CD8^+$ T cells, the optimal infection conditions for the in-house multi-vector pseudovirus needed to be determined. After carrying out the infection protocol described by Crawford et al. (2020) to determine the optimal cell line for infection, it was observed that the percentage of mCherry positive cells was relatively low, as depicted in **Figure 2.5**. To optimize the infection of H1299-E3 cells, various parameters were investigated including i) the adjustment of infection time and ii) the quantity of pseudovirus added to the H1299-E3 cells during infection. Since the use of 50 µl of pseudovirus generated a relatively low percentage of mCherry positivity in both cell lines tested, 100 µl of pseudovirus was tested at serial dilutions of pseudovirus to cells (1:1, 1:2 and 1:4) for subsequent experiments.

2.3.2.1. Incubation time-scale analysis

A time-scale analysis was carried out to evaluate the effect of incubation time by varying the duration after the addition of pseudovirus to the H1299-E3 cells. **Figure 2.6** (**A**) depicts the gating strategy used to determine the threshold for percentage mCherry positivity. The representative flow cytometry plots depicted in **Figure 2.6** (**B – E**) show the infection status of the H1299-E3 cells after infection with 100 µl multi-vector SARS-nCoV-2 spiked pseudovirus at each tested time point. These infection results, which were carried out in duplicate, suggested a dose-dependent decrease in the infection rate with increasing dilution of the pseudovirus. The uninfected control plots where no virus was added, served as a baseline to confirm that any increases in the percentage of mCherry positive cells were due to the addition of the pseudovirus at their respective dilutions. **Figure 2.6** (**F**) showed that the highest

fluorescence intensities were observed at the 72 h and 96 h time points at a 1:1 dilution, with **Figure 2.6** (**G**) confirming this observation. After testing the effect of both infection time and pseudovirus quantity on the infection rate, a high pseudovirus titre required for the measurement of killing activity could still not be obtained using multi-vector spiked pseudoviruses constructed by classical transfection. Due to the challenges faced in obtaining a significantly high pseudovirus fluorescence readout, a mechanical transfection method, nucleofection, was tested to improve the titre of the pseudovirus.

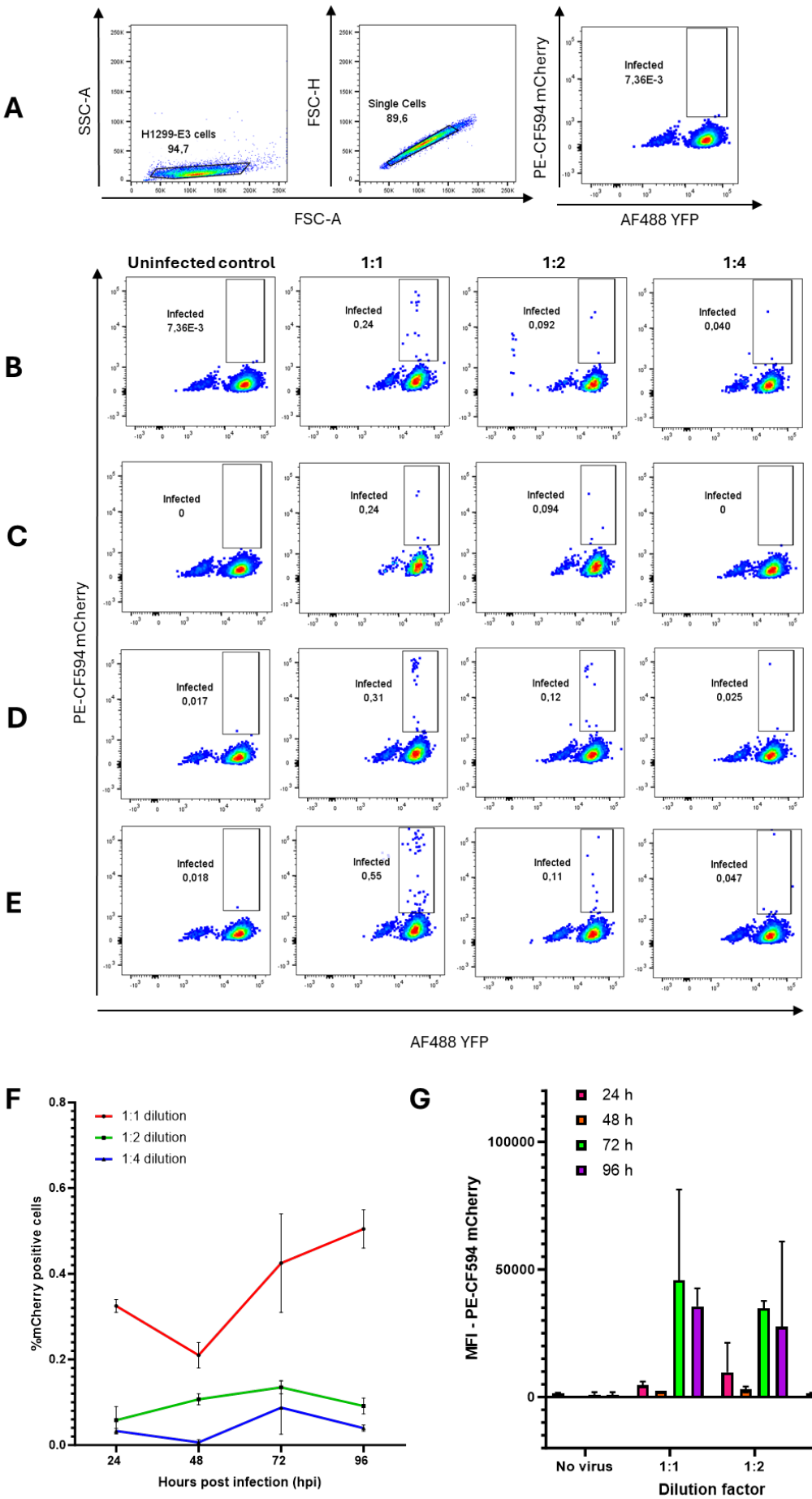
A
SSC-A
H1299-E3 cells
94,7
FSC-H
Single Cells
89,6
FSC-A
PE-CF594 mCherry
Infected
7,36E-3
AF488 YFP
Uninfected control
1:1
1:2
1:4
B
C
D
E
Infected
7,36E-3
Infected
0,24
Infected
0,092
Infected
0,040
Infected
0
Infected
0,24
Infected
0,094
Infected
0
Infected
0,017
Infected
0,31
Infected
0,12
Infected
0,025
Infected
0,018
Infected
0,55
Infected
0,11
Infected
0,047
PE-CF594 mCherry
AF488 YFP
F
1:1 dilution
1:2 dilution
1:4 dilution
%mCherry positive cells
0.0
0.2
0.4
0.6
0.8
24
48
72
96
Hours post infection (hpi)
G
24 h
48 h
72 h
96 h
MFI - PE-CF594 mCherry
0
50000
100000
No virus
1:1
1:2
1:4
Dilution factor

Figure 2.6.: Infection duration optimization for in-house multi-vector pseudovirus generated by classical transfection. (**A**) Gating strategy for uninfected control H1299-E3 cells, showing the main cell population and single cells, with no indication of infection in the PE-CF594 mCherry versus AF488 YFP plot. (**B**) Representative flow plots showing percentage of mCherry positive cells 24 h post infection in H1299-E3 cells at different dilutions (1:1, 1:2, 1:4). (**C**) Representative flow plots showing percentage of mCherry positive cells 48 h post infection in H1299-E3 cells at different dilutions. (**D**) Representative flow plots showing percentage of mCherry positive cells 72 h post infection in H1299-E3 cells at different dilutions. (**E**) Representative flow plots showing percentage of mCherry positive cells 96 h post infection in H1299-E3 cells at different dilutions. (**F**) Line graph illustrating the mean percentage of mCherry positive H1299-E3 cells following pseudovirus infection at various dilutions (1:1, 1:2, and 1:4) over time (n=2). The highest infection rates were observed at 96 h post-infection, particularly with the 1:1 dilution. Infection efficiency decreases with lower concentrations of pseudovirus. (**G**) Bar graph illustrating median fluorescence intensity (MFI) of infected H1299-E3 cells at each time point post infection.

2.3.3. Infection optimization of multi-vector pseudovirus generated by nucleofection

Nucleofection is an electroporation-based technology which introduces DNA into the cell nucleus through pulsed electric fields (Đorđević et al., 2022). The Amaxa™ 4D-Nucleofector™ kit is used to deliver a wide range of substrates, usually DNA, directly to the nuclei of target cells. Additionally, the pulse and transfection buffers are well-optimized to ensure minimal cytotoxicity thus preserving the cell functionality (Đorđević et al., 2022). A new batch of pseudoviruses were generated using the Amaxa™ 4D-Nucleofector™ kit manufacturer's protocol while maintaining the original multi-vector pseudovirus design used above. As done for the pseudoviruses generated by classical transfection, an identical incubation time-scale analysis was carried out for the nucleofection-generated pseudoviruses. The gating strategy in **Figure 2.7** (**A**) and representative plots (**Figures 2.7** (**B – E**)) showed the relationship between the dilution factor and pseudovirus fluorescence compared with an uninfected control. A higher percentage of mCherry-positive cells was expected for viruses generated by nucleofection compared to classical transfection as nucleofection was expected to be a more efficient transfection method. Indeed, it was observed that at a 1:1 dilution, the pseudovirus fluorescence peaked at the 72 h time point (**Figure 2.7** (**F)** and **(G**)) when the cells were infected by nucleofection-generated pseudoviruses compared to those generated by classical transfection which peaked at 96 h. As seen with the multi-vector pseudovirus generated by classical transfection, it was observed that higher concentrations of pseudovirus result in a higher percentage of mCherry positive cells, suggesting a dose-dependent infection efficiency.

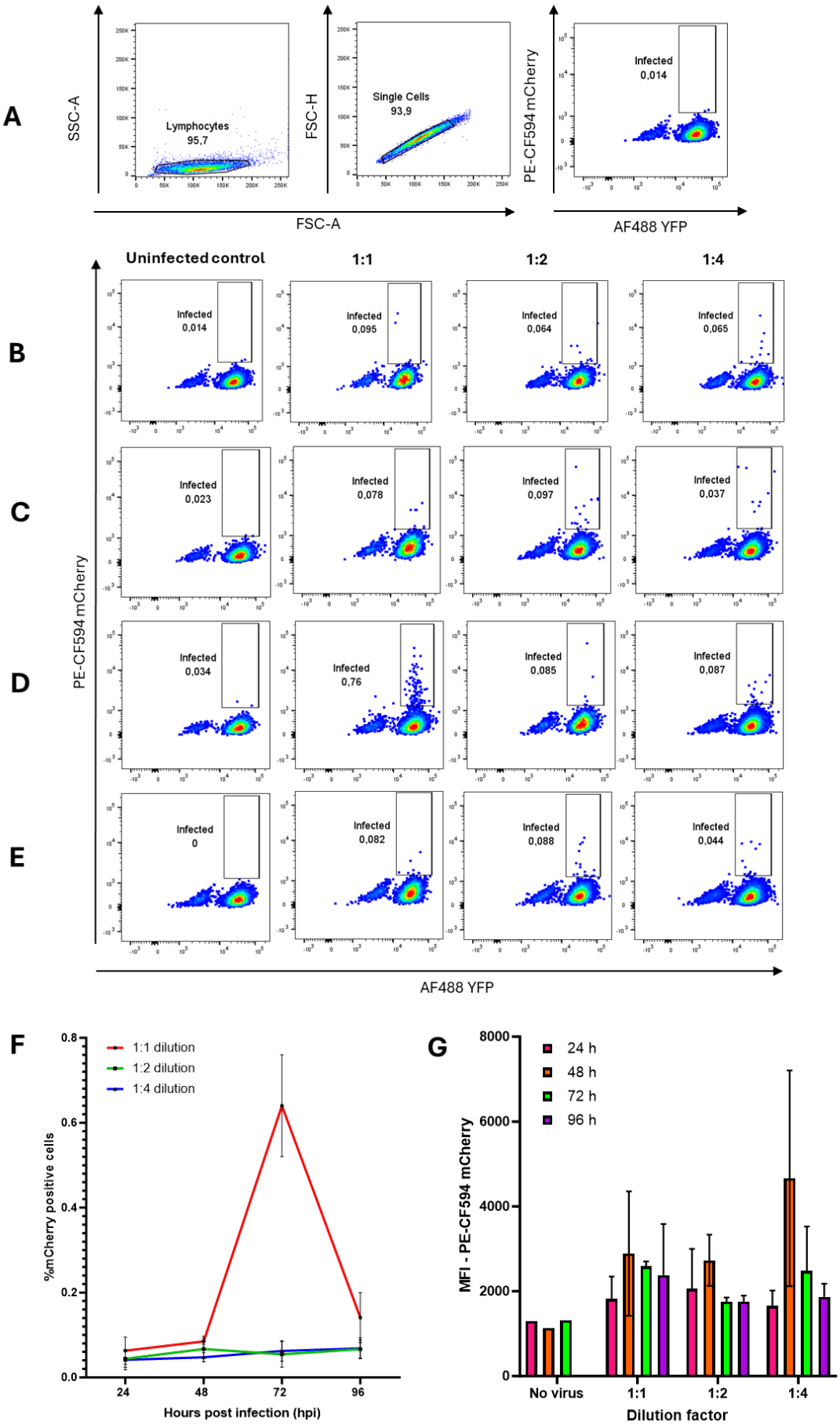
A
SSC-A
Lymphocytes
95,7
FSC-H
Single Cells
93,9
FSC-A
PE-CF594 mCherry
Infected
0,014
AF488 YFP
Uninfected control
1:1
1:2
1:4
B
Infected
0,014
Infected
0,095
Infected
0,064
Infected
0,065
C
Infected
0,023
Infected
0,078
Infected
0,097
Infected
0,037
D
Infected
0,034
Infected
0,76
Infected
0,085
Infected
0,087
E
Infected
0
Infected
0,082
Infected
0,088
Infected
0,044
PE-CF594 mCherry
AF488 YFP
F
1:1 dilution
1:2 dilution
1:4 dilution
%mCherry positive cells
0.0
0.2
0.4
0.6
0.8
24
48
72
96
Hours post infection (hpi)
G
24 h
48 h
72 h
96 h
MFI - PE-CF594 mCherry
0
2000
4000
6000
8000
No virus
1:1
1:2
1:4
Dilution factor

Figure 2.7.: Infection duration optimization for multi-vector pseudovirus generated by nucleofection. (**A**) Gating strategy for uninfected control H1299-E3 cells, showing the main cell population and single cells, with no indication of infection in the PE-CF594 mCherry versus AF488 YFP plot. (**B**) Representative flow plots showing percentage of mCherry positive cells 24 h post infection in H1299-E3 cells at different dilutions (1:1, 1:2, 1:4). (**C**) Representative flow plots showing percentage of mCherry positive cells 48 h post infection in H1299-E3 cells at different dilutions. (**D**) Representative flow plots showing percentage of mCherry positive cells 72 h post infection in H1299-E3 cells at different dilutions. (**E**) Representative flow plots showing percentage of mCherry positive cells 96 h post infection in H1299-E3 cells at different dilutions. (**F**) Line graph illustrating the mean percentage of mCherry positive H1299-E3 cells following pseudovirus infection at various dilutions (1:1, 1:2, and 1:4) over time (n=2). The highest infection rate was observed at 72 h post-infection, particularly with the 1:1 dilution. Infection efficiency decreased with lower concentrations of pseudovirus. (**G**) Bar graph illustrating median fluorescence intensity (MFI) of infected H1299-E3 cells at each time point post infection.

While the nucleofection-generated pseudoviruses showed an improved efficiency over classical transfection methods, with higher viral titres observed at an earlier time point, the current multi-vector pseudovirus design still leaves room for optimisation. To further enhance the transfection efficiency a two-vector pseudovirus design, which incorporates a critical spike protein mutation associated with increased infectivity, was implemented.

2.3.4. Infection comparison of untruncated two-vector pseudoviruses generated by classical transfection and nucleofection

Given the continued challenges faced in generating a high titre 5-vector pseudovirus by both these methods, a new 2-vector pseudovirus design was employed which has been used extensively in SARS-nCoV-2 neutralization assays (Cele et al., 2021, Riou et al., 2022). This design comprises a GFP reporter gene, which was used to measure pseudovirus fluorescence, with a D614G envelope vector. A two-vector system can offer better control over the expression of the transgene as there are fewer elements to regulate, and therefore easier to achieve a balanced expression of the necessary proteins (Dull et al., 1998). This is important for the correct assembly and functioning of the pseudovirus. Furthermore, while mCherry has its own benefits, such as longer wavelength emission which can reduce cellular autofluorescence, the increased brightness of GFP may make it a more effective reporter for certain laboratory experiments where sensitivity and detection limits are imperative (Shaner et al., 2005). It was therefore of interest to determine whether this pseudovirus design generated a higher titre pseudovirus when using either nucleofection or classical transfection methods, after the previously optimized infection time points, either 72 or 96 h post infection. For this reason, an infection comparison

was carried out on 293T-ACE2 cells to determine which transfection method and incubation time point generated pseudoviruses of a higher titre, as H1299-E3 cells are not compatible with the GFP reporter. An optimized VSV-GFP pseudovirus was used as a positive control to confirm that this experimental design is capable of producing a valid result (**Figure 2.8 (A – G)**). It is known that VSV has a wide tropism, with the ability to infect many cell types (Whitt, 2010). Given the ubiquitous nature of the VSV-GFP control virus, if the positive control does not yield the expected outcome, it may suggest issues with the experimental conditions or methodology. After infecting the cells for a period of 72 h and 96 h, a high proportion of infected cells was observed for the VSV-positive control, affirming that the overall infection protocol was efficient. At all dilutions and time points, nucleofection (**Figures 2.8** (**B**) and (**D**)) consistently resulted in a lower percentage of GFP positive cells than classical transfection. This suggested that classical transfection (**Figures 2.8** (**C**) and (**E**)) was a more efficient method for transfecting these cells with the pseudovirus.

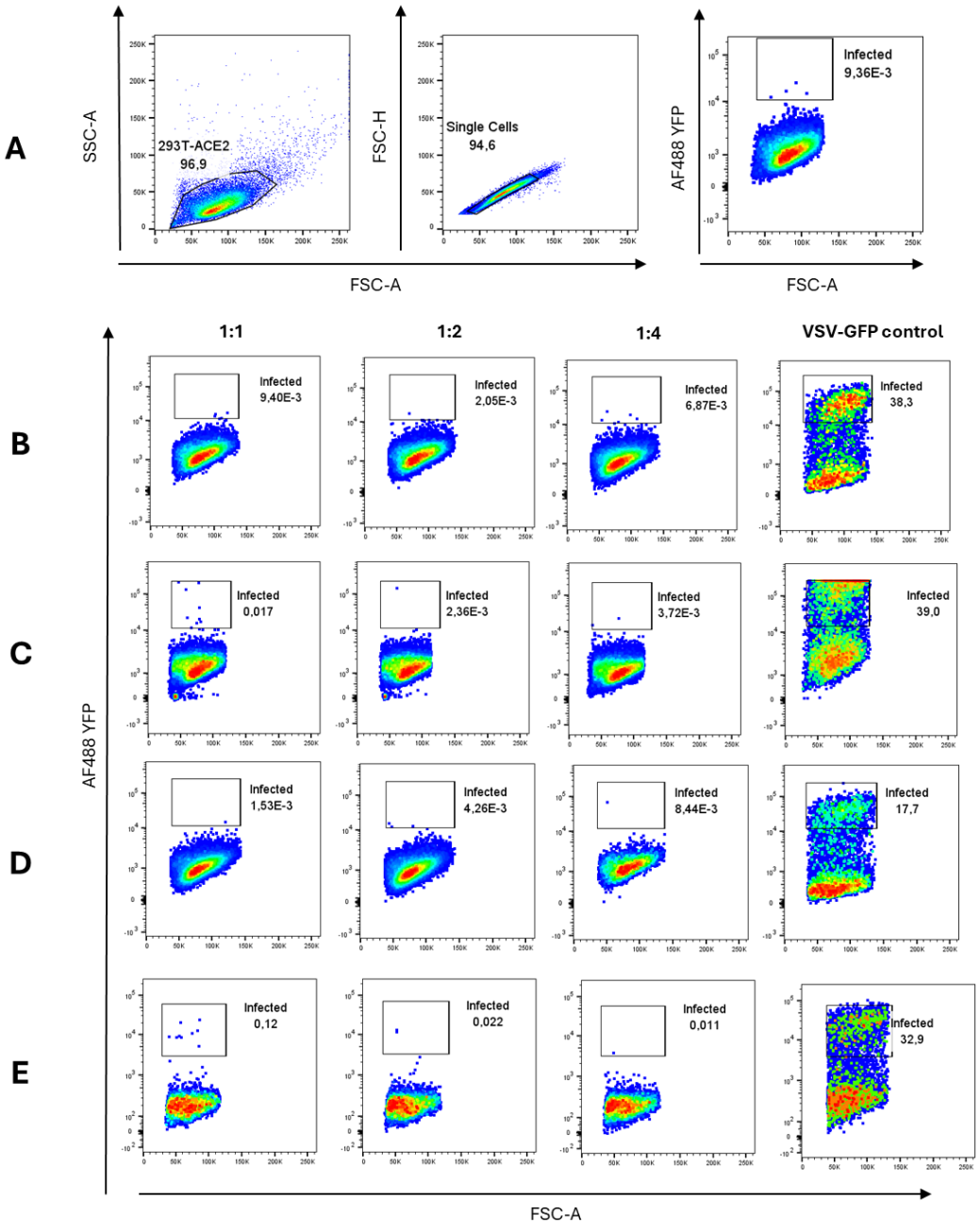
A
SSC-A
293T-ACE2
96,9
FSC-A
FSC-H
Single Cells
94,6
FSC-A
AF488 YFP
Infected
9,36E-3
FSC-A
1:1
1:2
1:4
VSV-GFP control
B
Infected
9,40E-3
Infected
2,05E-3
Infected
6,87E-3
Infected
38,3
C
Infected
0,017
Infected
2,36E-3
Infected
3,72E-3
Infected
39,0
D
Infected
1,53E-3
Infected
4,26E-3
Infected
8,44E-3
Infected
17,7
E
Infected
0,12
Infected
0,022
Infected
0,011
Infected
32,9
AF488 YFP
FSC-A

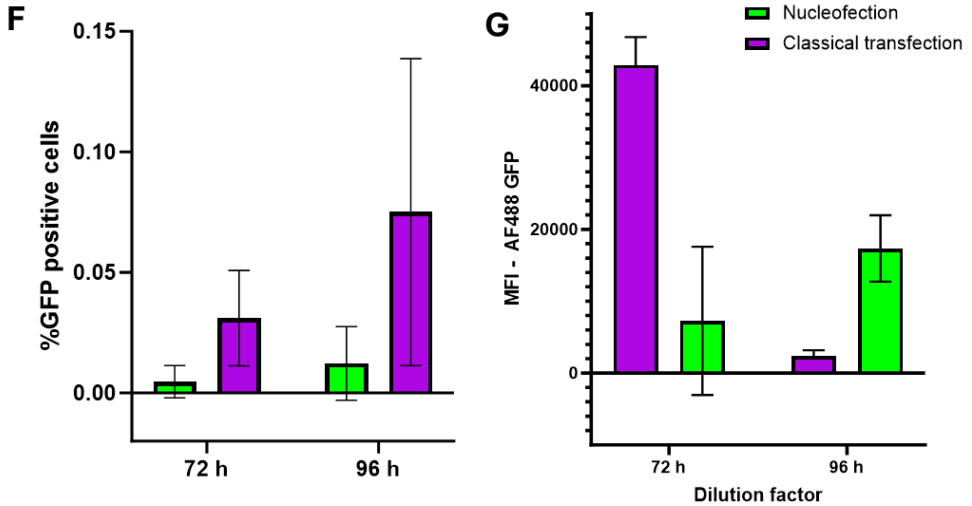
F
%GFP positive cells
0.15
0.10
0.05
0.00
72 h
96 h
G
Nucleofection
Classical transfection
MFI - AF488 GFP
40000
20000
0
72 h
96 h
Dilution factor

Figure 2.8.: Infection duration optimization for untruncated two-vector pseudovirus generated by nucleofection and classical transfection. (**A**) Gating strategy for uninfected control 293T-ACE2 cells after 72 h, showing the main cell population and single cells, with minimal infection in AF488 YFP vs. FSC-A plot. (**B**) Representative flow plots showing percentage of GFP positive cells 72 h post infection with untruncated two-vector pseudovirus generated by nucleofection in 293T-ACE2 cells at different dilutions (1:1, 1:2, 1:4), with the inclusion of a VSV-GFP control at a 1:4 dilution (n=2). (**C**) Representative flow plots showing percentage of GFP positive cells 72 h post infection with untruncated two-vector pseudovirus generated by classical transfection in 293T-ACE2 cells at different dilutions (1:1, 1:2, 1:4), with the inclusion of a VSV-GFP control at a 1:4 dilution. (**D**) Representative flow plots showing percentage of GFP positive cells 96 h post infection with untruncated two-vector pseudovirus generated by nucleofection in 293T-ACE2 cells at different dilutions (1:1, 1:2, 1:4), with the inclusion of a VSV-GFP control at a 1:4 dilution (n=2). (**E**) Representative flow plots showing percentage of GFP positive cells 96 h post infection with untruncated two-vector pseudovirus generated by classical transfection in 293T-ACE2 cells at different dilutions (1:1, 1:2, 1:4), with the inclusion of a VSV-GFP control at a 1:4 dilution (n=2). (**F**) Percentage graph showing GFP positive cells for 1:1 dilution 72 h and 96 h post infection. The highest percentage of GFP positive cells was observed 96 h post-infection with two-vector pseudovirus generated by classical transfection, particularly with the 1:1 dilution. Infection efficiency decreased with lower concentrations of pseudovirus. (**G**) Bar graph illustrating median fluorescence intensity (MFI) of infected 293T-ACE2 cells 72 h and 96 h post infection with two-vector pseudoviruses generated by nucleofection and classical transfection.

2.3.6. Generation of truncated spike two-vector pseudovirus

Several studies have noted different methods to increase the titre of spike protein-pseudotyped vectors (Yu et al., 2021, Chen et al., 2021) and a common method noted is the truncation of the spike protein cytoplasmic tail (Chen et al., 2021). It has been noted that SARS-nCoV-2 spike contains an endoplasmic reticulum (ER) retention signal at its C terminus, which is removed by the tail truncations of 13 amino acids or 18 to 21 amino acids that are frequently employed (Crawford et al., 2020). Compared to the full-length spike, these truncations were reported to generate ∼10- to 20-fold higher titres of VSV vectors (Chen et al., 2021). To generate pseudoviruses with a high titre, truncated D614G spike plasmids (National Institute of Communicable Diseases) were used to improve the original two-vector pseudovirus design. The pseudoviruses were generated by classical transfection for 96 h as this was the overall optimal transfection method and incubation time observed for the untruncated spike two-vector pseudovirus. An infection was carried out on 293T-ACE2 cells with the newly generated truncated spike pseudoviruses and the untruncated pseudoviruses to compare their infectivity percentages as a result of the altered spike protein. At a 1:1 dilution, the infectivity percentage of the truncated spiked pseudovirus was approximately three times higher than that observed for the untruncated spiked

pseudovirus. A higher infectivity percentage for the truncated spiked pseudovirus was also observed at a 1:2 dilution, although the infectivity percentage at a 1:4 dilution was higher for the untruncated spiked pseudovirus (**Figure 2.9** (**A** – **D**)).

2.3.6.1. Cell density comparison

In an attempt to further optimize the titre of the truncated spiked pseudoviruses, a cell density comparison was carried out with 293T-ACE2 cells where instead of adjusting the amount of pseudovirus used, the amount of cells seeded before pseudovirus infection was adjusted (~1.25×10^4, ~2.5×10^4, ~5×10^4 cells) as this could play a role in increasing the total amount of cells available for pseudovirus infection, thereby increasing the infectivity. It was observed that at higher cell seeding densities, the percentage of GFP positive decreased substantially when infected with the same dilution (1:1) of truncated and untruncated two-vector pseudovirus (**Figure 2.9** (**E** – **H**)).

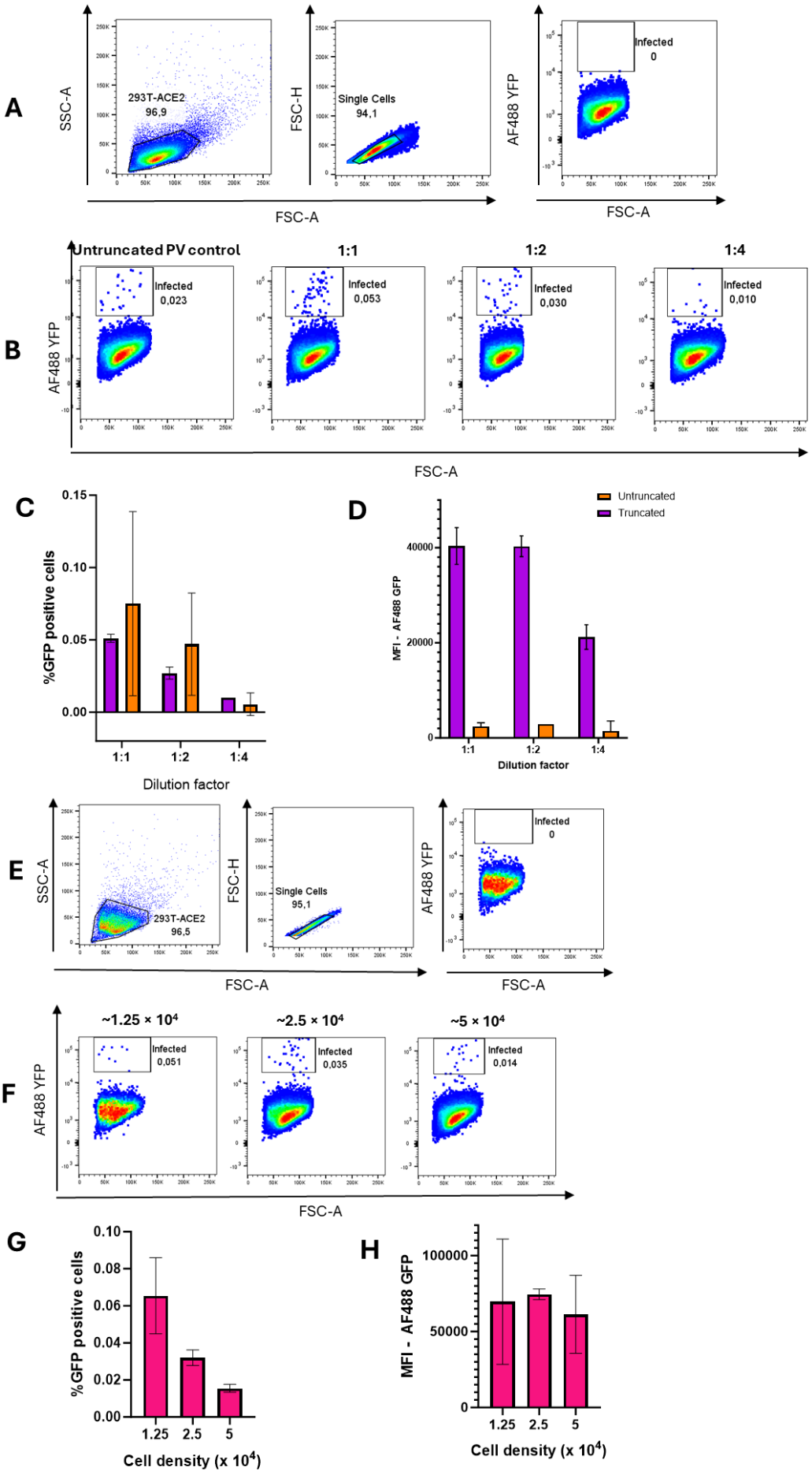
A
SSC-A
293T-ACE2
96,9
FSC-A
FSC-H
Single Cells
94,1
AF488 YFP
Infected
0
FSC-A
B
Untruncated PV control
1:1
1:2
1:4
AF488 YFP
Infected
0,023
Infected
0,053
Infected
0,030
Infected
0,010
FSC-A
C
%GFP positive cells
0.15
0.10
0.05
0.00
1:1
1:2
1:4
Dilution factor
D
Untruncated
Truncated
MFI - AF488 GFP
40000
20000
0
1:1
1:2
1:4
Dilution factor
E
SSC-A
293T-ACE2
96,5
FSC-A
FSC-H
Single Cells
95,1
AF488 YFP
Infected
0
FSC-A
F
~1.25 × 10⁴
~2.5 × 10⁴
~5 × 10⁴
AF488 YFP
Infected
0,051
Infected
0,035
Infected
0,014
FSC-A
G
%GFP positive cells
0.10
0.08
0.06
0.04
0.02
0.00
1.25
2.5
5
Cell density (x 10⁴)
H
MFI - AF488 GFP
100000
50000
0
1.25
2.5
5
Cell density (x 10⁴)

Figure 2.9.: Comparison between truncated two-vector pseudovirus and untruncated two-vector pseudovirus. (**A**) Gating strategy for uninfected control 293T-ACE2 cells after 96 h, showing the main cell population and single cells, with minimal infection in AF488 YFP vs. FSC-A plot. (**B**) Representative flow plots showing percentage of GFP positive cells 96 h post infection with truncated two-vector pseudovirus generated by classical transfection in 293T-ACE2 cells at different dilutions (1:1, 1:2, 1:4), with the inclusion of a untruncated two-vector pseudovirus control at a 1:1 dilution (n=2). (**C)** The highest percentage of GFP positive cells was observed 96 h post-infection with untruncated two-vector pseudovirus generated by classical transfection, particularly with the 1:1 dilution. (**D**) Bar graph illustrating median fluorescence intensity (MFI) of infected 293T-ACE2 cells 96 h post infection with truncated two-vector pseudoviruses classical transfection. (**E**) Gating strategy for uninfected control 293T-ACE2 cells after 96 h at a seeding density of ~1.25 × 10^4 cells, showing the main cell population and single cells, with minimal infection in AF488 YFP vs. FSC-A plot. (**F**) Representative flow plots showing percentage of GFP positive cells 96 h post infection with truncated two-vector pseudovirus generated by classical transfection in 293T-ACE2 cells at different seeding densities with (n=2). (**G**) Bar graph illustrating percentage GFP positive cells after infection of 293T-ACE2 cells 96 h post infection with two-vector pseudoviruses generated by classical transfection. (**H**) Bar graph illustrating median fluorescence intensity (MFI) for GFP positive cells after infection of 293T-ACE2 cells 96 h post infection with two-vector pseudoviruses generated by classical transfection.

After observing that the overall titres were still too low for an effective fluorescence readout, despite altering the pseudovirus design and plasmids used, a new fluorescence-based assay design was adopted, without the use of spiked pseudoviruses.

2.4. Discussion

The generation of a high titre SARS-nCoV-2 spiked pseudovirus is crucial for the quantification of killing activity upon the addition of cytotoxic $CD8^+$ T cells. This is due to the fact that the initial percentage of reporter fluorescence (in this case either mCherry or GFP) needs to be high enough at baseline without the addition of effector $CD8^+$ T cells to accurately assess the reduction in fluorescence intensity upon the addition of $CD8^+$ T cells, which would be a function of $CD8^+$-mediated killing. There are several reasons why despite extensive optimization efforts, achieving a high titre pseudovirus proved challenging. Firstly, the quality and purity of the plasmid DNA used for transfection may impact the efficiency of pseudovirus production, which may have in turn resulted in the low pseudovirus titres observed (Chong et al., 2021). It is also likely that the choice of transfection reagent, in this case PEI, and its compatibility with the cell line can affect the uptake of plasmid DNA (Longo et al., 2013). To mitigate these issues, further steps can be taken to ensure high-quality plasmid is being used, in addition to the DNA quality assessment that was previously carried out using a nanodrop. These include optimizing the choice and amount of transfection reagents being used as well as testing different commercially available plasmid preparation kits designed for high-yield and high-purity DNA (Chong et al., 2021). Cell harvesting techniques were crucial to avoid washing away of infected cells following different incubation times. Improper or rigorous washing may have caused cells to wash away, thereby resulting in low fluorescence intensity percentages observed. It should also be noted that the sensitivity and stability of the fluorescent reporter gene (for example, mCherry) used to measure infectivity can affect the detection of pseudovirus-infected cells (Thimmiraju et al., 2024). Low expression levels or rapid degradation of the reporter gene can lead to underestimation of infectivity rates. Ensuring that the reporter gene is under the control of a strong promoter for robust expression can help mitigate this (Thimmiraju et al., 2024).

2.4.1. Limitations

Interestingly, pseudoviruses generated using classical transfection methods showed overall higher infectivity percentages when compared with nucleofection-generated pseudoviruses for both the five-vector and two-vector model. Classical transfection, particularly when using reagents like PEI, is a well-established method that is generally less harsh on cells compared to nucleofection (Chong et al., 2021). Nucleofection involves the use of electrical pulses to introduce DNA into cells, which can be more efficient, but also more stressful to the cells, potentially leading to higher cell death and lower cell viability (Đorđević et al., 2022). This stress can reduce the number of viable cells capable of producing pseudovirus, thereby lowering the overall titres observed for nucleofection in **Figures 2.6** and **2.7**. Additionally, classical transfection methods allow for more gradual uptake of DNA, which can result in more stable and sustained expression of the transfected genes. This is particularly important for the production of pseudoviruses, where the coordinated expression of multiple plasmids is required (Chong et al., 2021). In this study, only two technical replicates per condition were carried out which may

potentially skew the results observed. The addition of three replicates instead of two would provide a more accurate average of the infection titre for each condition. Another important consideration in the generation of high-titre pseudoviruses is the choice between multi-vector and two-vector designs. The multi-vector design involves the use of multiple plasmids, each encoding different components necessary for pseudovirus assembly, namely the structural proteins, regulatory proteins, and the envelope protein outlined in **section 2.1**. The multi-vector system can be more complex and challenging to optimize, as it requires the co-transfection of several plasmids in precise ratios. For nucleofection in particular, the total volume of plasmid DNA, as per the Amaxa™ 4D-Nucleofector™ kit manufacturer's protocol, cannot exceed 10 µl which may prove difficult when handling multiple plasmid types. This can lead to lower transfection efficiency, as the likelihood of each cell taking up all necessary plasmids decreases with the number of plasmids being used (Carreño et al., 2024). In contrast, the two-vector design simplifies the transfection process by reducing the number of plasmids required. Typically, one plasmid encodes the envelope protein, while the other encodes the core and accessory proteins necessary for pseudovirus assembly. This approach can enhance transfection efficiency, as cells are more likely to take up both plasmids, leading to higher overall pseudovirus production (Carreño et al., 2024). The reduced complexity also minimizes the risk of recombination events, enhancing the safety profile of the pseudovirus system.

2.4.2. Future recommendations

Given that the use of a lentiviral packaging system used in this study generated low-titre pseudoviruses, using alternative pseudoviral packaging systems, such as VSV-G or MLV, may generate higher titre pseudoviruses. In addition, testing different SARS-nCoV-2 spike variants, as opposed to the wildtype spike used in this study, may offer enhanced immunogenicity.

2.5. Conclusion

In terms of safety, both pseudovirus designs are generally considered safe for use in biosafety level 2 laboratories, provided that the plasmids are carefully designed to eliminate any sequences that could enable replication (Crawford et al., 2020). The multi-vector system may require more rigorous validation to ensure that no unintended recombination events occur. On the other hand, the two-vector system, with its simpler design, may be easier to validate and monitor for safety. The choice between multi-vector and two-vector designs largely depends on the requirements of the study in question. While the pseudovirus approach for developing an assay to measure $CD8^+$ T cell responses to SARS-nCoV-2 did not yield an ideal titre, valuable insights were gained into the complexities of implementing a pseudovirus-based approach.

CHAPTER 3: A CFSE-BASED KILLING ASSAY TO MEASURE T CELL RESPONSES TO SARS-nCoV-2 VACCINATION

3.1. Introduction

For the pseudovirus-based direct killing assay, the aim was to co-culture $CD8^+$ T cells with pseudovirus-infected target cells. The specific killing of the target cell population would have been measured *in vitro* by tracking the loss of fluorescence, indicating the elimination of the target cells. As detailed in Chapter 2, the assays relied on a robust fluorescence readout to allow for the quantification of the killing activity. In this instance, a sufficient pseudovirus fluorescence signal was not achieved to allow for an accurate measurement of killing activity. Therefore, the lack of a robust readout signal in the pseudovirus approach prompted the adoption of an alternative fluorescent dye-based method for developing the CTL killing assay. This approach has been shown to produce a much stronger and more reliable signal, enabling the detection of CTL killing of labelled targets with greater sensitivity and reliability (Riss et al., 2004, Ingulli, 2007, Parish et al., 2009, Ndhlovu et al., 2019). One of the most commonly used fluorescent dyes for tracking cells *in vivo* is carboxyfluorescein diacetate succinimidyl ester (CFSE) which is able to passively diffuse into the cytoplasm of cells where it is cleaved by enzymes and becomes highly fluorescent as a result (Ingulli, 2007, Dalgaard et al., 2010). The CFSE dye conjugates with intracellular proteins and is retained in the cells without leakage, making it a versatile tool in the development of cytotoxicity assays without interfering with cellular functions (Ingulli, 2007).

CFSE is well-documented as a useful proliferation marker as the dye is long-lived and is distributed evenly among daughter cells upon cell division allowing resolution of up to eight to eleven rounds of cell division by flow cytometry (Quah et al., 2012, Lyons et al., 2013). The use of CFSE was originally described for studies of lymphocyte migration where purified spleen cells were labelled with CFSE and the proliferation of CFSE-labelled cells was expressed as a percentage of the response obtained with unlabelled cells (Weston and Parish, 1990). Here, labelled lymphocytes were detected by flow cytometry after intravenous injection into mice and it was observed that these labelled lymphocytes were detectable up to eight weeks post injection, making CFSE ideal for long term *in vivo* migration studies (Weston and Parish, 1990, Parish et al., 2009). More recently, Terrén et al. (2020) has described a protocol for the labelling and analysis of proliferation for human T and natural killer (NK) cells using CFSE. This involves preparing a stock solution of CFSE and then incubating the cells in a working solution of CFSE after which they are washed with fetal bovine serum (FBS) and cultured in medium under various conditions, with unstained cells serving as controls for proliferation analysis (Terrén et al., 2020). Similarly, Lyons et al. (2013) described a CFSE proliferation assay in which a single-cell suspension of the cells of interest were labelled with CFSE after which they were washed with the appropriate culture medium twice to ensure the removal of CFSE bound to protein within the supernatant, preventing any uptake of CFSE into bystander cells (Lyons et al., 2013).

Gaiha et al. (2019) and Collins et al. (2021) have also employed proliferation assays to measure the proliferation of $CD8^+$ T cells when exposed to HLA-optimal HIV peptides. Here, the individual HLA-optimal HIV peptides which were tailored to each participant's genotype were introduced to CFSE-labelled mononuclear cells and incubated at 37°C for six days after which they were assessed by flow cytometry. For this experiment, a negative control of cells which were not exposed to the peptides were included and positive controls included cells with anti-CD3 and anti-CD28 antibodies (Collins et al., 2021). Responses were assessed by the reduction of the fluorescence signal. The results revealed that HIV-specific CD8+ T cell proliferation is progressively and selectively impaired in individuals who experience aborted viral control (AC), compared to those with durable control (DC) (Collins et al., 2021). In addition to proliferation assays, CFSE-based cytotoxicity or killing assays have been employed in an array of studies owing to their advantages over traditional killing assays. Given that CFSE is a long-lived dye, this is particularly advantageous when assessing the killing activity of effector cells, for example $CD8^+$ T cells, over longer periods as opposed to the conventional 4-hour chromium-release killing assay (Brunner et al., 1968). Furthermore, the ability to measure cytotoxic responses over longer periods may offer insights into apoptotic pathways which act slowly, compared to rapid perforin-mediated cell death (Jedema et al., 2004).

3.1.1. CFSE-based killing assays

Jedema et al. (2004) has described a CFSE-based cytotoxicity assay used in monitoring immune responses against leukemic cells. The target cell populations were peripheral blood from a patient with acute myeloid leukaemia (AML) labelled with CFSE. After terminating the CFSE labelling reaction with fetal calf serum (FCS) and subsequent wash steps, the cells were plated in a 96-well plate at a concentration of ~5×10^4 cells per well. Thereafter, cytotoxic T lymphocytes (CTLs) were added at various effector-to-target cell ratios and incubated at 37°C. For this particular assay, specific antibodies were added to the cells and stained at different intervals (4 h, 24 h, 48 h and 72 h) before being analysed by flow cytometry. Here, the percentage survival at each of the time points was calculated by dividing the absolute number of viable CFSE-positive target cells by the absolute number of viable CFSE-positive target cells before the addition of CTLs, then multiplying the result by 100 (Jedema et al., 2004). This assay was particularly relevant in that it allowed for precise quantification of viable leukemic cells over time, demonstrating the dynamics of CTL-induced cell death over longer periods (Jedema et al., 2004). A similar assay involving K562 leukaemia cells, which were used as target cells, interestingly noted that labelling the K562 target cells with CFSE while the effector cells, lymphokine-activated killer (LAK) cells, were labelled with CellTrace Violet did not result in any cross-staining between the two cell populations during co-culturing when analysed by flow cytometry (Wu et al., 2021). This emphasized the versatility of CFSE when used in conjunction with other cellular dyes in the design of cytotoxicity assays.

In another study, Choi et al. (2019) has described a cytotoxicity assay in which mice were treated with antibodies to deplete regulatory T cells (Treg) or to block PD-1 interactions before being primed with C57SV fibrosarcoma cell line. Splenocytes were then recovered from the mice and pulsed with either irrelevant peptides or cognate peptides to create target cells after which they were labelled with different concentrations of CFSE to differentiate the peptides with which the cells were pulsed (Choi et al., 2019). The CFSE-labelled cells were then injected into the mice and after four hours, the mice were euthanized and the spleens were processed to analyse the CFSE-labelled target cells. Flow cytometry was then used to quantify the distinct CFSE-labelled target cell populations, allowing the specific lysis of each target cell population to be calculated (Choi et al., 2019). This cytotoxicity assay revealed the specific killing ability of CTLs in an *in vivo* setting, reflecting the actual number of antigen-specific CTLs (Choi et al., 2019). Barber et al. (2003), Byers et al. (2003) and Ingulli (2007) have also carried out cytotoxicity assays using mice and have demonstrated the mechanisms of target cell destruction by $CD8^+$ T cells *in vivo*. Choi et al. (2019) demonstrated that using CFSE at different concentrations to label cells allowed for the distinction between cell populations based on the addition of peptides. Additionally, Noto et al. (2013) described a cytotoxicity assay in which effector $CD8^+$ and target $CD4^+$ T cells were magnetically isolated. Here, the $CD4^+$ target cells were labelled with a low concentration and a high concentration of CFSE after which the low CFSE-labelled $CD4^+$ target cells were pulsed with a peptide of interest (Noto et al., 2013). To measure basal apoptosis, separate control wells were included with target cells alone during the effector and target cell co-culture phase and the cytolytic activity of antigen-specific $CD8^+$ cells was measured by flow cytometry.

Ndhlovu et al. (2019) employed a similar approach in the design of a CFSE-based killing assay to measure $CD8^+$ T cell responses in people living with HIV (Ndhlovu et al., 2019). This killing assay measured the ability of effector $CD8^+$ T cells to selectively kill target cells that were loaded with HIV-specific peptides. In this assay, autologous $CD4^+$ T cells were divided into two groups and labelled with different concentrations of CFSE (termed "$CFSE_{high}$" and "$CFSE_{low}$") to distinguish them. One group was pulsed with HLA class I matched optimal peptides, while the other group served as a control with irrelevant peptides. In the context of HIV, optimal peptides are known to be effectively presented by the individual's HLA class I molecules and are recognized by HIV-specific $CD8^+$ T cells. The irrelevant peptides are sequences of amino acids which are not recognized by the $CD8^+$ T cells specific to HIV. Target cells were then mixed and co-cultured with $CD8^+$ T cells at a 1:1 effector-to-target ratio. After a 4-hour incubation, the cells were analysed using flow cytometry to determine the selective elimination of antigen-presenting target cells. The killing capacity of the $CD8^+$ T cells was then calculated based on the percentage reduction of viable antigenic cells compared to control cells.

In designing a CFSE-based killing assay to measure $CD8^+$ T cell responses to SARS-nCoV-2 vaccination between people living with HIV (PLWH) and people living without HIV (PLWoH), a similar experimental design used by both Noto et al. (2013) and Ndhlovu et al. (2019) was utilized for this research project. The CFSE-based killing assay outlined in **Figure 3.1.** involves stimulating peripheral blood mononuclear cells (PBMCs) from SARS-nCoV-2-vaccinated individuals with SARS-nCoV-2-specific peptides of interest and expanding the cells over two weeks. After expansion, the $CD8^+$ T cells are then captured using magnetic beads after which the remaining lymphocytes, are labelled with two concentrations of CFSE to allow for their distinction during flow cytometry. One cell population is pulsed with SARS-nCoV-2-specific peptides while the other serves as a control population. Following the addition of the effector $CD8^+$ T cells at different effector-to-target cell ratios and an overnight incubation period, flow cytometry can be carried out to assess antigen-specific killing by the $CD8^+$ T cells. This assay may offer novel insights into the differences in cytotoxic potential of $CD8^+$ T cells between PLWH and PLWoH in a vaccinated cohort.

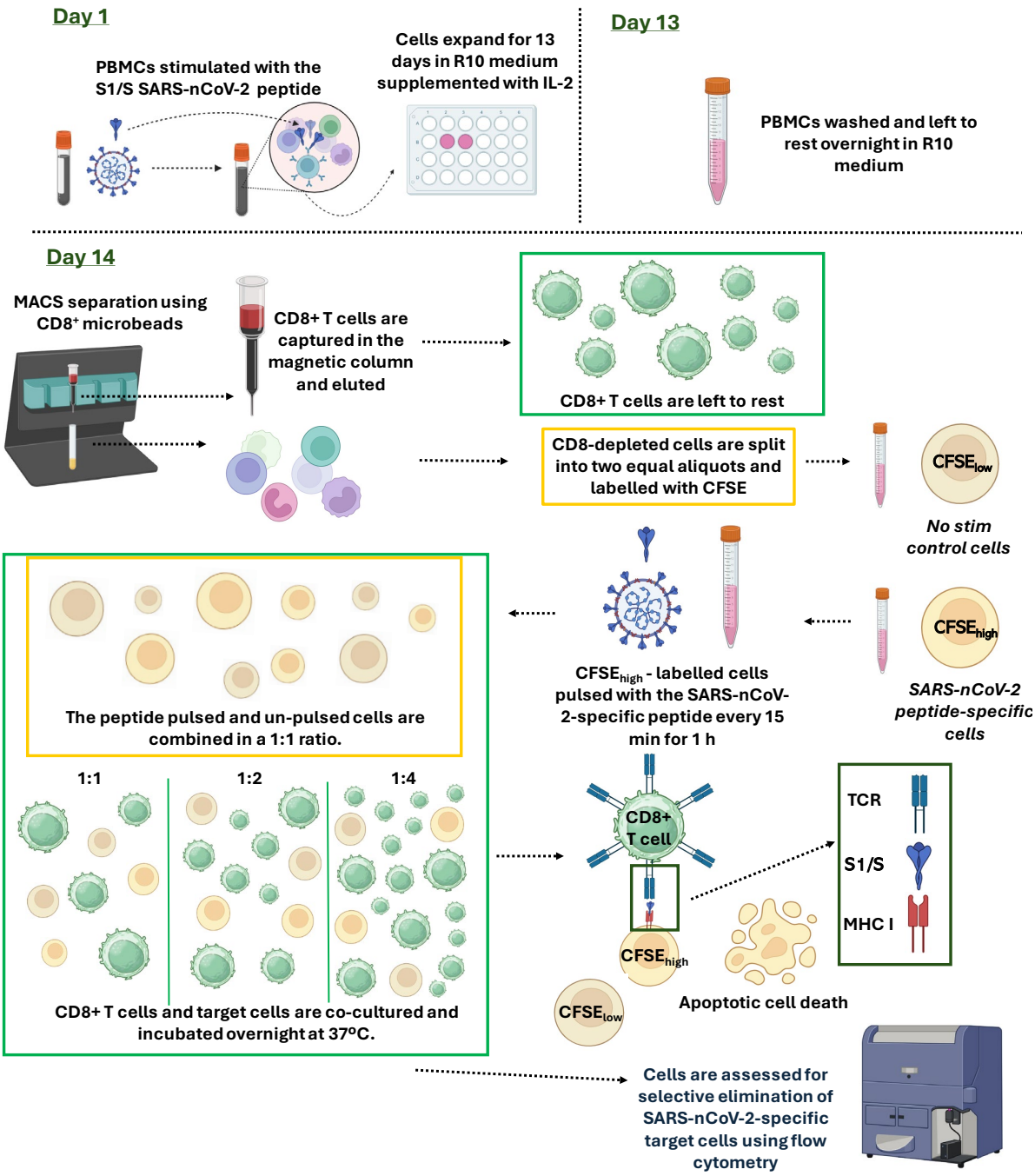

Figure 3.1.: Overview of the optimized CFSE-based killing assay to measure SARS-nCoV-2 specific $CD8^+$ T cell responses. The process begins on Day 1 with the stimulation of PBMCs using SARS-nCoV-2 peptides and continues until Day 13 with the expansion of cells in R10 medium supplemented with IL-2. On Day 14, $CD8^+$ T cells are isolated using MACS separation and then co-cultured with CFSE-labelled target cells that are either pulsed with the same SARS-nCoV-2-specific peptide or left un-pulsed. The assay setup includes various effector-to-target cell ratios (1:1, 1:2, 1:4) to determine optimal cytotoxicity, followed by flow cytometric analysis to assess the selective elimination of SARS-nCoV-2 peptide-specific target cells, reflecting the cytotoxic capability of the $CD8^+$ T cells.

Hypothesis:

Labelling target cells with different concentrations of CFSE, will provide a robust readout to measure killing by cytotoxic $CD8^+$ T cells. It is expected that this will demonstrate differential responses between people living with HIV (PLWH) and people living without HIV (PLWoH) who have been vaccinated against SARS-nCoV-2.

Aim:

To develop an optimized CFSE-readout killing assay to measure $CD8^+$ T cell responses against SARS-nCoV-2-specific target cells co-cultured with $CD8^+$ T cells isolated from PBMCs of PLWH and PLWoH vaccinated against SARS-nCoV-2.

Objectives:

1. Optimise CFSE labelling conditions and co-culture conditions using HIV-specific killing as a model $CD8^+$ T cell response system.
2. Optimize SARS-nCoV-2 spike peptide pulsing for *ex vivo* and T cell-expanded killing assays.
3. Determine optimal effector-to-target cell ratios to achieve robust cytotoxicity measurements.
4. Compare robustness of assay readouts under *ex vivo* with that of T cell expansion conditions.
5. Perform the optimized killing assay on PBMCs of multiple COVID-19-vaccinated participants.

3.2. Materials and methods

3.2.1. Study participants and sample collection

Optimization of CFSE labelling and co-culture conditions for the killing assay was conducted using PBMCs from study participants recruited in the HIV Pathogenesis Programme (HPP) Acute and Elite Controller cohorts and the FRESH (Females Rising through Education, Support, and Health) cohort. To assess the optimized killing assay, PBMCs were collected from study participants recruited in the Botswana-Harvard AIDS Institute Partnership (BHP) COVID-19 vaccine study. The BHP participants were all vaccinated against COVID-19 with either the AZD1222 (Oxford/AstraZeneca), Coronavac (Sinovac) or Ad26.COV2.S (Johnson and Johnson) vaccine. Written informed consent was obtained from all study participants. All samples were stored in liquid nitrogen at the AHRI Biorepository. Sample collection was approved by Biomedical Research Ethics Committee (BREC) at the University of KwaZulu-Natal.

3.2.2. General workflow of ex vivo CFSE killing assay

PBMCs were thawed and rested for 2 h at 37°C in 5% CO_2. Magnetic activated cell sorting (**section 3.2.6**), CFSE staining (**section 3.2.7**), peptide pulsing (**section 3.2.8**) and co-culturing (**section 3.2.9**) were performed and the cells were incubated for 16 to 18 h overnight at 37°C in 5% CO_2. The following day, antibody staining (**section 3.2.10**) was performed and $CD8^+$-mediated killing was quantified (**section 3.2.11**).

3.2.3. General workflow of CFSE killing assay for expanded T cells

On Day 1 of expansion, PBMCs were stimulated with either HIV-specific or SARS-nCoV-2-specific peptide pools in a 96-well plate overnight at 37°C in 5% CO_2. The cells were transferred to a 24-well plate the following day and fed with R10 medium supplemented with IL-2 every two to three days. On day 13 of expansion, expanded PBMCs were washed once with 10 ml fresh R10 medium and left to rest overnight at 37°C in 5% CO_2. After resting overnight, magnetic activated cell sorting (**section 3.2.6**), CFSE staining (**section 3.2.7**), peptide pulsing (**section 3.2.8**) and co-culturing (**section 3.2.9**) were performed and the cells were incubated for 16 to 18 h overnight at 37°C in 5% CO_2. The following day, antibody staining (**section 3.2.10**) was performed and $CD8^+$-mediated killing was quantified (**section 3.2.11**).

3.2.4. T cell expansion for PBMCs from PLWH

To expand HIV antigen-specific T cell populations, peripheral blood mononuclear cells (PBMCs) isolated from PLWH were stimulated with 20 µl each of 20 µM HIV Clade C Global Pool comprised of eight peptide pools spanning the HIV genome. This was carried out in a 96-well plate and incubated at 37°C in 5% CO_2 overnight. The cultured cells were then moved to a 24-well plate and were fed two to three times weekly with RPMI 1640 medium supplemented with heat-inactivated fetal bovine serum (FBS), 1% penicillin/streptomycin, 1% HEPES buffer and 1% L-glutamine (Gibco, Schwerte, Germany) and 100 U recombinant IL-2 (Miltenyi Biotec, Bergisch Gladbach, Germany). On Day 13 of expansion, the cells were washed twice with fresh medium, not containing IL-2 (R10 medium), and left to rest at 37°C in 5% CO_2 overnight.

3.2.5. T cell expansion for PBMCs from participants vaccinated against COVID-19

To expand SARS-nCoV-2 antigen-specific T cell populations, peripheral blood mononuclear cells (PBMCs) isolated from individuals vaccinated against SARS-nCoV-2 were stimulated with 3 µl each of SARS-nCoV-2 S and S1 (wildtype – WT, 2 µg/ml) (Miltenyi Biotec, Bergisch Gladbach, Germany) in a 96-well plate and incubated at 37°C in 5% CO_2 overnight. The cultured cells were then moved to a 24-well plate and were fed two to three times weekly with RPMI 1640 medium supplemented with heat-inactivated fetal bovine serum (FBS), 1% penicillin/streptomycin, 1% HEPES buffer and 1% L-glutamine (Gibco, Schwerte, Germany) and 100 U recombinant IL-2 (Miltenyi Biotec, Bergisch Gladbach, Germany). On Day 13 of expansion, the cells were washed twice with fresh medium, not containing IL-2 (R10 medium), and left to rest at 37°C in 5% CO_2 overnight.

3.2.6. Magnetic activated cell sorting (MACS) for $CD8^+$ isolation

For both *ex vivo* and expanded T cell conditions, the $CD8^+$ T cells were isolated from PBMCs using $CD8^+$ microbeads (Miltenyi Biotec, Bergisch Gladbach, Germany) as per the manufacturer's protocol. Briefly, the expanded cells were washed in R10 medium and centrifuged at 1800 rpm for 6 min. The cells were counted and the washing step was repeated with 2% MACS buffer (2% bovine serum albumin (BSA) (Sigma, Munich, Germany) in phosphate buffered saline (PBS) (Gibco, Schwerte, Germany)). The supernatant was decanted and resuspended in 80 µl MACS buffer with 20 µl $CD8^+$ microbeads. The volumes of buffer and beads were adjusted accordingly, depending on whether the cell counts obtained for the sample were greater than 1×10^7 cells. The solution was incubated at 4°C for 15 min after which 1 ml MACS buffer was added to the cells and centrifuged at 300 ×*g* for 10 min in a pre-cooled 4°C centrifuge. The supernatant was discarded and the cells were resuspended in 500 µl MACS buffer.

3.2.6.1. Magnetic separation

The MACS column (Miltenyi Biotec, Bergisch Gladbach, Germany) was placed in the magnetic field of a magnetic separation stand and rinsed with 1 ml MACS buffer to prevent drying out of the column. The cells were placed in the column, allowed to run through and collected in a clean 15 ml Falcon tube (Gibco, Schwerte, Germany). To ensure a higher purity of $CD8^+$ T cells, the cells were run through the column a second time and collected. The $CD8^+$ depleted cells were flushed with 6 ml MACS buffer and set aside. The $CD8^+$ T cells were eluted in a separate 15 ml Falcon tube by removing the column from the magnetic stand, placing 5 ml MACS buffer into the column and firmly pushing the plunger into the column.

3.2.7. CFSE staining of target cells

Staining with CFSE (ThermoFisher Scientific, Eugene, Oregon, United States) allows for separation of the two populations on flow plots based on the CFSE signal intensity. Following magnetic separation, the $CD8^+$ depleted cells and $CD8^+$ enriched cells were centrifuged at 1800 rpm for 6 min. The $CD8^+$ enriched cells were resuspended in 1 ml fresh R10 medium and left to rest at 37°C in 5% CO_2. The $CD8^+$ depleted cells were washed twice in 10 ml PBS and centrifuged at 1800 rpm for 6 min. The supernatant was discarded and the cells were separated into two equal aliquots. One aliquot was stained with a high concentration of CFSE ($CFSE_{high}$) and the other aliquot with a low concentration of CFSE ($CFSE_{low}$) for 7 min at 37°C in 5% CO_2. The standardised concentrations for the $CFSE_{high}$ and $CFSEl_{ow}$ dyes were 0.2 µg/µl and 0.001 µg/µl, respectively. On the day of staining, 1 µl of the CFSE stock (1 µg/µl) was diluted in 4 µl dimethyl sulfoxide (DMSO), after which 1 µl of the 0.2 µg/µl working stock was added to 6 ml PBS to make up the $CFSE_{high}$ labelling solution. To make up the $CFSEl_{ow}$ labelling solution, 1 µl of the CFSE stock (1 µg/µl) was diluted in 999 µl PBS, after which 1 µl of the 0.001 µg/µl working stock was added to 6 ml PBS. To terminate the CFSE staining reaction, 2 ml filtered heat-inactivated FBS (Gibco, Schwerte, Germany) was added to each stained aliquot and inverted before centrifugation at 1800 rpm for 6 min. The cells were washed twice with 10 ml fresh R10 medium after which the $CFSE_{low}$ cells were left to rest in 1 ml fresh R10 medium at 37°C in 5% CO_2.

3.2.8. Peptide pulsing

For both *ex vivo* and expanded T cell conditions, the $CFSE_{high}$-labelled cells were resuspended in fresh R10 medium in a 96-well plate. Based on the available cell quantity, an aliquot of cells was allocated to the un-pulsed target cell control well.

3.2.8.1. Peptide pulsing for PBMCs from PLWH

The $CFSE_{high}$-labelled cells were resuspended in 180 µl fresh R10 medium in a single well of a 96-well plate. To induce stimulation, 20 µl of 20 µM HIV Clade C Global Pool was added to the cells. The cells were mixed by gently pipetting up and down. The cells were then placed in the incubator for a total of 1 hr, with intermittent pipetting every 15 min. Following the incubation period, the cells were washed with 10 ml of R10 media, counted, and centrifuged at 1800 rpm for 6 min to eliminate the peptide. The supernatant was decanted, and the cells were resuspended in 1 ml of media per 1 million cells.

3.2.8.2. Peptide pulsing for PBMCs from participants vaccinated against COVID-19

The $CFSE_{high}$-labelled cells were resuspended in 194 µl fresh R10 medium in a single well of a 96-well plate. To induce stimulation, 3 µl each of PepTivator® SARS-CoV-2 Prot_S (2 µg/ml) and PepTivator® SARS-CoV-2 Prot_S1 (2 µg/ml) were pooled and added to the cells. The cells were mixed by gently pipetting up and down. The cells were then placed in the incubator for a total of 1 hr, with intermittent pipetting every 15 min. Following the incubation period, the cells were washed with 10 ml of R10 media, counted, and centrifuged at 1800 rpm for 6 min to eliminate the peptides. The supernatant was decanted, and the cells were resuspended in 1 ml of media per 1 million cells.

3.2.9. $CD8^+$ T cell and target cell co-culture

Following peptide pulsing, and resuspension of cells in R10 media (1 ml per million cells), the $CFSE_{high}$ and $CFSE_{low}$ cell populations were combined in a 1:1 ratio. These cells constituted the target cells, and a constant amount of this mixture was added to each experimental condition. Specifically, 100 µl of target cells, totalling 1×10^5 cells, were added to each well. The introduction of $CD8^+$ T cells was performed differentially based on the following target-to-effector cell ratios describe in **Table 3.1** below. Control wells were prepared by adding $\sim 1 \times 10^5$ target cells only to a separate well. This was also carried out for the un-pulsed target controls $\sim 1 \times 10^5$ $CD8^+$ T cells were added. The cells were incubated for 16 to 18 h overnight at 37°C in 5% CO2. Replicate conditions were included depending on cell availability. The cells were incubated for 16 to 18 h overnight at 37°C in 5% CO_2.

Table 3.1: Amount of cells allocated for each target-to-effector cell ratio during co-culture

Target-to-effector (T:E) ratio	**Amount of CFSE-labelled (target) cells per well**	**Amount of $CD8^+$ T (effector) cells per well**
1:1	$\sim 1 \times 10^5$	$\sim 1 \times 10^5$
1:2	$\sim 1 \times 10^5$	$\sim 2 \times 10^5$
1:3	$\sim 1 \times 10^5$	$\sim 3 \times 10^5$
1:4	$\sim 1 \times 10^5$	$\sim 4 \times 10^5$

3.2.10. Antibody staining and FACS readout of killing

Following the overnight incubation period, the plate was centrifuged at 2000 rpm for 6 min to pellet the cells. A surface antibody cocktail was prepared, with Live/Dead fixable aqua dead cell stain, anti-CD3 Brilliant Violet (BV) 711 (BioLegend, CA, United States), anti-CD4 BV650 (BD BioSciences, Franklin Lakes, NJ) and anti-CD8 (BV786) (BD BioSciences, Franklin Lakes, NJ). The supernatant from each well was decanted, and 40 µl of the surface antibody cocktail was added to each well. The plate was then incubated at room temperature for 20 min, with the entire plate covered in foil to maintain the integrity of the fluorescent labels. Following the incubation period, the cells were resuspended in 150 µl of 2% FBS in PBS per well and centrifuged at 2000 rpm for 6 min. The supernatant was decanted, and the cells were resuspended in 150 µl of PBS, supplemented with an additional 150 µl to ensure all cells were being decanted from the wells. The resuspended cells were then transferred to appropriately labelled cluster tubes and FACS tubes for analysis via flow cytometry on the LSRFortessa™ (BD BioSciences, Franklin Lakes, NJ). The initial gating on FSC-A vs. SSC-A selected the lymphocyte population based on cell size and granularity. Using FSC-H vs. FSC-A allowed for the exclusion of doublets, ensuring that only single cells are analysed. The next gate distinguished live cells from dead cells and subsequent gating on $CD3^+$ cells identified the T cell population. Within the T cell population, cells were further gated to distinguish between $CD4^+$ ($CD3^+CD4^+$) and $CD8^+$ T cells ($CD3^+CD8^+$). The CFSE fluorescence intensity was measured to identify the CFSE-labelled target cells that were subject to $CD8^+$ T cell-mediated killing.

3.2.11. Killing index quantification and statistical analyses

Killing index quantification was determined by generating killing curves for different participants and plotting the percentage elimination rate of target cells at various target-to-effector (T) ratios. The percentage elimination was calculated based on the following equation:

$$\frac{\%\ \text{CFSEhigh cells in No CD8 control} - \%\ \text{CFSEhigh cells in experimental condition}}{\%\ \text{CFSEhigh cells in No CD8 control}} \times 100$$

The killing curves were then generated and statistical analyses were performed using GraphPad Prism 10.0.3 (GraphPad Software, Inc, San Diego, CA. Analysis was carried out using simple linear regression to establish the effectiveness of $CD8^+$ T cell-mediated killing. The slope of the regression line, or gradient, represented the killing efficiency whereby a steeper slope indicated a higher killing capacity. This method allowed for a comparison of cytotoxic responses between different individuals or groups, such as people living with HIV (PLWH) and people living without HIV (PLWoH), vaccinated against SARS-nCoV-2.

3.3. Results

3.3.1. Optimization of CFSE dilutions for labelling of target cell populations

In order to measure direct killing of antigen-specific target cells, two different concentrations of CFSE were used to differentially label identical proportions of peptide-pulsed, $CD8^+$-depleted cells and un-pulsed $CD8^+$-depleted cells; with antigen-specificity being exhibited by autologous $CD8^+$ T cells only, reducing the number of peptide-pulsed cells, while un-pulsed cells remain constant. To achieve this differential fluorescence readout, $CFSE_{low}$ and $CFSE_{high}$ concentrations were arbitrarily assigned to un-pulsed and pulsed target cell respectively. Optimizing the respective concentrations of CFSE for labelling of target cells is therefore critical for accurate discrimination between the un-pulsed ($CFSE_{low}$) and pulsed ($CFSE_{high}$) populations ensures that the two target cell populations can be identified and analysed in flow cytometry, as carried out by Noto et al. (2013) and Ndhlovu et al. (2019). The precision in CFSE labelling directly affects the ability to measure selective killing of peptide-pulsed target cells by $CD8^+$ T cells. Insufficient or excessive concentrations CFSE may lead to overlapping signal intensities, thereby compromising the assay's accuracy. By establishing the optimal dilutions of CFSE necessary to distinguish between the peptide pulsed and un-pulsed populations, the sensitivity and specificity of the $CD8^+$ T cell killing assay is enhanced. This optimization is crucial for obtaining valid and reproducible results, which are important for the analysis of $CD8^+$ T cell-mediated cytotoxicity.

3.3.1.1. Determining optimal $CFSE_{low}$ dilution factor

As previously emphasised, determining the optimal $CFSE_{low}$ dilution is necessary to ensure accurate discrimination between un-pulsed, $CFSE_{low}$ and pulsed $CFSE_{high}$ labelled target cells in cytotoxicity assays. In this test, a standard working solution of $CFSE_{high}$ (1.67×10^{-4} µg/µl), was prepared by mixing 1 µl of 1 µg/µl stock CFSE with 6 ml of PBS, intended for achieving a high fluorescence intensity. This served as the base solution for subsequent dilutions. For the first dilution, 100 µl of the $CFSE_{high}$ stock solution was transferred into a new tube containing 900 µl of PBS, resulting in a 1:10 dilution intended to reduce the fluorescence intensity, thereby creating the first $CFSE_{low}$ population. This was repeated as 1:10 serial dilutions to achieve a 1:100 dilution and 1:1000 dilution respectively. It was expected that the $CFSE_{low}$ population will exhibit a lower fluorescence intensity that does not overlap with the $CFSE_{high}$ population when the labelled cells were combined. The results in **Figure 3.2** showed a distinct separation in fluorescence intensities when the fluorescence data of 1:1000 CFSE dilution was overlayed with that of the standard $CFSE_{high}$ concentration, permitting differentiation between the two different cell populations (**Figure 3.2**) . Therefore, a 1:1000 dilution was applied as the $CFSE_{low}$ concentration in subsequent experiments.

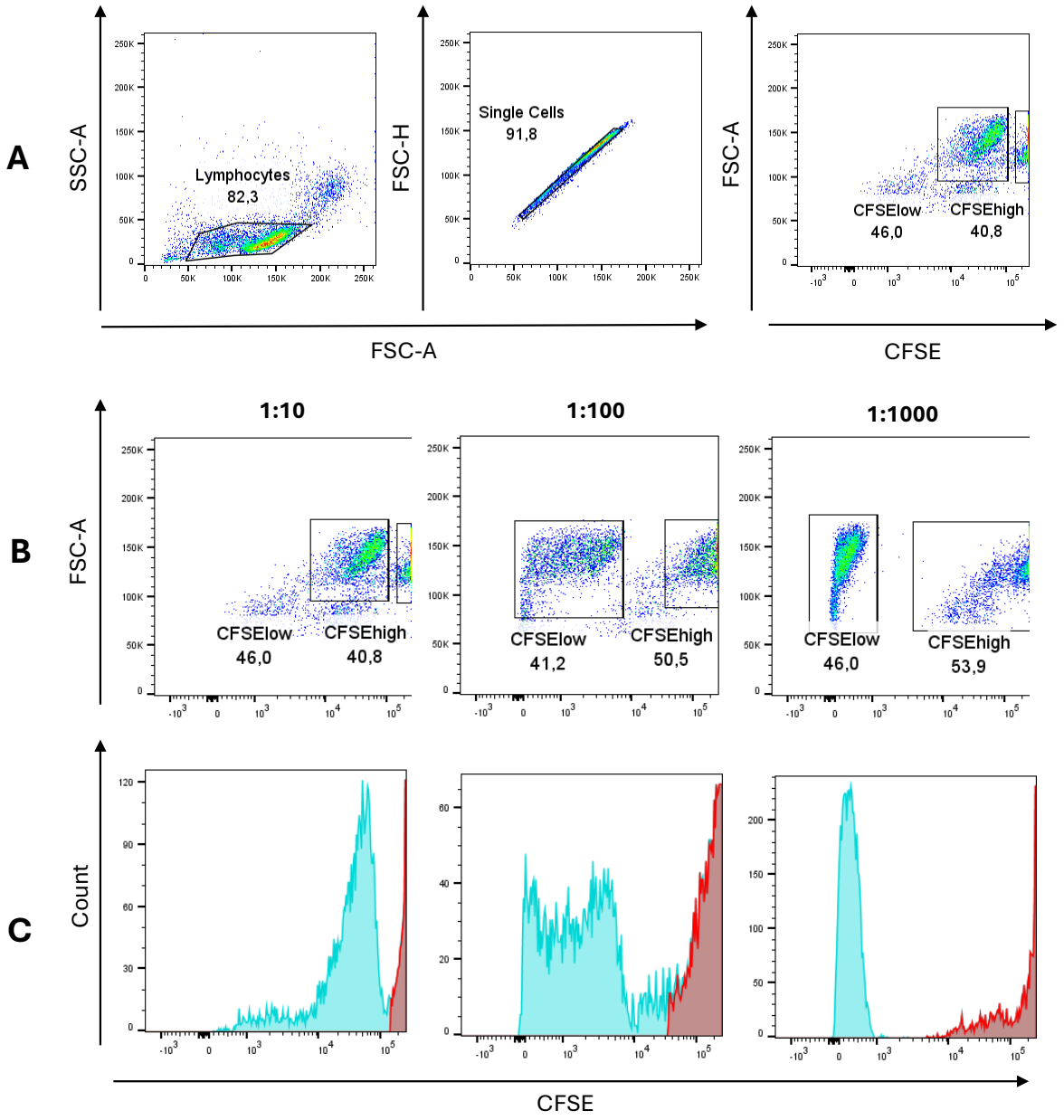

Figure 3.2: Optimisation of $CFSE_{low}$ concentration for differential labelling of peptide-pulsed and un-pulsed target cells. (**A**) Representative flow plot showing parent gating strategy, followed by differentiation between $CFSE_{low}$ and $CFSE_{high}$ populations based on CFSE fluorescence intensity for 1:10 dilution. (**B**) Analysis of $CFSE_{low}$ and $CFSE_{high}$ populations across various CFSE dilutions (1:10, 1:100, 1:1000), demonstrating the impact of dilution on the discrimination between differently labelled cell populations. (**C**) Histogram plots correlating with Panel B depicting analysis of $CFSE_{low}$ (blue) and $CFSE_{high}$ (red) populations across various CFSE dilutions (1:10, 1:100, 1:1000).

3.3.1.2. Determining optimal $CFSE_{high}$ dilution factor

In optimizing the dilution factor for the cells labelled with a low concentration of CFSE, it was observed that the signal intensity of the cells labelled with the standard stock concentration of CFSE was notably too high, beyond detectable limits when conducting flow cytometry analysis. Therefore, a $CFSE_{high}$ dilution series was assessed to optimise the appropriate $CFSE_{high}$ concentrations for quantifiable fluorescence intensity range for peptide-pulsed target cells. For this, the CFSE working volume was increased from 6 ml to 6.5 ml and 7 ml of PBS respectively to which 1 µl of CFSE (1 µg/µl) was added. The concentration for $CFSE_{low}$ was kept constant. It was observed that increasing the diluent volume to 6.5 ml produced a negligible change in the $CFSE_{high}$ fluorescence intensity compared to the standard protocol of 6 ml of PBS. Increasing the diluent to 7 ml PBS produced a distinct population, however a proportion of cells still produced fluorescence intensity beyond detection limits, requiring further optimization of $CFSE_{high}$ concentration (**Figure 3.3**).

Given that the fluorescence intensity of a proportion of $CFSE_{high}$ -labelled cells were still too high, the dye concentration was optimized by performing a dilution series of CFSE stock before further adding to 6 ml of PBS. The stock concentration of CFSE was serially diluted with dimethyl sulfoxide (DMSO) to make up a 1:10 and 1:100 dilution. Next, 1 µl of each CFSE dilution was added to separate tubes of PBS (6 ml). The concentration of $CFSE_{low}$ was kept consistent and an additional negative control, PBS with no CFSE, was added to validate that all CFSE labelled cells exhibited fluorescence above background. Following CFSE labelling, cells were stained with Live/Dead fixable aqua dead cell stain and CD3 antibodies, limiting the number of fluorescent channels to three (BV711, HV500 and FITC), taking care to limit the effect of spectral overlap compensation on the CFSE intensity. As depicted in (**Figure 3.4** (**A** – **D**)), the results of the CFSE staining across different dilutions including an unstained control in a population of lymphocytes showed that the standard stock concentration of CFSE was notably too high when labelling the cells. The 1:10 dilution, produced a reduced intensity within quantifiable ranges, yet still distinct from the $CFSE_{low}$ and unstained populations. At the 1:100 dilution, CFSE intensity began to overlap with that of the $CFSE_{low}$ population. Despite the 1:10 dilution showing a clear separation from the $CFSE_{low}$, the two populations were appearing notably close. Thus, an additional $CFSE_{high}$ dilution, a 1:5 dilution, was prepared and compared with the 1:10 dilution, as depicted in (**Figure 3.4** (**E**) and (**F**)). It was observed that the 1:5 dilution showed a clearer distinction from the $CFSE_{low}$ population when the cells were combined and stained for flow cytometry. Therefore, a 1:5 dilution was adopted as the stock concentration for the $CFSE_{high}$ cell population for subsequent experiments.

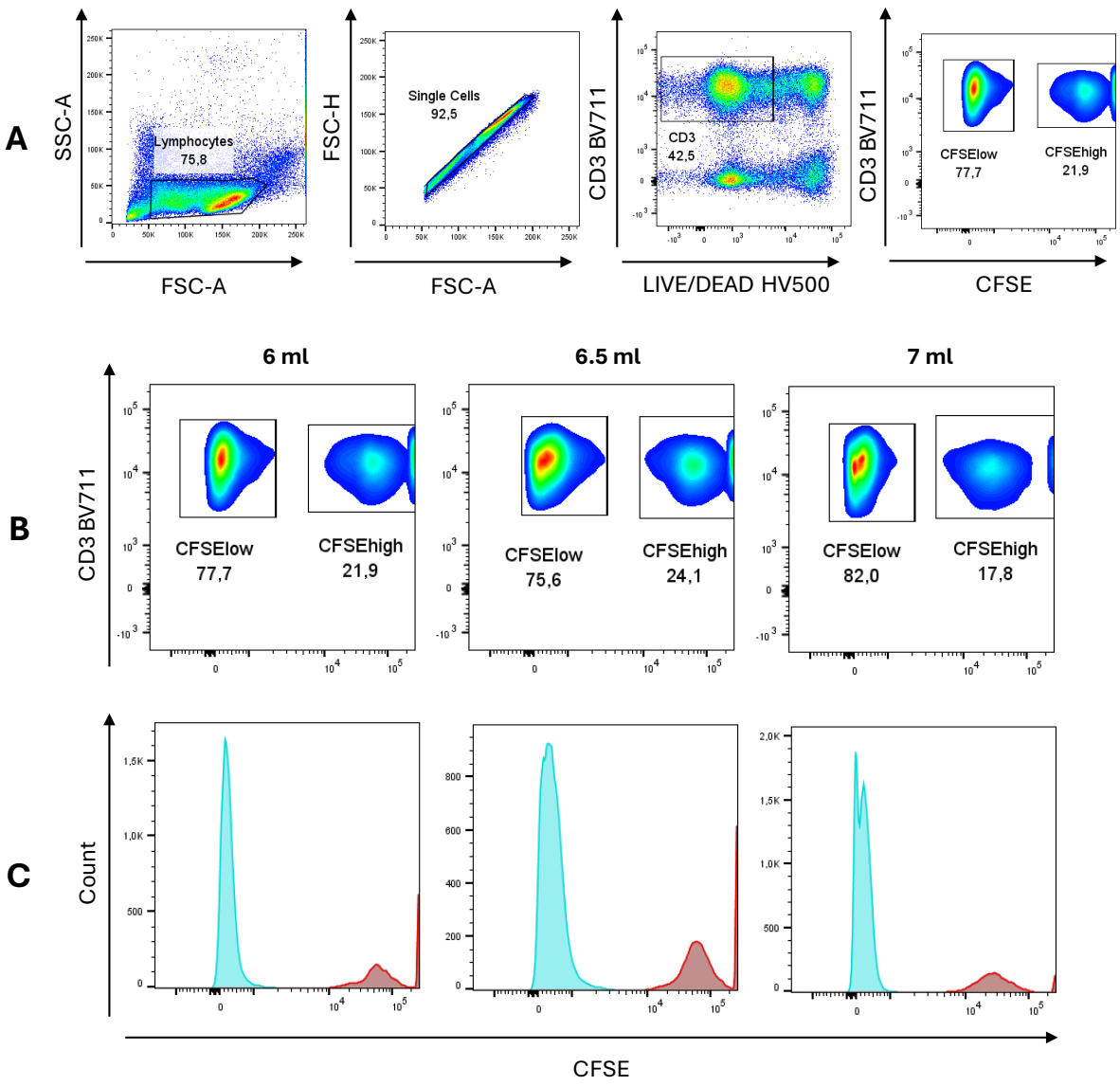

Figure 3.3.: Optimisation of $CFSE_{high}$ concentration for differential labelling of peptide-pulsed and un-pulsed target cells. (**A**) Representative flow plot showing gating strategy for identifying lymphocytes and single cells, followed by differentiation between $CFSEl_{ow}$ and $CFSE_{high}$ populations based on CFSE fluorescence intensity for cells stained with the standard CFSE stock concentration. (**B**) Analysis of $CFSE_{low}$ and $CFSE_{high}$ populations across various CFSE dilutions (6 ml, 6.5 ml, 7 ml), demonstrating the impact of dilution on the discrimination between differently labelled cell populations. (**C**) Histogram plots correlating with Panel B depicting analysis of $CFSE_{low}$ (blue) and $CFSE_{high}$ (red) populations across various CFSE dilutions (6 ml, 6.5 ml, 7 ml).

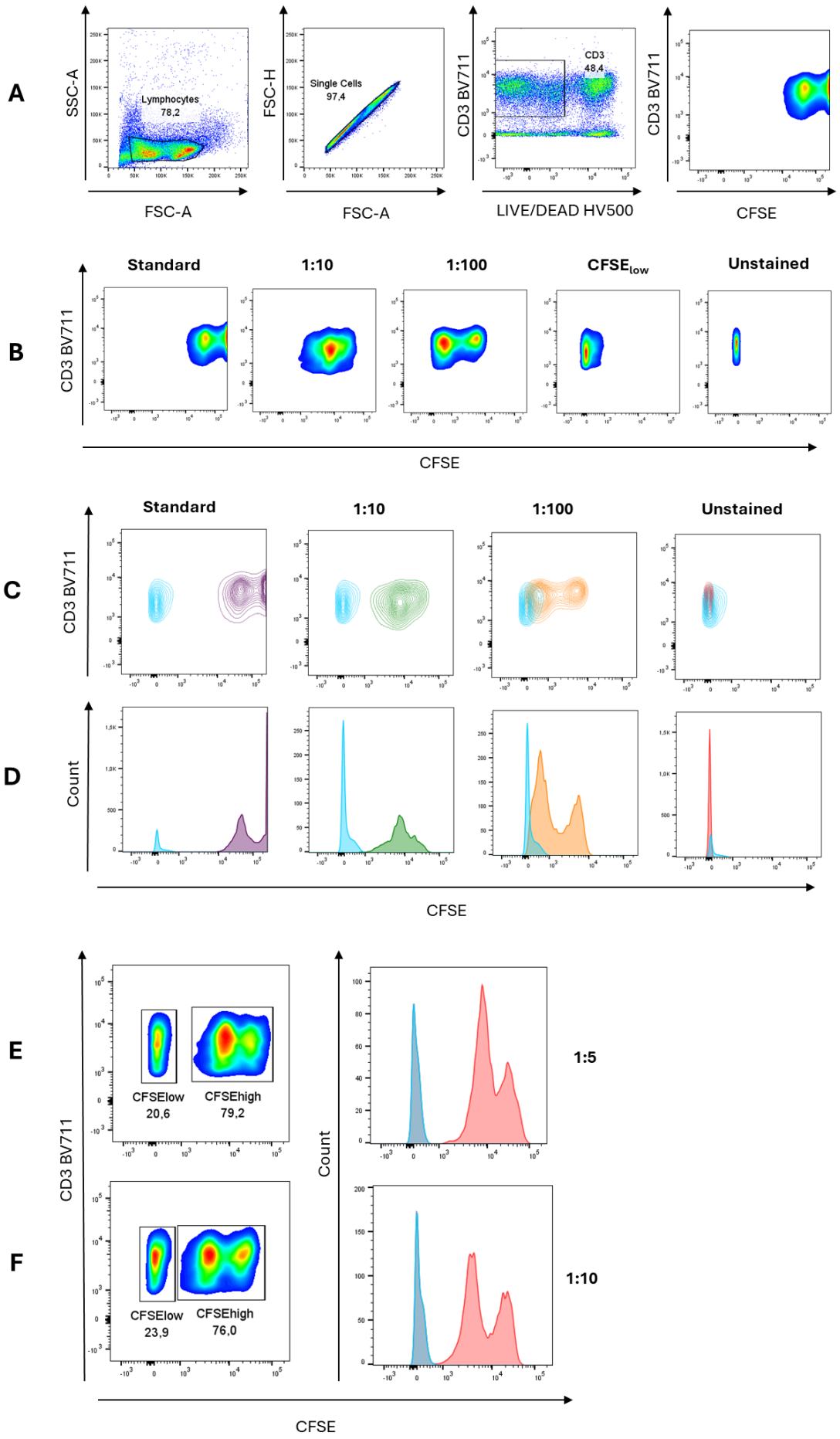
A
SSC-A
FSC-A
Lymphocytes
78,2
FSC-H
FSC-A
Single Cells
97,4
CD3 BV711
LIVE/DEAD HV500
CD3
48,4
CD3 BV711
CFSE
B
Standard
1:10
1:100
CFSElow
Unstained
CD3 BV711
CFSE
C
Standard
1:10
1:100
Unstained
CD3 BV711
D
Count
CFSE
E
CFSElow
20,6
CFSEhigh
79,2
1:5
F
CFSElow
23,9
CFSEhigh
76,0
1:10
CD3 BV711
Count
CFSE

Figure 3.4: Further optimisation of $CFSE_{high}$ concentration for differential labelling of peptide-pulsed and un-pulsed target cells. (**A**) Representative flow plots showing parent gating strategy and CFSE fluorescence intensity in live CD3+ cells (**B**) Scatter plots of CFSE intensity of CD3+ T cells across four different conditions: standard CFSE stock concentration, 1:10 dilution, 1:100 dilution, established $CFSE_{low}$ dilution and an unstained control, highlighting the impact of dilution on fluorescence intensity. (**C**) Superimposed contour plots showing the fluorescence intensity of the $CFSE_{high}$ labelled cells in relation to the $CFSE_{low}$ labelled cell population (in blue). (**D**) Histograms correlating with Panel C, quantifying the shifts in CFSE fluorescence across the different dilutions. (**E** + **F**) CFSE fluorescence analyses for cells labelled with a 1:5 and 1:10 dilution of CFSE, combined with cells labelled with the established $CFSE_{low}$ dilution.

3.3.2. Flow cytometry panel optimization

Given that the dilution factors for both the $CFSE_{low}$ and $CFSE_{high}$ cell populations were now optimized, a suitable flow cytometry staining panel needed to be established to ensure various cell populations can be correctly identified and characterized based on specific surface markers. A panel consisting of Live/Dead fixable aqua (HV500) dead cell stain, anti-CD3 Brilliant Violet (BV) 711, anti-CD4 BV650 and anti-CD8 BV786 was applied to further distinguish target cells as Live $CD3^+CD4^+$ from effector cells which were Live $CD3^+CD8^+$. As a control, to rule out signal loss from increasing the complexity of the compensation matrix, a subset of cells were alternatively stained with Live/Dead and CD3 BV711 only (**Figure 3.5 A**). Also, an additional counting step was added before the $CFSE_{low}$ and $CFSE_{high}$ labelled cell populations were combined to ensure an accurate comparison between the target and control populations could be carried out, which would enhance precise measurement of the specific cytotoxic activity of effector $CD8^+$ T cells in a killing readout. As depicted in **Figure 3.5** (**B**) the addition of $CD4^+$ and $CD8^+$ markers allowed for clear distinction of these cell populations during flow cytometry analysis without compromising CFSE intensity. The panel was thus accepted for subsequent flow cytometry analyses when examining killing activity by effector $CD8^+$ T cells.

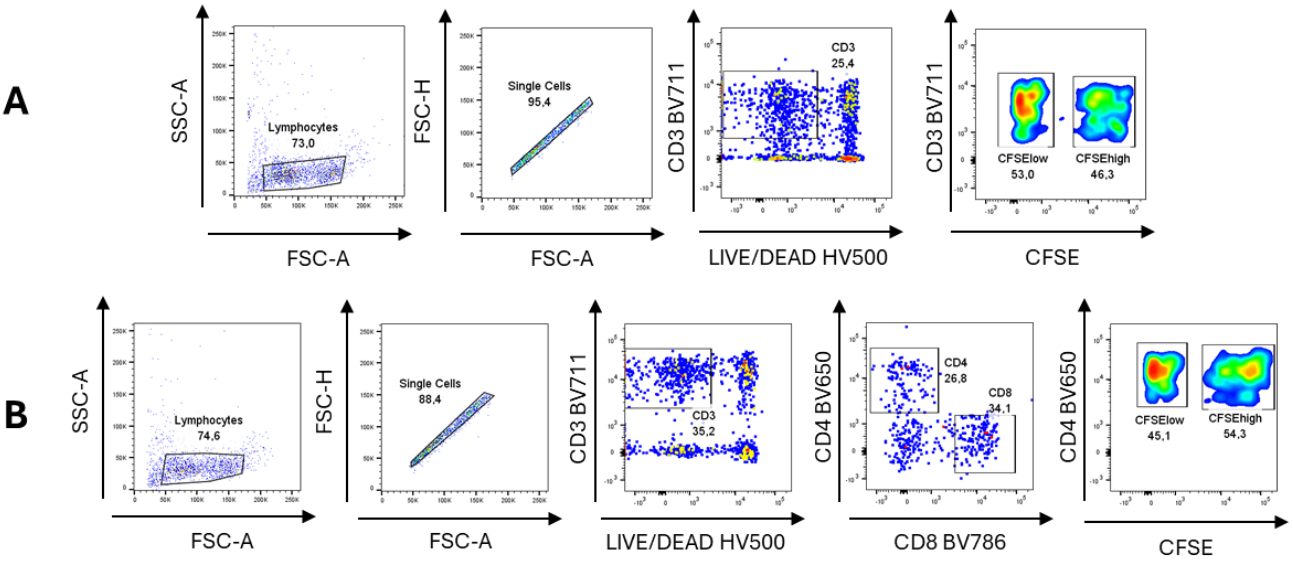

Figure 3.5: Flow cytometry analysis of CFSE-labelled cells stained with different cocktails of surface antibodies. (**A**) Representative flow plots showing gating strategy displaying lymphocyte population based on FSC-A vs. SSC-A, singlet discrimination using FSC-H vs. FSC-A, subsequent gating on $CD3^+$ T cells, and CFSE fluorescence intensity in live cells for cells stained with surface Stain A (**B**) Representative flow plots showing gating strategy displaying lymphocyte population based on FSC-A vs. SSC-A, singlet discrimination using FSC-H vs. FSC-A, subsequent gating on $CD3^+$ T cells, and CFSE fluorescence intensity in live $CD4^+$ T cells for cells stained with surface Stain B.

3.3.3. Testing the CFSE elimination assay in a model anti-viral immune response

Due to the novelty of SARS-nCoV-2, prior to performing the elimination assay in the COVID-19 context, it was first decided to test the assay in an established immune response context - that of $CD8^+$ T cell elimination of HIV-infected $CD4^+$ T cells – before using the assay to measure unknown SARS-nCoV-2 responses. Almost all individuals who are infected by HIV can mount $CD8^+$ T cell responses, including those who fail to control infection (Collins et al., 2020). This ensures that the optimized conditions, including magnetic activated cell sorting, $CFSE_{low}$ and $CFSE_{high}$ dilutions, the staining panel and peptide pulse conditions accurately reflect the ability of $CD8^+$ T cells to target and eliminate antigen-specific cells. Additionally, using PBMCs with known robust responses helped establish baseline data for future iterations of the killing assay. For this model killing assay, PBMCs from an HIV elite controller (Participant 1) were used to elucidate the antigen-specific killing activity of effector $CD8^+$ T cells in this participant by pulsing autologous CD8-depleted PBMCS with HIV-specific Global Pool (Clade C) peptides, comprising eight peptide pools spanning the HIV genome and combining peptide-pulsed and un-pulsed target cell populations at different ratios with autologous effector $CD8^+$ T cells. A control was added where $CD8^+$ effector cells were excluded to demonstrate the dependency of any observed cytotoxicity on the presence of antigen-specific $CD8^+$ T cells.

It was evident that at different ratios of target-to-effector cells, a dose-dependent killing response was observed, noted by a decrease in the percentage of $CFSE_{high}$ labelled cells following the addition of autologous $CD8^+$ T cells, illustrated in **Figure 3.6 (A**) and (**B**). The addition of the un-pulsed $CFSE_{high}$ labelled cell control, representing cells which are not HIV-specific, demonstrated the antigen-specificity of the observed killing response as this control was comparable to the "No $CD8^+$" control with similar distributions of $CFSE_{low}$ and $CFSE_{high}$ cell populations in both conditions. A killing assay run was carried out on an additional HIV acutely-infected patient sample to confirm the reproducibility of the killing assay. Due to limitations with the number of cells available for co-culturing, after performing the killing assay, a control containing un-pulsed $CFSE_{high}$ labelled cells could not be included. As expected, a dose-dependent killing response was observed for Participant 2 at different ratios of target-to-effector cells.

In the analysis of dose-dependent killing, generating killing curves for different participants is useful for understanding the effect of various clinical parameters, such as HIV status, on immune responses. In this case, the percentage elimination rate was calculated at each target-to-effector ratio, relative to the control population containing no CD8+ T cells, and plotted (Collins et al., 2021). Killing curves for both Participant 1 and Participant 2 (**Figure 3.6** (**C**) and (**D**)) were generated, as well as a simple linear regression line for each patient, to establish the effectiveness of CD8+ killing between these individuals as a function of the gradient of the trendline. It was expected that higher gradient values would denote greater killing capacity when comparing different patient samples. As observed in **Figure 3.6** (**E**), Participant 1 showed a higher killing efficiency, as indicated by a steeper slope, compared to Participant 2. Going forward, this analysis strategy was used to elucidate the $CD8^+$ T cell responses between PLWH and PLWoH vaccinated against SARS-nCoV-2.

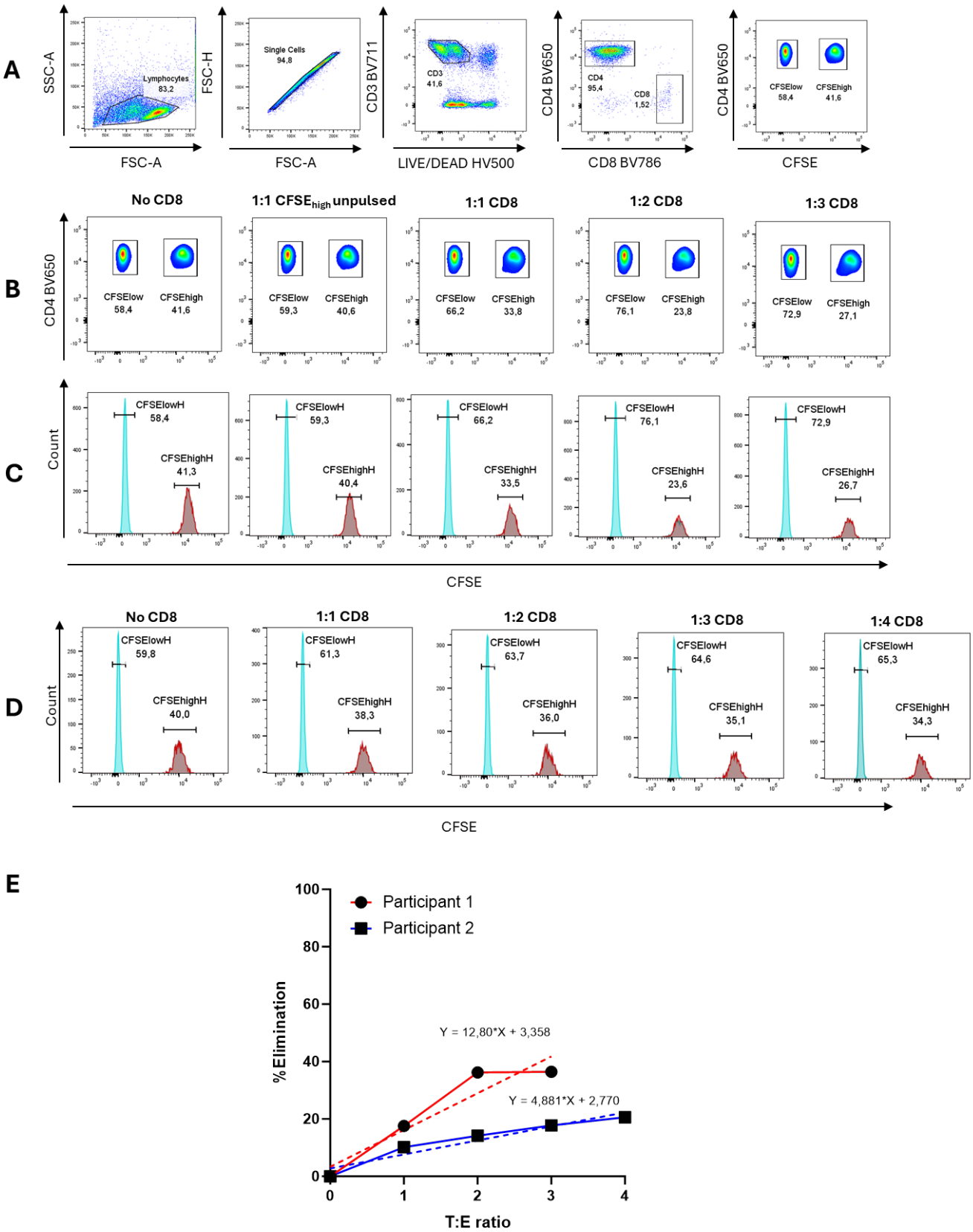
A
SSC-A
FSC-A
Lymphocytes
83,2
FSC-H
FSC-A
Single Cells
94,8
CD3 BV711
LIVE/DEAD HV500
CD3
41,6
CD4 BV650
CD8 BV786
CD4
95,4
CD8
1,52
CD4 BV650
CFSE
CFSElow
58,4
CFSEhigh
41,6
B
No CD8
1:1 CFSEhigh unpulsed
1:1 CD8
1:2 CD8
1:3 CD8
CD4 BV650
CFSElow 58,4
CFSEhigh 41,6
CFSElow 59,3
CFSEhigh 40,6
CFSElow 66,2
CFSEhigh 33,8
CFSElow 76,1
CFSEhigh 23,8
CFSElow 72,9
CFSEhigh 27,1
C
Count
CFSElowH 58,4
CFSEhighH 41,3
CFSElowH 59,3
CFSEhighH 40,4
CFSElowH 66,2
CFSEhighH 33,5
CFSElowH 76,1
CFSEhighH 23,6
CFSElowH 72,9
CFSEhighH 26,7
CFSE
D
No CD8
1:1 CD8
1:2 CD8
1:3 CD8
1:4 CD8
Count
CFSElowH 59,8
CFSEhighH 40,0
CFSElowH 61,3
CFSEhighH 38,3
CFSElowH 63,7
CFSEhighH 36,0
CFSElowH 64,6
CFSEhighH 35,1
CFSElowH 65,3
CFSEhighH 34,3
CFSE
E
Participant 1
Participant 2
% Elimination
Y = 12,80*X + 3,358
Y = 4,881*X + 2,770
T:E ratio
0
20
40
60
80
100
0
1
2
3
4

Figure 3.6.: HIV-specific killing assay to optimize CFSE readout. (**A**) Representative flow plots showing gating strategy displaying lymphocyte population based on FSC-A vs. SSC-A, singlet discrimination using FSC-H vs. FSC-A, subsequent gating on $CD3^+$ T cells, $CD4^+$ T cells, $CD8^+$ T cells and CFSE fluorescence intensity in live cells for the "No CD8 condition" in Participant 1. (**B**) Representative scatter plots for Participant 1 showing different co-culture ratios and controls. (**C**) Representative histogram plots corresponding with Panel B for Participant 1 (n=2). (**D** Representative histogram plots for Participant 2 showing different co-culture ratios and controls (n=3). (**E**) Killing curves for Participant 1 (red) and Participant 2 (blue) showing HIV-specific $CD8^+$ T cell killing activity between two patients across various target-to-effector (T:E) ratios. The graph illustrates the percentage of target cell elimination as a function of increasing E ratios, and linear regression lines (dotted) show the trend of target cell elimination for Participant 1 (red) and Participant 2 (blue), with corresponding equations provided for each participant's response curve. Participant 1 exhibited a steeper increase in cell elimination across the ratios compared to Participant 2.

3.3.4. Ex vivo killing assay using PBMCs isolated from SARS-nCoV-2 vaccinated individuals

Having established optimal target-to-effector cell ratios and controls in a controlled, model context, the assay could now be used to measure $CD8^+$ T cell killing activity in PBMCS from individuals who had been vaccinated against SARS-nCoV-2. For this, a PLWoH vaccinated with the Ad26.COV2.S COVID-19 vaccine from the previously described Botswana-Harvard AIDS Institute Partnership cohort was used to assess if cytolytic SARS-nCoV-2 $CD8^+$ T cell responses were elicited after vaccination. The killing curve depicted in **Figure 3.7** (**C**) showed that the percentage of target cell elimination remained consistently low across all ratios, indicated by the nearly flat slope in the graph. The linear regression model, represented by the equation Y=1.193X+1.694Y, suggested only a slight increase in killing efficiency as the number of CD8+ T cells increased relative to the target cells, however the overall change was minimal.

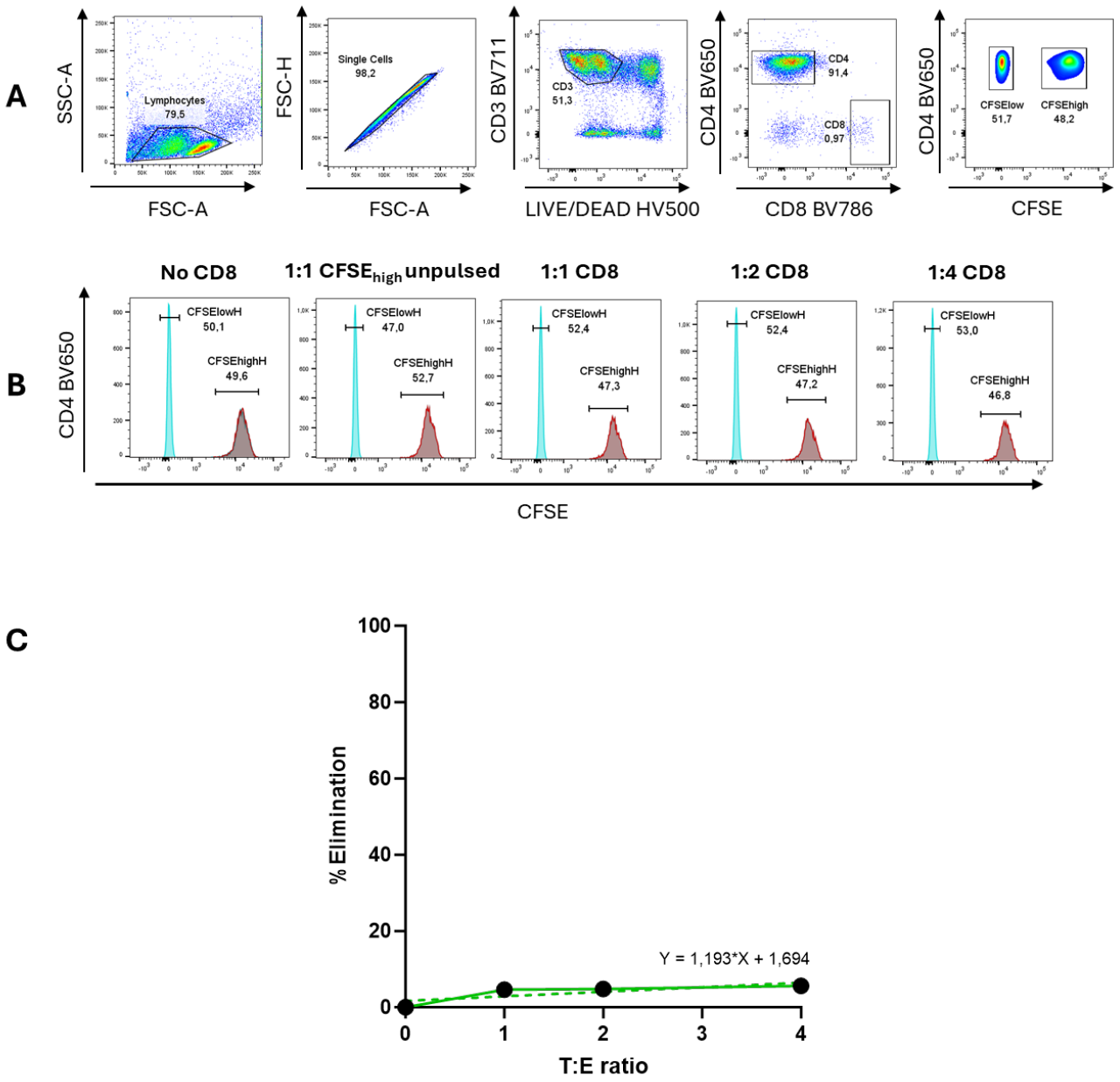

Figure 3.7: *Ex vivo* SARS-nCoV-2-specific killing assay. (**A**) Representative flow plots showing gating strategy displaying lymphocyte population based on FSC-A vs. SSC-A, singlet discrimination using FSC-H vs. FSC-A, subsequent gating on $CD3^+$ T cells, $CD4^+$ T cells, $CD8^+$ T cells and CFSE fluorescence intensity in live cells for the "No CD8 condition" in a PLWoH vaccinated with Ad26.COV2.S COVID-19 vaccine. (**B**) Histogram plots displaying $CD4^+$ T cell populations differentiated by CFSE intensity under varying conditions: No $CD8^+$ control, 1:1 $CFSE_{high}$ un-pulsed control, and increasing target-to-effector (T:E) ratios of 1:1, 1:2, and 1:4 $CD8^+$ T cells (n=1). (**C**) Killing curve showing the percentage of target cell elimination as a function of increasing effector ratios.

3.3.5. In vitro killing assay using expanded PBMCs isolated from PLWH

Expanding PBMCs in the presence of a specific peptide allows for the selective activation and proliferation of T cells that are specific to that peptide (Rosendahl Huber et al., 2014). This antigen-specific expansion helps to increase the proportion of T cells that are reactive to the target antigen, thereby leading to an easily quantifiable cytotoxic response during the killing assay. In addition, controlling the conditions under which the T cells are expanded and stimulated, such as the concentration of peptides and cytokines used, the killing assay protocol can be standardized compared to *ex vivo* killing assays (Sato et al., 2009). This standardization allows for more reproducible results across killing assays measured for different participants. A 14-day expansion was therefore carried out on PBMCs isolated from an HIV elite controller (Participant 1) after which the optimized killing assay was performed. It was observed that the killing index for this patient had markedly increased compared to *ex vivo* conditions, as depicted in the killing curves in **Figure 3.8** (**C**). The killing curve illustrates the expansion of antigen-specific $CD8^+$ T cells in *in vitro* conditions compared to *ex vivo*, as evidenced by steeper gradients in the *in vitro* killing curve. Therefore, 14-day culture expansions were performed for all subsequent participants prior to conducting killing assays.

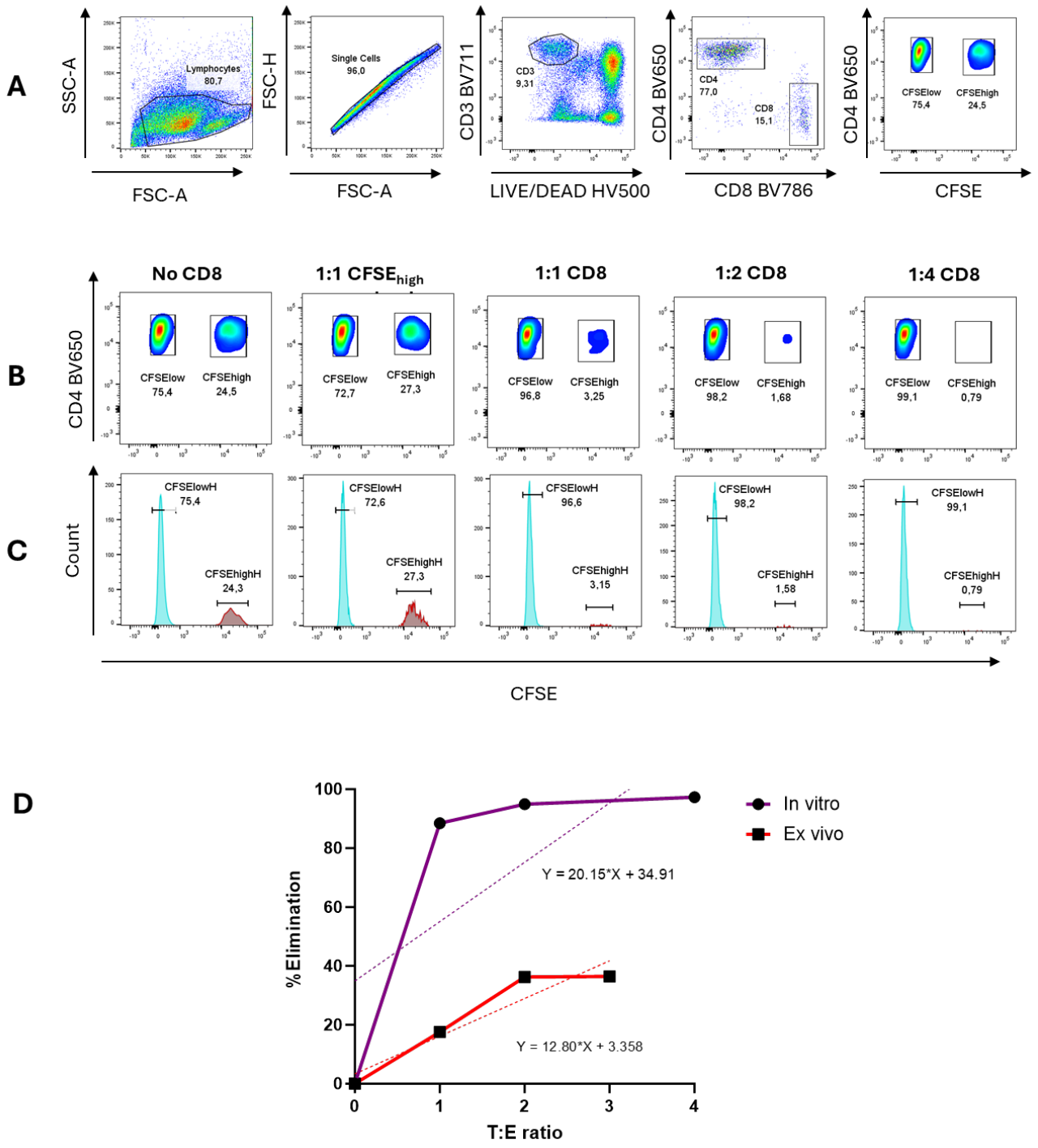

Figure 3.8: Comparison of *in vitro* and *ex vivo* HIV-specific killing assays. (**A**) Representative flow plots showing gating strategy displaying lymphocyte population based on FSC-A vs. SSC-A, singlet discrimination using FSC-H vs. FSC-A, subsequent gating on $CD3^+$ T cells, $CD4^+$ T cells, $CD8^+$ T cells and CFSE fluorescence intensity in live cells for the "No CD8 condition" in Participant 1. (**B**) Representative contour plots displaying $CD4^+$ T cell populations differentiated by CFSE intensity under varying conditions: No $CD8^+$ control, 1:1 $CFSE_{high}$ un-pulsed control, and increasing target-to-effector ratios of 1:1, 1:2, and 1:4 $CD8^+$ T cells (n=3). The effect of $CD8^+$ T cells which are still present in the

CD8-depleted fraction after MACS separation results in residual killing of the target cells. (**C**) Representative histogram plots corresponding with Panel B. (**D**) Killing curve comparing the percentage of target cell elimination as a function of increasing effector (E) ratios for Patient 1 at *in vitro* (purple) and *ex vivo* (red) conditions.

3.3.6. In vitro killing assay using expanded PBMCs isolated from COVID-19 vaccinated individuals

Using PBMCs expanded for 14 days, provided by the Botswana-Harvard AIDS Institute Partnership (BHP), an *in vitro* killing assay was conducted for people living with HIV (PLWH) and people living without HIV (PLWoH) who were vaccinated against COVID-19 to compare differences in their cytotoxic responses post-vaccination with three COVID-19 vaccinations.

3.3.6.1. AZD1222 (Oxford/AstraZeneca) vaccine

The killing curve in **Figure 3.9** (**B**) illustrates the cytotoxic response in a PLWH (light green line) where the percentage elimination rate increased as the concentration of $CD8^+$ T cells increased, with a regression line equation Y = 5.220X + 4.640. A similar relationship was observed in the PLWoH (orange line) where the percentage elimination rate increased as the concentration of $CD8^+$ T cells increased, with a regression line equation Y = 3.612X - 0.9530. The PLWH showed a slightly higher cytotoxic activity compared to the PLWoH, indicated by the steeper slope of the regression line for this patient which may imply variability in vaccine-induced immune responses between PLWH and PLWoH.

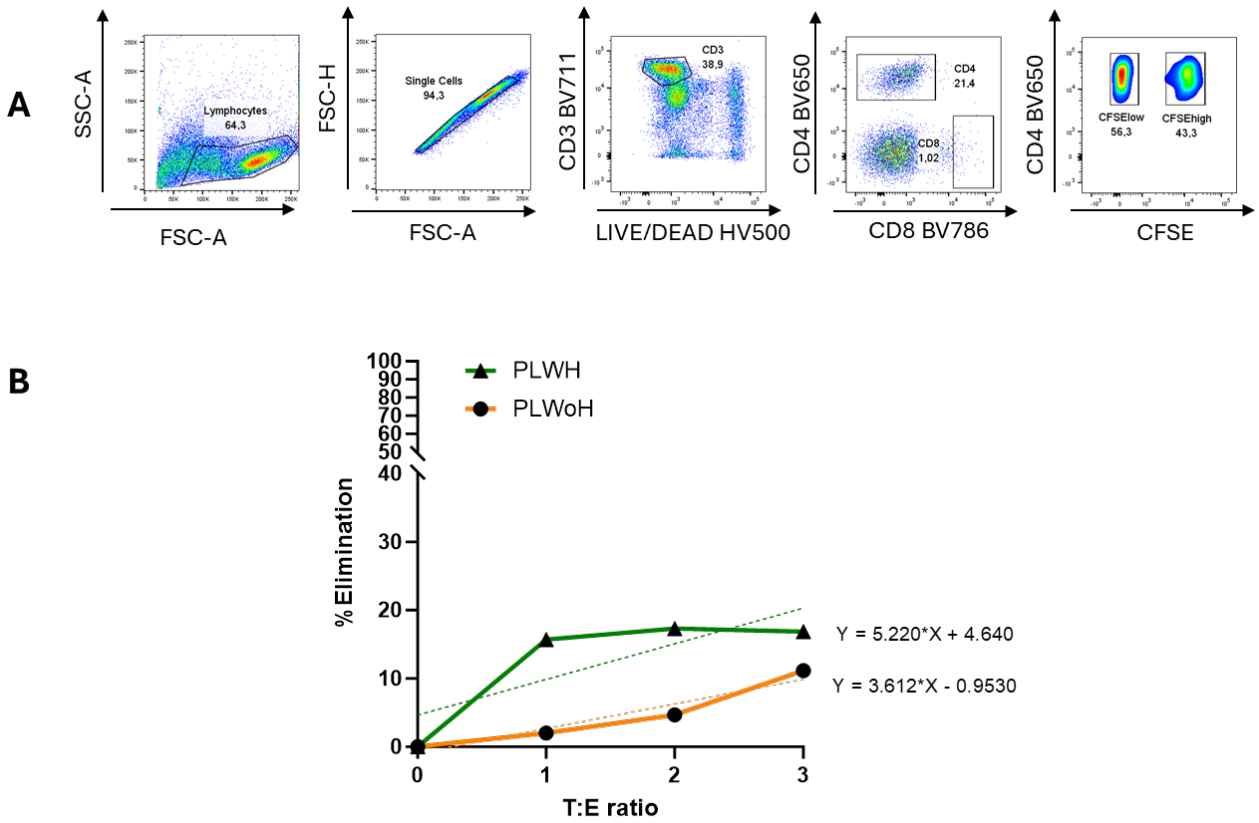

Figure 3.9.: Comparison of cytolytic CD8$^+$ T cell responses between PLWH and PLWoH vaccinated with AZD1222 (Oxford/AstraZeneca) COVID-19 vaccine. (**A**) Representative flow plots showing gating strategy displaying lymphocyte population based on FSC-A vs. SSC-A, singlet discrimination using FSC-H vs. FSC-A, subsequent gating on CD3$^+$ T cells, CD4$^+$ T cells, CD8$^+$ T cells and CFSE fluorescence intensity in live cells for the "No CD8 condition" in a PLWoH vaccinated with the AZD1222 COVID-19 vaccine. (**B**) Killing curve showing comparative cytotoxic response in a person living with HIV (PLWH) (light green) and a person living without HIV (PLWoH) (orange) vaccinated with the AZD1222 COVID-19 vaccine.

3.3.6.2. Coronavac (Sinovac) vaccine

The killing curve in **Figure 3.10** (**B**) illustrates the cytotoxic response in a PLWH (light green line) where the percentage elimination rate remained relatively low as the concentration of CD8$^+$ T cells increased, with a regression line equation Y = 0.8490X + 0.994. For the PLWoH (orange line) the percentage elimination rate increased slightly as the concentration of CD8$^+$ T cells increased, with a regression line equation Y = 2.573X - 0.5670. The slopes of both regression lines for each participant were relatively gentle indicating poor cytotoxic activity for these participants following vaccination, regardless of HIV status.

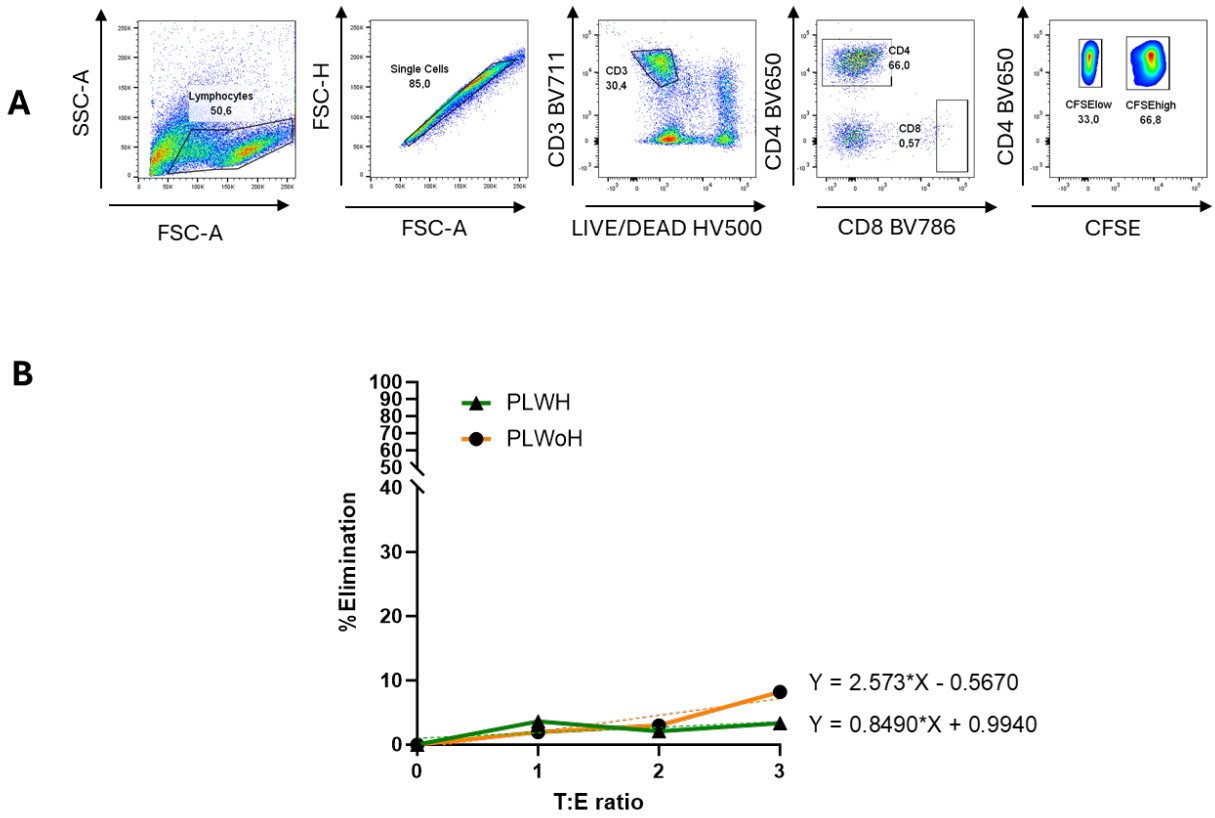

Figure 3.10.: Comparison of cytolytic $CD8^+$ T cell responses between PLWH and PLWoH vaccinated with Coronavac (Sinovac) COVID-19 vaccine. (**A**) Representative flow plots showing gating strategy displaying lymphocyte population based on FSC-A vs. SSC-A, singlet discrimination using FSC-H vs. FSC-A, subsequent gating on $CD3^+$ T cells, $CD4^+$ T cells, $CD8^+$ T cells and CFSE fluorescence intensity in live cells for the "No $CD8^+$ condition" in a PLWoH vaccinated with the Coronavac COVID-19 vaccine. (**B**) Killing curve showing comparative cytotoxic response in a person living with HIV (PLWH) (light green) and a person living without HIV (PLWoH) (orange) vaccinated with the Coronavac COVID-19 vaccine.

3.3.6.3. Ad26.COV2.S (Johnson and Johnson) vaccine

The killing curve in **Figure 3.11** (**B**) illustrates the cytotoxic response in a PLWH (light green line) where the percentage elimination rate increased as the concentration of $CD8^+$ T cells increased, with a regression line equation Y = 6.007X + 2.577. For the PLWoH (orange line) the percentage elimination rate increased slightly as the concentration of $CD8^+$ T cells increased, with a regression line equation Y=4.417X + 2.847. The PLWH showed a slightly higher cytotoxic activity compared to the PLWoH, indicated by the steeper slope of the regression line for this patient which may imply variability in vaccine-induced immune responses between PLWH and PLWoH.

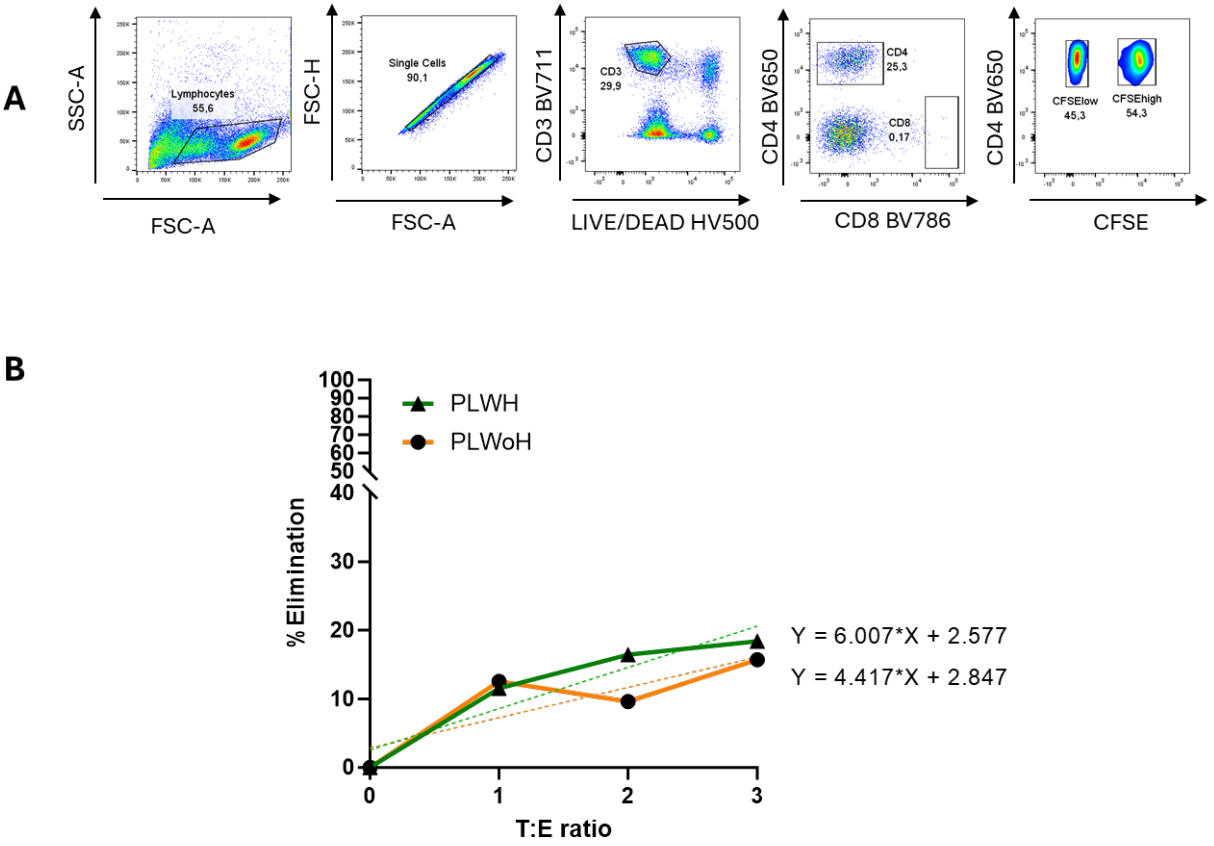

Figure 3.11.: Comparison of cytolytic $CD8^+$ T cell responses between PLWH and PLWoH vaccinated with Ad26.COV2.S (Johnson and Johnson) COVID-19 vaccine. (**A**) Representative flow plots showing gating strategy displaying lymphocyte population based on FSC-A vs. SSC-A, singlet discrimination using FSC-H vs. FSC-A, subsequent gating on $CD3^+$ T cells, $CD4^+$ T cells, $CD8^+$ T cells and CFSE fluorescence intensity in live cells for the "No CD8 condition" in a PLWoH vaccinated with the Ad26.COV2.S COVID-19 vaccine. (**B**) Killing curve showing comparative cytotoxic response in a person living with HIV (PLWH) (light green) and a person living without HIV (PLWoH) (orange) vaccinated with the Ad26.COV2.S COVID-19 vaccine.

3.4. Discussion

The optimized CFSE-based killing assay described in Chapter 3 leveraged the long-lived and highly fluorescent properties of carboxyfluorescein diacetate succinimidyl ester (CFSE) to track and quantify the cytotoxic activity of $CD8^+$ T cells over an extended period. Additionally, the results presented in this chapter demonstrated the assay's effectiveness in distinguishing between peptide-pulsed and un-pulsed target cells, allowing for the measurement of antigen-specific cytotoxic $CD8^+$ T cell responses. One of the main challenges in using CFSE is the potential for fluorescence overlap between differentially labelled cell populations. As described in the optimization section, achieving the correct CFSE concentrations was important to ensure the $CFSE_{low}$ and $CFSE_{high}$ populations could be distinguished. Notably, the efficiency of CFSE labelling can vary between different cell types and experimental conditions, as illustrated in **Figures 3.2** and **3.3**. Factors such as the cell size, membrane permeability, and well as variations between different batches of reconstituted CFSE, may lead to variability in fluorescence intensity (Dalgaard et al., 2010). This in turn affects the reproducibility of the assay, highlighting the necessity for the careful initial optimization steps carried out.

While CFSE is generally considered a non-toxic dye and does not interfere with cellular functions, high concentrations or prolonged exposure to CFSE can potentially impact cell viability and function (Ingulli, 2007). For this reason, the inclusion of a baseline "No $CD8^+$" control during the co-culture phase validated that any observed effects were due to the cytotoxic activity of CD8+ T cells, and were not artifacts of CFSE labelling. Furthermore, the inclusion of the "un-pulsed $CFSE_{high}$" control at a 1:1 dilution demonstrated the specificity of the $CD8^+$ T cell-mediated killing. By including target cells labelled with a high concentration of CFSE but not pulsed with the specific peptide, it could be determined whether the observed cytotoxic activity was truly antigen-specific. If the $CD8^+$ T cells were specific to the peptide, they would selectively kill the peptide-pulsed $CFSE_{high}$ target cells, The un-pulsed $CFSE_{high}$ target cells would largely remain unaffected in this instance, as illustrated in **Figures 3.5** (**B**) and **3.7** (**B**). Furthermore, the effect of residual or "leaky" $CD8^+$ T cells after MACS separation shown in **Figure 3.8** (**A**) may have played a role in the reduced $CFSE_{high}$ population size observed, even in the control conditions. This may be easily rectified with the addition of a second column in which the residual $CD8^+$ T cells can be properly captured prior to co-culturing target and effector cells to ensure an accurate an cleaner readout.

In measuring the $CD8^+$ T cell response, both an *ex vivo* and *in vitro* T cell expansion approach were compared. The *ex vivo* killing assay may show the immediate cytotoxic response, for example, post-vaccination. On the other hand, the *in vitro* killing assay provides a more comprehensive assessment of the cytotoxic potential of $CD8^+$ T cells by allowing for the expansion and activation of antigen-specific T cells. This approach is particularly useful to evaluate the long-term efficacy of vaccines and the potential for memory T cell responses (Farber et al., 2016, Gerritsen and Pandit, 2016, Jarjour et al.,

2021). **Figure 3.8** (**D**) showed the differences in $CD8^+$ T cell responses when cells are used post-isolation (*ex vivo*) versus after a period of expansion and activation (*in vitro*) in Participant 1, an HIV elite controller. The linear regression lines for both approaches provided a quantitative measure of the killing efficiency. The steeper slope of the *in vitro* regression line suggested a more robust cytotoxic response compared to the *ex vivo* approach. For vaccines targeting chronic infections like HIV, or emerging pathogens like SARS-nCoV-2, the ability to elicit robust and long-lived $CD8^+$ T cell responses is crucial (Almendro-Vázquez et al., 2023). The *in vitro* killing assay therefore provided a more comprehensive assessment of this potential.

In particular, Participant 1, a PLWH, was able to mount a robust $CD8^+$ T cell response, demonstrating that PLWH can achieve high levels of antigen-specific cytotoxicity, post-expansion. Notably, individuals who are elite controllers of HIV are able to maintain HIV RNA to less than 50 copies per ml in the absence of antiretroviral therapy (Walker, 2007). Such individuals with minimal T cell responses are able to suppress HIV *in vitro* due to a highly functional, broadly directed central memory T cell population (Ndhlovu et al., 2012). In an acutely infected PLWH (Participant 2), depicted in **Figure 3.6** (**E**), the less steep slope of the regression line indicated a lower killing efficiency compared to Participant 1. While $CD8^+$ T cells in acute HIV infection are able to perform antigen-specific killing to an extent, the lower killing efficiency compared to the elite controller suggests that the cytotoxic potential of $CD8^+$ T cells in acute HIV infection may be compromised. This is in line with studies which have highlighted that untreated HIV infection causes progressive $CD8^+$ T cell dysfunction (Jensen et al., 2015, Ferrari et al., 2011). These findings highlight the sensitivity of the CFSE-based killing assay in demonstrating differences in $CD8^+$-mediated killing between participants with varying HIV statuses.

When the optimized killing assay was tested on participants who were vaccinated against COVID-19, it was observed that the overall cytotoxic responses were generally low in all participants. This finding implies that first-generation COVID-19 vaccines did not generate robust CTL responses for these participants. In applying the *in vitro* CFSE-based killing assay to a cohort of participants comprised of PLWH and PLWoH from Botswana, notable differences were observed in the $CD8^+$ killing activities with regards to the HIV status and type of vaccination received by the chosen participants. It was observed that PLWH exhibited a stronger $CD8^+$ T cell cytotoxic response to the AZD1222 (Oxford/AstraZeneca) and Ad26.COV2.S (Johnson and Johnson) vaccines compared to PLWoH. This could suggest that these vaccines are capable of eliciting a more robust cellular immune response in PLWH, which may be beneficial for this group given the potential for HIV to compromise immunity. It should be noted, however, that the difference in the killing activities observed were marginal and the inclusion of more participants vaccinated with these vaccine types would be needed to draw any reasonable conclusions. It is also important to consider that the SARS-nCoV-2 spike-specific peptide pool that was used to stimulate cells in this assay may not have been highly antigenic, thereby resulting in poor killing efficiency of the $CFSEh_{igh}$ cells by $CD8^+$ T cells. This may be due to several factors such

as poor binding affinity to MHC molecules or lack of recognition by T cell receptors (Walls et al., 2020).

For the participants who received the Coronavac vaccine, similar cytotoxic responses were observed between PLWH and PLWoH. This indicated that this vaccine may not affect the $CD8^+$ T cell responses based on HIV status. Notably, the Oxford/AstraZeneca and Johnson and Johnson vaccines use viral vector platforms and appeared to elicit stronger $CD8^+$ T cell responses than the Sinovac vaccine, which uses an inactivated virus platform. The viral vector vaccines might therefore be more effective in stimulating cellular immunity, which is an important consideration for vaccine deployment, especially in PLWH. This has also been noted by Voysey et al. (2021) and Sadoff et al. (2021) who noted ~80% and ~85% efficacy of the Oxford/AstraZeneca and Johnson and Johnson vaccines against severe COVID-19 disease, respectively (Voysey et al., 2021, Sadoff et al., 2021). In comparison to the Sinovac vaccine, the vaccine efficacy varies among different populations but is maintained between ~50.4% and ~57.5% against mild to moderate COVID-19 (Palacios et al., 2021, Halperin et al., 2022). Overall, the optimized CFSE-based killing assay provided a sensitive and effective method for measuring antigen-specific cytotoxic $CD8^+$ T cell responses. This assay's application demonstrated differences in the $CD8^+$ T cell responses across various HIV statuses and COVID-19 vaccination types, demonstrating its potential to evaluate vaccine efficacy and immune responses among different populations.

3.4.1. Limitations

It is important to note the limitations associated with this study. The sample size of this particular study was low, therefore accurate conclusions about the efficacy of different COVID-19 vaccinations among differing HIV statuses could not be drawn. Furthermore, information regarding the $CD4^+$ counts, viral loads and ART statuses of the participants in the BHP cohort were not available. These are crucial considerations when performing analysis of individual $CD8^+$ T cell responses as they may influence the killing capacities observed. In addition, the chosen participants for this study were all female and therefore, larger sample sizes encompassing male and female participants would provide a more holistic depiction.

3.4.2 Future recommendations

The CFSE-based killing assay showed differences in the efficacy of vaccine-induced $CD8^+$ T cell responses for two vector-based vaccines and one inactivated virus vaccine in PLWH and PLWoH. Performing the assay on participants who have been vaccinated with mRNA vaccines such as BNT162b2 and mRNA-1273, which have largely been considered the most effective of the COVID-19 vaccines, may reveal interesting insights into vaccine-induced $CD8^+$ T cell responses for these

individuals (Polack et al., 2020, Reynolds et al., 2023). Furthermore, the inclusion of participants who are PLWH at different stages of infection, or perhaps different stages of treatment, may reveal information about the killing efficacy of $CD8^+$ T cells under these different conditions and how COVID-19 may modulate this. In terms of assay improvement, the use of other CellTrace dyes instead of or in addition to CFSE, such as CellTrace Violet and CellTrace Far Red, may be useful in distinguishing cell populations based on the addition of different SARS-nCoV-2-specific peptides. Dyes such as CellTrace Violet offer similar properties to CFSE and can be used in combination with CFSE to label different cell populations without spectral overlap (Wu et al., 2021). This has been reported by Collins et al. (2021) who used these dyes in an elimination assay to distinguish between peptide specific and non-specific cell populations (Collins et al., 2021). The CFSE-based killing assay has undoubtedly paved the way forward in enhancing our understanding of differences in the $CD8^+$ T cell response among PLWH and PLWoH and what these differences may imply for the development of optimal vaccinations for PLWH.

3.5. Conclusion

The optimized CFSE-based killing assay allowed for the distinction between peptide-pulsed and un-pulsed target cells, thereby allowing for the measurement of antigen-specific cytotoxic $CD8^+$ T cell responses. A challenge encountered in using CFSE was the potential for fluorescence overlap between differentially labelled cell populations, which required careful optimization of CFSE concentrations to ensure clear distinction between $CFSE_{low}$ and $CFSE_{high}$ populations. Variability in CFSE labelling efficiency due to factors such as cell type, membrane permeability, and batch differences highlighted the importance of initial optimization steps to ensure reproducibility. The inclusion of un-pulsed $CFSE_{high}$ controls demonstrated the specificity of $CD8^+$ T cell-mediated killing, confirming that any cytotoxic activity observed was truly antigen-specific. Comparing *ex vivo* and *in vitro* T cell expansion approaches revealed that *in vitro* assays provided a more comprehensive assessment of $CD8^+$ T cell cytotoxic potential, which is particularly useful for evaluating long-term vaccine efficacy and memory T cell responses. The study also highlighted differences in $CD8^+$ T cell responses among participants with varying HIV statuses, demonstrating the assay's sensitivity in detecting these differences. Notably, first-generation COVID-19 vaccines elicited generally low CTL responses, with viral vector vaccines showing stronger $CD8^+$ T cell responses compared to the inactivated virus vaccine. To enhance the current COVID-19 vaccines, peptides derived from the spike proteins of different SARS-nCoV-2 variants may offer enhanced immunogenicity when tested. These peptides have been identified as targets for eliciting strong T cell responses and may be more efficient alternatives to the wild type SARS-nCoV-2 spike peptides used in this study (Jackson et al., 2022). Overall, the optimized CFSE-

based killing assay provided a sensitive and effective method for measuring antigen-specific cytotoxic $CD8^+$ T cell responses.

CHAPTER 4: DISCUSSION/SYNTHESIS

Overall, two killing assays have been evaluated in this study. The pseudovirus-based killing assay uses pseudoviruses which have been engineered to express fluorescent reporter genes, such as mCherry or GFP, which mimic the infection process of SARS-nCoV-2. Target cells are infected with these pseudoviruses, leading to the expression of the fluorescent reporter gene within the cells (Donofrio et al., 2021). While this assay requires further optimization, it may offer specificity in measuring $CD8^+$ T cell responses against SARS-nCoV-2-infected cells and is safer to perform in a BSL2+ environment. In contrast, the CFSE-based killing assay involved labelling target cells with a non-radioactive fluorescent dye, CFSE. Using contrasting concentrations of CFSE, differential CFSE intensity was used to distinguish between SARS-nCoV-2 target cell populations and other populations of PBMCS, to monitor the loss of target cells in the presence of $CD8^+$ T cells. Both of these assays circumvent the limitations of traditional killing assays like the chromium release assay which uses radioactive materials (Brunner et al., 1968). In addition to being safer, these assays are more specific alternatives to evaluate cytotoxic responses over several timepoints, compared to a single time point offered by traditional assays. Here, the pseudovirus-based assay did not produce a robust fluorescence readout to measure $CD8^+$-mediated elimination of target cells. However, the CFSE-based assay was useful to compare cytolytic responses following COVID-19 vaccination in PLWH and PLWoH, both *in vitro* and *ex vivo.*

Conclusion

Developing a killing assay to measure T cell responses to SARS-nCoV-2 may contribute towards understanding immune responses to COVID-19. Such assays, including the pseudovirus-based and CFSE-based approaches, provide insights into the cytotoxic capabilities of CD8+ T cells, which are essential for controlling viral infections. Moreover, being able to assess these responses in different populations, such as PLWH, PLWoH and individuals with underlying co-morbidities, allows for a more holistic representation of the T cell repertoire to COVID-19 (Gutierrez et al., 2020). By accurately quantifying the ability of these T cells to eliminate virus-infected cells, researchers can evaluate the efficacy of vaccines and immune-based therapies, which is beneficial for the scientific community. Measuring T cell responses in a high-throughput manner may aid in large-scale studies of effective vaccines and therapeutics, contributing to better public health outcomes and preparedness for future pandemics.

CHAPTER 5: APPENDICES

Appendix A: BREC approval

22 May 2024

Miss Uvedhna Padia (218010260)
School of Lab Med & Medical Sc Medical School

Dear Miss Padia,

Protocol reference number: BREC/00006446/2023
Project title: A CD8 killing assay to measure T cell responses to infection with SARS-CoV-2
Degrees: MMedSci

EXPEDITED APPLICATION: APPROVAL LETTER

A sub-committee of the Biomedical Research Ethics Committee has considered and noted your application.

The conditions have been met and the study is given full ethics approval and may begin as from 22 May 2024. Please ensure that any outstanding site permissions are obtained and forwarded to BREC for approval before commencing research at a site.

This approval is valid for one year from 22 May 2024. To ensure uninterrupted approval of this study beyond the approval expiry date, an application for recertification must be submitted to BREC on RIG on the appropriate BREC form 2-3 months before the expiry date.

Any amendments to this study, unless urgently required to ensure safety of participants, must be approved by BREC prior to implementation.

Your acceptance of this approval denotes your compliance with South African National Research Ethics Guidelines (2015), South African National Good Clinical Practice Guidelines (2020) (if applicable) and with UKZN BREC ethics requirements as contained in the UKZN BREC Terms of Reference and Standard Operating Procedures, all available at http://research.ukzn.ac.za/Research-Ethics/Biomedical-Research-Ethics.aspx.

BREC is registered with the South African National Health Research Ethics Council (REC-290408-009). BREC has US Office for Human Research Protections (OHRP) Federal-wide Assurance (FWA 678).

The sub-committee's decision will be noted by a full Committee at its next meeting taking place on 11 June 2024.

Yours sincerely,

[redacted]

Prof S Singh
Chair: Biomedical Research Ethics Committee

Biomedical Research Ethics Committee
Chair: Professor S Singh
UKZN Research Ethics Office Westville Campus, Govan Mbeki Building
Postal Address: Private Bag X54001, Durban 4000
Email: BREC@ukzn.ac.za
Website: http://research.ukzn.ac.za/Research-Ethics/Biomedical-Research-Ethics.aspx

Appendix B: Media and reagents

HEK293T media

Reagent	Quantity	Supplier
Dulbecco's modified Eagle media (DMEM)	500 ml	Gibco, Schwerte, Germany
Heat-inactivated fetal bovine serum (FBS)	50 ml	Gibco, Schwerte, Germany
HEPES buffer (1 M)	5.5 ml	Gibco, Schwerte, Germany
Penicillin/streptomycin (10000 U/ml)	5.5 ml	Gibco, Schwerte, Germany

293T-ACE2 media

Reagent	Quantity	Supplier
Dulbecco's modified Eagle media (DMEM)	500 ml	Gibco, Schwerte, Germany
Heat-inactivated fetal bovine serum (FBS)	50 ml	Gibco, Schwerte, Germany
L-glutamine (200 mM)	5.5 ml	Gibco, Schwerte, Germany
Puromycin (3mg/ml)	1 µl per ml media	Gibco, Schwerte, Germany
Gentamycin (10mg/ml)	5 µl per ml media	Gibco, Schwerte, Germany

H1299-E3 media

Reagent	Quantity	Supplier
RPMI 1640 media	500 ml	Gibco, Schwerte, Germany
Heat-inactivated fetal bovine serum (FBS)	50 ml	Gibco, Schwerte, Germany
HEPES buffer (1 M)	5.5 ml	Gibco, Schwerte, Germany
Non-essential amino acids (100X)	5.5 ml	Gibco, Schwerte, Germany
Sodium pyruvate (100 mM)	5.5 ml	Gibco, Schwerte, Germany
L-glutamine (200 mM)	5.5 ml	Gibco, Schwerte, Germany

R10 media

Reagent	Quantity	Supplier
RPMI 1640 media	500 ml	Gibco, Schwerte, Germany
Heat-inactivated fetal bovine serum (FBS)	50 ml	Gibco, Schwerte, Germany
HEPES buffer (1 M)	5.5 ml	Gibco, Schwerte, Germany
L-glutamine (200 mM)	5.5 ml	Gibco, Schwerte, Germany

Trypsinization reagents

Reagent	Supplier
Trypsin-EDTA (1X)	Gibco, Schwerte, Germany
Phosphate buffered saline (PBS)	Gibco, Schwerte, Germany

Classical transfection reagents

Reagent	Quantity	Supplier
Dulbecco's modified Eagle media (DMEM)	500 ml	Gibco, Schwerte, Germany
Polyethyleneimine (PEI)	8 µl per condition	A gift from the HIV Pathogenesis Programme, Durban, South Africa

Nucleofection reagents

Reagent	Quantity	Supplier
Nucleofector™ solution	82 µl	Lonza, Basel, Switzerland
Supplement	18 µl	Lonza, Basel, Switzerland

MACS buffer

Reagent	Supplier
Bovine serum albumin (2% BSA)	(Sigma, Munich, Germany)
Phosphate buffered saline (PBS)	Gibco, Schwerte, Germany

CFSE reconstitution

Add 50 µl DMSO to 50 µg of lyophilized reagent to make a 1 µg/µl stock ((ThermoFisher Scientific, Eugene, Oregon, United States).

Peptide reconstitution

20 µM HIV Clade C Global Pool was gifted by Dr Tiza Nguni of the Ndhlovu Lab.

PepTivator® SARS-CoV-2 Prot_S (2 µg/ml) and PepTivator® SARS-CoV-2 Prot_S1 (2 µg/ml) were reconstituted by adding 200 µl distilled water to the lyophilized reagent (Miltenyi Biotec, Bergisch Gladbach, Germany).

Staining antibodies

Antibody	**Quantity**	**Supplier**
CD3 (BV711)	1 µl/well	BioLegend, CA, United States
CD4 (BV650)	1 µl/well	BD BioSciences, Franklin Lakes, NJ
CD8 (BV786)	1 µl/well	BD BioSciences, Franklin Lakes, NJ
Aqua Live/Dead (HV500)	0.3 µl/well	ThermoFisher Scientific, Eugene, Oregon, United States

Appendix C: Chapter 2 supplementary material

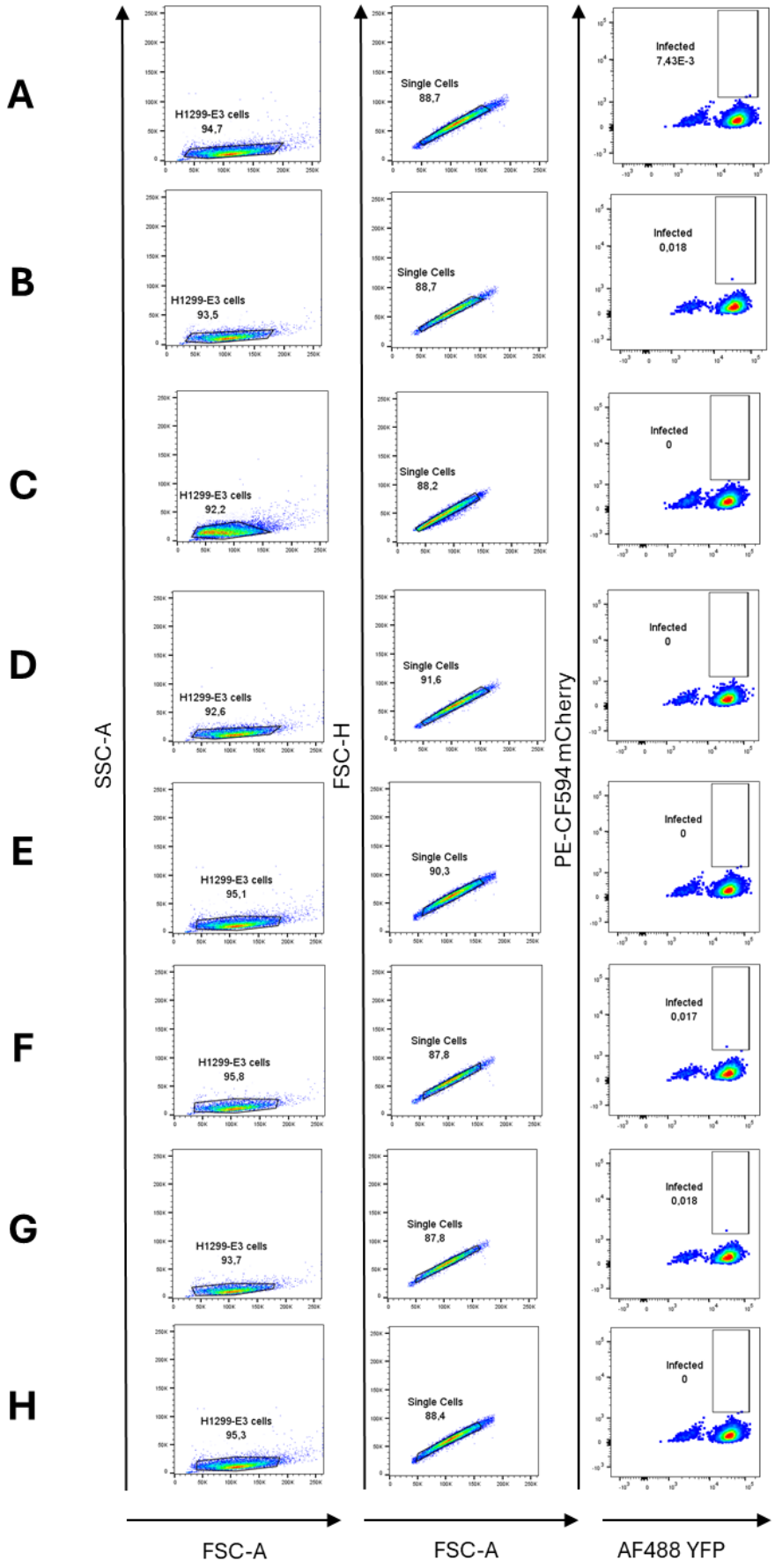

Figure C1: Uninfected H1299-E3 cell controls for infection duration optimization for in-house multi-vector pseudovirus generated by classical transfection. (**A**) 24 h post-infection (Replicate 1). (**B**) 24 h post-infection (Replicate 2). (**C**) 48 h post-infection (Replicate 1). (**D**) 48 h post-infection (Replicate 2). (**E**) 72 h post-infection (Replicate 1). (**F**) 72 h post-infection (Replicate 2). (**G**) 96 h post-infection (Replicate 1). (**H**) 96 h post-infection (Replicate 2).

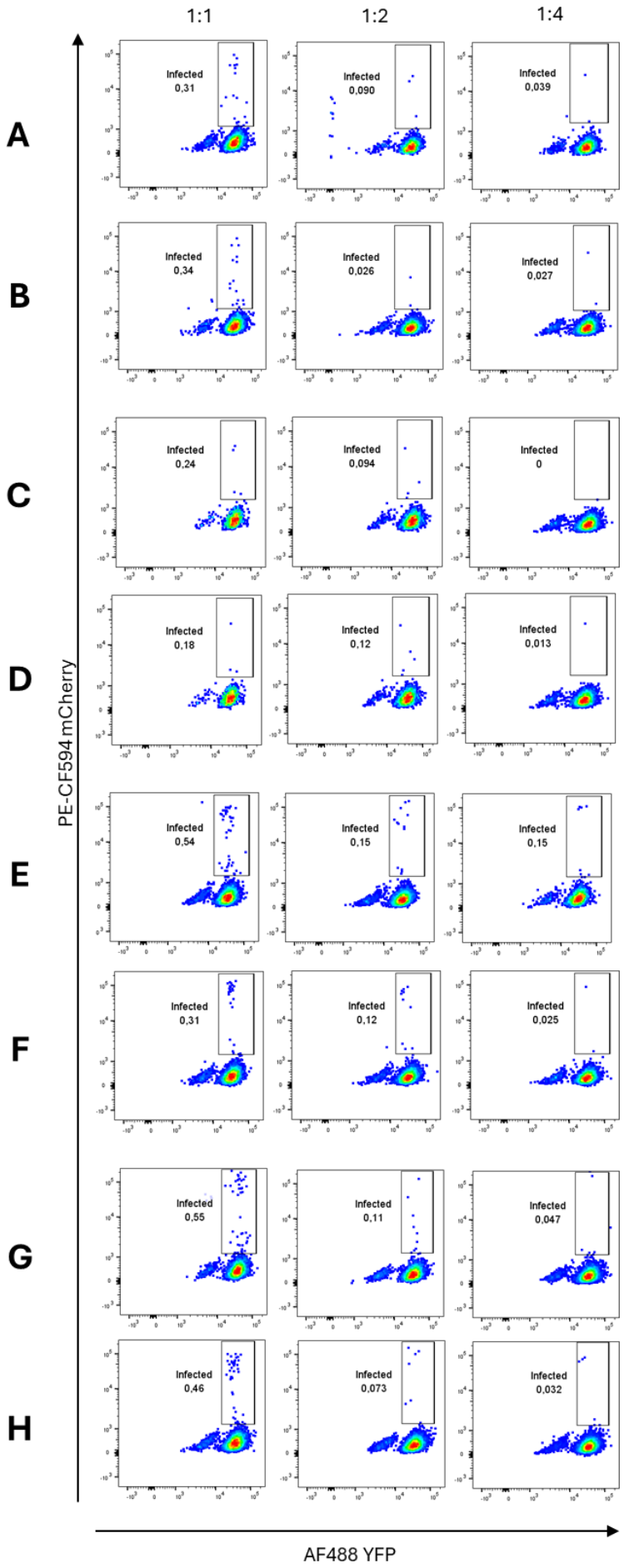
1:1
1:2
1:4
A
B
C
D
E
F
G
H
Infected 0,31
Infected 0,090
Infected 0,039
Infected 0,34
Infected 0,026
Infected 0,027
Infected 0,24
Infected 0,094
Infected 0
Infected 0,18
Infected 0,12
Infected 0,013
Infected 0,54
Infected 0,15
Infected 0,15
Infected 0,31
Infected 0,12
Infected 0,025
Infected 0,55
Infected 0,11
Infected 0,047
Infected 0,46
Infected 0,073
Infected 0,032
PE-CF594 mCherry
AF488 YFP

Figure C2: Infection duration optimization for in-house multi-vector pseudovirus generated by classical transfection at different time points. (**A**) 24 h post-infection (Replicate 1). (**B**) 24 h post-infection (Replicate 2). (**C**) 48 h post-infection (Replicate 1). (**D**) 48 h post-infection (Replicate 2). (**E**) 72 h post-infection (Replicate 1). (**F**) 72 h post-infection (Replicate 2). (**G**) 96 h post-infection (Replicate 1). (**H**) 96 h post-infection (Replicate 2).

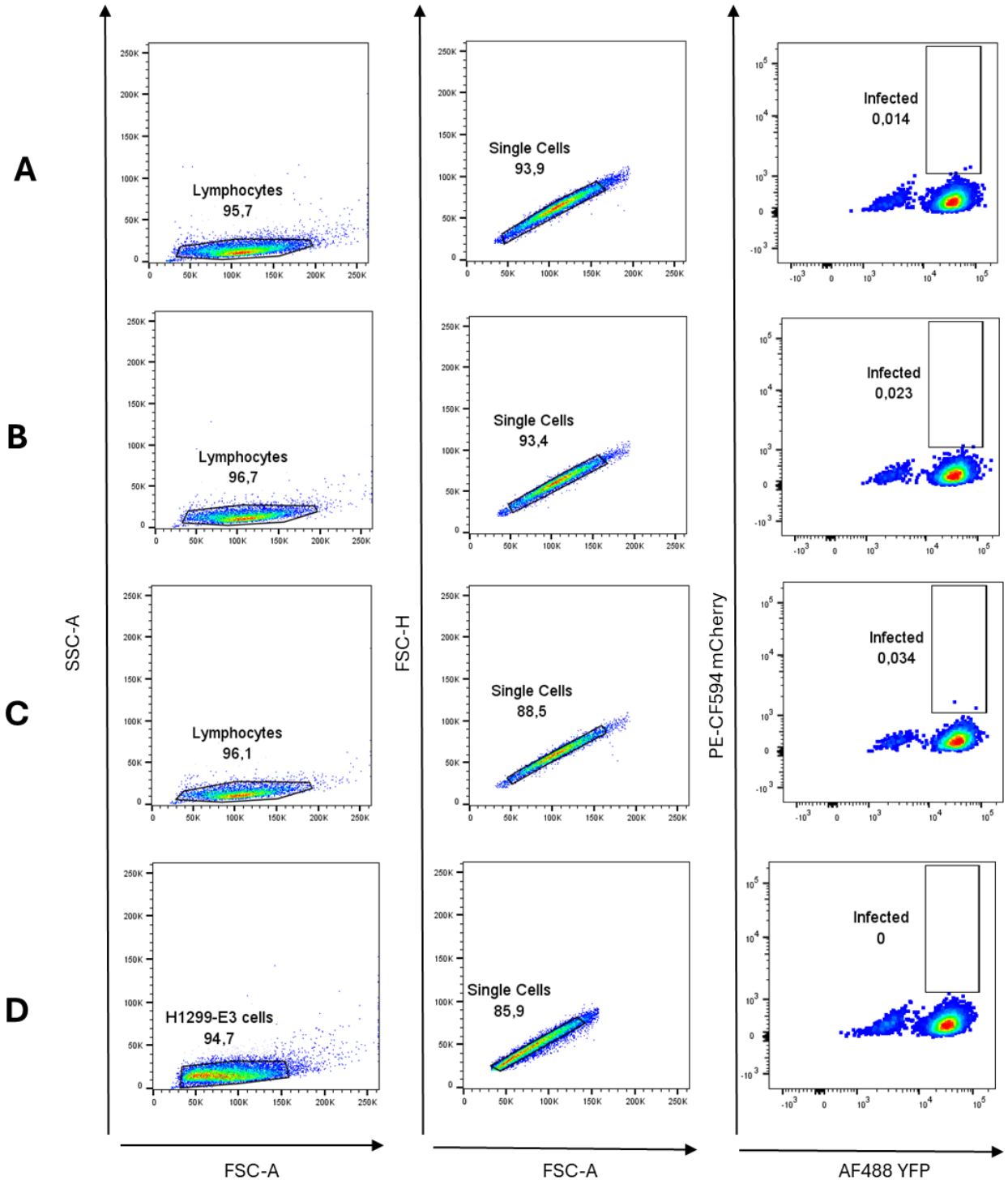

Figure C3: Uninfected H1299-E3 cell controls for infection duration optimization for multi-vector pseudovirus generated by nucleofection. (**A**) 24 h post-infection. (**B**) 48 h post-infection. (**C**) 72 h post-infection. (**D**) 96 h post-infection.

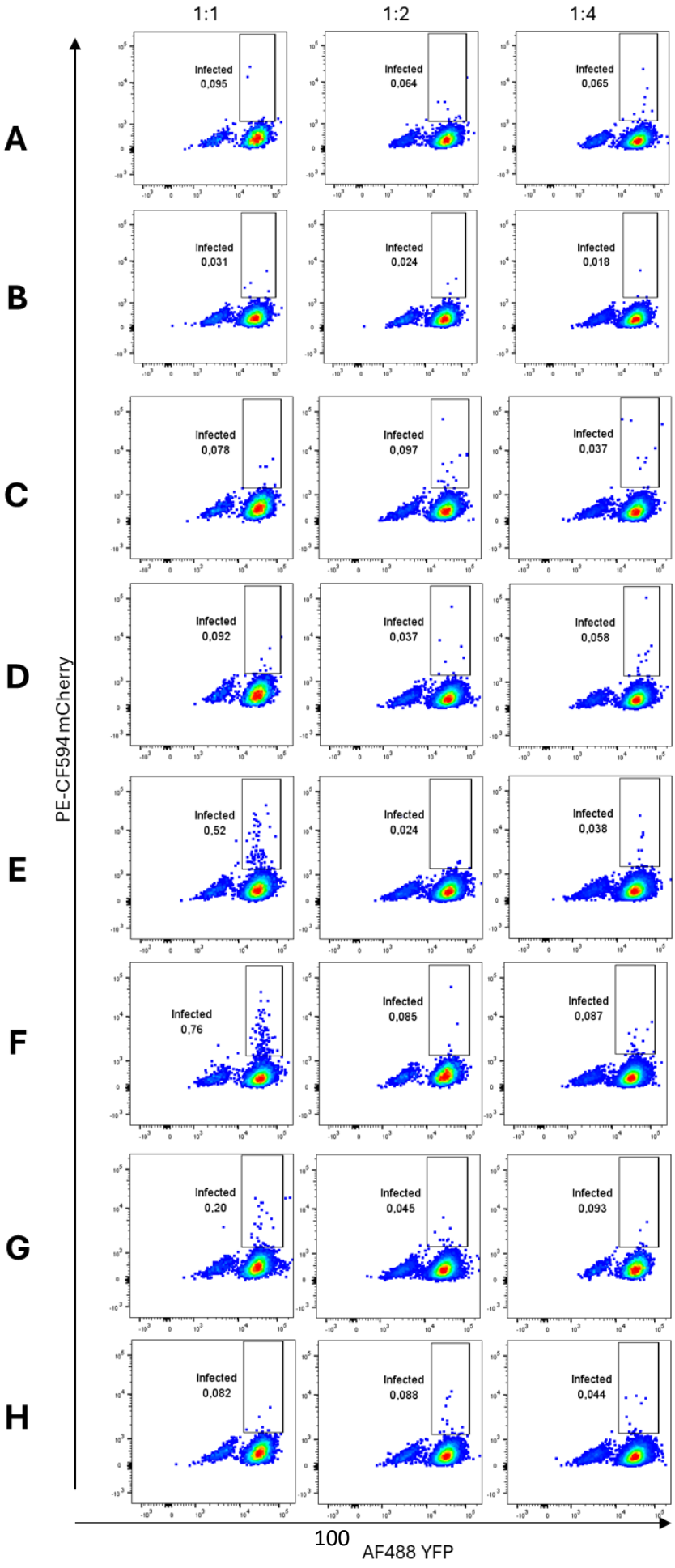
1:1
1:2
1:4
A
B
C
D
E
F
G
H
Infected 0,095
Infected 0,064
Infected 0,065
Infected 0,031
Infected 0,024
Infected 0,018
Infected 0,078
Infected 0,097
Infected 0,037
Infected 0,092
Infected 0,037
Infected 0,058
Infected 0,52
Infected 0,024
Infected 0,038
Infected 0,76
Infected 0,085
Infected 0,087
Infected 0,20
Infected 0,045
Infected 0,093
Infected 0,082
Infected 0,088
Infected 0,044
PE-CF594 mCherry
100
AF488 YFP

Figure C4: Infection duration optimization for in-house multi-vector pseudovirus generated by nucleofection at different time points. (**A**) 24 h post-infection (Replicate 1). (**B**) 24 h post-infection (Replicate 2). (**C**) 48 h post-infection (Replicate 1). (**D**) 48 h post-infection (Replicate 2). (**E**) 72 h post-infection (Replicate 1). (**F**) 72 h post-infection (Replicate 2). (**G**) 96 h post-infection (Replicate 1). (**H**) 96 h post-infection (Replicate 2).

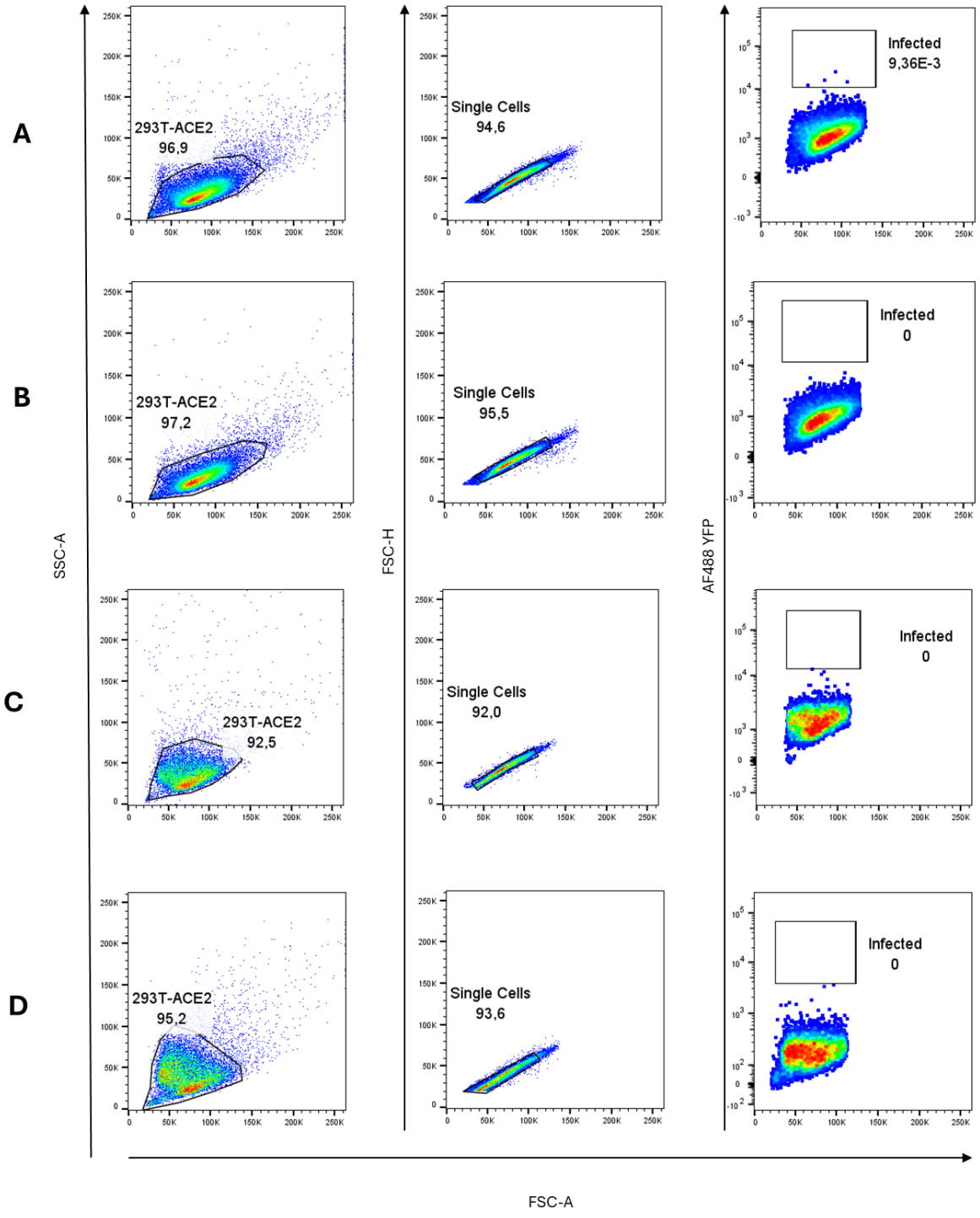

Figure C5: Uninfected 293T-ACE2 cell controls for infection duration optimization for two-vector pseudovirus generated by nucleofection and classical transfection. (**A**) 72 h post-infection for nucleofection-generated two-vector pseudovirus. (**B**) 72 h post-infection for classical transfection-generated two-vector pseudovirus. (**C**) 96 h post-infection for nucleofection-generated two-vector pseudovirus. (**D**) 96 h post-infection for classical transfection-generated two-vector pseudovirus.

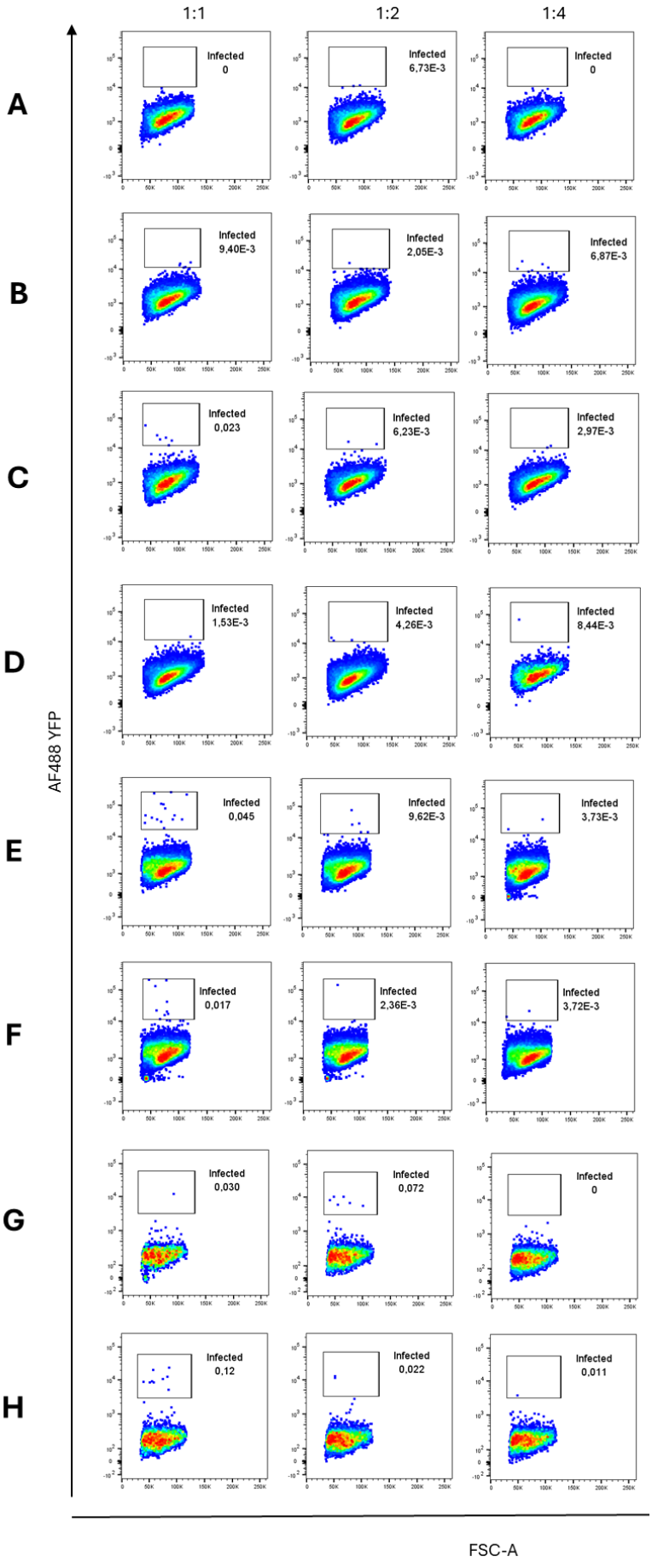
1:1
1:2
1:4
A
B
C
D
E
F
G
H
Infected 0
Infected 6,73E-3
Infected 0
Infected 9,40E-3
Infected 2,05E-3
Infected 6,87E-3
Infected 0,023
Infected 6,23E-3
Infected 2,97E-3
Infected 1,53E-3
Infected 4,26E-3
Infected 8,44E-3
Infected 0,045
Infected 9,62E-3
Infected 3,73E-3
Infected 0,017
Infected 2,36E-3
Infected 3,72E-3
Infected 0,030
Infected 0,072
Infected 0
Infected 0,12
Infected 0,022
Infected 0,011
AF488 YFP
FSC-A

Figure C7: Infection optimization for untruncated two-vector pseudovirus generated by nucleofection and classical transfection. (**A**) 72 h post-infection for nucleofection-generated two-vector pseudovirus (Replicate 1). (**B**) 72 h post-infection for nucleofection-generated two-vector pseudovirus (Replicate 2). (**C**) 72 h post-infection for classical transfection-generated two-vector pseudovirus (Replicate 1). (**D**) 72 h post-infection for classical transfection-generated two-vector pseudovirus (Replicate 2). (**E**) 96 h post-infection for nucleofection-generated two-vector pseudovirus (Replicate 1). (**F**) 96 h post-infection for nucleofection-generated two-vector pseudovirus (Replicate 2). (**G**) 96 h post-infection for classical transfection-generated two-vector pseudovirus (Replicate 1). (**D**) 96 h post-infection for classical transfection-generated two-vector pseudovirus (Replicate 2).

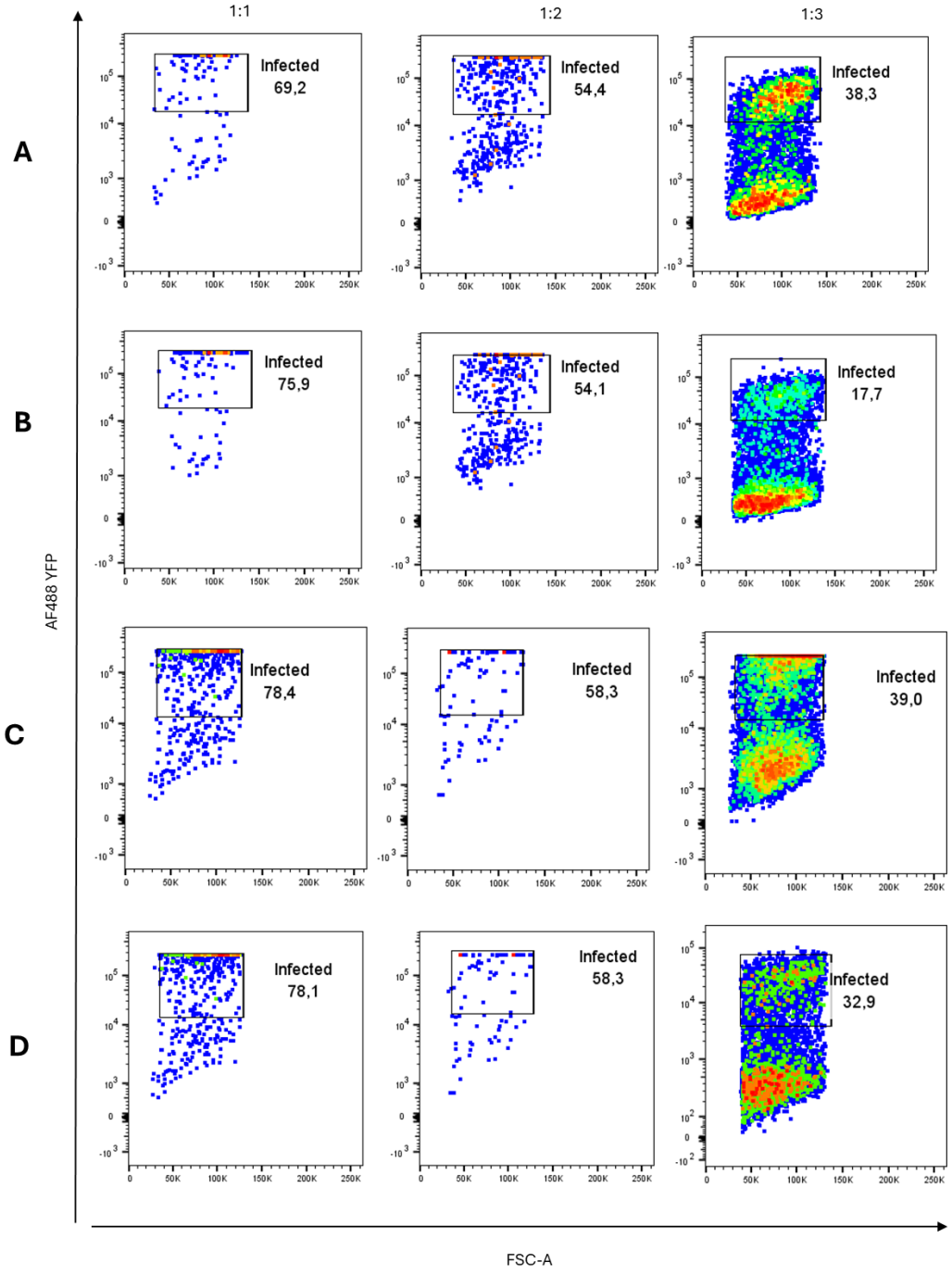

Figure C8: VSV-GFP control conditions at different dilutions. (**A**) 72 h post-infection. (**B**) 72 h post-infection. (**C**) 96 h post-infection. (**D**) 96 h post-infection.

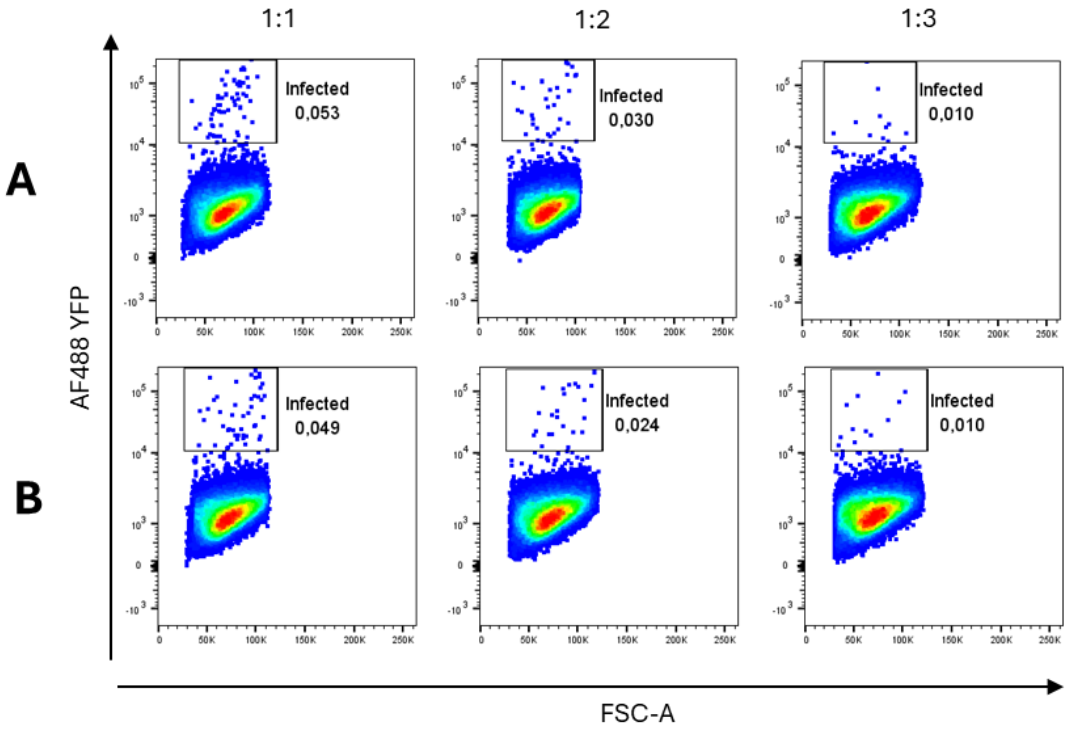

Figure C7: Infection optimization for untruncated two-vector pseudovirus generated by nucleofection and classical transfection.

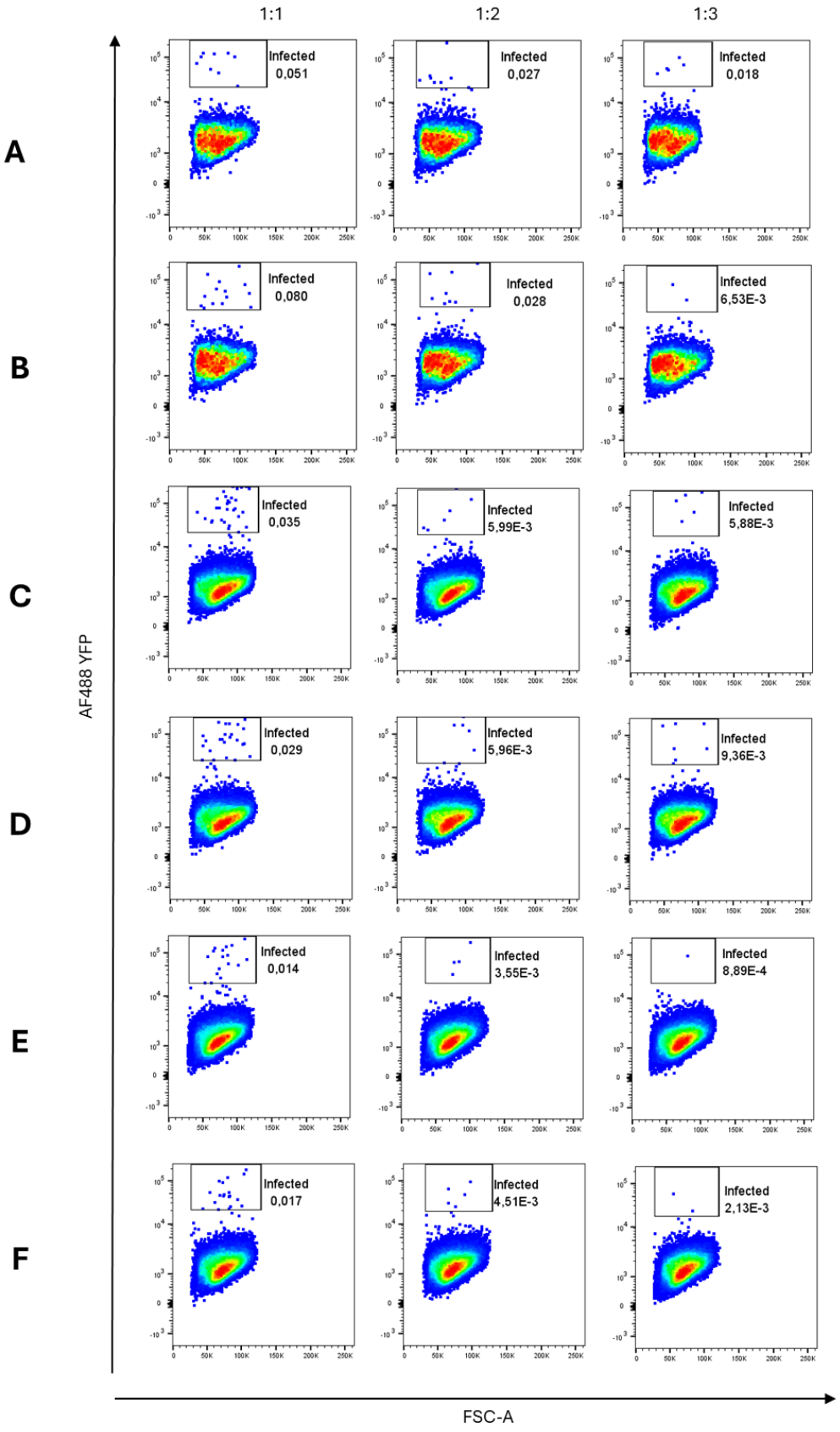
1:1
1:2
1:3
A
B
C
D
E
F
Infected 0,051
Infected 0,027
Infected 0,018
Infected 0,080
Infected 0,028
Infected 6,53E-3
Infected 0,035
Infected 5,99E-3
Infected 5,88E-3
Infected 0,029
Infected 5,96E-3
Infected 9,36E-3
Infected 0,014
Infected 3,55E-3
Infected 8,89E-4
Infected 0,017
Infected 4,51E-3
Infected 2,13E-3
AF488 YFP
FSC-A

Figure C8: Cell density comparison for truncated two-vector pseudovirus generated by classical transfection. (**A**) 1.25 × 10^4 cells (Replicate 1). (**B**) 1.25 × 10^4 cells (Replicate 2). (**C**) 2.5 × 10^4 cells (Replicate 1). (**D**) 2.5 × 10^4 cells (Replicate 2). (**E**) 5 × 10^4 cells (Replicate 1). (**F**) 5 × 10^4 cells (Replicate 2)

Appendix D: Turnitin report

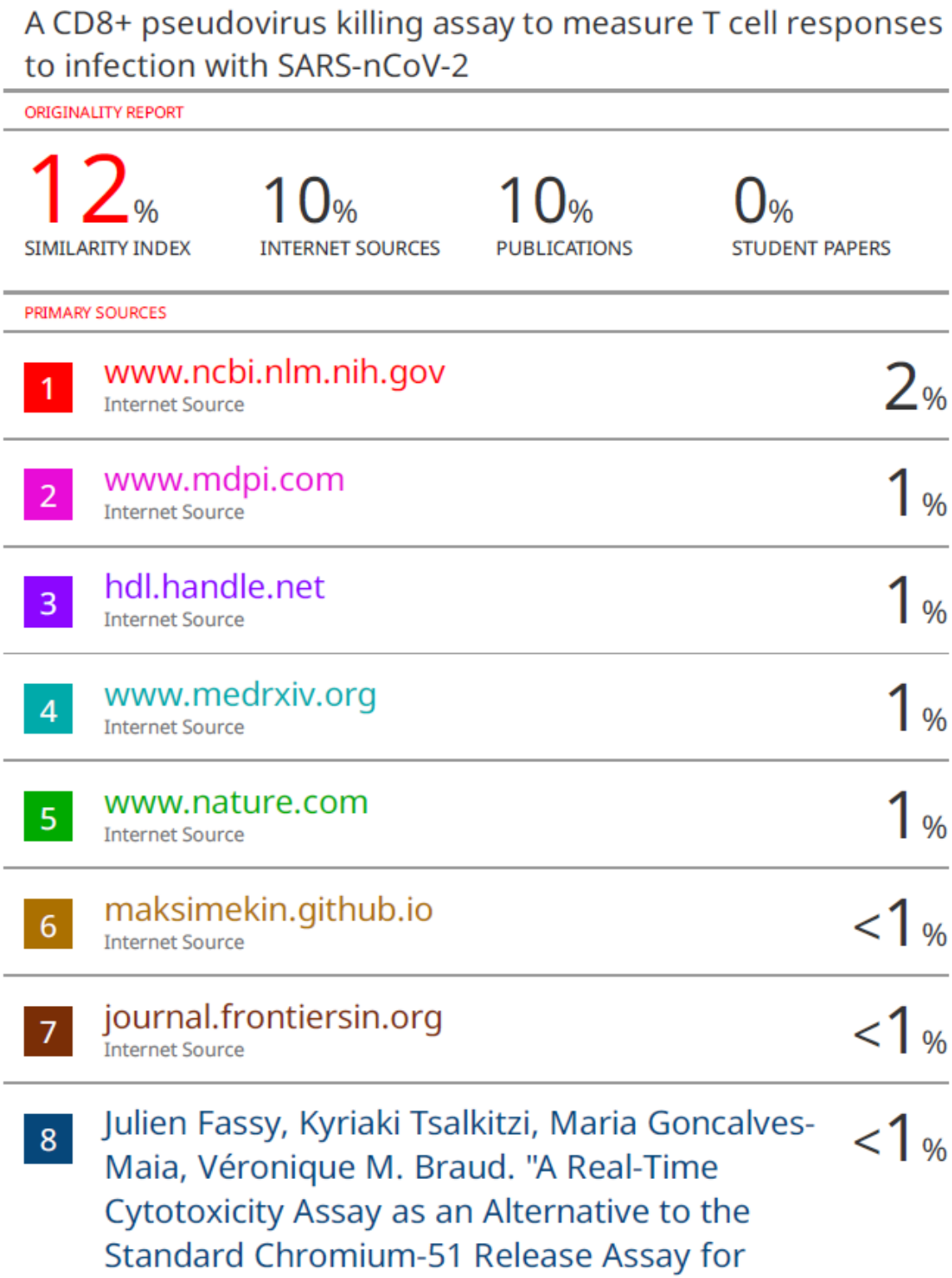

A CD8+ pseudovirus killing assay to measure T cell responses to infection with SARS-nCoV-2

ORIGINALITY REPORT

12%	10%	10%	0%
SIMILARITY INDEX	INTERNET SOURCES	PUBLICATIONS	STUDENT PAPERS

PRIMARY SOURCES

1	www.ncbi.nlm.nih.gov Internet Source	2%
2	www.mdpi.com Internet Source	1%
3	hdl.handle.net Internet Source	1%
4	www.medrxiv.org Internet Source	1%
5	www.nature.com Internet Source	1%
6	maksimekin.github.io Internet Source	<1%
7	journal.frontiersin.org Internet Source	<1%
8	Julien Fassy, Kyriaki Tsalkitzi, Maria Goncalves-Maia, Véronique M. Braud. "A Real-Time Cytotoxicity Assay as an Alternative to the Standard Chromium-51 Release Assay for	<1%

CHAPTER 6: REFERENCES

ABANI, O., ABBAS, A., ABBAS, F., ABBAS, M., ABBASI, S., ABBASS, H., ABBOTT, A., ABDALLAH, N., ABDELAZIZ, A. & ABDELFATTAH, M. 2021. Convalescent plasma in patients admitted to hospital with COVID-19 (RECOVERY): a randomised controlled, open-label, platform trial. *The Lancet,* 397**,** 2049-2059.

AFROUGH, B., DOWALL, S. & HEWSON, R. 2019. Emerging viruses and current strategies for vaccine intervention. *Clin Exp Immunol,* 196**,** 157-166.

ALI, A., MISHRA, R., KAUR, H. & BANERJEA, A. C. 2021. HIV-1 Tat: an update on transcriptional and non-transcriptional functions. *Biochimie,* 190**,** 24-35.

ALMENDRO-VÁZQUEZ, P., LAGUNA-GOYA, R. & PAZ-ARTAL, E. 2023. Defending against SARS-CoV-2: The T cell perspective. *Front Immunol,* 14**,** 1107803.

ALRUBAYYI, A., GEA-MALLORQUÍ, E., TOUIZER, E., HAMEIRI-BOWEN, D., KOPYCINSKI, J., CHARLTON, B., FISHER-PEARSON, N., MUIR, L., ROSA, A. & ROUSTAN, C. 2021. Characterization of humoral and SARS-CoV-2 specific T cell responses in people living with HIV. *Nature communications,* 12**,** 1-16.

AMICONE, M., BORGES, V., ALVES, M. J., ISIDRO, J., ZÉ-ZÉ, L., DUARTE, S., VIEIRA, L., GUIOMAR, R., GOMES, J. P. & GORDO, I. 2022. Mutation rate of SARS-CoV-2 and emergence of mutators during experimental evolution. *Evol Med Public Health,* 10**,** 142-155.

ANDREWS, N., TESSIER, E., STOWE, J., GOWER, C., KIRSEBOM, F., SIMMONS, R., GALLAGHER, E., THELWALL, S., GROVES, N., DABRERA, G., MYERS, R., CAMPBELL, C. N. J., AMIRTHALINGAM, G., EDMUNDS, M., ZAMBON, M., BROWN, K., HOPKINS, S., CHAND, M., LADHANI, S. N., RAMSAY, M. & LOPEZ BERNAL, J. 2022. Duration of Protection against Mild and Severe Disease by Covid-19 Vaccines. *N Engl J Med,* 386**,** 340-350.

ARAF, Y., AKTER, F., TANG, Y. D., FATEMI, R., PARVEZ, M. S. A., ZHENG, C. & HOSSAIN, M. G. 2022. Omicron variant of SARS-CoV-2: genomics, transmissibility, and responses to current COVID-19 vaccines. *Journal of medical virology,* 94**,** 1825-1832.

ARUNACHALAM, P. S., WIMMERS, F., MOK, C. K. P., PERERA, R., SCOTT, M., HAGAN, T., SIGAL, N., FENG, Y., BRISTOW, L., TAK-YIN TSANG, O., WAGH, D., COLLER, J., PELLEGRINI, K. L., KAZMIN, D., ALAAEDDINE, G., LEUNG, W. S., CHAN, J. M. C., CHIK, T. S. H., CHOI, C. Y. C., HUERTA, C., PAINE MCCULLOUGH, M., LV, H., ANDERSON, E., EDUPUGANTI, S., UPADHYAY, A. A., BOSINGER, S. E., MAECKER, H. T., KHATRI, P., ROUPHAEL, N., PEIRIS, M. & PULENDRAN, B. 2020. Systems biological assessment of immunity to mild versus severe COVID-19 infection in humans. *Science,* 369**,** 1210-1220.

ATLANI-DUAULT, L., LINA, B., CHAUVIN, F., DELFRAISSY, J. F. & MALVY, D. 2021. Immune evasion means we need a new COVID-19 social contract. *Lancet Public Health,* 6**,** e199-e200.

BARBER, D. L., WHERRY, E. J. & AHMED, R. 2003. Cutting edge: rapid in vivo killing by memory CD8 T cells. *J Immunol,* 171**,** 27-31.

BARTOSCH, B., DUBUISSON, J. & COSSET, F. L. 2003. Infectious hepatitis C virus pseudo-particles containing functional E1-E2 envelope protein complexes. *J Exp Med,* 197**,** 633-42.

BASTARD, P., ROSEN, L. B., ZHANG, Q., MICHAILIDIS, E., HOFFMANN, H. H., ZHANG, Y., DORGHAM, K., PHILIPPOT, Q., ROSAIN, J., BÉZIAT, V., MANRY, J., SHAW, E., HALJASMÄGI, L., PETERSON, P., LORENZO, L., BIZIEN, L., TROUILLET-ASSANT, S., DOBBS, K., DE JESUS, A. A., BELOT, A., KALLASTE, A., CATHERINOT, E., TANDJAOUI-LAMBIOTTE, Y., LE PEN, J., KERNER, G., BIGIO, B., SEELEUTHNER, Y., YANG, R., BOLZE, A., SPAAN, A. N., DELMONTE, O. M., ABERS, M. S., AIUTI, A., CASARI, G., LAMPASONA, V., PIEMONTI, L., CICERI, F., BILGUVAR, K., LIFTON, R. P., VASSE, M., SMADJA, D. M., MIGAUD, M., HADJADJ, J., TERRIER, B., DUFFY, D., QUINTANA-MURCI, L., VAN DE BEEK, D., ROUSSEL, L., VINH, D. C., TANGYE, S. G., HAERYNCK, F., DALMAU, D., MARTINEZ-PICADO, J., BRODIN, P., NUSSENZWEIG, M. C., BOISSON-DUPUIS, S., RODRÍGUEZ-GALLEGO, C., VOGT, G., MOGENSEN, T. H., OLER, A. J., GU, J., BURBELO, P. D., COHEN, J. I., BIONDI, A., BETTINI, L. R.,

D'ANGIO, M., BONFANTI, P., ROSSIGNOL, P., MAYAUX, J., RIEUX-LAUCAT, F., HUSEBYE, E. S., FUSCO, F., URSINI, M. V., IMBERTI, L., SOTTINI, A., PAGHERA, S., QUIROS-ROLDAN, E., ROSSI, C., CASTAGNOLI, R., MONTAGNA, D., LICARI, A., MARSEGLIA, G. L., DUVAL, X., GHOSN, J., TSANG, J. S., GOLDBACH-MANSKY, R., KISAND, K., LIONAKIS, M. S., PUEL, A., ZHANG, S. Y., HOLLAND, S. M., GOROCHOV, G., JOUANGUY, E., RICE, C. M., COBAT, A., NOTARANGELO, L. D., ABEL, L., SU, H. C. & CASANOVA, J. L. 2020. Autoantibodies against type I IFNs in patients with life-threatening COVID-19. *Science,* 370.

BENTLEY, E. M., MATHER, S. T. & TEMPERTON, N. J. 2015. The use of pseudotypes to study viruses, virus sero-epidemiology and vaccination. *Vaccine,* 33**,** 2955-62.

BEWLEY, K. R., COOMBES, N. S., GAGNON, L., MCINROY, L., BAKER, N., SHAIK, I., ST-JEAN, J. R., ST-AMANT, N., BUTTIGIEG, K. R., HUMPHRIES, H. E., GODWIN, K. J., BRUNT, E., ALLEN, L., LEUNG, S., BROWN, P. J., PENN, E. J., THOMAS, K., KULNIS, G., HALLIS, B., CARROLL, M., FUNNELL, S. & CHARLTON, S. 2021. Quantification of SARS-CoV-2 neutralizing antibody by wild-type plaque reduction neutralization, microneutralization and pseudotyped virus neutralization assays. *Nature Protocols,* 16**,** 3114-3140.

BRUNNER, K., MAUEL, J., CEROTTINI, J.-C. & CHAPUIS, B. 1968. Quantitative assay of the lytic action of immune lymphoid cells of 51Cr-labelled allogeneic target cells in vitro; inhibition by isoantibody and by drugs. *Immunology,* 14**,** 181.

BULLED, N. & SINGER, M. 2020. In the shadow of HIV & TB: A commentary on the COVID epidemic in South Africa. *Global public health,* 15**,** 1231-1243.

BUSHMAN, M., KAHN, R., TAYLOR, B. P., LIPSITCH, M. & HANAGE, W. P. 2021. Population impact of SARS-CoV-2 variants with enhanced transmissibility and/or partial immune escape. *Cell,* 184**,** 6229-6242.e18.

BYERS, A. M., KEMBALL, C. C., MOSER, J. M. & LUKACHER, A. E. 2003. Cutting edge: rapid in vivo CTL activity by polyoma virus-specific effector and memory CD8+ T cells. *J Immunol,* 171**,** 17-21.

CANTONI, D., MAYORA-NETO, M. & TEMPERTON, N. 2021. The role of pseudotype neutralization assays in understanding SARS CoV-2. *Oxford open immunology,* 2**,** iqab005.

CARREÑO, A., GUERRERO-YAGÜE, R., CASAL, E., MENDOZA, R. & CORCHERO, J. L. 2024. Tuning plasmid DNA amounts for cost-effective transfections of mammalian cells: when less is more. *Appl Microbiol Biotechnol,* 108**,** 98.

CASTRO DOPICO, X., OLS, S., LORÉ, K. & KARLSSON HEDESTAM, G. B. 2022. Immunity to SARS-CoV-2 induced by infection or vaccination. *Journal of Internal Medicine,* 291**,** 32-50.

CELE, S., GAZY, I., JACKSON, L., HWA, S. H., TEGALLY, H., LUSTIG, G., GIANDHARI, J., PILLAY, S., WILKINSON, E., NAIDOO, Y., KARIM, F., GANGA, Y., KHAN, K., BERNSTEIN, M., BALAZS, A. B., GOSNELL, B. I., HANEKOM, W., MOOSA, M. S., LESSELLS, R. J., DE OLIVEIRA, T. & SIGAL, A. 2021. Escape of SARS-CoV-2 501Y.V2 from neutralization by convalescent plasma. *Nature,* 593**,** 142-146.

CELE, S., KARIM, F., LUSTIG, G., SAN, J. E., HERMANUS, T., TEGALLY, H., SNYMAN, J., MOYO-GWETE, T., WILKINSON, E., BERNSTEIN, M., KHAN, K., HWA, S. H., TILLES, S. W., SINGH, L., GIANDHARI, J., MTHABELA, N., MAZIBUKO, M., GANGA, Y., GOSNELL, B. I., KARIM, S. S. A., HANEKOM, W., VAN VOORHIS, W. C., NDUNG'U, T., LESSELLS, R. J., MOORE, P. L., MOOSA, M. S., DE OLIVEIRA, T. & SIGAL, A. 2022. SARS-CoV-2 prolonged infection during advanced HIV disease evolves extensive immune escape. *Cell Host Microbe,* 30**,** 154-162.e5.

CHEN, H. Y., HUANG, C., TIAN, L., HUANG, X., ZHANG, C., LLEWELLYN, G. N., ROGERS, G. L., ANDRESEN, K., O'GORMAN, M. R. G., CHEN, Y. W. & CANNON, P. M. 2021. Cytoplasmic Tail Truncation of SARS-CoV-2 Spike Protein Enhances Titer of Pseudotyped Vectors but Masks the Effect of the D614G Mutation. *J Virol,* 95**,** e0096621.

CHEN, M. & ZHANG, X. E. 2021. Construction and applications of SARS-CoV-2 pseudoviruses: a mini review. *Int J Biol Sci,* 17**,** 1574-1580.

CHEN, Q., NIE, J., HUANG, W., JIAO, Y., LI, L., ZHANG, T., ZHAO, J., WU, H. & WANG, Y. 2018. Development and optimization of a sensitive pseudovirus-based assay for HIV-1

neutralizing antibodies detection using A3R5 cells. *Human Vaccines & Immunotherapeutics,* 14**,** 199-208.

CHEN, X., LI, R., PAN, Z., QIAN, C., YANG, Y., YOU, R., ZHAO, J., LIU, P., GAO, L., LI, Z., HUANG, Q., XU, L., TANG, J., TIAN, Q., YAO, W., HU, L., YAN, X., ZHOU, X., WU, Y., DENG, K., ZHANG, Z., QIAN, Z., CHEN, Y. & YE, L. 2020a. Human monoclonal antibodies block the binding of SARS-CoV-2 spike protein to angiotensin converting enzyme 2 receptor. *Cell Mol Immunol,* 17**,** 647-649.

CHEN, X., PAN, Z., YUE, S., YU, F., ZHANG, J., YANG, Y., LI, R., LIU, B., YANG, X. & GAO, L. 2020b. Disease severity dictates SARS-CoV-2-specific neutralizing antibody responses in COVID-19. *Signal transduction and targeted therapy,* 5**,** 180.

CHOI, J., MEILLEUR, C. E. & HAERYFAR, S. M. M. 2019. Tailoring In Vivo Cytotoxicity Assays to Study Immunodominance in Tumor-specific CD8+ T Cell Responses. *J Vis Exp*.

CHOI, J. Y. & SMITH, D. M. 2021. SARS-CoV-2 Variants of Concern. *Yonsei Med J,* 62**,** 961-968.

CHONG, Z. X., YEAP, S. K. & HO, W. Y. 2021. Transfection types, methods and strategies: a technical review. *PeerJ,* 9**,** e11165.

CIOTTI, M., CICCOZZI, M., TERRINONI, A., JIANG, W.-C., WANG, C.-B. & BERNARDINI, S. 2020. The COVID-19 pandemic. *Critical Reviews in Clinical Laboratory Sciences,* 57**,** 365-388.

COHEN, K. W., LINDERMAN, S. L., MOODIE, Z., CZARTOSKI, J., LAI, L., MANTUS, G., NORWOOD, C., NYHOFF, L. E., EDARA, V. V. & FLOYD, K. 2021. Longitudinal analysis shows durable and broad immune memory after SARS-CoV-2 infection with persisting antibody responses and memory B and T cells. *Cell Reports Medicine,* 2.

COLLINS, D. R., GAIHA, G. D. & WALKER, B. D. 2020. CD8+ T cells in HIV control, cure and prevention. *Nature Reviews Immunology,* 20**,** 471-482.

COLLINS, D. R., URBACH, J. M., RACENET, Z. J., ARSHAD, U., POWER, K. A., NEWMAN, R. M., MYLVAGANAM, G. H., LY, N. L., LIAN, X. & RULL, A. 2021. Functional impairment of HIV-specific CD8+ T cells precedes aborted spontaneous control of viremia. *Immunity,* 54**,** 2372-2384. e7.

CORBETT, K. S., FLYNN, B., FOULDS, K. E., FRANCICA, J. R., BOYOGLU-BARNUM, S., WERNER, A. P., FLACH, B., O'CONNELL, S., BOCK, K. W., MINAI, M., NAGATA, B. M., ANDERSEN, H., MARTINEZ, D. R., NOE, A. T., DOUEK, N., DONALDSON, M. M., NJI, N. N., ALVARADO, G. S., EDWARDS, D. K., FLEBBE, D. R., LAMB, E., DORIA-ROSE, N. A., LIN, B. C., LOUDER, M. K., O'DELL, S., SCHMIDT, S. D., PHUNG, E., CHANG, L. A., YAP, C., TODD, J. M., PESSAINT, L., VAN RY, A., BROWNE, S., GREENHOUSE, J., PUTMAN-TAYLOR, T., STRASBAUGH, A., CAMPBELL, T. A., COOK, A., DODSON, A., STEINGREBE, K., SHI, W., ZHANG, Y., ABIONA, O. M., WANG, L., PEGU, A., YANG, E. S., LEUNG, K., ZHOU, T., TENG, I. T., WIDGE, A., GORDON, I., NOVIK, L., GILLESPIE, R. A., LOOMIS, R. J., MOLIVA, J. I., STEWART-JONES, G., HIMANSU, S., KONG, W. P., NASON, M. C., MORABITO, K. M., RUCKWARDT, T. J., LEDGERWOOD, J. E., GAUDINSKI, M. R., KWONG, P. D., MASCOLA, J. R., CARFI, A., LEWIS, M. G., BARIC, R. S., MCDERMOTT, A., MOORE, I. N., SULLIVAN, N. J., ROEDERER, M., SEDER, R. A. & GRAHAM, B. S. 2020. Evaluation of the mRNA-1273 Vaccine against SARS-CoV-2 in Nonhuman Primates. *N Engl J Med,* 383**,** 1544-1555.

COX, J. H., FERRARI, G. & JANETZKI, S. 2006. Measurement of cytokine release at the single cell level using the ELISPOT assay. *Methods,* 38**,** 274-282.

CRAWFORD, K. H., EGUIA, R., DINGENS, A. S., LOES, A. N., MALONE, K. D., WOLF, C. R., CHU, H. Y., TORTORICI, M. A., VEESLER, D. & MURPHY, M. 2020. Protocol and reagents for pseudotyping lentiviral particles with SARS-CoV-2 spike protein for neutralization assays. *Viruses,* 12**,** 513.

CUI, J., LI, F. & SHI, Z.-L. 2019. Origin and evolution of pathogenic coronaviruses. *Nature reviews microbiology,* 17**,** 181-192.

DAI, L. & GAO, G. F. 2021. Viral targets for vaccines against COVID-19. *Nature Reviews Immunology,* 21**,** 73-82.

DALGAARD, T. S., NORUP, L. R., RUBBENSTROTH, D., WATTRANG, E. & JUUL-MADSEN, H. R. 2010. Flow cytometric assessment of antigen-specific proliferation in peripheral chicken T cells by CFSE dilution. *Veterinary Immunology and Immunopathology,* 138**,** 85-94.

DAN, J. M., LINDESTAM ARLEHAMN, C. S., WEISKOPF, D., DA SILVA ANTUNES, R., HAVENAR-DAUGHTON, C., REISS, S. M., BRIGGER, M., BOTHWELL, M., SETTE, A. & CROTTY, S. 2016. A cytokine-independent approach to identify antigen-specific human germinal center T follicular helper cells and rare antigen-specific CD4+ T cells in blood. *The Journal of Immunology,* 197**,** 983-993.

DAN, J. M., MATEUS, J., KATO, Y., HASTIE, K. M., YU, E. D., FALITI, C. E., GRIFONI, A., RAMIREZ, S. I., HAUPT, S. & FRAZIER, A. 2021. Immunological memory to SARS-CoV-2 assessed for up to 8 months after infection. *Science,* 371**,** eabf4063.

DANILOSKI, Z., JORDAN, T. X., ILMAIN, J. K., GUO, X., BHABHA, G., TENOEVER, B. R. & SANJANA, N. E. 2021. The Spike D614G mutation increases SARS-CoV-2 infection of multiple human cell types. *Elife,* 10.

DEEKS, S. G., OVERBAUGH, J., PHILLIPS, A. & BUCHBINDER, S. 2015. HIV infection. *Nature Reviews Disease Primers,* 1**,** 15035.

DEJNIRATTISAI, W., HUO, J., ZHOU, D., ZAHRADNÍK, J., SUPASA, P., LIU, C., DUYVESTEYN, H. M. E., GINN, H. M., MENTZER, A. J., TUEKPRAKHON, A., NUTALAI, R., WANG, B., DIJOKAITE, A., KHAN, S., AVINOAM, O., BAHAR, M., SKELLY, D., ADELE, S., JOHNSON, S. A., AMINI, A., RITTER, T. G., MASON, C., DOLD, C., PAN, D., ASSADI, S., BELLASS, A., OMO-DARE, N., KOECKERLING, D., FLAXMAN, A., JENKIN, D., ALEY, P. K., VOYSEY, M., COSTA CLEMENS, S. A., NAVECA, F. G., NASCIMENTO, V., NASCIMENTO, F., FERNANDES DA COSTA, C., RESENDE, P. C., PAUVOLID-CORREA, A., SIQUEIRA, M. M., BAILLIE, V., SERAFIN, N., KWATRA, G., DA SILVA, K., MADHI, S. A., NUNES, M. C., MALIK, T., OPENSHAW, P. J. M., BAILLIE, J. K., SEMPLE, M. G., TOWNSEND, A. R., HUANG, K. A., TAN, T. K., CARROLL, M. W., KLENERMAN, P., BARNES, E., DUNACHIE, S. J., CONSTANTINIDES, B., WEBSTER, H., CROOK, D., POLLARD, A. J., LAMBE, T., PATERSON, N. G., WILLIAMS, M. A., HALL, D. R., FRY, E. E., MONGKOLSAPAYA, J., REN, J., SCHREIBER, G., STUART, D. I. & SCREATON, G. R. 2022. SARS-CoV-2 Omicron-B.1.1.529 leads to widespread escape from neutralizing antibody responses. *Cell,* 185**,** 467-484.e15.

DEMERS, K. R., REUTER, M. A. & BETTS, M. R. 2013. CD8+ T-cell effector function and transcriptional regulation during HIV pathogenesis. *Immunological Reviews,* 254**,** 190-206.

DENG, X., GARCIA-KNIGHT, M. A., KHALID, M. M., SERVELLITA, V., WANG, C., MORRIS, M. K., SOTOMAYOR-GONZÁLEZ, A., GLASNER, D. R., REYES, K. R. & GLIWA, A. S. 2021. Transmission, infectivity, and neutralization of a spike L452R SARS-CoV-2 variant. *Cell,* 184**,** 3426-3437. e8.

DONG, Y., DAI, T., WEI, Y., ZHANG, L., ZHENG, M. & ZHOU, F. 2020. A systematic review of SARS-CoV-2 vaccine candidates. *Signal Transduction and Targeted Therapy,* 5**,** 237.

DONOFRIO, G., FRANCESCHI, V., MACCHI, F., RUSSO, L., ROCCI, A., MARCHICA, V., COSTA, F., GIULIANI, N., FERRARI, C. & MISSALE, G. 2021. A simplified SARS-CoV-2 pseudovirus neutralization assay. *Vaccines,* 9**,** 389.

ĐORĐEVIĆ, M., PAUNOVIĆ, V., JOVANOVIĆ TUCOVIĆ, M., TOLIĆ, A., RAJIĆ, J., DINIĆ, S., USKOKOVIĆ, A., GRDOVIĆ, N., MIHAILOVIĆ, M. & MARKOVIĆ, I. 2022. Nucleofection as an efficient method for alpha Tc1-6 cell line transfection. *Applied Sciences,* 12**,** 7938.

DULL, T., ZUFFEREY, R., KELLY, M., MANDEL, R. J., NGUYEN, M., TRONO, D. & NALDINI, L. 1998. A third-generation lentivirus vector with a conditional packaging system. *J Virol,* 72**,** 8463-71.

ELSNER, R. A. & SHLOMCHIK, M. J. 2020. Germinal center and extrafollicular B cell responses in vaccination, immunity, and autoimmunity. *Immunity,* 53**,** 1136-1150.

EVANS, J. P., ZENG, C., CARLIN, C., LOZANSKI, G., SAIF, L. J., OLTZ, E. M., GUMINA, R. J. & LIU, S.-L. 2022. Neutralizing antibody responses elicited by SARS-CoV-2 mRNA vaccination wane over time and are boosted by breakthrough infection. *Science Translational Medicine*.

FARBER, D. L., NETEA, M. G., RADBRUCH, A., RAJEWSKY, K. & ZINKERNAGEL, R. M. 2016. Immunological memory: lessons from the past and a look to the future. *Nature Reviews Immunology,* 16**,** 124-128.

FASSY, J., TSALKITZI, K., GONCALVES-MAIA, M. & BRAUD, V. M. 2017. A real-time cytotoxicity assay as an alternative to the standard chromium-51 release assay for measurement of human NK and T cell cytotoxic activity. *Current protocols in immunology,* 118**,** 7.42. 1-7.42. 12.

FENG, Y., ZHANG, Y., HE, Z., HUANG, H., TIAN, X., WANG, G., CHEN, D., REN, Y., JIA, L. & WANG, W. 2022. Immunogenicity of an inactivated SARS-CoV-2 vaccine in people living with HIV-1: a non-randomized cohort study. *EClinicalMedicine,* 43.

FERRARI, G., KORBER, B., GOONETILLEKE, N., LIU, M. K., TURNBULL, E. L., SALAZAR-GONZALEZ, J. F., HAWKINS, N., SELF, S., WATSON, S. & BETTS, M. R. 2011. Relationship between functional profile of HIV-1 specific CD8 T cells and epitope variability with the selection of escape mutants in acute HIV-1 infection. *PLoS pathogens,* 7**,** e1001273.

FIROUZABADI, N., GHASEMIYEH, P., MORADISHOOLI, F. & MOHAMMADI-SAMANI, S. 2023. Update on the effectiveness of COVID-19 vaccines on different variants of SARS-CoV-2. *Int Immunopharmacol,* 117**,** 109968.

FRANCIS, A. I., GHANY, S., GILKES, T. & UMAKANTHAN, S. 2022. Review of COVID-19 vaccine subtypes, efficacy and geographical distributions. *Postgrad Med J,* 98**,** 389-394.

FRATER, J., EWER, K. J., OGBE, A., PACE, M., ADELE, S., ADLAND, E., ALAGARATNAM, J., ALEY, P. K., ALI, M. & ANSARI, M. A. 2021. Safety and immunogenicity of the ChAdOx1 nCoV-19 (AZD1222) vaccine against SARS-CoV-2 in HIV infection: a single-arm substudy of a phase 2/3 clinical trial. *The lancet HIV,* 8**,** e474-e485.

FUKUSHI, S., WATANABE, R. & TAGUCHI, F. 2008. Pseudotyped vesicular stomatitis virus for analysis of virus entry mediated by SARS coronavirus spike proteins. *Methods Mol Biol,* 454**,** 331-8.

GAIHA, G. D., ROSSIN, E. J., URBACH, J., LANDEROS, C., COLLINS, D. R., NWONU, C., MUZHINGI, I., ANAHTAR, M. N., WARING, O. M., PIECHOCKA-TROCHA, A., WARING, M., WORRALL, D. P., GHEBREMICHAEL, M. S., NEWMAN, R. M., POWER, K. A., ALLEN, T. M., CHODOSH, J. & WALKER, B. D. 2019. Structural topology defines protective CD8(+) T cell epitopes in the HIV proteome. *Science,* 364**,** 480-484.

GAO, F., MORRISON, S. G., ROBERTSON, D. L., THORNTON, C. L., CRAIG, S., KARLSSON, G., SODROSKI, J., MORGADO, M., GALVAO-CASTRO, B., VON BRIESEN, H., BEDDOWS, S., WEBER, J., SHARP, P. M., SHAW, G. M. & HAHN, B. H. 1996. Molecular cloning and analysis of functional envelope genes from human immunodeficiency virus type 1 sequence subtypes A through G. The WHO and NIAID Networks for HIV Isolation and Characterization. *J Virol,* 70**,** 1651-67.

GAO, Q., BAO, L., MAO, H., WANG, L., XU, K., YANG, M., LI, Y., ZHU, L., WANG, N., LV, Z., GAO, H., GE, X., KAN, B., HU, Y., LIU, J., CAI, F., JIANG, D., YIN, Y., QIN, C., LI, J., GONG, X., LOU, X., SHI, W., WU, D., ZHANG, H., ZHU, L., DENG, W., LI, Y., LU, J., LI, C., WANG, X., YIN, W., ZHANG, Y. & QIN, C. 2020. Development of an inactivated vaccine candidate for SARS-CoV-2. *Science,* 369**,** 77-81.

GARCIA-BELTRAN, W. F., LAM, E. C., ST DENIS, K., NITIDO, A. D., GARCIA, Z. H., HAUSER, B. M., FELDMAN, J., PAVLOVIC, M. N., GREGORY, D. J., POZNANSKY, M. C., SIGAL, A., SCHMIDT, A. G., IAFRATE, A. J., NARANBHAI, V. & BALAZS, A. B. 2021. Multiple SARS-CoV-2 variants escape neutralization by vaccine-induced humoral immunity. *Cell,* 184**,** 2372-2383.e9.

GARCÍA-MONTERO, C., FRAILE-MARTÍNEZ, O., BRAVO, C., TORRES-CARRANZA, D., SANCHEZ-TRUJILLO, L., GÓMEZ-LAHOZ, A. M., GUIJARRO, L. G., GARCÍA-HONDUVILLA, N., ASÚNSOLO, A., BUJAN, J., MONSERRAT, J., SERRANO, E., ÁLVAREZ-MON, M., DE LEÓN-LUIS, J. A., ÁLVAREZ-MON, M. A. & ORTEGA, M. A. 2021. An Updated Review of SARS-CoV-2 Vaccines and the Importance of Effective Vaccination Programs in Pandemic Times. *Vaccines (Basel),* 9.

GERRITSEN, B. & PANDIT, A. 2016. The memory of a killer T cell: models of CD8+ T cell differentiation. *Immunology and cell biology,* 94**,** 236-241.

GRAALMANN, T., BORST, K., MANCHANDA, H., VAAS, L., BRUHN, M., GRAALMANN, L., KOSTER, M., VERBOOM, M., HALLENSLEBEN, M., GUZMÁN, C. A., SUTTER, G., SCHMIDT, R. E., WITTE, T. & KALINKE, U. 2021. B cell depletion impairs vaccination-induced CD8⁺ T cell responses in a type I interferon-dependent manner. *Annals of the Rheumatic Diseases,* 80**,** 1537-1544.

GRIBBLE, J., STEVENS, L. J., AGOSTINI, M. L., ANDERSON-DANIELS, J., CHAPPELL, J. D., LU, X., PRUIJSSERS, A. J., ROUTH, A. L. & DENISON, M. R. 2021. The coronavirus proofreading exoribonuclease mediates extensive viral recombination. *PLoS Pathog,* 17**,** e1009226.

GRIFONI, A., SIDNEY, J., VITA, R., PETERS, B., CROTTY, S., WEISKOPF, D. & SETTE, A. 2021. SARS-CoV-2 human T cell epitopes: Adaptive immune response against COVID-19. *Cell Host Microbe,* 29**,** 1076-1092.

GRIFONI, A., WEISKOPF, D., RAMIREZ, S. I., MATEUS, J., DAN, J. M., MODERBACHER, C. R., RAWLINGS, S. A., SUTHERLAND, A., PREMKUMAR, L., JADI, R. S., MARRAMA, D., DE SILVA, A. M., FRAZIER, A., CARLIN, A. F., GREENBAUM, J. A., PETERS, B., KRAMMER, F., SMITH, D. M., CROTTY, S. & SETTE, A. 2020. Targets of T Cell Responses to SARS-CoV-2 Coronavirus in Humans with COVID-19 Disease and Unexposed Individuals. *Cell,* 181**,** 1489-1501.e15.

GUAN, W. J., NI, Z. Y., HU, Y., LIANG, W. H., OU, C. Q., HE, J. X., LIU, L., SHAN, H., LEI, C. L., HUI, D. S. C., DU, B., LI, L. J., ZENG, G., YUEN, K. Y., CHEN, R. C., TANG, C. L., WANG, T., CHEN, P. Y., XIANG, J., LI, S. Y., WANG, J. L., LIANG, Z. J., PENG, Y. X., WEI, L., LIU, Y., HU, Y. H., PENG, P., WANG, J. M., LIU, J. Y., CHEN, Z., LI, G., ZHENG, Z. J., QIU, S. Q., LUO, J., YE, C. J., ZHU, S. Y. & ZHONG, N. S. 2020. Clinical Characteristics of Coronavirus Disease 2019 in China. *N Engl J Med,* 382**,** 1708-1720.

GUTIERREZ, L., BECKFORD, J. & ALACHKAR, H. 2020. Deciphering the TCR repertoire to solve the COVID-19 mystery. *Trends in pharmacological sciences,* 41**,** 518-530.

HADJADJ, J., YATIM, N., BARNABEI, L., CORNEAU, A., BOUSSIER, J., SMITH, N., PÉRÉ, H., CHARBIT, B., BONDET, V., CHENEVIER-GOBEAUX, C., BREILLAT, P., CARLIER, N., GAUZIT, R., MORBIEU, C., PÈNE, F., MARIN, N., ROCHE, N., SZWEBEL, T. A., MERKLING, S. H., TRELUYER, J. M., VEYER, D., MOUTHON, L., BLANC, C., THARAUX, P. L., ROZENBERG, F., FISCHER, A., DUFFY, D., RIEUX-LAUCAT, F., KERNÉIS, S. & TERRIER, B. 2020. Impaired type I interferon activity and inflammatory responses in severe COVID-19 patients. *Science,* 369**,** 718-724.

HALPERIN, S. A., YE, L., MACKINNON-CAMERON, D., SMITH, B., CAHN, P. E., RUIZ-PALACIOS, G. M., IKRAM, A., LANAS, F., GUERRERO, M. L. & NAVARRO, S. R. L. M. O. 2022. Final efficacy analysis, interim safety analysis, and immunogenicity of a single dose of recombinant novel coronavirus vaccine (adenovirus type 5 vector) in adults 18 years and older: an international, multicentre, randomised, double-blinded, placebo-controlled phase 3 trial. *The Lancet,* 399**,** 237-248.

HE, S., WAHEED, A. A., HETRICK, B., DABBAGH, D., AKHRYMUK, I. V., KEHN-HALL, K., FREED, E. O. & WU, Y. 2020. PSGL-1 Inhibits the Incorporation of SARS-CoV and SARS-CoV-2 Spike Glycoproteins into Pseudovirions and Impairs Pseudovirus Attachment and Infectivity. *Viruses,* 13.

HEYNDRICKX, L., VERMOESEN, T., VEREECKEN, K., KURTH, J., COPPENS, S., AERTS, L., OHAGEN, A., VAN HERREWEGE, Y., LEWI, P. & VANHAM, G. 2008. Antiviral compounds show enhanced activity in HIV-1 single cycle pseudovirus assays as compared to classical PBMC assays. *J Virol Methods,* 148**,** 166-73.

HIE, B., ZHONG, E. D., BERGER, B. & BRYSON, B. 2021. Learning the language of viral evolution and escape. *Science,* 371**,** 284-288.

HILL, M., TACHEDJIAN, G. & MAK, J. 2005. The packaging and maturation of the HIV-1 Pol proteins. *Current HIV research,* 3**,** 73-85.

HOBERNIK, D. & BROS, M. 2018. DNA Vaccines-How Far From Clinical Use? *Int J Mol Sci,* 19.

HODCROFT, E. B., DOMMAN, D. B., SNYDER, D. J., OGUNTUYO, K. Y., VAN DIEST, M., DENSMORE, K. H., SCHWALM, K. C., FEMLING, J., CARROLL, J. L. & SCOTT, R. S.

2021. Emergence in late 2020 of multiple lineages of SARS-CoV-2 Spike protein variants affecting amino acid position 677. *MedRxiv*.
HOFFMANN, M., KLEINE-WEBER, H., SCHROEDER, S., KRÜGER, N., HERRLER, T., ERICHSEN, S., SCHIERGENS, T. S., HERRLER, G., WU, N. H., NITSCHE, A., MÜLLER, M. A., DROSTEN, C. & PÖHLMANN, S. 2020. SARS-CoV-2 Cell Entry Depends on ACE2 and TMPRSS2 and Is Blocked by a Clinically Proven Protease Inhibitor. *Cell,* 181**,** 271-280.e8.
HÖFT, M. A., BURGERS, W. A. & RIOU, C. 2024. The immune response to SARS-CoV-2 in people with HIV. *Cellular & Molecular Immunology,* 21**,** 184-196.
HUESO, T., POUDEROUX, C., PÉRÉ, H., BEAUMONT, A.-L., RAILLON, L.-A., ADER, F., CHATENOUD, L., ESHAGH, D., SZWEBEL, T.-A. & MARTINOT, M. 2020. Convalescent plasma therapy for B-cell–depleted patients with protracted COVID-19. *Blood, The Journal of the American Society of Hematology,* 136**,** 2290-2295.
INGULLI, E. 2007. Tracing tolerance and immunity in vivo by CFSE-labeling of administered cells. *Methods Mol Biol,* 380**,** 365-76.
ISHO, B., ABE, K. T., ZUO, M., JAMAL, A. J., RATHOD, B., WANG, J. H., LI, Z., CHAO, G., ROJAS, O. L. & BANG, Y. M. 2020. Persistence of serum and saliva antibody responses to SARS-CoV-2 spike antigens in COVID-19 patients. *Science immunology,* 5**,** eabe5511.
IUCHI, K., OYA, K., HOSOYA, K., SASAKI, K., SAKURADA, Y., NAKANO, T. & HISATOMI, H. 2020. Different morphologies of human embryonic kidney 293T cells in various types of culture dishes. *Cytotechnology,* 72**,** 131-140.
IZAC, J. R., KWEE, E. J., TIAN, L., ELSHEIKH, E., GAIGALAS, A. K., ELLIOTT, J. T. & WANG, L. 2023. Development of a Cell-Based SARS-CoV-2 Pseudovirus Neutralization Assay Using Imaging and Flow Cytometry Analysis. *Int J Mol Sci,* 24.
JACKSON, B., BONI, M. F., BULL, M. J., COLLERAN, A., COLQUHOUN, R. M., DARBY, A. C., HALDENBY, S., HILL, V., LUCACI, A. & MCCRONE, J. T. 2021. Generation and transmission of interlineage recombinants in the SARS-CoV-2 pandemic. *Cell,* 184**,** 5179-5188. e8.
JACKSON, C. B., FARZAN, M., CHEN, B. & CHOE, H. 2022. Mechanisms of SARS-CoV-2 entry into cells. *Nature Reviews Molecular Cell Biology,* 23**,** 3-20.
JAGANATHAN, S., STIEBER, F., RAO, S. N., NIKOLAYEVSKYY, V., MANISSERO, D., ALLEN, N., BOYLE, J. & HOWARD, J. 2021. Preliminary evaluation of QuantiFERON SARS-CoV-2 and QIAreach anti-SARS-CoV-2 total test in recently vaccinated individuals. *Infectious Diseases and Therapy,* 10**,** 2765-2776.
JARJOUR, N. N., MASOPUST, D. & JAMESON, S. C. 2021. T cell memory: understanding COVID-19. *Immunity,* 54**,** 14-18.
JASSAT, W., MUDARA, C., OZOUGWU, L., WELCH, R., ARENDSE, T., MASHA, M., BLUMBERG, L., KUFA, T., PUREN, A., GROOME, M., GOVENDER, N., PISA, P., GOVENDER, S., SANNE, I., BRAHMBHATT, H., PARMLEY, L., WOLMARANS, M., ROUSSEAU, P., SELIKOW, A., BURGESS, M., HANKEL, L., PARKER, A. & COHEN, C. 2024. Trends in COVID-19 admissions and deaths among people living with HIV in South Africa: analysis of national surveillance data. *Lancet HIV,* 11**,** e96-e105.
JEDEMA, I., VAN DER WERFF, N. M., BARGE, R. M., WILLEMZE, R. & FALKENBURG, J. H. 2004. New CFSE-based assay to determine susceptibility to lysis by cytotoxic T cells of leukemic precursor cells within a heterogeneous target cell population. *Blood,* 103**,** 2677-82.
JENSEN, S. S., FOMSGAARD, A., LARSEN, T. K., TINGSTEDT, J. L., GERSTOFT, J., KRONBORG, G., PEDERSEN, C. & KARLSSON, I. 2015. Initiation of antiretroviral therapy (ART) at different stages of HIV-1 disease is not associated with the proportion of exhausted CD8+ T cells. *PloS one,* 10**,** e0139573.
JIANG, H., JIN, P., GUO, X., ZHU, J., WANG, X., WAN, P., WAN, J., LIU, J., LI, J. & ZHU, F. 2023. The 6-Month Antibody Durability of Heterologous Convidecia Plus CoronaVac and Homologous CoronaVac Immunizations in People Aged 18–59 Years and over 60 Years Based on Two Randomized Controlled Trials in China. *Vaccines,* 11**,** 1815.
KAN, A. K. C. & LI, P. H. 2023. Inactivated COVID-19 vaccines: potential concerns of antibody-dependent enhancement and original antigenic sin. *Immunol Lett,* 259**,** 21-23.

KANOKUDOM, S., CHANSAENROJ, J., SUNTRONWONG, N., ASSAWAKOSRI, S., YORSAENG, R., NILYANIMIT, P., AEEMJINDA, R., KHANARAT, N., VICHAIWATTANA, P., KLINFUENG, S., THONGMEE, T., KATANYUTANON, A., THANASOPON, W., ARAYAPONG, J., WITHAKSABUT, W., SRIMUAN, D., THATSANATORN, T., SUDHINARASET, N., WANLAPAKORN, N., HONSAWEK, S. & POOVORAWAN, Y. 2023. Safety and immunogenicity of a third dose of COVID-19 protein subunit vaccine (Covovax(TM)) after homologous and heterologous two-dose regimens. *Int J Infect Dis,* 126**,** 64-72.

KARIM, F., GAZY, I., CELE, S., ZUNGU, Y., KRAUSE, R., BERNSTEIN, M., KHAN, K., GANGA, Y., RODEL, H., MTHABELA, N., MAZIBUKO, M., MUEMA, D., RAMJIT, D., NDUNG'U, T., HANEKOM, W., GOSNELL, B., LESSELLS, R. J., WONG, E. B., DE OLIVEIRA, T., MOOSA, M. S., LUSTIG, G., LESLIE, A., KLØVERPRIS, H. & SIGAL, A. 2021a. HIV status alters disease severity and immune cell responses in Beta variant SARS-CoV-2 infection wave. *Elife,* 10.

KARIM, F., MOOSA, M., GOSNELL, B., CELE, S., GIANDHARI, J., PILLAY, S., TEGALLY, H., WILKINSON, E., SAN, J., MSOMI, N., MLISANA, K., KHAN, K., BERNSTEIN, M., MANICKCHUND, N., SINGH, L., RAMPHAL, U., TEAM, C.-K., HANEKOM, W., LESSELLS, R., SIGAL, A. & DE OLIVEIRA, T. 2021b. Persistent SARS-CoV-2 infection and intra-host evolution in association with advanced HIV infection. *medRxiv***,** 2021.06.03.21258228.

KARIM, F., RIOU, C., BERNSTEIN, M., JULE, Z., LUSTIG, G., VAN GRAAN, S., KEETON, R. S., UPTON, J.-L., GANGA, Y., KHAN, K., REEDOY, K., MAZIBUKO, M., GOVENDER, K., THAMBU, K., NGCOBO, N., VENTER, E., MAKHADO, Z., HANEKOM, W., VON GOTTBERG, A., HOQUE, M., KARIM, Q. A., ABDOOL KARIM, S. S., MANICKCHUND, N., MAGULA, N., GOSNELL, B. I., LESSELLS, R. J., MOORE, P. L., BURGERS, W. A., DE OLIVEIRA, T., MOOSA, M.-Y. S. & SIGAL, A. 2024. Clearance of persistent SARS-CoV-2 associates with increased neutralizing antibodies in advanced HIV disease post-ART initiation. *Nature Communications,* 15**,** 2360.

KARLSSON, A. C., HUMBERT, M. & BUGGERT, M. 2020. The known unknowns of T cell immunity to COVID-19. *Science Immunology,* 5**,** eabe8063.

KAYSER, V. & RAMZAN, I. 2021. Vaccines and vaccination: history and emerging issues. *Hum Vaccin Immunother,* 17**,** 5255-5268.

KEETON, R., RICHARDSON, S. I., MOYO-GWETE, T., HERMANUS, T., TINCHO, M. B., BENEDE, N., MANAMELA, N. P., BAGUMA, R., MAKHADO, Z. & NGOMTI, A. 2021. Prior infection with SARS-CoV-2 boosts and broadens Ad26. COV2. S immunogenicity in a variant-dependent manner. *Cell host & microbe,* 29**,** 1611-1619. e5.

KEETON, R., TINCHO, M. B., NGOMTI, A., BAGUMA, R., BENEDE, N., SUZUKI, A., KHAN, K., CELE, S., BERNSTEIN, M., KARIM, F., MADZORERA, S. V., MOYO-GWETE, T., MENNEN, M., SKELEM, S., ADRIAANSE, M., MUTITHU, D., AREMU, O., STEK, C., DU BRUYN, E., VAN DER MESCHT, M. A., DE BEER, Z., DE VILLIERS, T. R., BODENSTEIN, A., VAN DEN BERG, G., MENDES, A., STRYDOM, A., VENTER, M., GIANDHARI, J., NAIDOO, Y., PILLAY, S., TEGALLY, H., GRIFONI, A., WEISKOPF, D., SETTE, A., WILKINSON, R. J., DE OLIVEIRA, T., BEKKER, L.-G., GRAY, G., UECKERMANN, V., ROSSOUW, T., BOSWELL, M. T., BHIMAN, J. N., MOORE, P. L., SIGAL, A., NTUSI, N. A. B., BURGERS, W. A. & RIOU, C. 2022. T cell responses to SARS-CoV-2 spike cross-recognize Omicron. *Nature,* 603**,** 488-492.

KEMP, S. A., COLLIER, D. A., DATIR, R. P., FERREIRA, I. A., GAYED, S., JAHUN, A., HOSMILLO, M., REES-SPEAR, C., MLCOCHOVA, P. & LUMB, I. U. 2021. SARS-CoV-2 evolution during treatment of chronic infection. *Nature,* 592**,** 277-282.

KHAN, K., KARIM, F., GANGA, Y., BERNSTEIN, M., JULE, Z., REEDOY, K., CELE, S., LUSTIG, G., AMOAKO, D. & WOLTER, N. 2022. Omicron BA. 4/BA. 5 escape neutralizing immunity elicited by BA. 1 infection. *Nature communications,* 13**,** 4686.

KIESGEN, S., MESSINGER, J. C., CHINTALA, N. K., TANO, Z. & ADUSUMILLI, P. S. 2021. Comparative analysis of assays to measure CAR T-cell-mediated cytotoxicity. *Nature protocols,* 16**,** 1331-1342.

KLASSEN, S. A., SENEFELD, J. W., JOHNSON, P. W., CARTER, R. E., WIGGINS, C. C., SHOHAM, S., GROSSMAN, B. J., HENDERSON, J. P., MUSSER, J. & SALAZAR, E. The effect of convalescent plasma therapy on mortality among patients with COVID-19: systematic review and meta-analysis. Mayo Clinic Proceedings, 2021. Elsevier, 1262-1275.

KOHLMEIER, J. E., COOKENHAM, T., ROBERTS, A. D., MILLER, S. C. & WOODLAND, D. L. 2010. Type I interferons regulate cytolytic activity of memory CD8+ T cells in the lung airways during respiratory virus challenge. *Immunity,* 33**,** 96-105.

KRAUSE, R., SNYMAN, J., SHI-HSIA, H., MUEMA, D., KARIM, F., GANGA, Y., NGOEPE, A., ZUNGU, Y., GAZY, I., BERNSTEIN, M., KHAN, K., MAZIBUKO, M., MTHABELA, N., RAMJIT, D., LIMBO, O., JARDINE, J., SOK, D., WILSON, I. A., HANEKOM, W., SIGAL, A., KLØVERPRIS, H., NDUNG'U, T. & LESLIE, A. 2022. HIV skews the SARS-CoV-2 B cell response towards an extrafollicular maturation pathway. *Elife,* 11.

KUDLAY, D., KOFIADI, I. & KHAITOV, M. 2022. Peculiarities of the T cell immune response in COVID-19. *Vaccines,* 10**,** 242.

KUMAR, A., NARAYAN, R. K., PRASOON, P., KUMARI, C., KAUR, G., KUMAR, S., KULANDHASAMY, M., SESHAM, K., PAREEK, V. & FAIQ, M. A. 2021. COVID-19 mechanisms in the human body—What we know so far. *Frontiers in Immunology,* 12**,** 693938.

KUMMEROW, C., SCHWARZ, E. C., BUFE, B., ZUFALL, F., HOTH, M. & QU, B. 2014. A simple, economic, time-resolved killing assay. *Eur J Immunol,* 44**,** 1870-1872.

LE BERT, N., TAN, A. T., KUNASEGARAN, K., THAM, C. Y., HAFEZI, M., CHIA, A., CHNG, M. H. Y., LIN, M., TAN, N. & LINSTER, M. 2020. SARS-CoV-2-specific T cell immunity in cases of COVID-19 and SARS, and uninfected controls. *Nature,* 584**,** 457-462.

LI, J., HOU, L., GUO, X., JIN, P., WU, S., ZHU, J., PAN, H., WANG, X., SONG, Z. & WAN, J. 2022. Heterologous AD5-nCOV plus CoronaVac versus homologous CoronaVac vaccination: a randomized phase 4 trial. *Nature medicine,* 28**,** 401-409.

LI, Q., LIU, Q., HUANG, W., LI, X. & WANG, Y. 2018. Current status on the development of pseudoviruses for enveloped viruses. *Reviews in medical virology,* 28**,** e1963.

LI, Q., LIU, Q., HUANG, W., WU, J., NIE, J., WANG, M., ZHAO, C., ZHANG, L. & WANG, Y. 2017. An LASV GPC pseudotyped virus based reporter system enables evaluation of vaccines in mice under non-BSL-4 conditions. *Vaccine,* 35**,** 5172-5178.

LIMA, K. V. B., LIMA, L. N. G. C., RODRIGUES, Y. C. & SILVA, M. J. A. 2022. Innate immunity to SARS-CoV-2 infection: a review. *Epidemiology and Infection,* 150**,** e142.

LIU, C., GINN, H. M., DEJNIRATTISAI, W., SUPASA, P., WANG, B., TUEKPRAKHON, A., NUTALAI, R., ZHOU, D., MENTZER, A. J., ZHAO, Y., DUYVESTEYN, H. M. E., LÓPEZ-CAMACHO, C., SLON-CAMPOS, J., WALTER, T. S., SKELLY, D., JOHNSON, S. A., RITTER, T. G., MASON, C., COSTA CLEMENS, S. A., GOMES NAVECA, F., NASCIMENTO, V., NASCIMENTO, F., FERNANDES DA COSTA, C., RESENDE, P. C., PAUVOLID-CORREA, A., SIQUEIRA, M. M., DOLD, C., TEMPERTON, N., DONG, T., POLLARD, A. J., KNIGHT, J. C., CROOK, D., LAMBE, T., CLUTTERBUCK, E., BIBI, S., FLAXMAN, A., BITTAYE, M., BELIJ-RAMMERSTORFER, S., GILBERT, S. C., MALIK, T., CARROLL, M. W., KLENERMAN, P., BARNES, E., DUNACHIE, S. J., BAILLIE, V., SERAFIN, N., DITSE, Z., DA SILVA, K., PATERSON, N. G., WILLIAMS, M. A., HALL, D. R., MADHI, S., NUNES, M. C., GOULDER, P., FRY, E. E., MONGKOLSAPAYA, J., REN, J., STUART, D. I. & SCREATON, G. R. 2021a. Reduced neutralization of SARS-CoV-2 B.1.617 by vaccine and convalescent serum. *Cell,* 184**,** 4220-4236.e13.

LIU, Y., LIU, J., PLANTE, K. S., PLANTE, J. A., XIE, X., ZHANG, X., KU, Z., AN, Z., SCHARTON, D., SCHINDEWOLF, C., MENACHERY, V. D., SHI, P. Y. & WEAVER, S. C. 2021b. The N501Y spike substitution enhances SARS-CoV-2 transmission. *bioRxiv*.

LIU, Y. & YE, Q. 2022. Safety and Efficacy of the Common Vaccines against COVID-19. *Vaccines (Basel),* 10.

LONG, Q. X., LIU, B. Z., DENG, H. J., WU, G. C., DENG, K., CHEN, Y. K., LIAO, P., QIU, J. F., LIN, Y., CAI, X. F., WANG, D. Q., HU, Y., REN, J. H., TANG, N., XU, Y. Y., YU, L. H., MO, Z., GONG, F., ZHANG, X. L., TIAN, W. G., HU, L., ZHANG, X. X., XIANG, J. L., DU, H. X., LIU, H. W., LANG, C. H., LUO, X. H., WU, S. B., CUI, X. P., ZHOU, Z., ZHU, M. M., WANG, J., XUE, C. J., LI, X. F., WANG, L., LI, Z. J., WANG, K., NIU, C. C., YANG, Q. J.,

TANG, X. J., ZHANG, Y., LIU, X. M., LI, J. J., ZHANG, D. C., ZHANG, F., LIU, P., YUAN, J., LI, Q., HU, J. L., CHEN, J. & HUANG, A. L. 2020. Antibody responses to SARS-CoV-2 in patients with COVID-19. *Nat Med,* 26**,** 845-848.

LONGO, P. A., KAVRAN, J. M., KIM, M. S. & LEAHY, D. J. 2013. Transient mammalian cell transfection with polyethylenimine (PEI). *Methods Enzymol,* 529**,** 227-40.

LOU, F., LI, M., PANG, Z., JIANG, L., GUAN, L., TIAN, L., HU, J., FAN, J. & FAN, H. 2021. Understanding the Secret of SARS-CoV-2 Variants of Concern/Interest and Immune Escape. *Front Immunol,* 12**,** 744242.

LYONS, A. B., BLAKE, S. J. & DOHERTY, K. V. 2013. Flow cytometric analysis of cell division by dilution of CFSE and related dyes. *Curr Protoc Cytom,* Chapter 9**,** 9.11.1-9.11.12.

MALLONE, R., MANNERING, S., BROOKS-WORRELL, B., DURINOVIC-BELLO, I., CILIO, C., WONG, F. S. & SCHLOOT, N. 2011. Isolation and preservation of peripheral blood mononuclear cells for analysis of islet antigen-reactive T cell responses: position statement of the T-Cell Workshop Committee of the Immunology of Diabetes Society. *Clinical & Experimental Immunology,* 163**,** 33-49.

MARKOV, P. V., GHAFARI, M., BEER, M., LYTHGOE, K., SIMMONDS, P., STILIANAKIS, N. I. & KATZOURAKIS, A. 2023. The evolution of SARS-CoV-2. *Nature Reviews Microbiology,* 21**,** 361-379.

MAVHANDU, L. G., CHENG, H., BOR, Y.-C., TEBIT, D. M., HAMMARSKJOLD, M.-L., REKOSH, D. & BESSONG, P. O. 2020. Development of a pseudovirus assay and evaluation to screen natural products for inhibition of HIV-1 subtype C reverse transcriptase. *Journal of Ethnopharmacology,* 258**,** 112931.

MBUNGE, E. 2020. Effects of COVID-19 in South African health system and society: An explanatory study. *Diabetes & Metabolic Syndrome: Clinical Research & Reviews,* 14**,** 1809-1814.

MECKIFF, B. J., RAMÍREZ-SUÁSTEGUI, C., FAJARDO, V., CHEE, S. J., KUSNADI, A., SIMON, H., ESCHWEILER, S., GRIFONI, A., PELOSI, E., WEISKOPF, D., SETTE, A., AY, F., SEUMOIS, G., OTTENSMEIER, C. H. & VIJAYANAND, P. 2020. Imbalance of Regulatory and Cytotoxic SARS-CoV-2-Reactive CD4(+) T Cells in COVID-19. *Cell,* 183**,** 1340-1353.e16.

MELLOR, M. M., BAST, A. C., JONES, N. R., ROBERTS, N. W., ORDÓÑEZ-MENA, J. M., REITH, A. J. M., BUTLER, C. C., MATTHEWS, P. C. & DORWARD, J. 2021. Risk of adverse coronavirus disease 2019 outcomes for people living with HIV. *Aids,* 35**,** F1-f10.

MERCADO, N. B., ZAHN, R., WEGMANN, F., LOOS, C., CHANDRASHEKAR, A., YU, J., LIU, J., PETER, L., MCMAHAN, K., TOSTANOSKI, L. H., HE, X., MARTINEZ, D. R., RUTTEN, L., BOS, R., VAN MANEN, D., VELLINGA, J., CUSTERS, J., LANGEDIJK, J. P., KWAKS, T., BAKKERS, M. J. G., ZUIJDGEEST, D., ROSENDAHL HUBER, S. K., ATYEO, C., FISCHINGER, S., BURKE, J. S., FELDMAN, J., HAUSER, B. M., CARADONNA, T. M., BONDZIE, E. A., DAGOTTO, G., GEBRE, M. S., HOFFMAN, E., JACOB-DOLAN, C., KIRILOVA, M., LI, Z., LIN, Z., MAHROKHIAN, S. H., MAXFIELD, L. F., NAMPANYA, F., NITYANANDAM, R., NKOLOLA, J. P., PATEL, S., VENTURA, J. D., VERRINGTON, K., WAN, H., PESSAINT, L., VAN RY, A., BLADE, K., STRASBAUGH, A., CABUS, M., BROWN, R., COOK, A., ZOUANTCHANGADOU, S., TEOW, E., ANDERSEN, H., LEWIS, M. G., CAI, Y., CHEN, B., SCHMIDT, A. G., REEVES, R. K., BARIC, R. S., LAUFFENBURGER, D. A., ALTER, G., STOFFELS, P., MAMMEN, M., VAN HOOF, J., SCHUITEMAKER, H. & BAROUCH, D. H. 2020. Single-shot Ad26 vaccine protects against SARS-CoV-2 in rhesus macaques. *Nature,* 586**,** 583-588.

MINOR, P. D. 2015. Live attenuated vaccines: Historical successes and current challenges. *Virology,* 479-480**,** 379-92.

MIRTALEB, M. S., FALAK, R., HESHMATNIA, J., BAKHSHANDEH, B., TAHERI, R. A., SOLEIMANJAHI, H. & ZOLFAGHARI EMAMEH, R. 2023. An insight overview on COVID-19 mRNA vaccines: Advantageous, pharmacology, mechanism of action, and prospective considerations. *Int Immunopharmacol,* 117**,** 109934.

MISTRY, P., BARMANIA, F., MELLET, J., PETA, K., STRYDOM, A., VILJOEN, I. M., JAMES, W., GORDON, S. & PEPPER, M. S. 2021. SARS-CoV-2 Variants, Vaccines, and Host Immunity. *Front Immunol,* 12**,** 809244.

MITTAL, A., KHATTRI, A. & VERMA, V. 2022. Structural and antigenic variations in the spike protein of emerging SARS-CoV-2 variants. *PLOS Pathogens,* 18**,** e1010260.

MITTAL, A., MANJUNATH, K., RANJAN, R. K., KAUSHIK, S., KUMAR, S. & VERMA, V. 2020. COVID-19 pandemic: Insights into structure, function, and hACE2 receptor recognition by SARS-CoV-2. *PLoS Pathog,* 16**,** e1008762.

MOHSENI AFSHAR, Z., TAVAKOLI PIRZAMAN, A., KARIM, B., RAHIMIPOUR ANARAKI, S., HOSSEINZADEH, R., SANJARI PIREIVATLOU, E., BABAZADEH, A., HOSSEINZADEH, D., MIRI, S. R., SIO, T. T., SULLMAN, M. J. M., BARARY, M. & EBRAHIMPOUR, S. 2023. SARS-CoV-2 Omicron (B.1.1.529) Variant: A Challenge with COVID-19. *Diagnostics,* 13**,** 559.

MOSTAGHIMI, D., VALDEZ, C. N., LARSON, H. T., KALINICH, C. C. & IWASAKI, A. 2022. Prevention of host-to-host transmission by SARS-CoV-2 vaccines. *The Lancet Infectious Diseases,* 22**,** e52-e58.

MOYO-GWETE, T., MADZIVHANDILA, M., MKHIZE, N. N., KGAGUDI, P., AYRES, F., LAMBSON, B. E., MANAMELA, N. P., RICHARDSON, S. I., MAKHADO, Z., MESCHT, M. A. V. D., BEER, Z. D., VILLIERS, T. R. D., BURGERS, W. A., NTUSI, N. A. B., ROSSOUW, T., UECKERMANN, V., BOSWELL, M. T. & MOORE, P. L. 2022. Shared N417-Dependent Epitope on the SARS-CoV-2 Omicron, Beta, and Delta Plus Variants. *Journal of Virology,* 96**,** e00558-22.

MOYO-GWETE, T., RICHARDSON, S. I., KEETON, R., HERMANUS, T., SPENCER, H., MANAMELA, N. P., AYRES, F., MAKHADO, Z., MOTLOU, T., TINCHO, M. B., BENEDE, N., NGOMTI, A., BAGUMA, R., CHAUKE, M. V., MENNEN, M., ADRIAANSE, M., SKELEM, S., GOGA, A., GARRETT, N., BEKKER, L. G., GRAY, G., NTUSI, N. A. B., RIOU, C., BURGERS, W. A. & MOORE, P. L. 2023. Homologous Ad26.COV2.S vaccination results in reduced boosting of humoral responses in hybrid immunity, but elicits antibodies of similar magnitude regardless of prior infection. *medRxiv*.

MULLIGAN, M. J., LYKE, K. E., KITCHIN, N., ABSALON, J., GURTMAN, A., LOCKHART, S., NEUZIL, K., RAABE, V., BAILEY, R., SWANSON, K. A., LI, P., KOURY, K., KALINA, W., COOPER, D., FONTES-GARFIAS, C., SHI, P.-Y., TÜRECI, Ö., TOMPKINS, K. R., WALSH, E. E., FRENCK, R., FALSEY, A. R., DORMITZER, P. R., GRUBER, W. C., ŞAHIN, U. & JANSEN, K. U. 2020. Phase I/II study of COVID-19 RNA vaccine BNT162b1 in adults. *Nature,* 586**,** 589-593.

MUNIS, A. M., BENTLEY, E. M. & TAKEUCHI, Y. 2020. A tool with many applications: vesicular stomatitis virus in research and medicine. *Expert opinion on biological therapy,* 20**,** 1187-1201.

MURPHY, R. E. & SAAD, J. S. 2020. The interplay between HIV-1 Gag binding to the plasma membrane and Env incorporation. *Viruses,* 12**,** 548.

NAARDING, M. A., FERNANDEZ, N., KAPPES, J. C., HAYES, P., AHMED, T., ICYUZ, M., EDMONDS, T. G., BERGIN, P., ANZALA, O. & HANKE, T. 2014. Development of a luciferase based viral inhibition assay to evaluate vaccine induced CD8 T-cell responses. *Journal of immunological methods,* 409**,** 161-173.

NAHASS, G. R., SALOMON-SHULMAN, R. E., BLACKER, G., HAIDER, K., BROTHERTON, R., TEAGUE, K., YIU, Y. Y., BREWER, R. E., GALLOWAY, S. D. & HANSEN, P. 2021. Intramuscular SARS-CoV-2 vaccines elicit varying degrees of plasma and salivary antibody responses as compared to natural infection. *Medrxiv***,** 2021.08. 22.21262168.

NDHLOVU, Z. M., KAZER, S. W., NKOSI, T., OGUNSHOLA, F., MUEMA, D. M., ANMOLE, G., SWANN, S. A., MOODLEY, A., DONG, K., REDDY, T., BROCKMAN, M. A., SHALEK, A. K., NDUNG'U, T. & WALKER, B. D. 2019. Augmentation of HIV-specific T cell function by immediate treatment of hyperacute HIV-1 infection. *Sci Transl Med,* 11.

NDHLOVU, Z. M., PROUDFOOT, J., CESA, K., ALVINO, D. M., MCMULLEN, A., VINE, S., STAMPOULOGLOU, E., PIECHOCKA-TROCHA, A., WALKER, B. D. & PEREYRA, F. 2012. Elite controllers with low to absent effector CD8+ T cell responses maintain highly functional, broadly directed central memory responses. *J Virol,* 86**,** 6959-69.

NELSON, G., BUZKO, O., SPILMAN, P., NIAZI, K., RABIZADEH, S. & SOON-SHIONG, P. 2021. Molecular dynamic simulation reveals E484K mutation enhances spike RBD-ACE2 affinity and the combination of E484K, K417N and N501Y mutations (501Y. V2 variant) induces

conformational change greater than N501Y mutant alone, potentially resulting in an escape mutant. *BioRxiv*, 2021.01. 13.426558.

NG'UNI, T. L., MUSALE, V., NKOSI, T., MANDOLO, J., MVULA, M., MICHELO, C., KARIM, F., MOOSA, M. Y. S., KHAN, K., JAMBO, K. C., HANEKOM, W., SIGAL, A., KILEMBE, W. & NDHLOVU, Z. M. 2023. Low pre-existing endemic human coronavirus (HCoV-NL63)-specific T cell frequencies are associated with impaired SARS-CoV-2-specific T cell responses in people living with HIV. *Front Immunol,* 14**,** 1291048.

NIE, J., LI, Q., WU, J., ZHAO, C., HAO, H., LIU, H., ZHANG, L., NIE, L., QIN, H., WANG, M., LU, Q., LI, X., SUN, Q., LIU, J., FAN, C., HUANG, W., XU, M. & WANG, Y. 2020a. Establishment and validation of a pseudovirus neutralization assay for SARS-CoV-2. *Emerg Microbes Infect,* 9**,** 680-686.

NIE, J., LI, Q., WU, J., ZHAO, C., HAO, H., LIU, H., ZHANG, L., NIE, L., QIN, H., WANG, M., LU, Q., LI, X., SUN, Q., LIU, J., FAN, C., HUANG, W., XU, M. & WANG, Y. 2020b. Quantification of SARS-CoV-2 neutralizing antibody by a pseudotyped virus-based assay. *Nature Protocols,* 15**,** 3699-3715.

NKOSI, T., CHASARA, C., PAPADOPOULOS, A. O., NGUNI, T. L., KARIM, F., MOOSA, M.-Y. S., GAZY, I., JAMBO, K., HANEKOM, W. & SIGAL, A. 2022. Unsuppressed HIV infection impairs T cell responses to SARS-CoV-2 infection and abrogates T cell cross-recognition. *Elife,* 11**,** e78374.

NOTO, A., NGAUV, P. & TRAUTMANN, L. 2013. Cell-based flow cytometry assay to measure cytotoxic activity. *J Vis Exp*, e51105.

OGBE, A., PACE, M., BITTAYE, M., TIPOE, T., ADELE, S., ALAGARATNAM, J., ALEY, P. K., ANSARI, M. A., BARA, A. & BROADHEAD, S. 2022. Durability of ChAdOx1 nCoV-19 vaccination in people living with HIV. *JCI insight,* 7.

OHAGEN, A., DEVITT, A., KUNSTMAN, K. J., GORRY, P. R., ROSE, P. P., KORBER, B., TAYLOR, J., LEVY, R., MURPHY, R. L., WOLINSKY, S. M. & GABUZDA, D. 2003. Genetic and functional analysis of full-length human immunodeficiency virus type 1 env genes derived from brain and blood of patients with AIDS. *J Virol,* 77**,** 12336-45.

OKUMA, K., MATSUURA, Y., TATSUO, H., INAGAKI, Y., NAKAMURA, M., YAMAMOTO, N. & YANAGI, Y. 2001. Analysis of the molecules involved in human T-cell leukaemia virus type 1 entry by a vesicular stomatitis virus pseudotype bearing its envelope glycoproteins. *J Gen Virol,* 82**,** 821-830.

ORY, D. 1996. A stable human-derived packaging cell line for production of high titer retrovirus/vesicular stomatitis virus G psuedotypes. *Proc. Natl Acad. Sci. USA,* 93**,** 11 400-11 406.

OU, X., LIU, Y., LEI, X., LI, P., MI, D., REN, L., GUO, L., GUO, R., CHEN, T., HU, J., XIANG, Z., MU, Z., CHEN, X., CHEN, J., HU, K., JIN, Q., WANG, J. & QIAN, Z. 2020. Characterization of spike glycoprotein of SARS-CoV-2 on virus entry and its immune cross-reactivity with SARS-CoV. *Nat Commun,* 11**,** 1620.

OYAERT, M., DE SCHEERDER, M.-A., VAN HERREWEGE, S., LAUREYS, G., VAN ASSCHE, S., CAMBRON, M., NAESENS, L., HOSTE, L., CLAES, K. & HAERYNCK, F. 2022. Evaluation of humoral and cellular responses in SARS-CoV-2 mRNA vaccinated immunocompromised patients. *Frontiers in immunology,* 13**,** 858399.

PALACIOS, R., BATISTA, A. P., ALBUQUERQUE, C. S. N., PATIÑO, E. G., SANTOS, J. D. P., TILLI REIS PESSOA CONDE, M., PIORELLI, R. D. O., PEREIRA JÚNIOR, L. C., RABONI, S. M. & RAMOS, F. 2021. Efficacy and safety of a COVID-19 inactivated vaccine in healthcare professionals in Brazil: the PROFISCOV study.

PALM, A.-K. E. & HENRY, C. 2019. Remembrance of things past: long-term B cell memory after infection and vaccination. *Frontiers in immunology,* 10**,** 478641.

PARISH, C. R., GLIDDEN, M. H., QUAH, B. J. C. & WARREN, H. S. 2009. Use of the intracellular fluorescent dye CFSE to monitor lymphocyte migration and proliferation. *Curr Protoc Immunol,* Chapter 4**,** 4.9.1-4.9.13.

PENG, X., OUYANG, J., ISNARD, S., LIN, J., FOMBUENA, B., ZHU, B. & ROUTY, J.-P. 2020. Sharing CD4+ T Cell Loss: When COVID-19 and HIV Collide on Immune System. *Frontiers in Immunology,* 11.

PETRONE, L., SETTE, A., DE VRIES, R. D. & GOLETTI, D. 2023. The Importance of Measuring SARS-CoV-2-Specific T-Cell Responses in an Ongoing Pandemic. *Pathogens,* 12**,** 862.

POH, C. M., ZHENG, J., CHANNAPPANAVAR, R., CHANG, Z. W., NGUYEN, T. H., RÉNIA, L., KEDZIERSKA, K., PERLMAN, S. & POON, L. L. 2020. Multiplex screening assay for identifying cytotoxic CD8+ T cell epitopes. *Frontiers in immunology,* 11**,** 513441.

POLACK, F. P., THOMAS, S. J., KITCHIN, N., ABSALON, J., GURTMAN, A., LOCKHART, S., PEREZ, J. L., PÉREZ MARC, G., MOREIRA, E. D., ZERBINI, C., BAILEY, R., SWANSON, K. A., ROYCHOUDHURY, S., KOURY, K., LI, P., KALINA, W. V., COOPER, D., FRENCK, R. W., JR., HAMMITT, L. L., TÜRECI, Ö., NELL, H., SCHAEFER, A., ÜNAL, S., TRESNAN, D. B., MATHER, S., DORMITZER, P. R., ŞAHIN, U., JANSEN, K. U. & GRUBER, W. C. 2020. Safety and Efficacy of the BNT162b2 mRNA Covid-19 Vaccine. *N Engl J Med,* 383**,** 2603-2615.

POURCHER, V., BELIN, L., SOULIE, C., ROSENZWAJG, M., MAROT, S., LACOMBE, K., VALIN, N., PIALOUX, G., CALIN, R. & PALACIOS, C. 2022. High seroconversion rate and SARS-CoV-2 Delta neutralization in people with HIV vaccinated with BNT162b2. *AIDS,* 36**,** 1545-1552.

PREMKUMAR, L., SEGOVIA-CHUMBEZ, B., JADI, R., MARTINEZ, D. R., RAUT, R., MARKMANN, A. J., CORNABY, C., BARTELT, L., WEISS, S. & PARK, Y. 2020. The receptor-binding domain of the viral spike protein is an immunodominant and highly specific target of antibodies in SARS-CoV-2 patients. *Science immunology,* 5**,** eabc8413.

PRIMORAC, D., VRDOLJAK, K., BRLEK, P., PAVELIĆ, E., MOLNAR, V., MATIŠIĆ, V., ERCEG IVKOŠIĆ, I. & PARČINA, M. 2022. Adaptive Immune Responses and Immunity to SARS-CoV-2. *Frontiers in Immunology,* 13.

QI, H., LIU, B., WANG, X. & ZHANG, L. 2022. The humoral response and antibodies against SARS-CoV-2 infection. *Nature Immunology,* 23**,** 1008-1020.

QUAH, B. J., WIJESUNDARA, D. K., RANASINGHE, C. & PARISH, C. R. 2012. Fluorescent target array killing assay: a multiplex cytotoxic T-cell assay to measure detailed T-cell antigen specificity and avidity in vivo. *Cytometry Part A,* 81**,** 679-690.

RAMASAMY, R. 2020. Nasal conditioning of inspired air, innate immunity in the respiratory tract and SARS-CoV-2 infectivity.

RAVLIĆ, S., KURTOVIĆ, T., CVETKO KRAJINOVIĆ, L., HEĆIMOVIĆ, A., MILOŠ, M., MATELJAK LUKAČEVIĆ, S., MARKOTIĆ, A. & HALASSY, B. 2023. What can neutralizing antibodies tell us about the quality of immunity in COVID-19 convalescents and vaccinees? *Hum Vaccin Immunother,* 19**,** 2270310.

REYNOLDS, L., DEWEY, C., ASFOUR, G. & LITTLE, M. 2023. Vaccine efficacy against SARS-CoV-2 for Pfizer BioNTech, Moderna, and AstraZeneca vaccines: a systematic review. *Frontiers in Public Health,* 11**,** 1229716.

RINALDO, C., HUANG, X.-L., FAN, Z., DING, M., BELTZ, L., LOGAR, A., PANICALI, D., MAZZARA, G., LIEBMANN, J. & COTTRILL, M. 1995. High levels of anti-human immunodeficiency virus type 1 (HIV-1) memory cytotoxic T-lymphocyte activity and low viral load are associated with lack of disease in HIV-1-infected long-term nonprogressors. *Journal of Virology,* 69**,** 5838-5842.

RIOU, C., KEETON, R., MOYO-GWETE, T., HERMANUS, T., KGAGUDI, P., BAGUMA, R., VALLEY-OMAR, Z., SMITH, M., TEGALLY, H., DOOLABH, D., IRANZADEH, A., TYERS, L., MUTAVHATSINDI, H., TINCHO, M. B., BENEDE, N., MARAIS, G., CHINHOYI, L. R., MENNEN, M., SKELEM, S., DU BRUYN, E., STEK, C., NETWORK, S. A. C. I., DE OLIVEIRA, T., WILLIAMSON, C., MOORE, P. L., WILKINSON, R. J., NTUSI, N. A. B. & BURGERS, W. A. 2022. Escape from recognition of SARS-CoV-2 variant spike epitopes but overall preservation of T cell immunity. *Science Translational Medicine,* 14**,** eabj6824.

RISS, T., NILES, A., MORAVEC, R., KARASSINA, N. & VIDUGIRIENE, J. 2004. Cytotoxicity Assays: In Vitro Methods to Measure Dead Cells. 2019 May 1. *Assay Guidance Manual [Internet]. Bethesda (MD): Eli Lilly & Company and the National Center for Advancing Translational Sciences*.

ROBBIANI, D. F., GAEBLER, C., MUECKSCH, F., LORENZI, J. C., WANG, Z., CHO, A., AGUDELO, M., BARNES, C. O., GAZUMYAN, A. & FINKIN, S. 2020. Convergent antibody responses to SARS-CoV-2 in convalescent individuals. *Nature,* 584**,** 437-442.

ROSENDAHL HUBER, S., VAN BEEK, J., DE JONGE, J., LUYTJES, W. & VAN BAARLE, D. 2014. T cell responses to viral infections - opportunities for Peptide vaccination. *Front Immunol,* 5**,** 171.

RYDYZNSKI MODERBACHER, C., RAMIREZ, S. I., DAN, J. M., GRIFONI, A., HASTIE, K. M., WEISKOPF, D., BELANGER, S., ABBOTT, R. K., KIM, C., CHOI, J., KATO, Y., CROTTY, E. G., KIM, C., RAWLINGS, S. A., MATEUS, J., TSE, L. P. V., FRAZIER, A., BARIC, R., PETERS, B., GREENBAUM, J., OLLMANN SAPHIRE, E., SMITH, D. M., SETTE, A. & CROTTY, S. 2020. Antigen-Specific Adaptive Immunity to SARS-CoV-2 in Acute COVID-19 and Associations with Age and Disease Severity. *Cell,* 183**,** 996-1012.e19.

SADOFF, J., GRAY, G., VANDEBOSCH, A., CÁRDENAS, V., SHUKAREV, G., GRINSZTEJN, B., GOEPFERT, P. A., TRUYERS, C., FENNEMA, H. & SPIESSENS, B. 2021. Safety and efficacy of single-dose Ad26. COV2. S vaccine against Covid-19. *New England Journal of Medicine,* 384**,** 2187-2201.

SAHA, M. N., TANAKA, A., JINNO-OUE, A., SHIMIZU, N., TAMURA, K., SHINAGAWA, M., CHIBA, J. & HOSHINO, H. 2005. Formation of vesicular stomatitis virus pseudotypes bearing surface proteins of hepatitis B virus. *J Virol,* 79**,** 12566-74.

SAITO, A., NASSER, H., URIU, K., KOSUGI, Y., IRIE, T., SHIRAKAWA, K., SADAMASU, K., KIMURA, I., ITO, J. & WU, J. 2021. SARS-CoV-2 spike P681R mutation enhances and accelerates viral fusion.

SALATA, C., CALISTRI, A., ALVISI, G., CELESTINO, M., PAROLIN, C. & PALÙ, G. 2019. Ebola virus entry: from molecular characterization to drug discovery. *Viruses,* 11**,** 274.

SANDERS, D. A. 2002. No false start for novel pseudotyped vectors. *Current opinion in biotechnology,* 13**,** 437-442.

SATO, K., KONDO, M., SAKUTA, K., HOSOI, A., NOJI, S., SUGIURA, M., YOSHIDA, Y. & KAKIMI, K. 2009. Impact of culture medium on the expansion of T cells for immunotherapy. *Cytotherapy,* 11**,** 936-946.

SCHEIBENBOGEN, C., ROMERO, P., RIVOLTINI, L., HERR, W., SCHMITTEL, A., CEROTTINI, J.-C., WOELFEL, T., EGGERMONT, A. M. & KEILHOLZ, U. 2000. Quantitation of antigen-reactive T cells in peripheral blood by IFNγ-ELISPOT assay and chromium-release assay: a four-centre comparative trial. *Journal of immunological methods,* 244**,** 81-89.

SCHMIDT, K. G., HARRER, E. G., TASCILAR, K., KÜBEL, S., EL KENZ, B., HARTMANN, F., SIMON, D., SCHETT, G., NGANOU-MAKAMDOP, K. & HARRER, T. 2022. Characterization of serum and mucosal SARS-CoV-2-antibodies in HIV-1-infected subjects after BNT162b2 mRNA vaccination or SARS-CoV-2 infection. *Viruses,* 14**,** 651.

SCHWARZ, M., MZOUGHI, S., LOZANO-OJALVO, D., TAN, A. T., BERTOLETTI, A. & GUCCIONE, E. 2022. T cell immunity is key to the pandemic endgame: How to measure and monitor it. *Curr Res Immunol,* 3**,** 215-221.

SEOW, J., GRAHAM, C., MERRICK, B., ACORS, S., PICKERING, S., STEEL, K. J., HEMMINGS, O., O'BYRNE, A., KOUPHOU, N. & GALAO, R. P. 2020. Longitudinal observation and decline of neutralizing antibody responses in the three months following SARS-CoV-2 infection in humans. *Nature microbiology,* 5**,** 1598-1607.

SETH, R. B., SUN, L. & CHEN, Z. J. 2006. Antiviral innate immunity pathways. *Cell Research,* 16**,** 141-147.

SETTE, A. & CROTTY, S. 2021. Adaptive immunity to SARS-CoV-2 and COVID-19. *Cell,* 184**,** 861-880.

SEYEDPOUR, S., KHODAEI, B., LOGHMAN, A. H., SEYEDPOUR, N., KISOMI, M. F., BALIBEGLOO, M., NEZAMABADI, S. S., GHOLAMI, B., SAGHAZADEH, A. & REZAEI, N. 2021. Targeted therapy strategies against SARS-CoV-2 cell entry mechanisms: A systematic review of in vitro and in vivo studies. *J Cell Physiol,* 236**,** 2364-2392.

SHANER, N. C., STEINBACH, P. A. & TSIEN, R. Y. 2005. A guide to choosing fluorescent proteins. *Nature Methods,* 2**,** 905-909.

SHANG, J., WAN, Y., LUO, C., YE, G., GENG, Q., AUERBACH, A. & LI, F. 2020. Cell entry mechanisms of SARS-CoV-2. *Proceedings of the National Academy of Sciences,* 117**,** 11727-11734.

SHEIKHSHAHROKH, A., RANJBAR, R., SAEIDI, E., SAFARPOOR DEHKORDI, F., HEIAT, M., GHASEMI-DEHKORDI, P. & GOODARZI, H. 2020. Frontier Therapeutics and Vaccine Strategies for SARS-CoV-2 (COVID-19): A Review. *Iran J Public Health,* 49**,** 18-29.

SHERINA, N., PIRALLA, A., DU, L., WAN, H., KUMAGAI-BRAESCH, M., ANDRÉLL, J., BRAESCH-ANDERSEN, S., CASSANITI, I., PERCIVALLE, E., SARASINI, A., BERGAMI, F., DI MARTINO, R., COLANERI, M., VECCHIA, M., SAMBO, M., ZUCCARO, V., BRUNO, R., SACHS, M., OGGIONNI, T., MELONI, F., ABOLHASSANI, H., BERTOGLIO, F., SCHUBERT, M., BYRNE-STEELE, M., HAN, J., HUST, M., XUE, Y., HAMMARSTRÖM, L., BALDANTI, F., MARCOTTE, H. & PAN-HAMMARSTRÖM, Q. 2021. Persistence of SARS-CoV-2-specific B and T cell responses in convalescent COVID-19 patients 6-8 months after the infection. *Med,* 2**,** 281-295.e4.

SINTYA, E., WEDARI, N. L. P. H., PRANATA, I. W. A. & BUDAYANTI, N. N. S. 2021. Antiviral mechanisms targeting regulatory genes Tat and Rev to defeat latent HIV-1 infected T cells: a literature review. *Journal of Clinical Microbiology and Infectious Diseases,* 1**,** 16-23.

SPINELLI, M. A., PELUSO, M. J., LYNCH, K. L., YUN, C., GLIDDEN, D. V., HENRICH, T. J., DEEKS, S. G. & GANDHI, M. 2022. Differences in post-mRNA vaccination severe acute respiratory syndrome coronavirus 2 (SARS-CoV-2) immunoglobulin G (IgG) concentrations and surrogate virus neutralization test response by human immunodeficiency virus (HIV) status and type of vaccine: a matched case-control observational study. *Clinical Infectious Diseases,* 75**,** e916-e919.

STEFFEN, I. & SIMMONS, G. 2016. Pseudotyping Viral Vectors With Emerging Virus Envelope Proteins. *Curr Gene Ther,* 16**,** 47-55.

STEWART, S. A., DYKXHOORN, D. M., PALLISER, D., MIZUNO, H., YU, E. Y., AN, D. S., SABATINI, D. M., CHEN, I. S., HAHN, W. C., SHARP, P. A., WEINBERG, R. A. & NOVINA, C. D. 2003. Lentivirus-delivered stable gene silencing by RNAi in primary cells. *Rna,* 9**,** 493-501.

SUTHAR, M. S., ZIMMERMAN, M. G., KAUFFMAN, R. C., MANTUS, G., LINDERMAN, S. L., HUDSON, W. H., VANDERHEIDEN, A., NYHOFF, L., DAVIS, C. W., ADEKUNLE, O., AFFER, M., SHERMAN, M., REYNOLDS, S., VERKERKE, H. P., ALTER, D. N., GUARNER, J., BRYKSIN, J., HORWATH, M. C., ARTHUR, C. M., SAAKADZE, N., SMITH, G. H., EDUPUGANTI, S., SCHERER, E. M., HELLMEISTER, K., CHENG, A., MORALES, J. A., NEISH, A. S., STOWELL, S. R., FRANK, F., ORTLUND, E., ANDERSON, E. J., MENACHERY, V. D., ROUPHAEL, N., MEHTA, A. K., STEPHENS, D. S., AHMED, R., ROBACK, J. D. & WRAMMERT, J. 2020. Rapid Generation of Neutralizing Antibody Responses in COVID-19 Patients. *Cell Rep Med,* 1**,** 100040.

TAKADA, A., ROBISON, C., GOTO, H., SANCHEZ, A., MURTI, K. G., WHITT, M. A. & KAWAOKA, Y. 1997. A system for functional analysis of Ebola virus glycoprotein. *Proc Natl Acad Sci U S A,* 94**,** 14764-9.

TAKESHITA, M., NISHINA, N., MORIYAMA, S., TAKAHASHI, Y., ISHII, M., SAYA, H., KONDO, Y., KANEKO, Y., SUZUKI, K., FUKUNAGA, K. & TAKEUCHI, T. 2022. Immune evasion and chronological decrease in titer of neutralizing antibody against SARS-CoV-2 and its variants of concerns in COVID-19 patients. *Clinical Immunology,* 238**,** 108999.

TAN, A. T., LIM, J. M., LE BERT, N., KUNASEGARAN, K., CHIA, A., QUI, M. D., TAN, N., CHIA, W. N., DE ALWIS, R. & YING, D. 2021. Rapid measurement of SARS-CoV-2 spike T cells in whole blood from vaccinated and naturally infected individuals. *The Journal of clinical investigation,* 131.

TAO, K., TZOU, P. L., NOUHIN, J., GUPTA, R. K., DE OLIVEIRA, T., KOSAKOVSKY POND, S. L., FERA, D. & SHAFER, R. W. 2021. The biological and clinical significance of emerging SARS-CoV-2 variants. *Nature Reviews Genetics,* 22**,** 757-773.

TATSUO, H., OKUMA, K., TANAKA, K., ONO, N., MINAGAWA, H., TAKADE, A., MATSUURA, Y. & YANAGI, Y. 2000. Virus entry is a major determinant of cell tropism of Edmonston and

wild-type strains of measles virus as revealed by vesicular stomatitis virus pseudotypes bearing their envelope proteins. *J Virol,* 74**,** 4139-45.

TEGALLY, H., WILKINSON, E., GIOVANETTI, M., IRANZADEH, A., FONSECA, V., GIANDHARI, J., DOOLABH, D., PILLAY, S., SAN, E. J., MSOMI, N., MLISANA, K., VON GOTTBERG, A., WALAZA, S., ALLAM, M., ISMAIL, A., MOHALE, T., GLASS, A. J., ENGELBRECHT, S., VAN ZYL, G., PREISER, W., PETRUCCIONE, F., SIGAL, A., HARDIE, D., MARAIS, G., HSIAO, N.-Y., KORSMAN, S., DAVIES, M.-A., TYERS, L., MUDAU, I., YORK, D., MASLO, C., GOEDHALS, D., ABRAHAMS, S., LAGUDA-AKINGBA, O., ALISOLTANI-DEHKORDI, A., GODZIK, A., WIBMER, C. K., SEWELL, B. T., LOURENÇO, J., ALCANTARA, L. C. J., KOSAKOVSKY POND, S. L., WEAVER, S., MARTIN, D., LESSELLS, R. J., BHIMAN, J. N., WILLIAMSON, C. & DE OLIVEIRA, T. 2021. Detection of a SARS-CoV-2 variant of concern in South Africa. *Nature,* 592**,** 438-443.

TERRÉN, I., ORRANTIA, A., VITALLÉ, J., ZENARRUZABEITIA, O. & BORREGO, F. 2020. CFSE dilution to study human T and NK cell proliferation in vitro. *Methods Enzymol,* 631**,** 239-255.

THIMMIRAJU, S. R., KIMATA, J. T. & POLLET, J. 2024. Pseudoviruses, a safer toolbox for vaccine development against enveloped viruses. *Expert Rev Vaccines,* 23**,** 174-185.

TIAN, D., SUN, Y., ZHOU, J. & YE, Q. 2022. The global epidemic of SARS-CoV-2 variants and their mutational immune escape. *J Med Virol,* 94**,** 847-857.

TIAN, J.-H., PATEL, N., HAUPT, R., ZHOU, H., WESTON, S., HAMMOND, H., LOGUE, J., PORTNOFF, A. D., NORTON, J., GUEBRE-XABIER, M., ZHOU, B., JACOBSON, K., MACIEJEWSKI, S., KHATOON, R., WISNIEWSKA, M., MOFFITT, W., KLUEPFEL-STAHL, S., EKECHUKWU, B., PAPIN, J., BODDAPATI, S., JASON WONG, C., PIEDRA, P. A., FRIEMAN, M. B., MASSARE, M. J., FRIES, L., BENGTSSON, K. L., STERTMAN, L., ELLINGSWORTH, L., GLENN, G. & SMITH, G. 2021. SARS-CoV-2 spike glycoprotein vaccine candidate NVX-CoV2373 immunogenicity in baboons and protection in mice. *Nature Communications,* 12**,** 372.

TORMO, N., GIMÉNEZ, E., MARTÍNEZ-NAVARRO, M., ALBERT, E., NAVALPOTRO, D., TORRES, I., GIMENO, C. & NAVARRO, D. 2022. Performance comparison of a flow cytometry immunoassay for intracellular cytokine staining and the QuantiFERON® SARS-CoV-2 test for detection and quantification of SARS-CoV-2-Spike-reactive-IFN-γ-producing T cells after COVID-19 vaccination. *European Journal of Clinical Microbiology & Infectious Diseases,* 41**,** 657-662.

TURNER, C. T., BROWN, J., SHAW, E., UDDIN, I., TSALIKI, E., ROE, J. K., POLLARA, G., SUN, Y., HEATHER, J. M., LIPMAN, M., CHAIN, B. & NOURSADEGHI, M. 2021. Persistent T Cell Repertoire Perturbation and T Cell Activation in HIV After Long Term Treatment. *Front Immunol,* 12**,** 634489.

VADAKKAN, T. J., CULVER, J. C., GAO, L., ANHUT, T. & DICKINSON, M. E. 2009. Peak multiphoton excitation of mCherry using an optical parametric oscillator (OPO). *J Fluoresc,* 19**,** 1103-9.

VAN BAALEN, C. A., KWA, D., VERSCHUREN, E. J., REEDIJK, M. L., BOON, A. C. M., DE MUTSERT, G., RIMMELZWAAN, G. F., OSTERHAUS, A. D. M. E. & GRUTERS, R. A. 2005. Fluorescent Antigen–Transfected Target Cell Cytotoxic T Lymphocyte Assay for Ex Vivo Detection of Antigen-Specific Cell-Mediated Cytotoxicity. *The Journal of Infectious Diseases,* 192**,** 1183-1190.

VAN DOREMALEN, N., LAMBE, T., SPENCER, A., BELIJ-RAMMERSTORFER, S., PURUSHOTHAM, J. N., PORT, J. R., AVANZATO, V. A., BUSHMAKER, T., FLAXMAN, A., ULASZEWSKA, M., FELDMANN, F., ALLEN, E. R., SHARPE, H., SCHULZ, J., HOLBROOK, M., OKUMURA, A., MEADE-WHITE, K., PÉREZ-PÉREZ, L., EDWARDS, N. J., WRIGHT, D., BISSETT, C., GILBRIDE, C., WILLIAMSON, B. N., ROSENKE, R., LONG, D., ISHWARBHAI, A., KAILATH, R., ROSE, L., MORRIS, S., POWERS, C., LOVAGLIO, J., HANLEY, P. W., SCOTT, D., SATURDAY, G., DE WIT, E., GILBERT, S. C. & MUNSTER, V. J. 2020. ChAdOx1 nCoV-19 vaccine prevents SARS-CoV-2 pneumonia in rhesus macaques. *Nature,* 586**,** 578-582.

VARDHANA, S., BALDO, L., MORICE, W. G. & WHERRY, E. J. 2022. Understanding T cell responses to COVID-19 is essential for informing public health strategies. *Science immunology,* 7**,** eabo1303.

VARGHA, D. & WILKINS, I. 2023. Vaccination and Pandemics. *Isis,* 114**,** S50-S70.

VOYSEY, M., CLEMENS, S. A. C., MADHI, S. A., WECKX, L. Y., FOLEGATTI, P. M., ALEY, P. K., ANGUS, B., BAILLIE, V. L., BARNABAS, S. L., BHORAT, Q. E., BIBI, S., BRINER, C., CICCONI, P., COLLINS, A. M., COLIN-JONES, R., CUTLAND, C. L., DARTON, T. C., DHEDA, K., DUNCAN, C. J. A., EMARY, K. R. W., EWER, K. J., FAIRLIE, L., FAUST, S. N., FENG, S., FERREIRA, D. M., FINN, A., GOODMAN, A. L., GREEN, C. M., GREEN, C. A., HEATH, P. T., HILL, C., HILL, H., HIRSCH, I., HODGSON, S. H. C., IZU, A., JACKSON, S., JENKIN, D., JOE, C. C. D., KERRIDGE, S., KOEN, A., KWATRA, G., LAZARUS, R., LAWRIE, A. M., LELLIOTT, A., LIBRI, V., LILLIE, P. J., MALLORY, R., MENDES, A. V. A., MILAN, E. P., MINASSIAN, A. M., MCGREGOR, A., MORRISON, H., MUJADIDI, Y. F., NANA, A., O'REILLY, P. J., PADAYACHEE, S. D., PITTELLA, A., PLESTED, E., POLLOCK, K. M., RAMASAMY, M. N., RHEAD, S., SCHWARZBOLD, A. V., SINGH, N., SMITH, A., SONG, R., SNAPE, M. D., SPRINZ, E., SUTHERLAND, R. K., TARRANT, R., THOMSON, E. C., TÖRÖK, M. E., TOSHNER, M., TURNER, D. P. J., VEKEMANS, J., VILLAFANA, T. L., WATSON, M. E. E., WILLIAMS, C. J., DOUGLAS, A. D., HILL, A. V. S., LAMBE, T., GILBERT, S. C. & POLLARD, A. J. 2021. Safety and efficacy of the ChAdOx1 nCoV-19 vaccine (AZD1222) against SARS-CoV-2: an interim analysis of four randomised controlled trials in Brazil, South Africa, and the UK. *Lancet,* 397**,** 99-111.

WAJNBERG, A., AMANAT, F., FIRPO, A., ALTMAN, D. R., BAILEY, M. J., MANSOUR, M., MCMAHON, M., MEADE, P., MENDU, D. R. & MUELLERS, K. 2020. Robust neutralizing antibodies to SARS-CoV-2 infection persist for months. *Science,* 370**,** 1227-1230.

WALKER, B. D. 2007. Elite control of HIV Infection: implications for vaccines and treatment. *Top HIV Med,* 15**,** 134-6.

WALLS, A. C., PARK, Y. J., TORTORICI, M. A., WALL, A., MCGUIRE, A. T. & VEESLER, D. 2020. Structure, Function, and Antigenicity of the SARS-CoV-2 Spike Glycoprotein. *Cell,* 181**,** 281-292.e6.

WANG, C., LI, W., DRABEK, D., OKBA, N., VAN HAPEREN, R., OSTERHAUS, A. D., VAN KUPPEVELD, F. J., HAAGMANS, B. L., GROSVELD, F. & BOSCH, B.-J. 2020. A human monoclonal antibody blocking SARS-CoV-2 infection. *Nature communications,* 11**,** 1-6.

WANG, L., NICOLS, A., TURTLE, L., RICHTER, A., DUNCAN, C. J., DUNACHIE, S. J., KLENERMAN, P. & PAYNE, R. P. 2023a. T cell immune memory after covid-19 and vaccination. *BMJ Med,* 2**,** e000468.

WANG, Z., ZHONG, K., WANG, G., LU, Q., LI, H., WU, Z., ZHANG, Z., YANG, N., ZHENG, M., WANG, Y., NIE, C., ZHOU, L. & TONG, A. 2023b. Loss of furin site enhances SARS-CoV-2 spike protein pseudovirus infection. *Gene,* 856**,** 147144.

WESTON, S. A. & PARISH, C. R. 1990. New fluorescent dyes for lymphocyte migration studies. Analysis by flow cytometry and fluorescence microscopy. *J Immunol Methods,* 133**,** 87-97.

WHERRY, E. J. & AHMED, R. 2004. Memory CD8 T-cell differentiation during viral infection. *J Virol,* 78**,** 5535-45.

WHITT, M. A. 2010. Generation of VSV pseudotypes using recombinant ΔG-VSV for studies on virus entry, identification of entry inhibitors, and immune responses to vaccines. *Journal of virological methods,* 169**,** 365-374.

WHITTAKER, G. R., DANIEL, S. & MILLET, J. K. 2021. Coronavirus entry: how we arrived at SARS-CoV-2. *Curr Opin Virol,* 47**,** 113-120.

WILKINSON, T. M., LI, C. K., CHUI, C. S., HUANG, A. K., PERKINS, M., LIEBNER, J. C., LAMBKIN-WILLIAMS, R., GILBERT, A., OXFORD, J., NICHOLAS, B., STAPLES, K. J., DONG, T., DOUEK, D. C., MCMICHAEL, A. J. & XU, X. N. 2012. Preexisting influenza-specific CD4+ T cells correlate with disease protection against influenza challenge in humans. *Nat Med,* 18**,** 274-80.

WILLIAMSON, E. J., WALKER, A. J., BHASKARAN, K., BACON, S., BATES, C., MORTON, C. E., CURTIS, H. J., MEHRKAR, A., EVANS, D., INGLESBY, P., COCKBURN, J.,

MCDONALD, H. I., MACKENNA, B., TOMLINSON, L., DOUGLAS, I. J., RENTSCH, C. T., MATHUR, R., WONG, A. Y. S., GRIEVE, R., HARRISON, D., FORBES, H., SCHULTZE, A., CROKER, R., PARRY, J., HESTER, F., HARPER, S., PERERA, R., EVANS, S. J. W., SMEETH, L. & GOLDACRE, B. 2020. Factors associated with COVID-19-related death using OpenSAFELY. *Nature,* 584**,** 430-436.

WOLDEMESKEL, B. A., KARABA, A. H., GARLISS, C. C., BECK, E. J., WANG, K. H., LAEYENDECKER, O., COX, A. L. & BLANKSON, J. N. 2022. The BNT162b2 mRNA vaccine elicits robust humoral and cellular immune responses in people living with human immunodeficiency virus (HIV). *Clinical Infectious Diseases,* 74**,** 1268-1270.

WU, F., ZHAO, S., YU, B., CHEN, Y.-M., WANG, W., SONG, Z.-G., HU, Y., TAO, Z.-W., TIAN, J.-H. & PEI, Y.-Y. 2020. A new coronavirus associated with human respiratory disease in China. *Nature,* 579**,** 265-269.

WU, X., ZHANG, Y., LI, Y. & SCHMIDT-WOLF, I. G. H. 2021. Improvements in Flow Cytometry-Based Cytotoxicity Assay. *Cytometry A,* 99**,** 680-688.

XIANG, Q., LI, L., WU, J., TIAN, M. & FU, Y. 2022. Application of pseudovirus system in the development of vaccine, antiviral-drugs, and neutralizing antibodies. *Microbiological Research***,** 126993.

YANG, J., WANG, W., CHEN, Z., LU, S., YANG, F., BI, Z., BAO, L., MO, F., LI, X., HUANG, Y., HONG, W., YANG, Y., ZHAO, Y., YE, F., LIN, S., DENG, W., CHEN, H., LEI, H., ZHANG, Z., LUO, M., GAO, H., ZHENG, Y., GONG, Y., JIANG, X., XU, Y., LV, Q., LI, D., WANG, M., LI, F., WANG, S., WANG, G., YU, P., QU, Y., YANG, L., DENG, H., TONG, A., LI, J., WANG, Z., YANG, J., SHEN, G., ZHAO, Z., LI, Y., LUO, J., LIU, H., YU, W., YANG, M., XU, J., WANG, J., LI, H., WANG, H., KUANG, D., LIN, P., HU, Z., GUO, W., CHENG, W., HE, Y., SONG, X., CHEN, C., XUE, Z., YAO, S., CHEN, L., MA, X., CHEN, S., GOU, M., HUANG, W., WANG, Y., FAN, C., TIAN, Z., SHI, M., WANG, F.-S., DAI, L., WU, M., LI, G., WANG, G., PENG, Y., QIAN, Z., HUANG, C., LAU, J. Y.-N., YANG, Z., WEI, Y., CEN, X., PENG, X., QIN, C., ZHANG, K., LU, G. & WEI, X. 2020a. A vaccine targeting the RBD of the S protein of SARS-CoV-2 induces protective immunity. *Nature,* 586**,** 572-577.

YANG, L., PEI, R. J., LI, H., MA, X. N., ZHOU, Y., ZHU, F. H., HE, P. L., TANG, W., ZHANG, Y. C., XIONG, J., XIAO, S. Q., TONG, X. K., ZHANG, B. & ZUO, J. P. 2021. Identification of SARS-CoV-2 entry inhibitors among already approved drugs. *Acta Pharmacol Sin,* 42**,** 1347-1353.

YANG LITAO, Y. L., PENG HUI, P. H., ZHU ZHAOLING, Z. Z., LI GANG, L. G., HUANG ZITONG, H. Z., ZHAO ZHIXIN, Z. Z., KOUP, R., BAILER, R. & WU CHANGYOU, W. C. 2006. Long-lived effector/central memory T-cell responses to severe acute respiratory syndrome coronavirus (SARS-CoV) S antigen in recovered SARS patients.

YANG, R., HUANG, B., A, R., LI, W., WANG, W., DENG, Y. & TAN, W. 2020b. Development and effectiveness of pseudotyped SARS-CoV-2 system as determined by neutralizing efficiency and entry inhibition test in vitro. *Biosaf Health,* 2**,** 226-231.

YI, S. A., NAM, K. H., YUN, J., GIM, D., JOE, D., KIM, Y. H., KIM, H. J., HAN, J. W. & LEE, J. 2020. Infection of Brain Organoids and 2D Cortical Neurons with SARS-CoV-2 Pseudovirus. *Viruses,* 12.

YOUNG, A. 2022. T cells in SARS-CoV-2 infection and vaccination. *Therapeutic Advances in Vaccines and Immunotherapy,* 10**,** 25151355221115011.

YU, J., LI, Z., HE, X., GEBRE, M. S., BONDZIE, E. A., WAN, H., JACOB-DOLAN, C., MARTINEZ, D. R., NKOLOLA, J. P. & BARIC, R. S. 2021. Deletion of the SARS-CoV-2 spike cytoplasmic tail increases infectivity in pseudovirus neutralization assays. *Journal of virology,* 95**,** e00044-21.

ZAHRADNÍK, J., MARCIANO, S., SHEMESH, M., ZOLER, E., CHIARAVALLI, J., MEYER, B., RUDICH, Y., DYM, O., ELAD, N. & SCHREIBER, G. 2021. SARS-CoV-2 RBD in vitro evolution follows contagious mutation spread, yet generates an able infection inhibitor. *BioRxiv***,** 2021.01. 06.425392.

ZETTL, F., MEISTER, T. L., VOLLMER, T., FISCHER, B., STEINMANN, J., KRAWCZYK, A., V'KOVSKI, P., TODT, D., STEINMANN, E., PFAENDER, S. & ZIMMER, G. 2020. Rapid

Quantification of SARS-CoV-2-Neutralizing Antibodies Using Propagation-Defective Vesicular Stomatitis Virus Pseudotypes. *Vaccines (Basel),* 8.

ZHANG, G. F., MENG, W., CHEN, L., DING, L., FENG, J., PEREZ, J., ALI, A., SUN, S., LIU, Z., HUANG, Y., GUO, H. & GAO, S. J. 2022. Neutralizing antibodies to SARS-CoV-2 variants of concern including Delta and Omicron in subjects receiving mRNA-1273, BNT162b2, and Ad26.COV2.S vaccines. *J Med Virol,* 94**,** 5678-5690.

ZHANG, Q., BASTARD, P., LIU, Z., LE PEN, J., MONCADA-VELEZ, M., CHEN, J., OGISHI, M., SABLI, I. K. D., HODEIB, S., KOROL, C., ROSAIN, J., BILGUVAR, K., YE, J., BOLZE, A., BIGIO, B., YANG, R., ARIAS, A. A., ZHOU, Q., ZHANG, Y., ONODI, F., KORNIOTIS, S., KARPF, L., PHILIPPOT, Q., CHBIHI, M., BONNET-MADIN, L., DORGHAM, K., SMITH, N., SCHNEIDER, W. M., RAZOOKY, B. S., HOFFMANN, H. H., MICHAILIDIS, E., MOENS, L., HAN, J. E., LORENZO, L., BIZIEN, L., MEADE, P., NEEHUS, A. L., UGURBIL, A. C., CORNEAU, A., KERNER, G., ZHANG, P., RAPAPORT, F., SEELEUTHNER, Y., MANRY, J., MASSON, C., SCHMITT, Y., SCHLÜTER, A., LE VOYER, T., KHAN, T., LI, J., FELLAY, J., ROUSSEL, L., SHAHROOEI, M., ALOSAIMI, M. F., MANSOURI, D., AL-SAUD, H., AL-MULLA, F., ALMOURFI, F., AL-MUHSEN, S. Z., ALSOHIME, F., AL TURKI, S., HASANATO, R., VAN DE BEEK, D., BIONDI, A., BETTINI, L. R., D'ANGIO, M., BONFANTI, P., IMBERTI, L., SOTTINI, A., PAGHERA, S., QUIROS-ROLDAN, E., ROSSI, C., OLER, A. J., TOMPKINS, M. F., ALBA, C., VANDERNOOT, I., GOFFARD, J. C., SMITS, G., MIGEOTTE, I., HAERYNCK, F., SOLER-PALACIN, P., MARTIN-NALDA, A., COLOBRAN, R., MORANGE, P. E., KELES, S., ÇÖLKESEN, F., OZCELIK, T., YASAR, K. K., SENOGLU, S., KARABELA Ş, N., RODRÍGUEZ-GALLEGO, C., NOVELLI, G., HRAIECH, S., TANDJAOUI-LAMBIOTTE, Y., DUVAL, X., LAOUÉNAN, C., SNOW, A. L., DALGARD, C. L., MILNER, J. D., VINH, D. C., et al. 2020. Inborn errors of type I IFN immunity in patients with life-threatening COVID-19. *Science,* 370.

ZHENG, M. 2021. Cellular Tropism of SARS-CoV-2 across Human Tissues and Age-related Expression of ACE2 and TMPRSS2 in Immune-inflammatory Stromal Cells. *Aging Dis,* 12**,** 718-725.

ZHENG, Y., LARRAGOITE, E. T., WILLIAMS, E., LAMA, J., CISNEROS, I., DELGADO, J. C., SLEV, P., RYCHERT, J., INNIS, E. A., COIRAS, M., RONDINA, M. T., SPIVAK, A. M. & PLANELLES, V. 2021. Neutralization assay with SARS-CoV-1 and SARS-CoV-2 spike pseudotyped murine leukemia virions. *Virol J,* 18**,** 1.

ZHOU, B., THAO, T. T. N., HOFFMANN, D., TADDEO, A., EBERT, N., LABROUSSAA, F., POHLMANN, A., KING, J., PORTMANN, J., HALWE, N. J., ULRICH, L., TRÜEB, B. S., KELLY, J. N., FAN, X., HOFFMANN, B., STEINER, S., WANG, L., THOMANN, L., LIN, X., STALDER, H., POZZI, B., DE BROT, S., JIANG, N., CUI, D., HOSSAIN, J., WILSON, M., KELLER, M., STARK, T. J., BARNES, J. R., DIJKMAN, R., JORES, J., BENARAFA, C., WENTWORTH, D. E., THIEL, V. & BEER, M. 2020a. SARS-CoV-2 spike D614G variant confers enhanced replication and transmissibility. *bioRxiv*.

ZHOU, P., YANG, X. L., WANG, X. G., HU, B., ZHANG, L., ZHANG, W., SI, H. R., ZHU, Y., LI, B., HUANG, C. L., CHEN, H. D., CHEN, J., LUO, Y., GUO, H., JIANG, R. D., LIU, M. Q., CHEN, Y., SHEN, X. R., WANG, X., ZHENG, X. S., ZHAO, K., CHEN, Q. J., DENG, F., LIU, L. L., YAN, B., ZHAN, F. X., WANG, Y. Y., XIAO, G. F. & SHI, Z. L. 2020b. A pneumonia outbreak associated with a new coronavirus of probable bat origin. *Nature,* 579**,** 270-273.

ZHU, Y., YU, D., YAN, H., CHONG, H. & HE, Y. 2020. Design of Potent Membrane Fusion Inhibitors against SARS-CoV-2, an Emerging Coronavirus with High Fusogenic Activity. *J Virol,* 94.